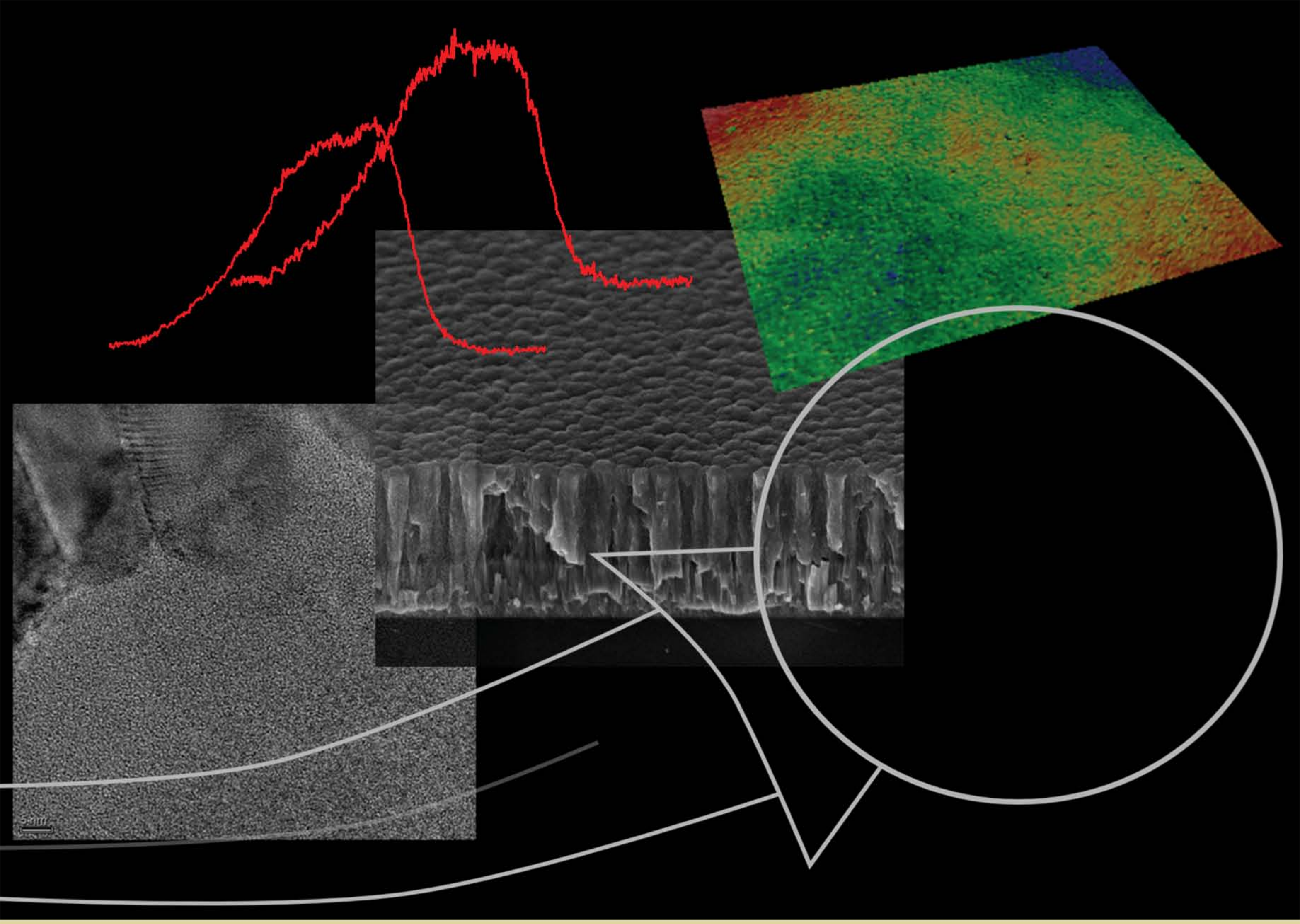

Ana Isabel Costa Escudeiro

NANOCOMPOSITE ZrC/a-C(:H) COATINGS FOR POTENTIAL APPLICATIONS ONTO BIOMEDICAL IMPLANTS

Doctoral Thesis in Mechanical Engineering, branch Surface Engineering, supervised by Professor Doctor Albano Augusto Cavaleiro Rodrigues de Carvalho and Professor Doctor Tomas Polcar, submitted to the Department of Mechanical Engineering, Faculty of Sciences and Technology of the University of Coimbra.

2014

· U C ·

Universidade de Coimbra

· U C ·

FCTUC FACULDADE DE CIÊNCIAS
E TECNOLOGIA
UNIVERSIDADE DE COIMBRA

DEPARTAMENTO DE ENGENHARIA MECÂNICA

Nanocomposite ZrC/a-C(:H) coatings for potential application onto biomedical implants

Ana Isabel Costa Escudeiro

Doctoral Thesis in Mechanical Engineering, branch Surface Engineering, submitted to the Department of Mechanical Engineering, Faculty of Sciences and Technology of the University of Coimbra

Supervisors

Professor Doctor Albano Cavaleiro

Professor Doctor Tomas Polcar

Coimbra

2014

Tecnical Sheet:

Author: Ana Isabel Costa Escudeiro

Title: Nanocomposite ZrC/a-C(:H) coatings for portential applications onto biomedical implants

Editor: Department of Mechanical Engineering, Faculty of Science and Technology

Cover: The cover images shows four different figures that briefly summarize the different steps undergo during the thesis:

Top left: Raman spectra of the a-C (left) and a-C_Zr(4) (right) films.

Top right: 3D profile of the as-deposited a-C_Zr(4) film.

Bottom left: Cross sectional TEM BF micrograph of a-C_Zr(14) film.

Bottom right: Hip prosthesis stylization.

Centre: Cross-sectional SEM micrograph of a-C_Zr(4) film.

Others finantial support:

PhD scholarship financed by:
(SFRH/BD/75071/2010)

Aos meus pais e irmão

Peanuts by Schulz

AGRADECIMENTOS/ACKNOLEGMENTS

A realização de um trabalho de investigação, como uma tese doutoramento, envolve um sem número de pessoas e instituições que direta ou indiretamente contribuíram para o levar a bom porto, e aos quais não posso deixar de expressar os mais sinceros agradecimentos.

Em primeiro lugar quero expressar mais uma vez um profundo agradecimento ao Professor Doutor Albano Cavaleiro pela confiança que sempre depositou em mim, bem como pela inesgotável paciência e pela perpétua disponibilidade sempre demonstradas durante toda a realização desta tese. Enfim, obrigada pela amizade e pelas infindáveis conversas e discussões que me fizeram crescer não só ao nível científico mas também como pessoa. I would also like to thank Doctor Tomas Polcar for everything: from THE famous email, which has completely shaken my PhD and made it possible, to his friendship, thanks Tomas!

Gostaria de agradecer ao Professor Valdemar, como presidente do CEMUC, pela oportunidade que me concedeu de trabalhar num centro de investigação com elevados padrões de qualidade.

Presto também um agradecimento geral a todos os elementos do SEG, do grupo de Nanomateriais e Microfabricação e do grupo de Tecnologia do CEMUC. No entanto, não posso deixar de expressar um agradecimento especial ao André, à Ritinha, à Noora, ao Filipe, à Maria João, à Ana e ao Joca porque, para além da amizade, a ajuda de cada um estará sempre na minha mente. Os agradecimentos estendem-se naturalmente a todos os colaboradores do Led&Mat do IPN, em particular ao Eng. João Paulo e Eng. Ana Manaia, ao Rui, ao Tó e ao Nelson, por toda a disponibilidade e partilha de conhecimentos.

My acknowledgments should be extended to other elements from foreigner institutions that also made this thesis possible: João Vitor, Tomas Vitù, and Karolina (from the *Czech Technical University*), Maria João, Bob, Robin, Carol, Elmira, Dmytri, Newton, Chris and all elements from the *Rush University Medical Center* for all the help and hospitality. A special thank to Doctor Markus Wimmer and Doctor Mathew Mathew for the opportunity of being part of such an excellent group as the section of Tribology and for all the scientific support and consideration during my stay in Chicago.

Cabe ainda um agradecimento à Fundação para a Ciência e Tecnologia pela concessão da bolsa de doutoramento SFRH/BD/75071/2010 sem a qual a realização do mesmo teria sido muito dificultada.

Por fim gostaria de agradecer à minha família, principalmente aos meus pais e irmão a quem dedico esta tese, aos meus primos Isabel, Zé, Cátia e, mais recentemente, ao pequeno Francisco, à minha Madrinha e aos meu avós que sempre compreenderam as minhas ausências e visitas de médico. Sem esquecer a minha segunda família, um grande obrigado aos meus amigos, amici and friends, e a todos aqueles que surgiram na minha vida por algum motivo relacionado com o desenvolvimento desta tese / and thank you all who are now, somehow, part of my life due to this thesis. Agradeço-vos do fundo do coração todo o apoio, carinho e motivação, ainda que não compreendessem muito bem que tipo de "filmes" fazia. Nada disto seria possível sem vós. ☺

Obrigada por me fazerem acreditar!

RESUMO

A longevidade de implantes biomédicos tem vindo a ser associada à libertação de partículas para o organismo e à sua interação com todos os elementos do meio envolvente. Das mais problemáticas encontram-se os resíduos de polietileno provenientes das combinações metal-polímero e os iões metálicos das metal-metal causando reações inflamatórias agudas nos tecidos que suportam o implante levando à sua consequente falha. A utilização da engenharia de superfícies, nomeadamente através da deposição de revestimentos finos, para reduzir a produção e libertação de partículas de desgaste e iões é cada vez mais apontada como uma possível solução. No entanto, foram reportados problemas de adesão *in service* que limitam a sua implantação e uso clínico.

Esta tese incide na síntese e caracterização de revestimentos nanocompósitos de carbono amorfo incorporado com nanopartículas de ZrC com potencial para melhorarem o tempo de vida de implantes biomédicos. Os revestimentos foram depositados por co-pulverização catódica por magnetrão em atmosfera reativa ($Ar+CH_4$) e inerte (Ar), permitindo o crescimento de filmes hidrogenados e não hidrogenados, respetivamente. O primeiro grande desafio que motivou a realização deste trabalho foi a necessidade de melhorar a adesão dos revestimentos o que foi possível com a interposição de uma intercamada em gradiente composta por Ti/TiN/TiNC entre o revestimento e o substrato.

A incorporação de diferentes teores de Zr na matriz de carbono amorfo foi possível variando o número de pastilhas de Zr colocadas no alvo de grafite. Assim, foram produzidos filmes com teores em Zr num intervalo de 0 a 14 %at. e de 0 a 10 %at. para os filmes sem e com H, respetivamente. Os filmes apresentaram uma estrutura nanocompósita consistindo em nanopartículas de ZrC (diâmetro entre 1 a 2.2 nm) distribuídas aleatoriamente numa matriz de carbono. A presença dos nanocristais permitiu a diminuição das tensões residuais dos filmes não-hidrogenados e hidrogenados melhorando a adesão dos revestimentos e influenciando fortemente as propriedades mecânicas dos revestimentos: maior dureza (H) e módulo de Young (E). Os revestimentos com cristalites mais pequenas revelaram um comportamento elástico mais favorável (maiores valores de H/E e H^3/E^2) o que se revelou particularmente importante quando os revestimentos foram depositados em substratos com baixa capacidade de resistir a carga de contacto, tais como o Ti puro (CP-Ti) e a liga de Ti (Ti6Al4V). No que diz respeito às propriedades tribológicas dos revestimentos quando testados contra bolas de Ti6Al4V, os filmes dopados com Zr demonstraram um comportamento independente das condições ambientais do teste (ao ar e em soluções fisiológica e contendo proteínas). No entanto, o desgaste do contracorpo diminuiu.

Do ponto de vista biomédico, a presença de nanocristias de ZrC desempenhou um papel fundamental, alterando as propriedades físico-químicas dos revestimentos: aumentou o ângulo de contacto e, consequentemente, melhorou a adsorção de proteína. Na realidade, a capacidade de efetivamente adsorver proteínas demonstrou ser particularmente importante na proteção das superfícies ao deslizarem em contacto direto.

De modo a avaliar o desgaste dos revestimentos contra materiais poliméricos, os revestimentos foram testados num equipamento pino disco multidirecional que replica o movimento "cruzado" que ocorre entre os materiais constituintes das próteses articulares. Apesar da interposição de uma intercamada otimizada em gradiente e melhor adesão devido à incorporação de Zr nos filmes, os filmes dopados delaminaram após alguns milhares de ciclos. O efeito sinergético entre os diferentes mecanismos de corrosão devido à presença de fluidos corpóreos, e as elevadas tensões cíclicas de corte podem ter sido a causa da falha da interface e da consequente delaminação do filme.

Palavras Chave: Filmes nanocompósitos de ZrC; Carbono amorfo; ZrC/a-C(:H); Biotribologia; DLC

ABSTRACT

The release of particulate matter derived from biomedical implants has been considered determinant for their long-term survival. Polyethylene debris derived from polymer-on-metal coupling together with the metal ion release on metal-on-metal pairs appear to cause the most pronounced tissue reactions which may induce inflammatory reactions associated with the ultimate failure of the implant. The use of surface engineering, namely coating technology, offers an alternative approach in order to reduce the production of the wear debris. However, a critical feature for such an alternative technology is the adhesion of the coating on the metallic substrates after implantation and clinical use.

This thesis deals with the synthesis and characterization of nanocomposite ZrC amorphous carbon (a-C) coatings with potential to improve the life time of biomedical implants. The coatings were deposited by dc magnetron sputtering in reactive (Ar+CH_4) and non-reactive (Ar) atmosphere in order to produce hydrogenated and non-hydrogenated coatings, respectively. The first challenge to motivate this work was the need for high adhesion of the coatings. The critical loads (and thus adhesion) of the coatings has strongly increased with the application of a Ti/TiN/TiNC gradient layer between coating and substrate.

Zr was incorporated into the C-matrix by varying the number of Zr pellets embedded in a graphite target. Different Zr contents, ranging from 0 to 14 at.% for non-hydrogenated coatings and 0 to 10 at.% for the hydrogenated ones, were obtained. Nanocomposite based films consisting of small ZrC nanoparticles (1 to 2.2 nm) randomly distributed in the C-matrix for Zr content as low as 3 at.% were achieved. The presence of such nanocrystals relaxed the non-hydrogenated and hydrogenated films, thus improving the adhesion of the coatings and strongly influencing the overall mechanical properties of the coatings: high hardness (H) and Young modulus (E). Coatings with small crystallites revealed more favourable elastic-plastic response (lower H/E and H^3/E^2) which was particularly important when depositing on low load carrying capacity substrates such as commercial pure titanium (CP-Ti) and titanium alloy (Ti6Al4V). Regarding the tribological properties of the coatings sliding against Ti6Al4V balls, the Zr-doped coatings behaviour was almost independent of the environmental conditions (ambient air, physiological and protein-containing solutions). Nevertheless, the counterbody wear was lower when compared to that of sliding pure carbon films. From the biomedical point of view, the presence of ZrC nanocrystals played an important role by changing the physicochemical properties of the coatings: increasing contact angle and, consequently, enhancing albumin adsorption. This was particularly important, since the ability to effectively adsorb proteins protected both surfaces from rubbing in direct contact.

In order to evaluate the wear behaviour against polymeric materials, Zr-containing films were tribologically tested in multidirectional pin-on-disk equipment, which replicated the “cross-shear” motion occurring between the mating components of a joint prosthesis. Despite the use of an optimized gradient interlayer scheme and improved adhesion by incorporation of Zr into the C-matrix, the Zr-containing film delaminated after several million of cycles. The synergetic effect of stress-induced corrosion through biological fluid and high cyclic shear stress may have caused interface fatigue and subsequent delamination of the coatings.

Keywords: Nanocomposite ZrC; Amorphous carbon; ZrC/a-C(:H); Biotribology; DLC

PAPERS INCLUDED IN THE THESIS

The thesis is based on 7 published/submitted papers listed below and which are referred to in the text by Roman numerals. Some results which have neither been published nor exist in manuscript are also included. Reprints of the papers can be found in the annexes.

I. **DLC(H) Doped with Zr Coatings for Orthopaedics Applications: Adhesion Properties**
A. Escudeiro, T. Polcar and A. Cavaleiro
55th Annual Technical Conference Proceedings, ed: Society of Vaccum Coaters, **2012**

II. **a-C(:H) and a-C(:H)_Zr coatings deposited on biomedical Ti-based substrates: Tribological properties**
A. Escudeiro, T. Polcar and A. Cavaleiro
Thin Solid Films 538 **(2013)** 89-96

III. **Indentation and scratch testing of DLC-Zr coatings on ultrafine-grained titanium processed by high-pressure torsion**
C.T. Wang, A. Escudeiro, T. Polcar, A. Cavaleiro, R.J.K. Wood, N. Gao and T.G. Langdon
Wear, 306, 1-2 **(2013)** 304-310

IV. **Adsorption of bovine serum albumin on Zr co-sputtered a-C(:H) films: implication on wear behavior**
A. Escudeiro, T. Polcar and A. Cavaleiro
Journal of Mechanical Behavior of Biomedical Materials 39 **(2014)** 316-327

V. **Sliding Properties of Zr-DLC Coatings: The effect of Tribolayer Formation**
T. Vitù, A. Escudeiro, T. Polcar and A. Cavaleiro
Surface and Coating Technology 258 **(2014)** 734-745

VI. **Tribological Behavior of uncoated and DLC-coated CoCr and Ti-alloy in contact with UHMWPE and PEEK counterbodies**
A. Escudeiro, M.A. Wimmer, T. Polcar and A. Cavaleiro
Tribology International, under review

VII. **Structural and Mechanical properties of nanocrystalline Zr co-sputtered a-C(:H) amorphous films**
A. Escudeiro, N.N. Figueiredo, T. Polcar and A. Cavaleiro
Applied Surface Science 325 **(2015)** 64-72

Other publications to which the author has contributed:

Influence of Ag on mechanical and Tribological behavior of DLC coatings
N.K. Manninen, F. Ribeiro, A. Escudeiro, T. Polcar, S. Carvalho and A. Cavaleiro
Surface and Coatings Technology 232 **(2013)** 290-300

Tribological behaviour a-C and a-C:H films doped with Ti in biological solutions
A. Escudeiro, T. Polcar, and A. Cavaleiro
Vacuum 85 **(2011)** 12: 1144-1148

Carbon-based coatings doped by copper: Tribological and mechanical behavior in olive oil lubrication
R.M. Balestra, A.M.G. Castro, M. Evaristo, A. Escudeiro, P. Mutafov, T. Polcar and A. Cavaleiro
Surface and Coatings Technology 205 **(2011)** 85: 79-83

LIST OF SYMBOLS AND ABREVIATIONS

θ	Position of the diffraction peak	[°]
θ_{water}	Water contact angle	[°]
λ	Wavelength	[Å] or [nm]
ν	Poisson ratio	
σ_{RS}	Residual stress	[GPa]
Ø	Diameter	[mm]
ASTM	American Society for Testing and Materials	
BF	Bright Field	
BM20	Bending magnet 20	
BSA	Bovine Serum Albumin	
CC	Crevice Corrosion	
CEMUC	Centro de Engenharia Mecânica da Universidade de Coimbra	
CEMUP	Centro de Engenharia Mecânica de Universidade do Porto	
CFR	Carbon-Fiber Reinforced	
CoC	Ceramic on Ceramic	
CoCrMo	Cobalt-chrome alloy	
CoP	Ceramic on Polymer	
COF	Coefficient of Friction	
CP	Commercial Pure	
CVD	Chemical Vapour Deposition	
DC	Direct Current	
DLC	Diamond-Like Carbon	
$d_{s\text{-}t}$	Substrate-to-target distance	[nm]
E	Young Modulus	[GPa]
EBS	Non- Rutherford Backscattering Spectrometry	
EDS	Electron Dispersive X-ray Spectrometry	
EELS	Electron Energy Loss Spectroscopy	

EN	European Norm	
EPMA	Electron Probe Micro Analysis	
ERD	Elastic Recoil Detection	
ESRF	European Synchrotron Radiation Facility	
FAT	Fixed Analyser Transmission	
FEG	Field Emission Gun	
FIB	Focus Ion Beam	
FTT	Fourier Fast Transform	
FWHM	Full Width at Half Maximum	
GIF	Gatan Image Filter	
H	Hardness	[GPa]
HPT	High Pressure Torsion	
HR	High resolution	
IBA	Total Ion Beam Analysis	
ICDD	International Centre of Diffraction Data	
Lc, Lc_1, Lc_2, Lc_3	Critical Load	
Mc	Million cycles	
MoM	Metal on metal	
MoP	Metal on polymer	
NA	Not Analysed	
nc	Nanocrystalline	
NCD	Nano crystalline diamond	
p	p value	
PE	Polyethylene	
PEEK	Polyetheretherketone	
PIXE	Particle-induced X-ray emission	
PS	Physiological Solution	
PTFE	Polytetrafluoroethylene	
PVD	Physical Vapour Deposition	
PyC	Pyrolytic carbon	

R_a	Average surface roughness	[nm]
RBS	Rutherford Backscattering Spectrometry	
R-C	Rockwell-C indentation	
RH	Relative Humidity	
Rms	Roughness mean square	[nm]
ROBL-MRH	Material Research station of the Rossendorf Beam Line	
rpm	Rotation per min	
SAED	Selected Area Electron Diffraction	
SEM	Scanning Electron Microscopy	
SCC	Stress-corrosion cracking	
SNK	Student-Newman-Keuls	
SS	Stainless Steel	
TEM	Transmission Electron Microscopy	
THA	Total hip arthroplasty	
Ti6Al4V	Titanium alloy	
TJA	Total joint arthroplasty	
TJR	Total joint replacement	
TKA	Total knee arthroplasty	
UFG	Ultrafine-grained	
V_F	Volume Fraction	
UHMWPE	Ultra-high molecular weight polyethylene	
XPS	X-ray Photoelectron Spectroscopy	
XRD	X-ray Diffraction	
YTZ	Ytria stabilized zirconia	
ZTA	Zirconia tounghened alumina	

TABLE OF CONTENTS

LIST OF FIGURES

LIST OF TABELS:

INTRODUCTION

Joint prosthesis is an artificial joint implanted into the human body to replace the natural articulating system, which has lost its functionality. The total joint arthroplasties decreasing pain and improving locomotion have gained increasing importance in orthopaedic surgery. The usage of joint prostheses entered the clinical practice mostly in the 70s; however, the design of endoprostheses dates back to the 14th century.

The materials used for artificial implants should fulfil several criteria, such as good mechanical properties, structural stability, corrosion resistance and suitable interaction with human cell environment. A wide range of materials is used as a bearing surface, from ceramics (e.g. alumina and zirconia) through metals (e.g. stainless steel, CoCr alloys and titanium and its alloys) to polymers (e.g. UHMWPE and PEEK). However, it is estimated that the average survival rate of an implant is of 10 to 15 years. It is particularly limiting for young patients with expected intense physical activity. Revision surgeries are complicated and expensive with outcomes that are often not as successful as that of the original joint replacement.

Aseptic loosening has been identified as the major problem associated with implant failure. Demanding contact conditions coupled with the aggressive body environment causes the generation of the wear debris which, by acute host-tissue reactions, tend to aggravate and speed up the failure of the biomaterial. Wear is thus a critical factor for prostheses, implants and other medical devices and its reduction is still an ongoing scientific and technological challenge. It is evident that the reduction of wear and subsequent extension of the life span of a joint prosthesis would improve quality of life and have positive economic impact.

Numerous attempts have been done in the last years to improve the life time of the prosthesis ranging from changing the overall bulk material, surface modification of the bulk material or the use of coatings. Nevertheless, there is still no ideal solution that effectively prevents the failure of implants. Surface modification has been considered one of the most promising approaches to improve the mechanical and tribological properties together with biocompatibility of the prostheses. Therefore, hard coatings as diamond-like carbon (DLC), transition metal nitrides and carbides, and surface modification of metals have been have been widely studied for improving the wear and corrosion resistance. Unfortunately, the major problem associated with coatings is the poor adhesion to the substrate due to the high residual stress and poor chemical bonding between the film and the substrate. Consequently, the coatings are prone to delaminate which results in rapid failure of the coated implant. The presence of body fluids is an extremely important factor to be considered. The natural lubrication minimizes the shearing damage and decreases the friction energy loss. However, in artificial joint, the lubrication effect depends on many factors, such as surface treatment or coating properties, surface roughness, mechanical properties of the implant and many more, which might strongly limit the efficiency of natural lubricants and lead to catastrophic failure of the implant with partial or complete loss of functionality.

This thesis contributes to this area by the study of diamond-like carbon alloyed with zirconium as a potential coating for orthopaedic materials.

1. Hypothesis

The production of wear particles from the replacements of metal on metal (MoM) and metal on polymer (MoP) joints replacement and their detrimental effects on body have been a continual problem since they were first implanted. Surface modifications are believed to have the potential to reduce the wear of joint prosthesis. Many studies have been carried out focused mainly on the deposition of DLC; however, there is still limited success today due to adhesion problems of the coatings.

Nanocomposite films are known to show extremely low wear and good adhesion and have been successfully used in industry such as machine tooling. The deposition of nanocomposite structure is based on atoms with different chemical affinity that can form immiscible phases providing huge improvements in both mechanical and tribological properties. When incorporating small amounts of a metallic element in an amorphous carbon matrix a nanocomposite structure is likely to be achieved. In this case, a decrease of the residual stresses are expected with the consequent improvement of the adhesion of the coatings. Experimental and clinical studies support the general consensus that Zr compounds are biocompatible and exhibit low toxicity. Thus, amorphous carbon alloyed with Zr should fulfil the implant tribological and adhesive criteria without losing its biocompatiblility.

2. Aims

This thesis seeks to contribute to wide efforts to solve the problems of inadequate artificial joint from a tribological perspective. The overall objective of this thesis is the development of nanocomposite coatings to improve the DLC performance under conditions similar to that of biomedical implants. The key idea was to combine the excellent mechanical and tribological properties of pure amorphous carbon (a-C) coatings with the specific characteristics of nanocomposite coatings. The aims of this thesis were could be then given as follows:

- To develop a-C(:H) coatings alloyed with with Zr (with different metal content and morphologies) in order to achieve a nanocomposite structured material by magnetron sputtering, using reactive ($Ar+CH_4$) and non-reactive (Ar) atmospheres.
- To thoroughly understand the deposition process and the characterization of the chemical composition and structure of the coating as a function of the depositions conditions;
- To optimize the adhesion of the coatings onto Ti-based substrates by developing a functional graded interlayer.
- To study the functional properties of the coatings in relation to their physical and chemical properties as well as their mechanical and tribological properties.
- To evaluate the interaction between the films and simulated body fluids and to characterize the influence of exposure conditions on the surface state and physical properties.
- To select the best coating candidates in relation to their tribological properties (wear and friction) and long term stability in simulating body fluid environments.

3. Thesis structure

Apart from this introductory chapter, the thesis consists of five main chapters. Chapter I presents the state of the art in the area of biomedical implants focused on protective coatings. It outlines the basis of knee anatomy and its failure, followed by the replacements that are available, the shortcoming of current replacements and the use of coatings as a method to improve their properties. Chapter II describes the deposition process and the parameters used for the coatings deposition. Special attention to the optimization of the coatings was paid, namely coatings adhesion, chemical composition and deposition rate. Chapter III is dedicated to fundamental characterization of the ZrC/a-C coatings including: chemical composition and bonding, morphology, microstructure, mechanical properties (hardness, residual stress, Young modulus and critical loads) and tribological properties in ambient air and in physiological solution. Chapter IV is focused on the physicochemical properties of the coatings by means of surface energy and protein adsorption assessment. The tribological properties of the coatings under simulated body fluid environments were also evaluated. Chapter V describes the evaluation of selected coatings sliding against ultra-high molecular weight polyethylene (UHMWPE) and polyetheretherketone (PEEK) polymeric materials in a multidirectional pin-on-disc, which replicates the typical movement in joint prosthesis. Finally, the thesis concludes with a summary of the main outcomes and future research topics that should be taken into consideration when using coatings for biomedical implants.

CHAPTER I

The gross anatomy of synovial joints is first described with emphasis on present failures and possible solutions. The history and development of joint prostheses is briefly referred in order to identify the deficiencies and the typical failure modes. The materials choice is probably the most important feature. A summary of the most common and alternative materials (bulk and surface engineered materials) used nowadays is presented. Moreover, a comprehensive overview on diamond-like carbon coatings, promising surface treatment of joint replacements, will be exposed as a possible way for improving their life span. Finally, the goal of this thesis is presented.

1. Joint Prosthesis

1.1. The natural synovial joint and its failure

An articulation, or joint, is a place where two different bones come together. They are usually associated with movement although that is not always the case. Many joints allow only limited movement and others even allow no apparent movement [1]. The structure of a given joint is directly correlated with its degree of motion. This study will focus on the mobile synovial joints. Figure 1.1 shows the structure of a typical synovial joint.

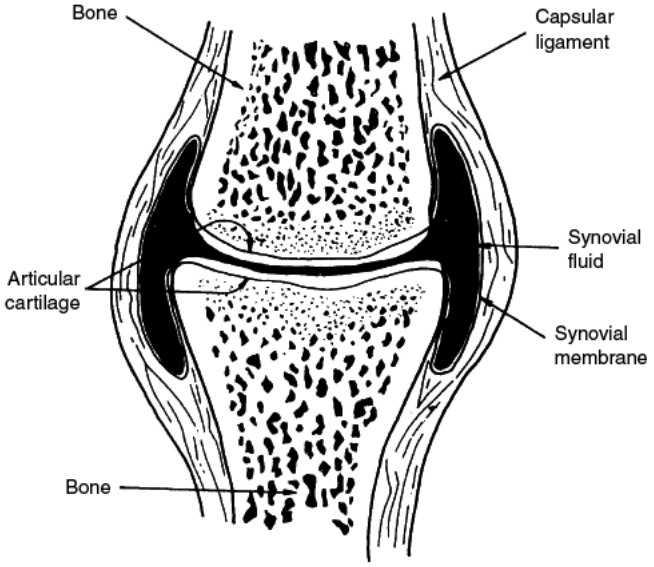

Figure 1.1 Representation of synovial joint (Adapted from [2]).

The synovial joint is a fluid containing joint (*synovial fluid*) that may look like a simple joint but it is anatomically one of the most complexes. Most of the joints that unite bones of the appendicular skeleton are synovial: hip, knee, ankle, shoulder, elbow and finger; reflecting their far greater mobility [1]. All synovial joints are covered with a thin layer of hyaline cartilage called *articular cartilage,* which promotes the sliding between bones and presents particular mechanical properties: resistance to compression (proteoglycans and water) and to shear stress (collagen) [2]. The articular surfaces are enclosed in a synovial joint cavity, surrounded by a joint capsule containing synovial fluid. This fluid is derived from the blood plasma but contains higher protein content, hyaluronic acid, glycoproteins, proteinases, and collengases. Therefore, this fluid has non-Newtonian characteristics (viscosity and viscoelastic effects that are shear rate depending) providing a slippery weight-bearing film that reduces friction between the cartilage (typical healthy human joint coefficient of friction (COF) 0.005-0.04) [3, 4]. Although the main function of the synovial fluid is to act as a lubricant during the movement, it also gives nutrients to the cartilage by diffusion, it absorbs shocks and it rids the joint cavity of microbes and cellular debris, due to the presence of phagocytic cells [3-5]. For more information on biochemistry, structure and properties of articular synovial joint references [6-9] are suggested as further reading.

The joint function can be easily affected due to accident, heredity or disease (such as *arthritis*). All the structures composing the synovial joint are liable to assume a diseased action both individually and collectively, including deformity, instability and loss of motion, which is commonly associated with severe pain and functional disability [9]. Articular cartilage is the most affected one. Its function to absorb shocks by the elasticity can be lost, if the balance of growth factors and enzymes is changed. The treatments vary between pharmacological and, in worse cases, chirurgical replacement of total or part of the joint by a prosthetic device (*arthroplasty*) [10, 11]. Indeed, the number of total joint arthroplasties (TJAs) is increasing relatively fast. For instance, a total of approximately 1,324,000 primary and revision knee procedures are carried out annually worldwide (data from 18 countries, based on international arthroplasty registers reports) [12] and it is expected that the number of TJA in 2020 will rise by 98% [13, 14].

1.2 A survey of artificial joints

The main reasons that lead to the implant of a joint prosthesis are unsustainable pain and difficulties in movements [15]. Joint implants are designed to replace biological materials that have been damaged (cartilage and/or bone) by articulating joint surfaces and synthetic materials.

The first total knee and hip arthroplasties (TKA and THA, respectively) were performed in 1890 by T. Gluck using cemented ivory. The few implants made had to be removed after a few months, mainly because of inadequate sterilization techniques [16]. Four years later, JE Pean substituted the proximal shoulder with platinum endoprosthesis [17]. During the World War II, materials originally manufactured for airplanes, automobiles, clocks and radios were taken “off-the-shelf” by surgeons and applied in the medical field (glass, titanium, stainless steel, metacrylates, Teflon®, nylon, polyurethanes, etc) but the real advance came in the 1950s with the principle of low-friction arthroplasty, initially developed for the hip by Charnley [18,19]. After numerous material combinations, in 1962, Charnley successfully implanted ultra-high molecular weight polyethylene (UHMWPE) articulated against a metallic femoral head; it was used by over a million of patients and it significantly improved their mobility [18-20]. His developments remain the gold standard bearing surface combination and basic tribological design for total joint replacements (TJRs). Table 1.1 shows the main articular prosthesis and its components used nowadays. There have been several innovations regarding strength, shape, function and behaviour of the stem which holds the prosthesis into the bone, but surfaces have changed very little indeed since Charnley first replaced polytetrafluoroethylene (PTFE) by UHMWPE.

Table 1.1 Types of TJR (Adapted from [21]).

Joint	Type
Hip	Ball and socket
Knee	Hinged, semiconstrained, surface resurfacing, unicompartment or bicompartment
Shoulder	Ball and socket
Ankle	Surface replacement
Elbow	Hinged, semiconstrained, surface resurfacing
Wrist	Ball and socket, space filler
Finger	Hinged, space filler

TJRs have been successfully implanted for over 30 years [20]. The success of the replacement is strongly related to the overall medical condition of the patient, the behaviour of the different materials used to produce the implants and the surgeon ability and experience [22]. Moreover, with a proper patient selection in terms of sex, age, bodyweight, profession and activity, good to excellent results can be achieved: 80% survivorship at 25 years for Charnley-type hip prosthesis [23] and 94% at 15 years for knee replacements [24]. However, the average survival rate of the implants is of 10-15 years [25, 26]. Unfortunately, with the increasing demand of prosthetic devices by younger people (< 65 years) this is not satisfactory. In fact, it is estimated that until 2030 these patients will represent the majority of the primary and revision TJR [27] due to more active lifestyles. This may also be synonymous of a growth in revision surgeries which are more costly, technically more difficult and also more complicated than primary arthroplasty, suggesting that this market will increase in the next few years. It is thus not surprising that the global market for joint prosthesis is worth US$56 billion by 2017, spurred by a multitude of factors including a aging global population, the rising incidence of degenerative joint diseases, and improving healthcare infrastructures in developing countries [28]. Besides, the development of durable and improved materials and implants is also expected to contribute to the market's growth.

1.2.1. Artificial joint failure and the role of wear

"*All prostheses will fail sometime. It is a race between the life of the patient and the life of the prosthesis*" [29]. Between 2000 and 2012 the top seven reasons for revision surgeries were, in order of proportion: aseptic loosening, infection, polyethylene (PE) wear, instability, pain/stiffness, osteolysis and malposition/malalignment [30, 31]. Failure due to instability and malposition is beyond the scope of this thesis but it lies on better surgeons training and the use of computer guided surgery [22]. On the other hand, implant loosening is mainly associated with biological potential of wear debris and consequently intimately related to the materials used [26]. Considering the nature of joint prosthesis, wear debris can be generated at any interface: at the articular surfaces, at the cement interfaces, with the bone and the implant, and at the junctions between any modular features in the main implant. Loosening and wear are then strongly related to each other by making the prosthetic failure a tribological issue.

Along with wear, friction is also another important issue. Excessive friction causes high torque loads that can be transmitted to the bone-implant interface and result in pain and instability [32]. It is therefore important to improve lubrication mechanisms and the use of low friction material combination in order to reduce friction. Even though wear will always be an intrinsic issue for biomaterials, it can be reduced having by taking the tribological aspects of the joint into consideration and proving materials that suit the natural synovial lubrication.

The presence of body fluids is also very important in the material degradation. Phagocytosis of wear debris by macrophages induces an inflammatory reaction associated with the release of cytokines and other inflammatory mediators. Once osteolysis has occurred, it tends to progress and may ultimately lead to implant failure [18, 33].

1.3 Current and alternative materials for joint prosthesis

1.3.1 State of the art

The implant design should fulfil the kinematic and dynamic load transfer characteristics of the natural joint [21] and should be patient- and pathology-related.

This section will only focus on material variations, especially materials used as bearing surfaces.

The implant components require desirable properties such as strength, high wear resistance, low Young modulus (close to the bone or cartilage), high ductility, high fracture toughness and high corrosion resistance [34]. Biocompatiblility is a vital parameter that must also be taken into account since the material should be implanted in the human body. In other words, as a foreign-body, the degree to which the homeostatic mechanisms is perturbed and the extent to which pathophysiologic conditions are created and undergo resolution is also an issue [18]. Decades of basic and clinical experimentation have resulted in a vast number of material combinations ranging from every class of materials. Generally though, there are only a few materials that have an optimal mix of those properties. The current standards include materials from all classes of materials: titanium and its alloys, cobalt-chrome alloys (CoCrMo), UHMWPE with or without cross-linking, alumina (Al_2O_3) or zirconia (ZrO_2) stabilized with ytria or toughened with alumina (YSZ and ZTA, respectively). These materials can be then combined by meanings of hard/soft (metal on polymer, MoP, and ceramic on polymer, CoP) and hard/hard (metal on metal, MoM, and ceramic on ceramic, CoC) combinations.

Table I.2 lists the relevant combination of materials based on the market leaders: DePuy, Zimmer, Biomet®, Smith & Nephew and Stryker® Corporation [25, 28].

Table I.2 Biomaterials for TJR and its properties and applications (Adapted from [21]).

Materials	Properties	Application
CoCrMo alloy (cast or wrought)	Heavy, hard, stiff High wear resistance	Stem, head (ball) Cup, porous coating, Metal backing
Ti alloys (Ti6Al6V)	Low stiffness Fatigue Resistance Low wear resistance Corrosion resistance	Stem, porous coating Metal backing
Pure Ti	Excellent osseointegration	Porous coating
Tantalum (*Trabecular Metal*)	Excellent osseointegration Good mechanical strength	Porous structure
Alumina (Al_2O_3)	Hard, Brittle High wear resistance	Ball, Cup
Zirconia (YSZ or ZTA)	Heavy and high toughness High wear resistance	Ball
UHMWPE (with or without crosslinking)	Low friction, wear debris Low creep resistance	Cup

It is worth noting that the way materials are processed, such as precision casting or forging (metal alloys), machining, grinding, grit blasting or other surfacing techniques, can also widely influence the properties of the prosthetic materials [35]. References [3, 9, 36-40] provide a deeper understanding of the fundamental properties of the materials and the influence of material processing for ensuring the desired performance of the implant devices. Besides extended research and testing, finding the optimal materials is a continuous effort of success and failures in search of perfection. Tribo-corrosive processes of metallic materials can increase the number of metallic ions in local tissues and systemically which may cause dramatic necrotic and inflammatory reactions in the surrounding tissues [33, 41]. Ceramics can be considered as the most preferred materials for joint endoprosthesis due to negligible body reaction to wear [26, 42, 43]. However, such materials can undergo brittle fracture [43, 44] and squeaking [45, 46], which can cause severe and complex problems. On the other hand, polymeric materials are soft and their wear resistance is strongly limited [38]. Searching for materials for a longer lasting implant is still an ongoing bioengineering challenge.

1.3.2 New promising bulk materials

The most obvious option to change the tribological properties is to replace the overall bulk material with a new one that generates less wear with adverse biological interactions. Using this approach, the new material has to ensure lubrication under physiological condition together with appropriate mechanical strength, corrosion resistance and biocompatibility.

Non-oxide ceramics

Silicon nitride (Si_3N_4) has been considered as a reliable material for TJA due to higher strength and fracture toughness compared to alumina and zirconia and its excellent wear characteristics [42, 47, 48]. Long-term *in vivo* exposure did not reveal any adverse biological reaction making it a biocompatible and non-toxic material [49, 50]. However, some controversial results have been reported suggesting the presence of a nanometric oxidized layer (SiO_2) that significantly improves third-body wear [51, 52]. Nevertheless, the first silicon nitride total hip joint was implanted in 2011 [53].

Sapphire

The purest aluminium oxide form with no porosity or grain boundaries has shown very low and stable friction coefficient (0.05-0.10) as well as an extraordinary high wear capacity [54]. Biocompatibility, biochemical inertness and low cost make the sapphire friction pair very attractive for endoprotheses. In fact, 5 sapphire heads had already been implanted with no complication reported within 5 year [53].

Vitamin E stabilized UHMWPE

Vitamin E is an antioxidant agent that improves the oxidation resistance of irradiated UHMWPE. When incorporated in the UHMWPE, it helps to eliminate the free radicals within the polymer which are partially responsible for the delamination type of wear, the primary cause of failure of UHMWPE [38, 55]. Moreover, it has been also shown that Vitamin E-doped polymers present superior crack and wear resistance and maintain its fatigue strength [56]. However, long-term studies to establish the effectiveness of vitamin E as an effective anti-oxidant *in vivo* are required.

Polyetheretherketone (PEEK) and carbon-fiber reinforced (CFR-PEEK) form

PEEK and its composites have been used for UHMWPE replacement due to their biocompatibility, high strength, stiffness, fatigue and wear resistance [57-59]. Moreover, the wear performance is strongly related to the presence or absence of CFR [59] and, when reinforced, the type [60], amount and orientation of incorporated carbon-fibers [61]. Moreover, PEEK wear particles were found to be less cytotoxic than UHMWPE [62]. In fact, in 2001, 30 alumina femoral heads against CFR-PEEK liners were implanted and 28 months after implantation only one liner had to be revised due to trauma [63]. The clinical study was expanded to a total of 121 patients by 2003. However, no published data is available yet. On the other hand, a recent study has found that two CFR-PEEK varieties increase cytokine expression that may suggest a proinflamatory potential *in vivo* [64].

1.3.3 Surface modification and coatings

Implant surface is the most important issue in the modern TJR due to direct interaction with the body fluids. Wear and corrosion are then likely to occur on bearing surfaces rather than in the bulk material. Therefore, the use of surface modification can retain the desired mechanical properties of bulk material while modifying only the properties of the outmost surface. Furthermore, ceramic coating can improve wear and corrosion resistance and minimize metal ion release. The use of coatings can also help hard tissue compatibility by promoting bone growth. Goodman [65] has published an excellent review on biologic coatings for orthopaedic implants that facilitate osseointegration and mitigate possible adverse tissue responses including the foreign body reaction and implant infections. Here we list the most studied variations of thin films and coating prepared through different methods.

Carbon-based coatings

Carbon-based coatings are one of the most used for a wide range of applications from the automotive industry to medical devices. From the biomedical point of view, the most common forms are:

(i) Diamond-like carbon (DLC), which exhibits a peculiar amorphous structure that gives them properties between diamond and graphite. They are generally characterized by high hardness, low friction, high wear resistance, an excellent environmental behaviour and biocompatibility [66-69]. Unfortunately, retrieved femoral heads had shown numerous pits and spots of local coating delamination and crevice corrosion [70]. Thus, adhesion problems are still an ongoing issue due to an inadequate bonding at the interface between metallic substrate and coating and high residual stress [71]. Recently, research has been done to improve the wear properties and the adhesion strength of DLC coatings; it will be discussed more in detail in the next session.

(ii) Nano crystalline diamond (NCD) is hard, smooth, corrosion and wear resistant, which makes it suitable to TJR application [72]. Despite the excellent results from *in vitro* testing in a mandibular simulator [73], the excessive residual stresses due to impurities at the grain boundaries affects their adhesion and may cause delamination [74]. No clinical studies are available so far.

(iii) Pyrolytic carbon (PyC) is a material with a good fatigue resistance, wettability and wear properties as well as a modulus of elasticity very close to the cortical bone [75, 76]. It has been applied to small joints, such as proximal interphalangeal [77] and metacarpophalangeal [78] joints with a survival rate of 81.4% within 10 year [79]. However, the use of PyC for load-bearing application still needs further *in vitro* consideration.

Surface modifications of metals

OXINIUM™ (Smith and Nephew, Memphis, TN) is the commercial name for surface oxidized zirconium. Technically this ceramic surface layer is not considered a coating but an intrinsically formed oxidation layer on the bulk metal surface 5 to 10 μm thick [55]. The main principle is to oxidize a metallic zirconium alloy by means of thermal diffusion to create ZrO_2 on the surface [55, 80]. This oxide layer offers good wear properties and adhesion to the metallic substrate avoiding the metal ion release and associated hypersensitivity [55]. However, retrieved femoral Oxinium™ heads have demonstrated loss of the Oxinium™ layer with exposure of the underlying substrate; moreover, an extensive damage to the polyethylene counterbody was also observed [67, 81].

Nitrides and Carbides

Metal nitrides, carbides and carbonitrides (TiN, WC, TiCN, TiAlN, etc.) has been considered the most appropriate as hard and wear resistant coatings [82]. Brilliant golden colour TiN coatings have been also used in several biomedical applications [53, 83]. Later, a variety of nitride coatings was prepared using chromium [84], silicon [85, 86] or zirconium [87] instead of titanium. Moreover, silver incorporation into such matrices as an antibacterial agent has also been subject of recent studies [88-90]. The mechanical and corrosion resistance can be improved or maintained allowing a limited Ag release to the environment to confer the aimed antibacterial properties. TiN coatings have been used in hip, knee, ankle and shoulder replacements and continue to be the main coating solution available on the market. However, Raimondi and Pietrabissa [91] retrieved four implants at two to eight years of follow-up and argued that TiN-coated titanium alloy femoral heads were inadequate in the task of resisting *in vivo* third-body wear. Moreover, a recent study [92] has shown a case of *in vivo* fracture of a TiN-coated femoral component after 3 year implantation. Debonding of the component may be the cause for stress fracture. The extreme hardness of the coatings and their adhesion resistance on the softer metal is apparently the major limitation of their use.

2. Diamond-like carbon (DLC)

DLC is an amorphous carbon (a-C) or hydrogenated amorphous carbon (a-C:H) thin film material containing both sp^3- and sp^2-hybridized carbon atoms, which give it structure and intermediate properties between diamond and graphite [68]. The abbreviation DLC can thus stand not for a specific coating but for a class of hard C-based material [66]. DLC sp^2/sp^3 ratio and hydrogen content are strongly influenced by the deposition technique; DLC coatings can be prepared by either chemical vapour deposition (CVD – only hydrogenated coatings) or physical vapour deposition (PVD – both hydrogenated and non-hydrogenated films) technologies [66, 68]. The sp^2/sp^3 ratio can be relatively easily varied and alter the whole properties of the coating. For instance, sp^2-rich coatings commonly show low coefficient of friction in dry condition but a higher wear rate than sp^3-rich ones [66]. Furthermore, the DLC films present a unique tribological behaviour. During sliding the outmost layers are transformed into graphite and transfer to the partner surface forming the so-called transfer layer, which protects the sliding surfaces from wear. The build-up of such layer strongly depends on the environment and testing conditions [66]. In addition, the graphitic layer acts as solid lubricant and low friction is then achieved. An introduction to the fundamental properties and applications of DLC coatings can be found in a number of review papers such as [66, 68, 82, 93-95]. In the next paragraphs, the possibilities and limitations of such coating for the joint replacement field will be highlighted.

Diamond-like carbon has emerged as a potential coating for joint replacements mainly due to its high hardness, low friction coefficient, high wear and corrosion resistance, bio- and hemo-compatibility and excellent smoothness. The use of such coatings in the orthopaedic field has been widely studied over the past years. A comprehensive overview of biomedical applications on DLC coatings can be found elsewhere [71, 96-103]. Early testing showed excellent tribo-corrosion performance, low toxicity to the body, and healthy interaction with the cells in the body; some of the coatings heve reached the market and been clinically implanted. In fact, Ching [104] has recently published a study on surface coatings used as orthopaedic implants showing that DLC coatings are the most frequently used coatings (61%) in artificial joints. Despite outstanding tribological and chemical properties and good short-term results, all coated prostheses failed within 2 to 10 years *in vivo* due to delamination problems [105-107].

One of the main obstacles to the use of DLC coatings is that high internal stress (> 3 GPa) is developed during the deposition process [108]. As expected, also here the sp^2/sp^3 ratio is important. Indeed, Dearnley [109] found that the higher the sp^3-C bonds the higher the internal compressive stress, which can be as high as 10 GPa. Unfortunately, high internal stress is commonly associated with debonding problems [66, 108] especially on soft metallic substrates [110]. In addition, the adhesion problems can also be related to the interface nature between the coating and substrate [71, 111]. Many attempts have been done to minimizes such issues: (i) deposition of a metallic interlayer, such Ti, Cr, Si, Zr or Ta [112-114] or a gradient transition layer (e.g. Me/MeC, Me/MeN, or Me/MeN/MeNC, where Me is the metallic element) to prevent distinct boundaries [115-117]; (ii) doping of carbon film with light (H, N, F, etc.) or metallic element (Si, Ti, Cr, Ti, etc) [66, 116, 118, 119]; (iii) changing the deposition parameters such as applying bias polarization [120]; and/or (iv) etching of the substrates [121]. Moreover, when implanted *in vivo*, it is expected that the corrosive body environment will further enhance coating premature failure [70, 71, 122]. In 2003, Taeger et al. [106] analysed a retrieved Ti6Al4V implant coated by DLC (no interlayer applied) and showed the presence of delaminated areas which might trigger adverse body reaction and consequent aseptic loosening. In 2007, Joyce [105] analysed a retrieved DLC coated CoCrMo metartarsophalangeal prostheses (Si interlayer) which also failed after 4 years *in service,* showing pinholes, imperfections, substrate flaws and scratches that allow the body fluids to penetrate underneath the coating (see Figure I.2a and b). Cracks can then propagate along the DLC/metal interface and enhance the delamination through stress-corrosion cracking (SCC) and crevice corrosion (CC) (see Figure I.2c and d). Hauert and co-workers have summarized the knowledge in the field in references [70, 71, 107, 114].

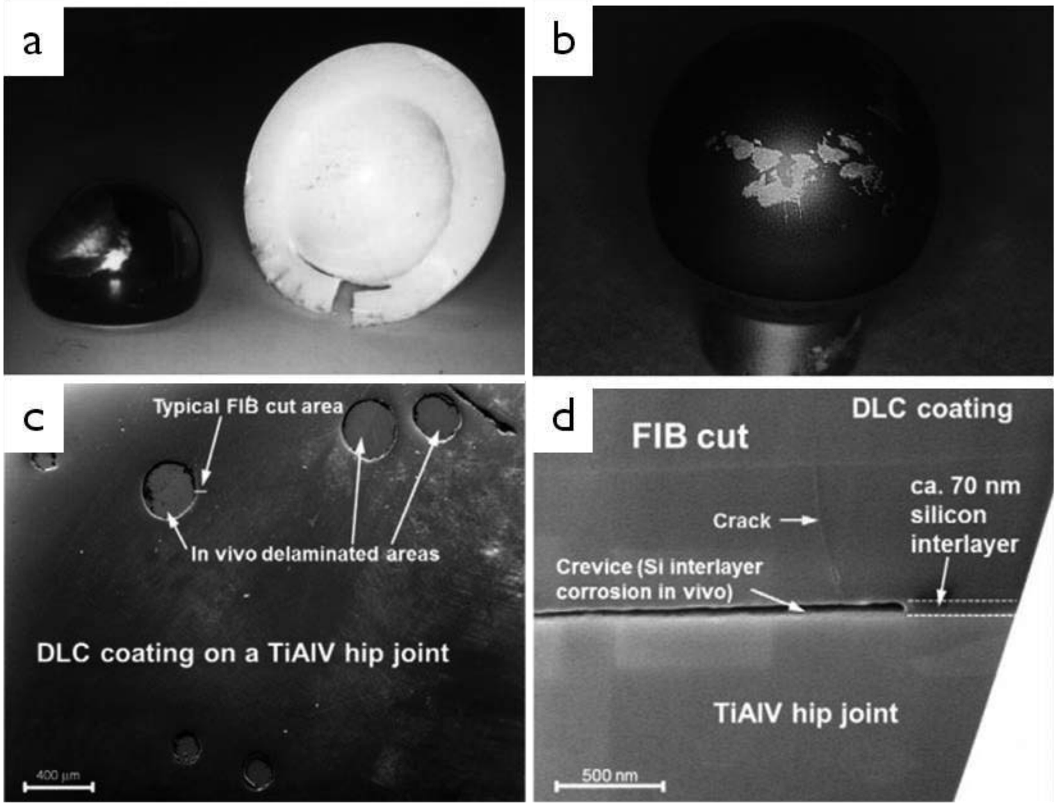

Figure I.2 (a) Retrieved DLC coated hip joint ball and correspondent UHMWPE acetabular component. (b) Numerous pits and confluent and irregular shaped larger defects in load bearing zones in the formerly articulating surface revealing the metallic substrate underneath. (c) Scanning electron microscopy (SEM) micrograph of the delaminated zones on DLC-coating and (d) the correspondent FIB cross-sectional cut near a delaminated area revealing the dissolution of the Si-based adhesion-promoting layer under the DLC due to crevice corrosion. (Adapted from [70, 106]).

Metal-alloying of DLC is another method to improve DLC properties. Even though metal co-sputtered carbon films differ from pure carbon films, it is possible to tune the properties for a desired application but still maintaining the typical amorphous structure. It was found that alloying the DLC coatings not only decreases the residual stress but also influences tribological, mechanical and electrical properties [66, 116, 123, 124], as well as the ion and protein adsorption and the cell reactions [66, 71, 125]. Alloying elements range from metallic (Ti, W, Si, Cr etc.) to non-metallic elements (H, N, P, etc.); an excellent review summarizing the results has been published by Sanchéz-López in Reference [66]. If carbide-forming elements are introduced above a certain concentration, a nanocomposite structure can be achieved: nanocrystalline (nc)-MeC embedded in an amorphous-carbon matrix [126-128]. In fact, Meng [126-127] reported a maximum concentration for Ti dissolution in the matrix as 1-2% and 4-8% in a-C:H and a-C matrix, respectively; for higher concentration nc-TiC nanocomposites are formed. The most common transition metals used as alloying materials are Ti, W, Cr and Nb [66]. Voevodin and co-workers pioneered nanostructured materials [119, 129]. For instance, when alloying with Ti, the TiC/DLC systems exhibit a large amount of grain boundaries between the nc-TiC phase and the amorphous DLC matrix, which effectively enhances the hardness and toughness of the coatings, limiting crack initiation and/or terminating further crack growth and film delamination [115, 119, 120, 130-133]. Moreover, such nanocomposite structure could also lower the friction and wear and significantly improve load carrying capacity [129]. Apparently, encapsulation of finer grains of hard nc-TiC within the amorphous DLC matrix restricts dislocation activity, diverts and arrests macrocracks development, and maintains the high level of hardness [120, 132], see Figure I.3.

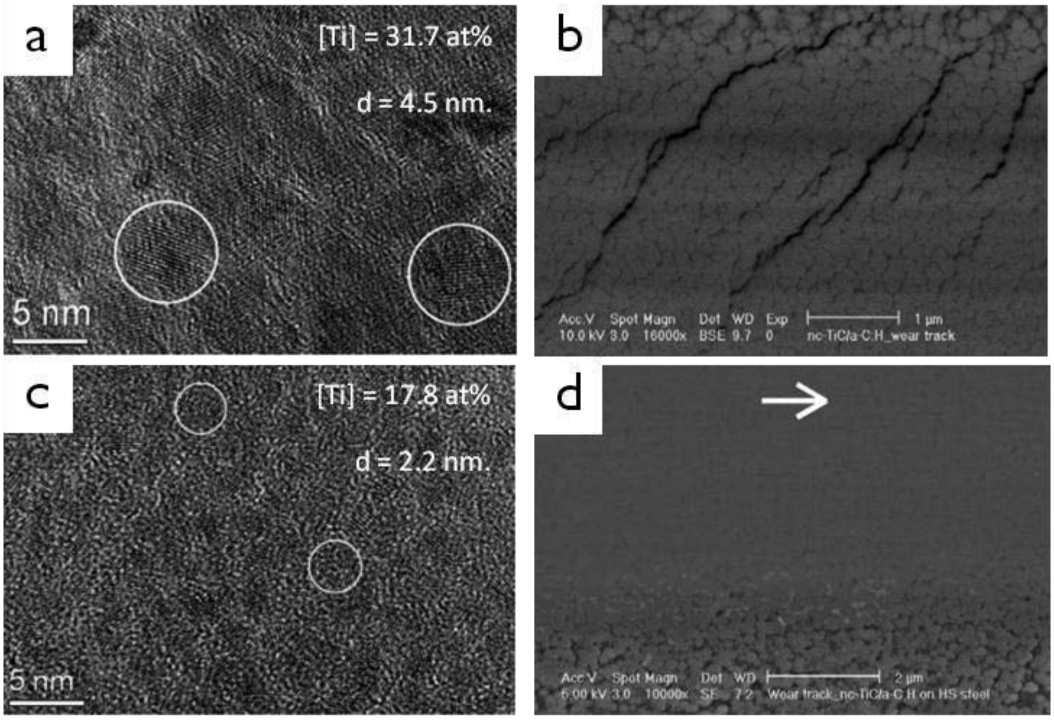

Figure I.3 (a) and (c) shows the HR-TEM micrographs of the evenly distributed and well separated TiC nanograins and (b) and (d) SEM micrographs of the corresponding the wear track under the same wear conditions. (Adapted from [132, 133]).

From the biomedical point of view, the introduction of alloying elements will modify the typical biological properties of DLC coatings. Ti [134], Si and F [135], Ca and P [71], N [136], Ag [137], Zr [138] and, more recently, Ta [139] are the most common doping materials which may enhance blood and cell compatibility due to surface chemistry modifications. Among these Ti has gained much interest owing to its biocompatible and tribological properties. Several authors [140, 141] found that proteins adsorbed on surface as a function of Ti content. Protein adsorption is the first event occurring after implantation which signalizes the overall biological response. Moreover, the ability of naturally forming TiO_2 by interaction with air improves corrosion resistance and may add affinity and biocompatibility, compared to pure a-C(:H) films. It was found that Ti-alloyed a-C(:H) stimulated osteoblast (bone producing cells) differentiation and inhibited osteoclast (bone resorbing cells) cell activity compared to a-C(:H) films [141, 142]. In the light of that Bruinink et al. [143] have studied the possible toxic effect of Ti-containing and pure a-C:H particles in the case of unexpected delamination of the coating *in service*: only pure films did not exhibit inflammatory induced response. Thus, Ti-containing DLC coatings may be suitable to bone related implants by improving fixation and enhanced osteo/osseointegration but not for load-bearing prostheses. It is still not clear how alloyed materials would perform *in vivo* due to a lack of adequate analysis of surface interacting with body fluids. However, it is expected that changes in surface chemistry could be beneficial for a successful *in vivo* performance if appropriate elements are used.

3. The Main Goal of the thesis

The use of alloyed DLC coating has revealed good biomedical potential together with an enhancement of the fundamental properties of the coating. Zirconium as a bulk material has shown low-toxicity, biocompatibility, high corrosion resistance and excellent tribological properties [144, 145]. Zr is a strong carbide forming element such as Ti but it differs slightly in the mechanical properties. The use of transition metals as doping elements is not new and has improved mechanical and tribological properties of the coatings due to the catalysis effect of the metal on DLC formation [66, 119, 146-149]. Moreover, the potential of protective high-strength material for biomechanical purposes is dependent on the average grain size due to the grain boundary effect typical of nanocomposite structures, as explained before. Thus, zirconium can be considered as a promising doping element competitive to Ti. In fact, Kao [150] has reported that an addition of 4-16 at.% Zr can considerable improve the tribological properties including the friction coefficient in dry environment. Kumar et al. [138, 151] and Wang et al. [116] have reported excellent pitting and crevice corrosion resistance of Zr-DLC coatings. Zr naturally forms a zirconium oxide layer considered as bioinert [152], which may enhance corrosion resistance [144]. Moreover, Tsutsumi et al. [153] and Manivasagam et al. [154] have found that such layer is more stable on Zr than on Ti when immersed in Hank's solution, which makes the Zr more passive and protective than Ti but also less bioreactive [155]. Thus, the incorporation of Zr is expected to decrease osseointegration compared to Ti-containing DLC coatings. In summary, the combination of the nc-ZrC and amorphous-C phases with a functionally graded interface might provide excellent toughness, high resistance to adhesive failure and corrosive resistance under severe biotribological situations.

The main goal of this thesis was then to produce nanostructered Zr-containing DLC coatings with different Zr concentration and evaluate their possible use in load-bearing biomedical application such as articular prosthesis in order to minimize the wear and the prosthetic intrinsic problems.

CHAPTER II

The deposition of hydrogenated and non-hydrogenated DLC and Zr-containing DLC coatings onto Ti grade 2 and 5 ELI is described in this chapter together with a brief summary of the characterization techniques. Since the adhesion of the coatings onto the metallic substrates has been used as one of the main optimization parameters, it will be exhaustively analysed as well.

1. Introduction

This chapter is dedicated to the deposition and optimization of the hydrogenated and non-hydrogenated DLC and Zr-containing DLC coatings. The coatings were deposited by using reactive and non-reactive magnetron sputtering, respectively, on biomedical grade Ti substrates: Ti grade 2 (commercial pure (CP-) Ti) and Ti grade 5 ELI (Ti6Al4V). Ti-based materials are interesting candidates for biomedical applications because of the known milder tissue reactions of their degradation products compared with Co-Cr alloy and Ni-containing steels [33, 41]. In fact, a recent study [156] has shown a patient from New England with an apparent heart failure that underwent an orthotopic heart transplantation; after 13 months it was discovered that such problem came from a huge Co- and Cr-ion release from his bilateral DePuy metal on metal hip prosthesis and needed revision surgery. However, Ti-based materials are soft and their tribological properties are poor [9, 157, 158]. Therefore, the use of coating is a promising approach to improve their tribological properties. As described in Chapter I, a potential limitation of coatings is their adhesion to the substrate, which is directly related to the chemical bonds between the layers as well as the elastic properties of both bulk material and coating. The deposition of hard coating on a relatively soft substrate such as Ti is an enormous challenge. The high gradient in superficial hardness can result in coating chipping off due to different elastic behaviour under high punctual loads (thin ice effect) [26, 110, 159, 160]. Therefore, after summarizing the main information concerning the deposition of the films and their characterization, this Chapter is dedicated to the optimization of the coatings deposition; in particular, some aspects not covered in the published papers, which are the basis of the thesis, will be discussed: (i) an exhaustive study on the effect of the interlayers design on the adhesion of the coatings on Ti-based substrates in order to avoid *in service* delamination and fracture of the coating and (ii) the analysis of the influence of the wear of the Zr pellets on the final results of the chemical composition and deposition rate of the coatings.

2. Coatings deposition and characterization

2.1 Deposition Process

DLC coatings can be produced by a variety of deposition processes. In general, the processes are very complex regarding the physical and chemical phenomena underlying the coating growth. In fact, the final coating structure strongly depends on the deposition technique. In this study, magnetron sputtering was the chosen technique to develop pure and Zr-containing amorphous carbon coatings. Figure II.1 shows the deposition chamber and configuration as well as the schematic representation of the final deposition parameters. Two parallel magnetrons were in a close-field unbalanced configuration to enhance the magnetic flux density in the chamber and to provide more efficient electron trap.

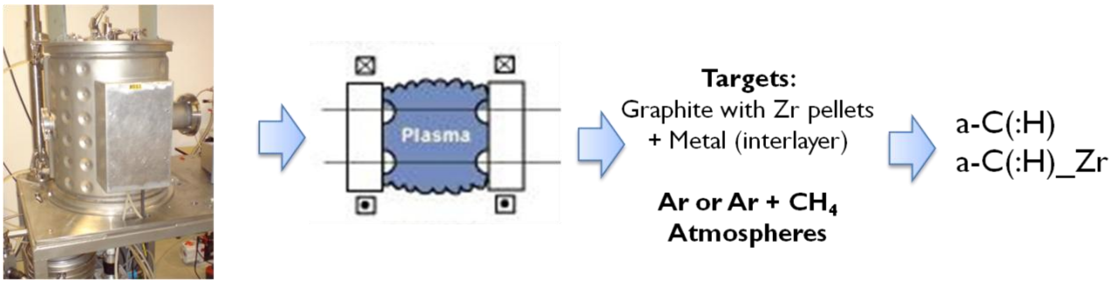

Figure II.1 Picture and schematic representation of the deposition chamber and deposition parameters.

Several parameters were kept constant for all depositions, such as the geometry of the deposition chamber, the magnetic field, a constant position of the inlets of the sputtering gas, the base pressure ($< 10^{-3}$ Pa), the substrate-to-target distance (d_{s-t}=170 mm), the substrate holder rotation (18 rpm) and the substrate thermal condition (no intentional heating was used). In addition, the C-target power density was also kept constant at 7.5 $W.cm^{-2}$. The use of negative substrate bias was also invariable in all deposition. For that, a pulsed-DC power supply was connected to the substrate holder with a pulsed frequency of 250 kHz and a bias voltage of -50 V. Two main combinations of conventional process parameters were used for the development of both hydrogenated and non-hydrogenated coatings: reactive (Ar/CH_4) and non-reactive atmospheres (Ar), respectively. The Ar flow was maintained at 45 sccm in order to reach the working pressure of ~0.4 Pa. For the deposition of hydrogenated coatings methane gas was introduced in the chamber to initiate the reactive process. The Ar gas flow was fixed at 40 sccm and the CH_4 gas flow at 5 sccm, in order to keep the working pressure constant.

2.2 Coating characterization methods

To understand the influence of the deposition parameters on the functional properties of the coatings, several characterization methods were used. The properties of the coatings were analysed in a first attempt with basic characterization: chemical composition, thickness and adhesion to the substrate. Si wafers and glass were generally used for microstructure and surface characterization and polished metallic substrates for mechanical and tribological properties assessment. Once proper deposition parameters had been determined, coatings were simultaneously deposited on appropriate substrates (i.e. CP-Ti and Ti6Al4V).

2.2.1 Chemical composition:

The chemical composition of the coatings was evaluated by electron probe microanalyses (EPMA), CAMECA Camebax SX 50 model. The applied voltage was 10 keV corresponding to a maximum penetration below 2 μm for C-based coatings. The values of the chemical composition were the average of 3-5 different measurements in different points of the sample. Unfortunately, this technique cannot evaluate hydrogen content. Therefore, in order to also evaluate the hydrogen content, the films were analysed by a full total ion beam analysis (IBA) – Rutherford backscattering (RBS), non-Rutherford elastic backscattering (EBS), elastic recoil detection (ERD) and particle-induced X-Ray emission (PIXE) self-consistently – used by the DataFurnace code (NDFv9.4f [161]). The experiments were conducted at Surrey Ion Beam Center, University of Surrey as part of a European grant under the SPIRIT[1] - project program. Detail experimental parameters can be found in Paper IV.

Chemical composition information of particular zones of the coated samples was also achieved during scanning electron microscopy (SEM) and transmission electron microscopy (TEM) through energy dispersive X-ray spectrometry (EDS) connected to both microscopes. During X-ray photoelectron spectroscopy (XPS) the chemical composition could also be evaluated through the analysis of the relative peak intensities, corrected by experimental determined sensitive factors.

2.2.2 Thickness, morphology and surface topography

The thickness of the films was evaluated by 2D optical profilometer (Perthometer S4P) using a substrate/coating step. A boron nitride drop was placed on a

---

[1] **SPIRIT** – represents an Integrated Infrastructure Initiative (I3) funded by the European Commission. The main goal of SPIRIT is to grant public and industrial researchers from Europe free access to leading European ion beam facilities and R&D providers, which deliver ions in an energy range from ~10 keV up to 100 MeV for the modification and analysis of solid surfaces, interfaces, thin films and nanostructured systems. The main application areas are materials, biomedical and environmental research and technology [162].

Si substrate and removed with acetone after the deposition, leaving a step on the coated surface. This method was applied to measure the thickness of the coatings in order to optimize the deposition time. The thickness of the coating was also compared and checked by direct measurements in cross-section observation in SEM (FEI Quanta 400FEG E SEM, at CEMUP). The deposition rates were calculated from the film thickness and the sputtering time.

SEM was also used to get a general idea of the morphology of the coatings. Additional to plan-view, fractured cross-section of the coated samples were regularly studied as they often allow a straightforward observation of the coating morphology, cohesion and adhesion to the substrate. A quantitative complementary method to examine the surface morphology was the analysis of the surface roughness. The average surface roughness (R_a) and the roughness mean square (Rms) were evaluated by atomic force microscopy (AFM – Buker Innova) - 5x5 μm^2 line scan – and scanning white light interferometer 3D optical profilometer (Zygo New Vision). The AFM images depicted in Chapter III were performed in 3x3 μm^2 line scan.

2.2.3 Structure and microstructure

The phase identification was performed by using X-ray diffraction (XRD). A single circle diffractometer (Philips X'Pert) has been used with CoK_α radiation (λ = 1.789 Å) generator operated at 40keV. For more precise measurements, some samples were analysed in a six-circle goniometer (at the Materials Research station of the Rossendorf beam line (ROBL-MRH) located at the bending magnet 20 (BM20) at the European Synchrotron Radiation Facility (ESRF) in Grenoble) with an incident X-ray beam monochromatized to an energy of 11.5 keV (λ = 1.078 Å). To increase the signal from the coating and to identify any crystalline phase, a grazing angle incidence XRD was performed, hereby the sample surface was tilted 2° in relation to the beam. The phase identification was done by comparing the position of the peaks with those of standard phases existing in the International Center for Diffraction Data (ICDD) database [163]. Even though the observed peaks were quite broad, due to small grain sizes typical of nanostructured materials, the XRD patterns were fitted using a Voigt function permitting the determination of several characteristics such as peak position (2θ), peak intensity and full width at half maximum (FWHM) that can be used for estimate an average size of the diffracting crystal through the Scherrer formula [164].

The structural analysis was complemented by TEM using a FEI Tecnai G2 T20 microscope with a LaB_6 filament operated at 200 kV and a FEI Titan 80-300 microscope equipped with field emission gun (FEG) and Gatan image filter (GIF) Tridium and operated at 300kV. Both bright field (BF) imaging and selected area electron diffraction (SAED) were carried out. SAED was performed with an aperture size of ~100 nm in diameter. Electron energy loss spectroscopy (EELS) was also used to reveal the bonding state of the elements present in the film. TEM specimens were prepared using an FEI Versa3D focus ion beam – scanning electron microscope (FIB-SEM). The experiments were carried out at Chalmers TH after a successful application to a European grant under the ESTEEM 2[2] project program.

Raman spectroscopy (Xplora, Horiba, DPSS laser, λ = 532 nm) was used to characterize the amorphous carbon phases present on DLC and Zr-containing DLC coatings. The peaks were fitted using two Gaussian peaks following the procedure described elsewhere [166].

2.2.4 Surface physicochemical characterization

Chemical bonding was investigated using X-ray photoelectron spectroscopy (XPS). The electron binding energy is specific for each element and orbital, thus enabling the elemental identification. The XPS analysis was performed using a Kratos AXIS Ultra with VISION software for data acquisition and CASAXPS software for data analysis. The analysis was carried out with a monochromatic Al Kα X-ray source (1486.7 eV), operating at 15kV (90 W), in FAT mode (Fixed Analyser Transmission), with a pass energy of 40 eV for regions ROI and 80 eV for survey. Data acquisition was performed with a pressure lower than 10^{-6} Pa, and a charge neutralisation system was used. The binding energy scale was charge referenced to the C 1s at 285 eV. The spectra were acquired on as deposited surface and after sputter-cleaning with Ar^+ ion gun in order to remove any residual contamination. The deconvolution of the spectra was performed using the CasaXPS program, in which an adjustment of the peaks was performed by using peak fitting with Gaussian/Lorentzian peak shape and Shirley type background subtraction. The relevant peak positions, as found in literature, are given in Paper VII.

The contact angle measurements were performed through the “static“-sessile drop method. Drops were generated with a Krüs GmbH G-23 goniometer at ~20 °C

---

[2] **ESTEEM 2** – represents a *European Netwotrk for Electon Microscopy* integrated infrastructure providing access for the academic and industrial research community in the physical sciences to some of the most powerful characterization techniques available at the nanoscale. Transnational access to ESTEEM2 centres is obtained through a transparent, simple peer review process based on merit and scientific priorities. Service to users is supported by a networking programme which addresses key issues such as specimen preparation, data interpretation through theory and simulation, and standardization of protocols and methodologies [165].

and room humidity (50%). The surface energy was calculated using the Owens equation [167] based on the contact angle measurements of the different liquids: water, glycerin ($C_3H_8O_2$), formamide (CH_3NO) and diiodomethane (CH_3I_2) [167, 168]. The interaction with bovine serum albumin (BSA) was studied by immersion of the samples in a 2 ml BSA containing solution (4 mg.ml^{-1}) diluted with a basic solution (NaCl: 9 (g/l); EDTA: 0.2 (g/l); Tris: 27 (g/l); sodium azide: 0.3%, pH 7.6) for 24 h at 4 °C. The amount of total immobilized protein was calculated using the Bradford reagent against a standard BSA calibration curve. After immersion, all samples were washed with water Mili-Q for eventual detachment of non-chemisorbed proteins. The detached proteins were also taken into account for the protein quantification using the same method described above. The samples were then air-dried for 24h before the XPS spectra were recorded. More info can be found in Paper IV.

2.2.5 Mechanical Properties

The residual stress (σ_{RS}) was calculated by the curvature or deflection method using the corrected Stoney equation [169]. The coatings were deposited on thin stainless steel (SS) 304 discs (Ø 25 x 0.5 mm) and the curvature radius was evaluated by 2D profilometer before and after deposition.

The hardness (*H*) and Young modulus (E) of the coatings were evaluated by depth-sensing indentation (Micromaterials Nanotest) using a Berkovich indenter. The normal stylus load was 5 mN (indentation depth approx. 150 nm); To have reliable *H* values, 32 indentations from 2 distinct areas on the sample were performed. Furthermore, the reduced Young modulus was derived from the indentation measurements by standard Oliver and Pharr method [170]. The Young modulus was then calculated by using the following parameters: E_i = 1140 GPa and ν_i = 0.07 for the diamond indenter [170] and ν = 0.3 for the coating [66] (ν is the Poisson ratio).

The adhesion of the coatings was evaluated by scratch test and the Rockwell-C (R-C) adhesion test, regulated by European standards (EN) 1071-3 [171] and 1071-8 [172], respectively. Both techniques use a Rockwell-C indenter: spherical diamond 120° tip with a diameter of 200 µm (CSM Instruments). The main difference between these techniques is that in the scratch test the spherical end of the indenter slides against the surface, while in the R-C the indenter penetrates into the material. For scratch test, an increasing applied load with a loading speed of 10 N.mm^{-1} and a range of 2-50N was used. During R-C testing, the normal load was dependent on the hardness of the substrate: for soft metallic substrates (< 54 HRC) a load of 981 N and for harder metallic substrates (> 54 HRC) a load of 1471 N [172] was applied. These tests are strongly influenced by the elastic properties of both film and substrate, the thickness of the film, etc [66, 173]. Thus, M2 Steel was used as a reference material to study the adhesion of the coatings; then Ti-based substrates (CP-Ti and Ti6Al4V) were used to predict the adhesion *in service* of the coatings. The results of the tests were qualitatively evaluated by comparing the optical microscope images (100X magnifications). To determine the adhesion strength of coatings by scratch test, three critical loads were considered: Lc_1, the lower critical load corresponding to the first cracks that occured (cohesive failure); Lc_2, the upper critical load defined as the load where the first spallation/flaking of the film is observed; and Lc_3, the load where penetration of the coating is detected in the centre of the scratch [171]. On the other hand, the crack network and degree of delamination of the indentation, resulting from R-C test were analysed based on adhesion quality charts and classified into six categories from HF1 to HF6, where HF1-HF4 is considered as acceptable failure while HF5-HF6 corresponds to unacceptable failure [9]. For more details see Paper I.

2.2.6 Tribological Properties

Wear testing was performed using a pin-on-disc CSM tribometer. Three different environments were tested: ambient air (relative humidity (RH) 30%); physiological solution (PS; 0.9 % NaCl water solution) and diluted foetal bovine serum (BSA, prepared according to ASTM F732 [174]). The tests were carried out against a Ti6Al4V ball with a diameter of 8 mm. The temperature was maintained constant at 37±2 °C for the lubricated tests. All measurements were provided with a normal load of 1N and linear speed of 0.2 $m.s^{-1}$. The maximum Hertzian pressures for ball-on-plate contact were almost identical close to 360 MPa (Ti6Al4V and Cp-Ti). The standard number of cycles was 10 000. Uncoated Ti-based substrates were also tested under the same conditions for comparison. Detail information can be found in Papers II and IV. A test closer to the *in service* application was also performed by using a multidirectional pin-on-disc (OrthoPod®, AMTI Inc.). These tests were carried out against UHMWPE and PEEK pins under a protein containing solution (BSA, protein concentration of 30g/mL). The temperature of the lubrication media was maintained at 37°C. The pins were subject to a 15 mm X 15 mm square motion pattern with a cycle frequency of 1 Hz and a constant applied load that generated a nominal contact pressure of 1.5 MPa. Paper VI presents a more detailed description of this particular experimental process.

The tribological behaviour was examined with respect to the friction coefficient and the wear rate. The surface and wear track topography was evaluated by using 3D profile measurements whereas the ball wear rate was calculated from optical inspection of the spherical wear cap (optical microscopy). On the other hand, gravimetric weight loss for the polymeric pins was used to calculate the volumetric wear loss (according to ASTM F2025 [175] and F732 [174]). The differences in the wear rate between UHMWPE and PEEK articulating against coating and uncoated materials were evaluated statistically by using students' tests. One-way analysis of variance (ANOVA) followed by the Student-Newman-Keuls (SNK) method was used to determine pairwise differences between each polymer group. The level of significance was set to p = 0.05.

3. Coating optimization

3.1 Adhesion and interlayer optimization

The biotribological performance of DLC coatings is strongly related to the adhesion of the coating to the metallic substrate. As referred to in Chapter I, it is indeed the main drawback for its use as load-bearing implants. Thus, one of the main requisites is that the coatings should adhere to the substrate not only after deposition but also *in service*.

To enhance adhesion, the substrate should be carefully cleaned with degreasing agents to remove surface contaminants and subsequently dried before being placed into the deposition chamber [176]. As a result, prior to be placed into the deposition chamber all substrates were ultrasonically cleaned with alcohol, acetone and distilled water for 15 min each. After the vacuum chamber was at the desired base pressure, substrate plasma cleaning was performed to remove surface oxides in Ar^+ atmosphere at a pressure of ~0.3 Pa for 1h with a bias voltage of -650 V allowing a self-current of ~1.0 A. A power of 600 W and 1000 W was also applied on the C and metal targets, respectively, during substrate cleaning to enhance the ionization of the glow discharge and to clean up the oxide contamination layer on top of the targets (note that the targets were covered by a shutter in order to avoid cross contamination of the targets and substrates). Even though the pre-cleaning and ion-cleaning steps are crucial for a good adhesion [176] the adhesion strength was insufficient when depositing pure DLC coatings directly on steel (see Figure II.2). It was then necessary to optimize the adhesion of the coatings onto metallic substrates by other methods.

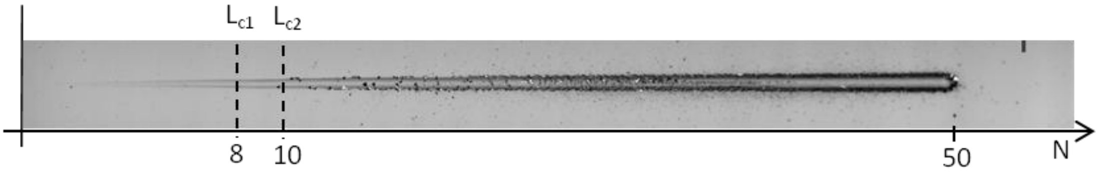

Figure II.2 Scratch test at increasing load on a-C coating deposited without interlayer.

3.1.1 Adhesion interlayer optimization

The deposition of a metallic and/or gradient transition layer between the functional coating and the substrate to improve the adhesion onto metallic substrates is not new and it has been considered as one of the most successful methods for improving adhesion, as mentioned in Chapter I. Thus, in this study the optimization of the adhesive layer was focused on the interface material between substrate and functional coating.

Many attempts to choose the best adhesive layer were carried out based on compositional gradient layer along the coating thickness using Zr, Cr and Ti as metallic elements. After etching, the bias voltage was switched to -50 V and a Me/MeN/MeCN(Zr) or Me/MeC (where Me stands for the metal element: Zr, Cr or Ti) composite gradient layer was deposited for 20 min, applying a constant power of 2000 W to the Me target. Me target was firstly sputtered in a pure Ar atmosphere (Ar flow 35 sccm); then, when necessary, nitrogen was introduced (17 sccm). The deposition of the functional coating (hydrogenated and non-hydrogenated) was then initiated by ramping up the power on the graphite target (without embedded Zr pellets) and ramping down the Me target power to zero and the nitrogen flux. Figure II.3 shows the different designed interlayers tested in this study.

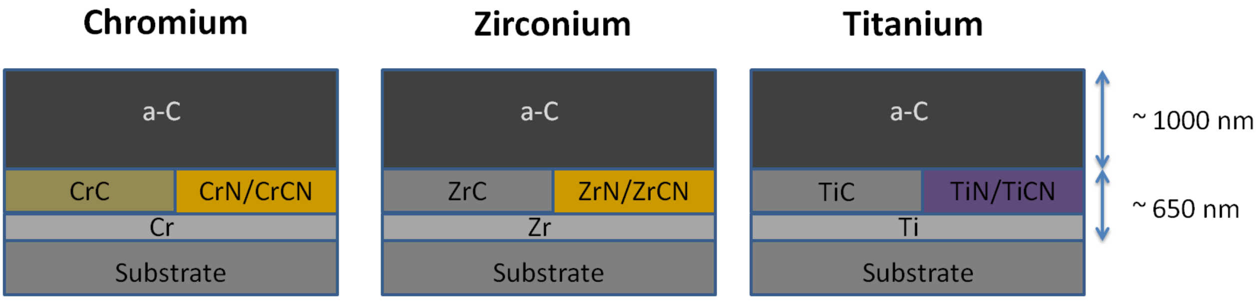

Figure II.3 Schematic representation of the different design of tested adhesion layers.

The adhesion strength was then measured by scratch test and it is shown in Figure II.4. Typically, the adhesion improving layer is usually based on the same alloying element [148, 177]. Unfortunately, when using Zr as metal element, the coating catastrophically delaminated due to the presence of ZrC brittle phase, especially when a ZrN layer was used. Cr/CrC, Cr/CrN/CrCN and Ti/TiN/TiNC were then found to be the best options for the development of a functional adhesive gradient layer. In fact, Cr has been the most widely used element for improving the adhesion of DLCs [66]. Although it has been reported that the use of Cr as interlayer might release less Cr-ion compared to a Co-Cr alloy typically used as an implant material [116, 178], it was decided to avoid chromium if possible. Ti/TiN/TiNC was then used as an interlayer material.

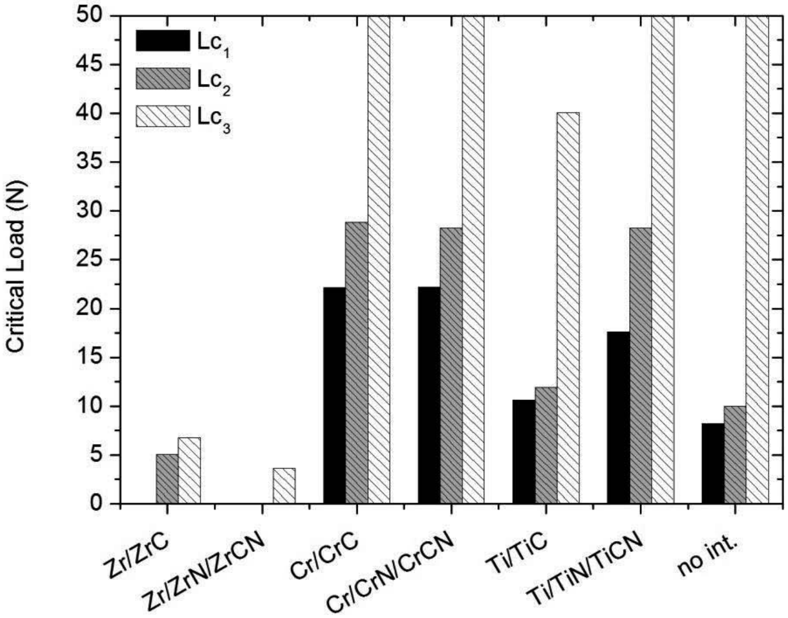

Figure II.4 Critical loads of a-C coated with the different designed interlayers on steel substrates.

It is also important to notice that using Ti as a metal element should also minimize the differences in the thermal expansion coefficients between the substrate and the coating when deposited on Ti-based substrates. The perfect match between Young modulus of the Ti-based substrate and the interlayer, as well as the subsequently gradation of the composition towards the coating side, may improve the compatibility between the film and substrate materials and, consequently, the adhesion [117]. Figure II.5 shows the cross-sectional TEM BF images showing the columnar morphology of TiN and the presence of an amorphous second gradient layer (TiCN(Zr)) between Ti/TiN and the DLC functional coating. By starting the coating growth from an amorphous phase, fewer discontinuities between the interlayer and the top coating would be expected, thusly improving the overall adhesion of the coating.

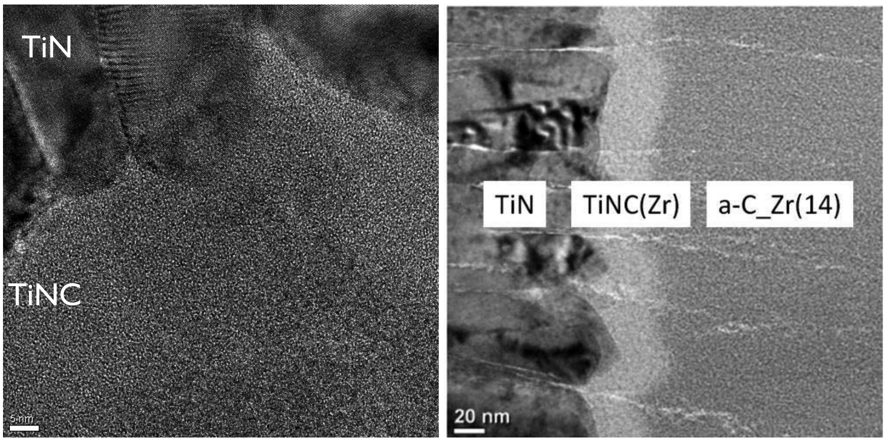

Figure II.5 Cross sectional TEM BF-images of a-C_Zr(14).

3.1.2 Adhesion onto Ti-based substrates

The adhesion of DLC films varies with the substrate and it is related to the chemical interaction between the film and substrate surfaces, the microstructural defects in the film-substrate interface and the compressive stress levels in the film [121]. The deposition of DLC coatings on soft biomedical substrates such as Ti-based materials is a continuous challenge due to substrate plastic deformation, which could cause fracture and delamination of the coating [110, 159, 160]. The coatings were deposited on CP-Ti and Ti6Al4V. It is worth noting that CP-Ti is softer than Ti6Al4V: 1.5 GPa and 3.1 GPa, both respectively [179] much softer than the M2 steel (8.2 GPa) originally used for the interlayer deposition optimization. Typical scratches produced by the adhesion test are shown in Figure II.6. As expected, the adhesion results were very sensitive to the mechanical properties of the substrate. Piling-up along the edges of the scratch track, which was clearly observed in both substrate materials, indicated plastic deformation (Figure II.6a and c). The plastic deformation was much more evident in the case of CP-Ti substrates, i.e. it was visible for lower loads. Figures II.6b and d show the scratches of a-C coatings deposited on CP-Ti and Ti6Al4V, respectively. The scratch tracks were much wider for the softer CP-Ti substrates when an identical load was applied leading to the destruction of a-C films; a harder substrate (Ti6Al4V/a-C) yielded improved coating adhesion and wear resistance.

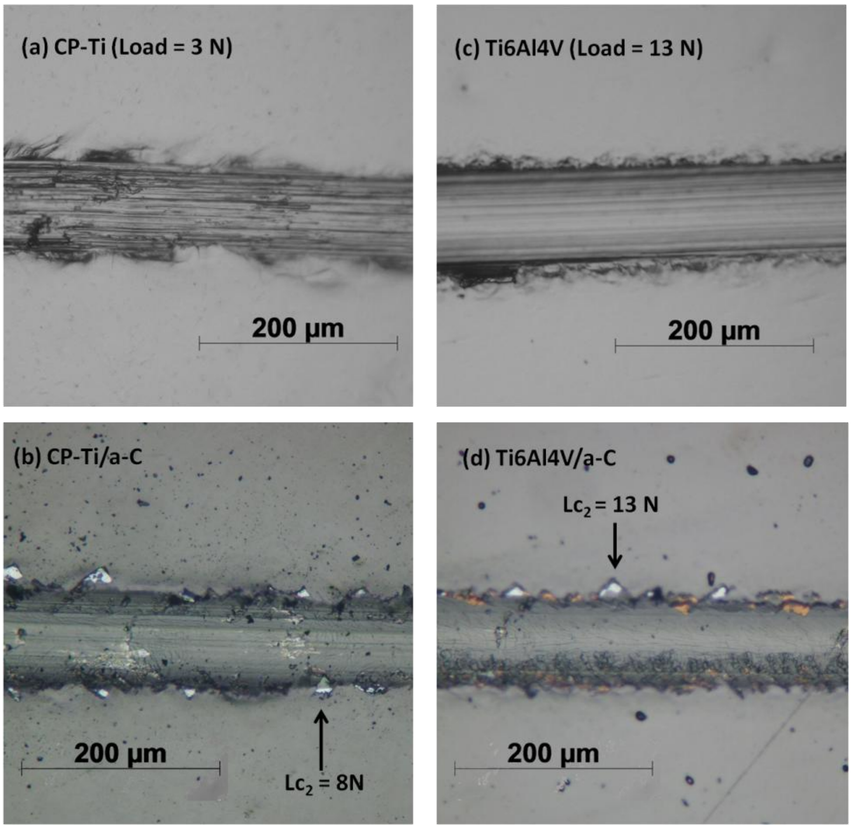

Figure II.6 Optical images of typical scratch tracks performed on (a) uncoated CP-Ti and (c) Ti6Al4V and a-C deposited on (b) CP-Ti and (d)Ti6Al4V. Scratch direction is from right to left. The arrows show the adhesive critical load Lc_2.

3.2 Chemical composition

For the deposition of Zr-containing films, Zr could be introduced either by the use of a Zr target or a Zr-C composite target (graphite target with Zr pellets). The former cannot be used due mainly to the impossibility of using very low target power to achieved nanocomposite films (very low Zr content) since the sputtering yield of Zr is almost 4 times higher than C [180]. Moreover, since only two target materials can be used (graphite and metal) with such magnetron sputtering configuration and Zr did not revealed sufficient adhesion when used as interlayer material, a Ti target should also be add to the deposition chamber. Thus, Zr Ø 5 mm pellets were embedded into the erosion area of the graphite target in order to deposit nanocomposite Zr alloyed DLC coatings. The targets (Ti and graphite) and the pellets were supplied by Testbourne Ltd with purity level of 99.99%. Figure II.7 shows the schematic representation of target and pellets.

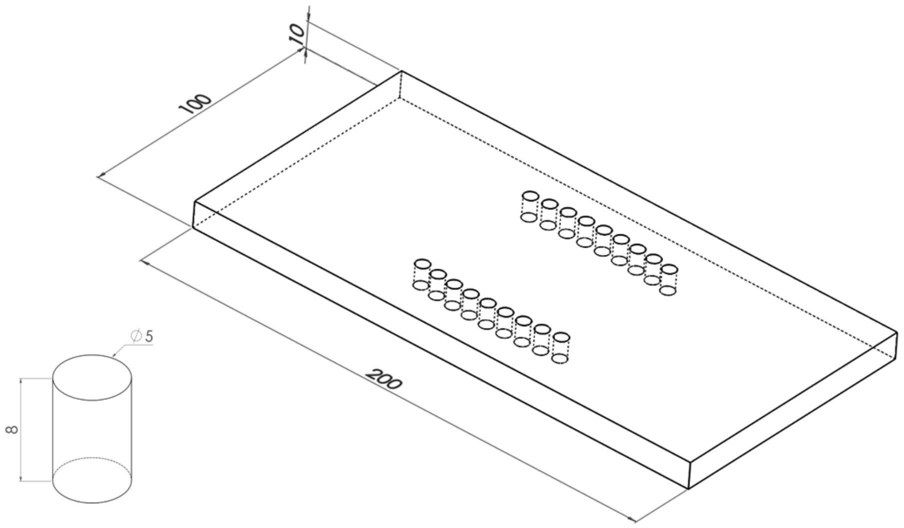

Figure II.7 Schematic representation of the mixed graphite target and the Zr pellets used to deposit Zr-containing DLC. The Zr pellets can be easily removed from the erosion zone and changed by C pellets to adjust the Zr content in the films. The target was glue to the Cu plate with a thermoplastic conductive silver ink (Sun Chemical®) to improve conductivity and then clamped by the target holder. All units in the Figure are in mm.

To synthesize coatings with the desired chemical compositions an interactive process of calibration and tuning of deposition parameters was used. The alloying of DLC coating with Zr was possible by incorporating different number of Zr pellets into the erosion zone of the C-target. However, co-sputtering with a mixed target is far from a simple process; it depends on the target / pellets aging, i.e., the erosion degree of both target and pellets. Thus, to achieve the desired compositions, the number of Zr pellets needed to be continuously adapted. Figure II.8 gathers all the results of chemical composition obtained by EPMAand shows how a different relative erosion area (A_{Zr}/A_C) was needed to achieve the desired Zr content. As expected, the higher the number of Zr pellets (higher A_{Zr}/A_C), the higher the Zr content.

For non-hydrogenated coatings, the Zr content was varied and set constant at values of approximately 0, 4, 7, 9 and 14 at.% (coatings are hereinafter denominated as a-C_Zr(X), with X = 0, 4, 7, 9, 14). When introducing methane to the Ar atmosphere, the deposition process tends to be different due to both the incorporation of another carbon source and the poisoning effect on the Zr pellets. Under reactive atmosphere, the formation of compounds on top of the metallic target can occur and change the sputtering rates of the metallic element [176]. However, in this case, for the same number of Zr pellets, the Zr content was only slightly lower when compared to non-hydrogenated films. Thus, Zr contents of approximately 0, 3, 5, 8 and 10 at.% were obtained (coatings are hereinafter denominated as a-C:H_Zr(X), with X = 0, 3, 5, 8, 10). It is thus expected that Zr pellets poisoning was almost negligible [181].

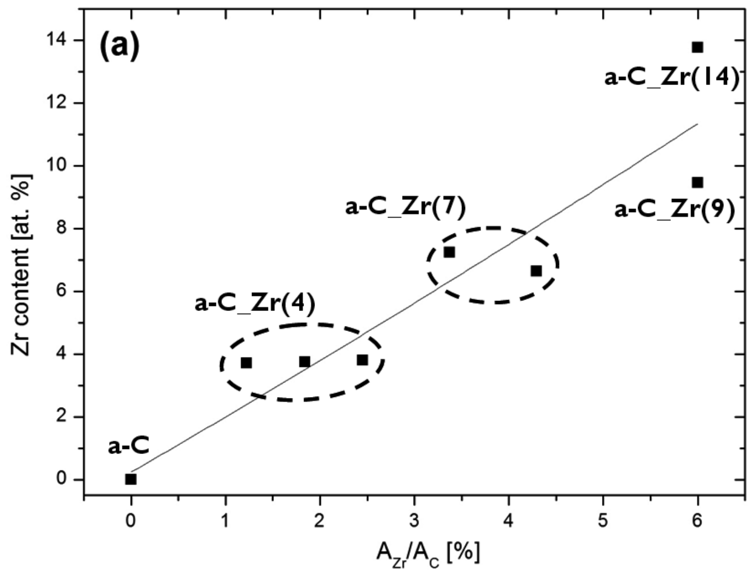

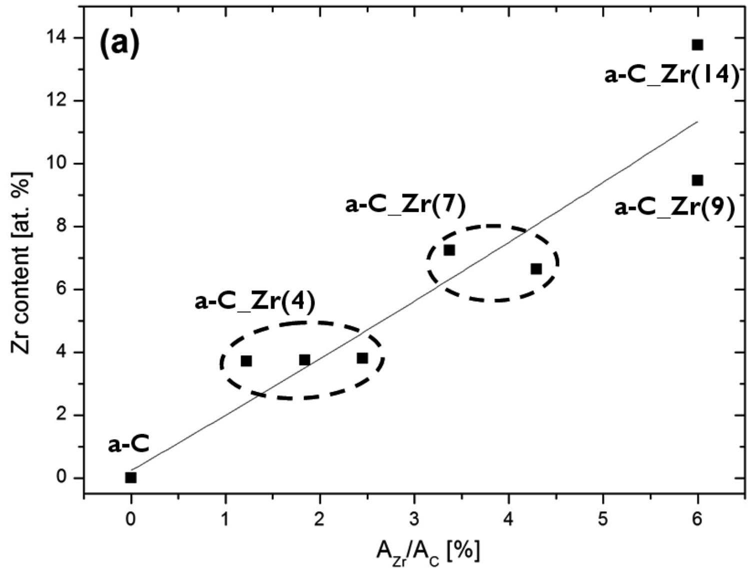

Figure II.8 Zr content as a function of relative erosion area (A_C/A_{Zr}): (a) non-hydrogenated and (b) hydrogenated coatings. The insets are the correspondent names that will be used during this work.

3.3 Deposition rate

The greatest disadvantage of using magnetron sputtering to deposit DLC films is that carbon presents a very low sputtering yield compared to many other elements. Therefore, the deposition rate is relatively slow. The incorporation of a carbonaceous gas precursor (such as CH_4) and/or the incorporation of the Zr pellets can provide coatings at higher deposition rates, since another carbon source is added and Zr has higher sputtering yield compared to C [180]. When depositing films for tribological applications, the thickness of the coating is one of the most important parameters to take into account [82] and it obviously depends on the deposition rate. Thus, the sputtering time needed to be adjusted in order to deposit the films with similar thickness 1.5 – 1.7 μm.

Figure II.9 shows the deposition rate as a function of Zr content for both hydrogenated and non-hydrogenated coatings. As expected, the deposition rate was strongly related to the deposition conditions. In general, for both non-hydrogenated and hydrogenated coatings the deposition rate increases with the increase of Zr content, as a consequence of the higher sputtering rate of Zr in relation to C. In addition, when a carbonaceous gas was introduced, the deposition rate was almost the double when compared to H-free coatings. The reactive gas worked as a rich carbon source increasing the available carbon into the chamber [177]. Finally, the importance of the erosion status of the Zr pellets on the deposition rate should be remarked. As shown in the Figure II.8, to get approximately the same Zr content (e.g. 4 at.%), different A_{Zr}/A_C ratios have to be used, which also influenced the deposition rate. Therefore, this knowledge was extremely important for the optimization of the coating deposition to achieve the desired Zr content and thickness for a specific film.

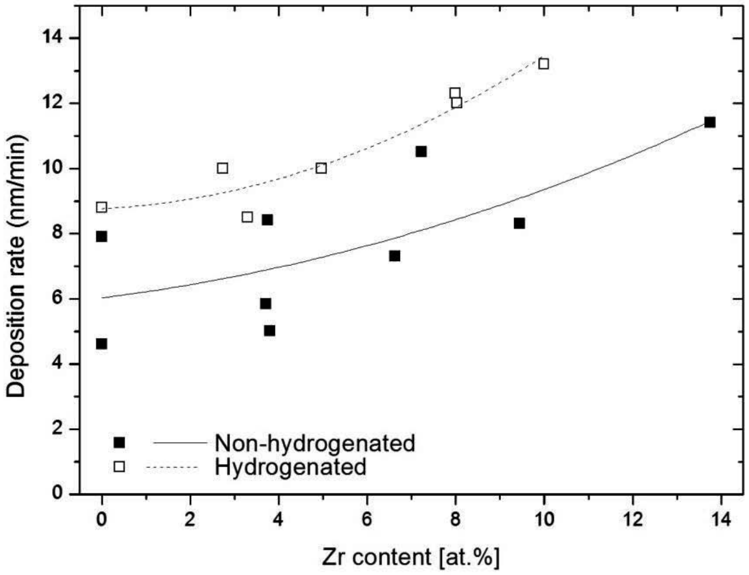

Figure II.9 Deposition rate as a function of the Zr content.

4. Conclusions

DLC and Zr-containing DLC coatings were successfully deposited onto steel and soft biomedical Ti-based substrates by magnetron sputtering in reactive and non-reactive atmosphere. Embedded pellets were used as Zr source; however, the erosion level of the target was found to be an issue. Therefore, it was important to study first the Zr content evolution as a function of A_C/A_{Zr}. When using reactive magnetron sputtering, the Zr content was slightly lower than that of non-hydrogenated coatings, since CH_4 worked as a second carbon source; the poisoning effect of Zr pellets had a negligible effect on the deposition rate. The deposition rate was also influenced by the deposition conditions, in particular the erosion level of the target, the number of Zr pellets and the deposition in reactive mode. Thus, in order to maintain the thickness constant the sputtering time needed to be adjusted in accordance with the actual deposition rate.

The adhesion of the coatings was used as an optimization parameter since a-C coatings presented insufficient adhesion without an interlayer. Various attempts were performed based on a functional gradient layer. Ti/TiN/TiNC was chosen as the most suitable option with respect to the adhesion strength and the substrate material (Ti-based). Even though Cr/CrC presented good adhesion results, the use of such layer is not recommended for the final application due to possible toxicity. The adhesion of the coatings on Ti-based materials was found to be substrate related. Ti6Al4V offered better load-support compared to CP-Ti.

CHAPTER III

This chapter deals with the basic physical and chemical characterization of Zr-containing a-C and a-C(:H) coatings, in particular their chemical composition, morphology and structure. The influence of both Zr and H on the mechanical and tribological properties is also discussed.

The main results of this chapter were presented in **Papers I**, **II**, **III**, **IV**, **V** and **VII.**

1. Introduction

The central question of this Chapter is whether composition, microstructure morphology and properties of the material are correlated. The deposition of pure and Zr- and H-containing films has been evaluated in an exploratory manner in Chapter II. During this Chapter the task of correlating nanostructure and fundamental properties, and subsequently the tribological behaviour, is developed. The results were fully expanded and supported by the author's papers I-V and VII. Thus, the microstructure and phase composition have been studied in Paper VII. The adhesion of the coatings on Ti-based substrates was extensively analysed in Paper I and III. In Paper II and V, the correlation between mechanical and basic tribological properties (ambient air) with structure was evaluated and, finally, Paper IV reports to the H content of the films and their density, together with the study of the tribological behaviour of the coatings under a corrosive medium (physiological solution).

2. Characterization of DLC nanocomposite films

2.1 Coating characterization

Two series of coatings were investigated: hydrogenated and non-hydrogenated, with different Zr contents. Table III.1 shows the chemical composition obtained by IBA.

Table III.1 Chemical composition and density measured by IBA of the coatings.

Samples	**Chemical Composition**				**Density** [g/cm^3]
	C [at.%]	Ar [at.%]	**Zr [at.%]**	H [at.%]	
a-C_Zr(9)	90.3	0.6	**9.0**	0.2	3.1
a-C_Zr(7)	88.1	3.0	**7.4**	1.5	3.9
a-C_Zr(4)	91.4	3.8	**3.8**	0.9	3.3
a-C	94.0	4.4	**-**	1.6	2.6
a-C:H_Zr(8)	67.6	1.9	**5.7**	24.8	2.8
a-C:H_Zr(5)	71.3	1.0	**4.8**	22.9	2.3
a-C:H_Zr(3)	64.1	1.1	**3.3**	31.5	3.1
a-C:H	61.3	0.6	**-**	38.1	1.9

It is important to notice that, as a result of the incorporation of H, for hydrogenated coatings the Zr content was slightly lower than that measured by EPMA (Chapter II, Figure II.8b). The use of a reactive atmosphere (Ar+CH_4) led to H incorporation diminishing from 38 down to 23 at.% with increasing Zr content. The density was strongly related to H and Zr contents, although with antagonist effects. In general, the incorporation of H into the C-matrix decreased the density of the coatings compared to non-hydrogenated films. In contrast, Zr co-sputtered films were denser than pure films (Paper IV). Figure III.1 shows the fractured cross-sectional SEM micrographs of selected hydrogenated and non-hydrogenated coatings. Pure a–C films presented a typical columnar growth. Although the incorporation of Zr did not reveal any significant morphological change, Zr, as a transition metal, can substitute the carbon atoms in the rigid C–C and C-H network distorting the electron density distribution [182] and, thus, decreasing the coordination defects and increasing the density of the coatings. On the other hand, the coating growth in a reactive atmosphere is influenced by the high mobility of carbonaceous species that may destroy the columnar boundaries leading to a glassy and compact morphology [120, 131].

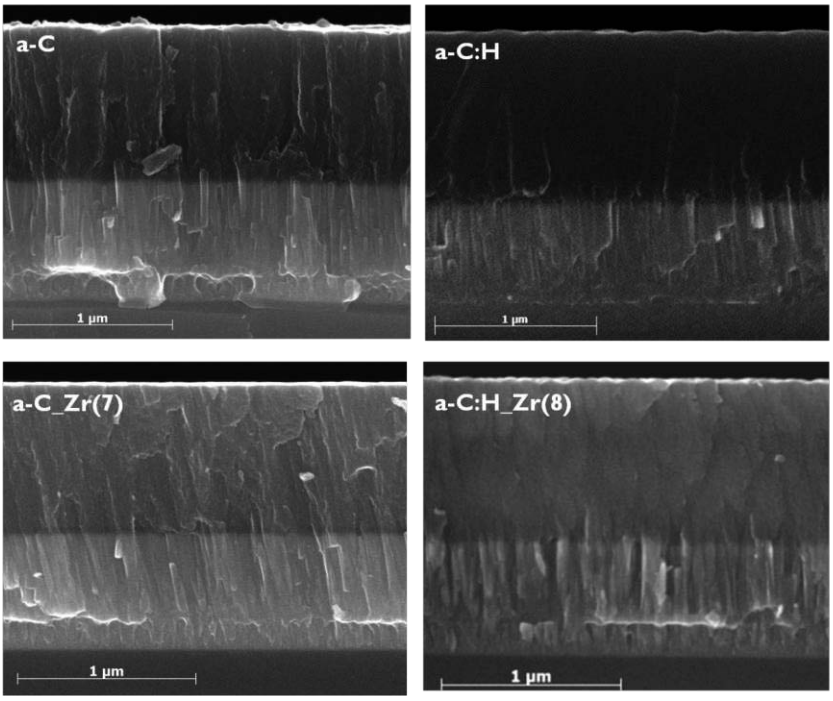

Figure III.1 SEM micrographs of fractured cross-section of non-hydrogenated (a-C and a-C_Zr(7)) and hydrogenated coatings (a-C:H and a-C:H_Zr(8)).

AFM contact-mode scans of the surface of the coatings are displayed in Figure III.2, together with the correspondent roughness values. Zr-containing films show very smooth surface regardless of hydrogen content, whereas pure hydrogenated and non-hydrogenated coatings showed dissimilar surface topographies. The a-C columnar growth is associated with the cauliflower-like patterned surface, with the consequent increase in the roughness, different from the glassy/compact morphology of a-C:H films that leads to a smooth and featureless surface. A complete morphological and topographical analysis can be found in Paper VII.

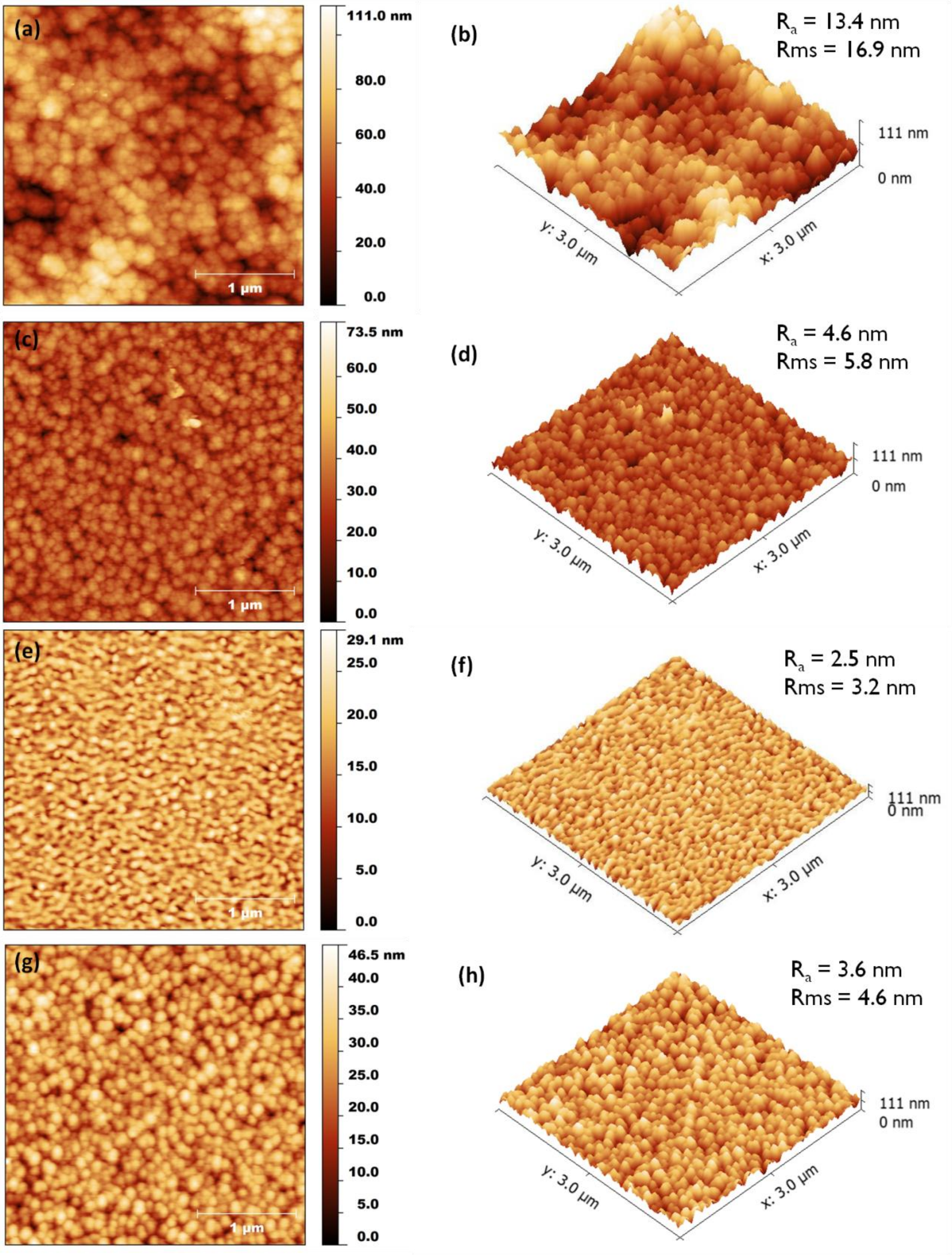

Figure III.2 AFM micrographs showing the topography of (a,b) a-C, (c,d) a-C_Zr(14), (e,f) a-C:H and (g,h) a-C:H_Zr(8) films deposited on Si wafers. The 3D in the right column corresponds to the 2D in the left column.

2.2 Structure and chemical bonding

The structure and chemical bonding of the coatings has been investigated using XRD, TEM, XPS and Raman. From XRD, pure a-C and a-C:H coatings were characterized as amorphous (Figure III.3); visible peaks were exclusively indexed as interlayer (Ti/TiN). When the coatings were alloyed with Zr, a broad peak typical of a nanocrystalline structure appeared near ZrC(111) and ZrC(200) phase. Figure III.4 shows the a-C_Zr(14) film diffractogram with the fitted peaks. The fitting procedure enabled us to find the exact position of the ZrC peaks and the calculation of the particle size by applying the Scherrer formula. The crystallite size slightly increased from 1.0 to 2.2 nm for Zr content of 4 and 14 at.%, respectively. A similar trend was observed for hydrogenated coatings: increasing the Zr content increases the crystalline size (1.5 nm for 10 at.%).

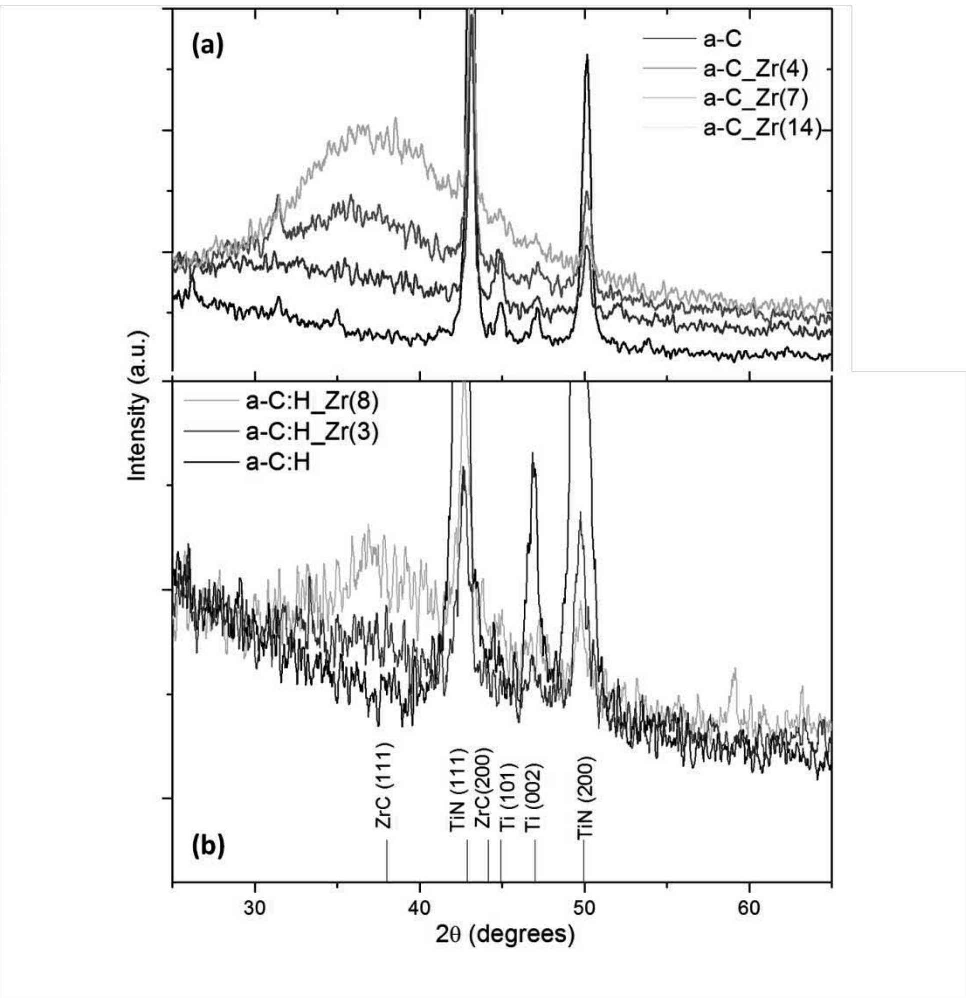

Figure III.3 Grazing-angle X-Ray diffractograms of (a) non-hydrogenated and (b) hydrogenated series of coatings with different Zr content.

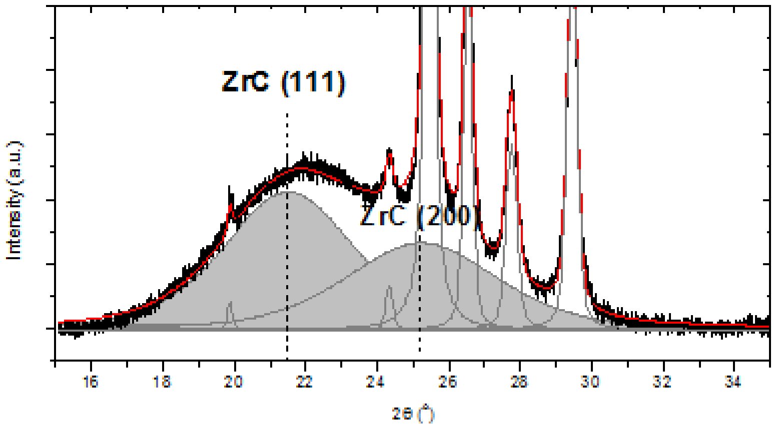

Figure III.4 Grazing-angle X-ray diffractogram of the coating a-C_Zr(14). The measured data are displayed as black line and the fitted curves as red line.

XPS of C 1s region (Figure III.5) allowed a clearl identification of C–C bonds (from the amorphous carbon phase). When Zr was incorporated in the C-matrix, a new peak appeared and grew at ~283.5 eV. Thus, it was expected that the interaction and/or bonding between zirconium and C would be different from the typical Zr-C bond of bulk ZrC (282.3 eV) [183]. A peak between typical C-Me and C-C bonds has been reported by many authors for nc-MeC/a-C systems (Me = Zr, Ti and Nb) [184-189] and it is suggested to originate from interfacial state at the carbide and amorphous matrix interface (Me-C*). The presence of nanocrystallites can enhance charge transfer between the positive metal element and the C-matrix [128, 189] leading to an electron deficiency and, consequently, weakening the Me-C bond [188]. Moreover, since such interface region was predicted to be around 1 nm [187], most of the ZrC bonds in our case are expected to show the typical positive binding energy shifts in the core levels of both C1s and Zr3d (not shown), characteristic of small ZrC nanoparticles (C-Zr*) [189, 190]. A detailed analysis of XPS data is given in Paper VII.

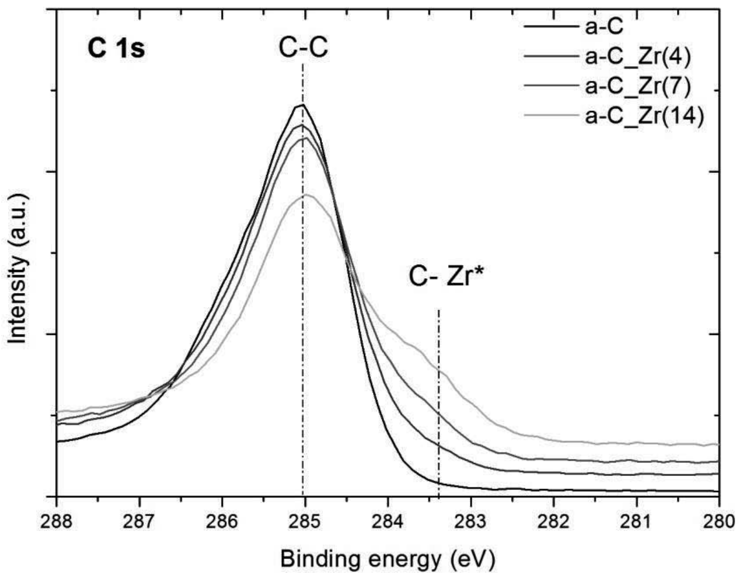

Figure III.5 XPS C1s spectra from the non-hydrogenated series of coatings with different Zr content.

TEM BF investigations were performed on selected coatings to support the results of XRD and XPS analyses. Figure III.6a highlights embedded ZrC nc-phase nanocrystals in a-C-Zr(14) film (blue line). Analysis by fast Fourier transform (FFT) (Figure III.6b) and diffraction images showed that the fringes corresponded to the lattice planes of the ZrC phase. The nc-ZrC crystals were randomly distributed in the C-matrix with a particle size of approximately 2 nm, as predicted by XRD. For lower Zr content (4 at.%), the nc-phase identification in TEM was very difficult due to the smaller grain size (~1nm). The matrix separation widths were estimated by using the Mathematica software to model the particle distribution taking into consideration the nanoparticle volume fraction (V_F) and the ZrC nanoparticles size for a unit cell of 20 x 20 x 5 nm^3 (Paper VII). In all cases the matrix separation widths were high enough (>> particle size) to effectively isolate the nanoparticles and to limit the grain growth via diffusion and coalescence [185].

Zr-containing films could be then structurally characterized as nanocomposite structures consisting of ZrC nanoparticles embedded in an amorphous C-matrix.

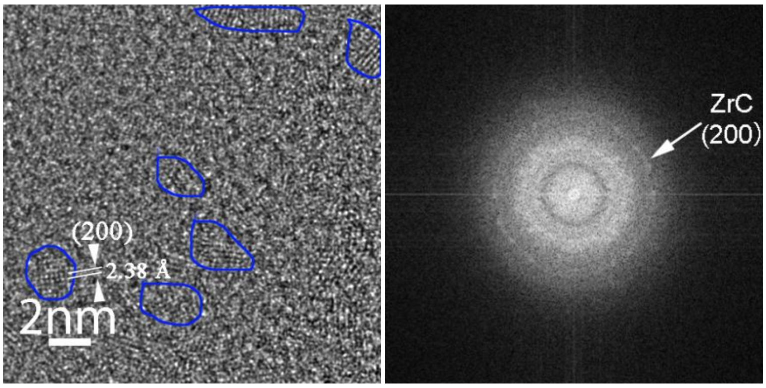

Figure III.6 (a) TEM BF images of the a-C_Zr(14) film and (b) FFT diffraction fringes with phase identification.

Raman spectra were used to characterize the amorphous carbon matrix (Paper II). Figure III.7 shows I_D/I_G ratio and the G peak position as a function of Zr content. The presence of Zr and H played an important role in the formation of aromatic rings and, in the organization and size of the C-clusters, typically demonstrated by the increase of D peak intensity (i.e. I_D/I_G ratio) either when comparing films with and without H or for increasing Zr content. Unexpectedly, the trend of the shift of G peak position for higher wavenumbers (also typical of graphitization), which should follow I_D/I_G ratio, was not systematically observed. The interface bonding induced by the presence of nc-ZrC phase may influence the vibration modes of sp^2 C=C binding modes and the graphitization of the C-matrix [177, 191] can be responsible for that anomalous behaviour for higher Zr content.

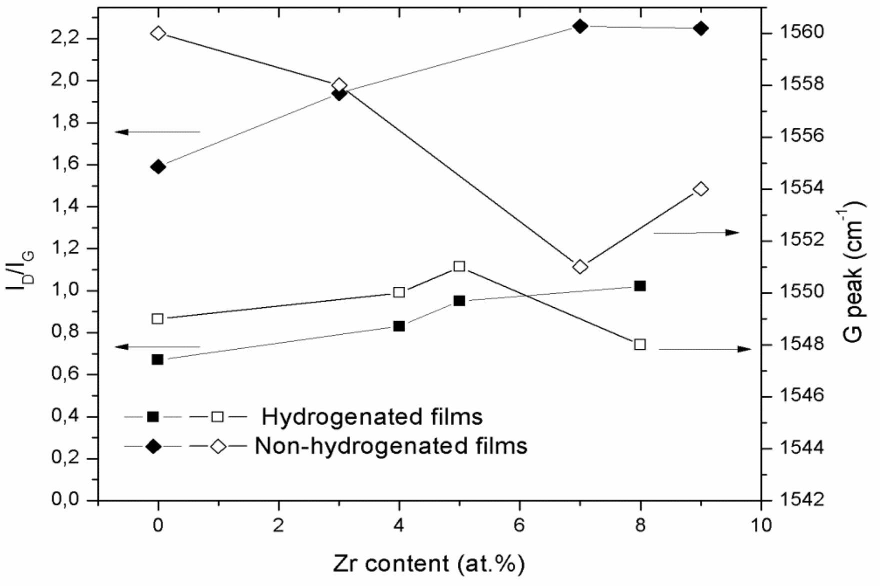

Figure III.7 I_D/I_G ratio and G peak position as a function of Zr content.

2.3 Mechanical properties of the coatings

The properties of nanocomposites are largely controlled by their microstructure. In this thesis, the main differences were associated with the amount of Zr in the a-C matrix and, consequently, the content of nc-ZrC phase. Residual stress, hardness and Young modulus have been reported in Paper II and VII. Table III.2 shows the mechanical properties of the deposited coatings.

Table III.2 Mechanical properties of the coatings.

Samples	σ_{RS} [GPa]	H [GPa]	E [GPa]	H/E	H^3/E^2 [GPa]
a-C_Zr(14)	0.3±0.06	11.9±0.5	137±2	0.09	0.09
a-C_Zr(7)	1.0±0.6	11.7±0.4	126±1	0.09	0.10
a-C_Zr(4)	1.6±0.3	10.7±0.9	114±17	0.09	0.10
a-C	1.9±0.6	10.9±0.3	105±10	0.10	0.12
a-C:H_Zr(10)	1.4±0.4	12.7±0.6	120±1	0.11	0.14
a-C:H_Zr(8)	1.9±0.3	12.2±0.5	114±3	0.11	0.14
a-C:H_Zr(3)	1.9±0.05	10.0±2	87±3	0.12	0.13
a-C:H	2.5±0.8	8.9±0.3	70±1	0.13	0.14

Generally speaking, hydrogenated films exhibited higher compressive residual stress, higher hardness and better elastic behaviour than non-hydrogenated films. The incorporation of H is known to induce modification of the amorphous carbon matrix (decrease in the I_D/I_G ratio), which suggests a less graphitic matrix. Furthermore, the glassy microstructure made the relaxation of the films harder. Both factors contributed to a higher compressive residual stresses in hydrogenated films. On the other hand, alloying with Zr allowed the relaxation of the films. The presence of nc-ZrC helped breaking the C–C bonds (more graphite-like) and, consequently, facilitated the relaxation and decreased the stress. The hardness and, especially, the Young modulus varied as a function of composition. Globally, for both hydrogenated and non-hydrogenated coatings, the hardness increased as a function of Zr content; this trend was more pronounced for hydrogenated films. In fact, the hardness of nanocomposite films is typically influenced by size, orientation and shape of the embedded nanograins [129]. Since small nc-ZrC (< 3 nm) were dispersed in a thick C-matrix (see Section 2.2), hardness was only slightly different when compared to pure films [128, 129, 192]. On the other hand, the presence of H in the gas phase and the difference in the degree of ion bombardment during deposition may contribute to the observed differences in hydrogenated coatings: the higher the hydrogen/carbon ratio, the lower the hardness (pure a-C:H film exhibits the highest H content, see Table III.1) [126, 127]. A growing trend of the Young modulus could also be observed with the increase of Zr content. The embedded nc-ZrC phase, which has a higher Young modulus if compared to the a-C matrix [193], influenced the elastic properties of the whole system making it more rigid (Paper II and VII). Other important parameters for hard coatings performance is H/E and H^3/E^2 ratios, which are closely related to the wear resistance [194]. Since the hardness was almost independent from the Zr content, both ratios have slightly decreased with the increase of Zr content. The presence of hydrogen resulted in a marked increase of H/E and H^3/E^2. As expected, the lack of columnar boundaries (i.e. glassy microstructure, see section 2.1) together with the modified nature of carbon matrix by hydrogen led to slightly higher hardness values. The wear resistance is then expected to be higher for hydrogenated films.

The cohesion/adhesion of the coatings was assessed by determination of the critical load (Lc) through scratch-testing. Since the adhesion of the coating is strongly influenced by the substrate mechanical properties, the coatings were first deposited onto hardened steel (M2) in order to effectively evaluate the influence of Zr and H. As a global trend, Zr-alloying improved the critical load values, in particular Lc_2 (first observed spallation/flaking), which is related to adhesion failures (see Figure III.8). The observed decrease in the residual stresses and the improvement of the density of the columnar microstructure with the addition of Zr were the main factors to influence the increase of Lc values.

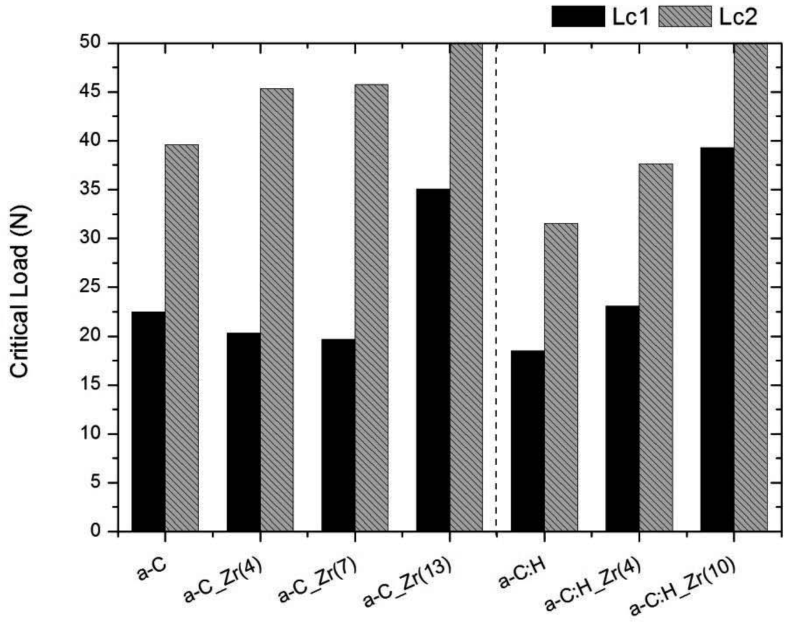

Figure III.8 Critical load of non-hydrogenated and hydrogenated coatings deposited on steel substrates.

As seen in Chapter II, the deposition of DLC on soft substrates is a continuous challenge. Once Ti-based substrates were chosen as final substrates, Zr-containing and pure films were also deposited on such substrates. Table III.3 shows the results achieved for scratch (critical loads: Lc_1, Lc_2 and Lc_3) and Rockwell-C adhesion tests (HF1-HF6) performed on CP-Ti and Ti6Al4V substrates. The adhesion properties are explained in detail in Paper I and II.

Table III.3 Adhesive properties of the coatings on Ti6Al4V and CP-Ti.

Sample	Ti6Al4V Scratch test [N]			R-C test	CP-Ti Scratch test [N]			R-C test
	Lc_1	Lc_2	Lc_3		Lc_1	Lc_2	Lc_3	
a-C	7.0±2	12.7±2	35.8±16	HF3	4.5±0.2	7.9±3	33.8±3	HF3
a-C_Zr(4)	6.2±0.7	13.1±1	36.3±5	HF3	4.4±0.4	8.0±2	35.5±3	HF3
a-C_Zr(7)	7.5±0.7	10.7±1	> 50	HF3	4.4±0.4	9.3±0.9	> 50	HF2
a-C:H	5.6±2	12.1±3	>50	HF3	4.8±2	6.3±3	12.0±6	HF5
a-C:H_Zr(3)	7.9±0.5	10.9±1	38.7±2	HF3	4.4±1	8.4±0.08	38.9±8	HF3
a-C:H_Zr(5)	6.7±0.7	12.2±2	37.8±0.6	HF3	4.6±0.2	10.2±0.07	35.7±1	HF3
a-C:H_Zr(8)	6.3±0.6	12.8±1	> 50	HF3	4.8±0.5	5.7±0.6	14.4±1	HF5

Although no significant differences in adhesion were observed between Zr-alloyed and a-C(:H) films, the adhesion strength was substrate dependent. When deposited on Ti6Al4V, the coatings revealed higher Lc's than when deposited on CP-Ti. Nevertheless, the critical loads were always lower when compared to those on steel (see Figure III.8) showing the underlying substrate at relatively low loads (Lc_3 value). In fact, Ti6Al4V is 2 times harder than CP-Ti but softer than M2 steel (see Chapter II, Section 3.1). Plastic deformation was then higher on CP-Ti than on Ti6Al4V being the main reason for early failure of the coatings. Nevertheless, the elastic properties of the Ti-based substrates were strongly enhanced by the deposition of a protective coating layer delaying the onset plastic yielding and the subsequent failure *in service* (Paper II).

In order to estimate the capability of the coating to follow substrate plastic deformation, R-C indentation tests were performed (see Table III.3). Again, for Ti6Al4V there was no significant difference between coatings, with all of them showing acceptable failure (HF2-HF3). However, when deposited on CP-Ti, some differences were observed on hydrogenated coatings: a-C:H and a-C:H_Zr(8) exhibit large-scale delamination at the indentation edges (unacceptable failure – HF5). Even though hydrogenated coatings exhibit higher elastic strain to failure (H/E ratio) and higher plastic deformation resistance (H^3/E^2 ratio) than non-hydrogenated films, they present high residual stress.

Moreover, high pile-up could lead to higher wear of the counterbody; thus the use of CP-Ti is expected to provide inferior tribological properties and to increase the risk of counterbody damage during sliding tests as demonstrated in the next section.

The effect of the substrate hardness on the DLC coating performance was further highlighted through a collaborative project with the University of Southampton. By changing the mechanical properties of the substrate with surface pre-treatments the cohesion/adhesion could be strongly enhanced [195]. High pressure torsion (HPT)[3] was applied to CP-Ti substrates; the microstructure was refined from coarse-grained to ultrafine-grained (UFG) and, consequently, the hardness of the substrate was increased. In general, from these tests it could be concluded that the coatings deposited on either HPT-processed CP-Ti and Ti6Al4V substrates showed similar scratch-test and indentation behaviour (Paper III).

2.4 Tribological properties

The tribological properties of the coatings were primarily assessed by pin-on-disc experiments against Ti6Al4V balls. The tests were conducted in two different environments: ambient air (RH = 30%) and physiological solution (PS). Testing in PS aims not only to predict the wear behavior but also to evaluate the synergistic effect of wear and corrosion in the presence of water and salt ions, that can both contribute for the degradation of the coatings [116, 197]. Figure III.9 and III.10 shows the friction coefficient and wear rates for hydrogenated and non-hydrogenated coatings deposited on CP-Ti and Ti6Al4V substrates in ambient air and PS, respectively. The values for uncoated substrates are also shown for comparison. Paper II and IV described in detail the tribological properties of the coating in ambient air and PS, respectively.

Under both testing conditions, the coefficient of friction was found to be independent of the substrate material. In general, coated substrates presented better tribological properties when compared to uncoated ones. In ambient air, pure non-hydrogenated films showed the lowest COF (~0.10), which slightly increased when Zr was added. On the other hand, hydrogenated coatings did not show any significant difference in COF. The same behaviour was observed when tested in PS, i.e. no significant difference between coatings (COF ~0.13). Moreover, the wear of the coatings was also similar, except for a-C_Zr(9) on CP-Ti; nevertheless, it was three orders of

---

[3] ***High pressure torsion (HPT)*** is a method used in metal processing to tailor the microstructure and properties. The metal is subject to a compressive force and concurrent torsional straining which causes severe plastic deformation without changing the overall dimensions of the material [196]

magnitude lower than that of uncoated samples. The wear of the counterbody decreased with the incorporation of Zr into the C(:H)-matrix.

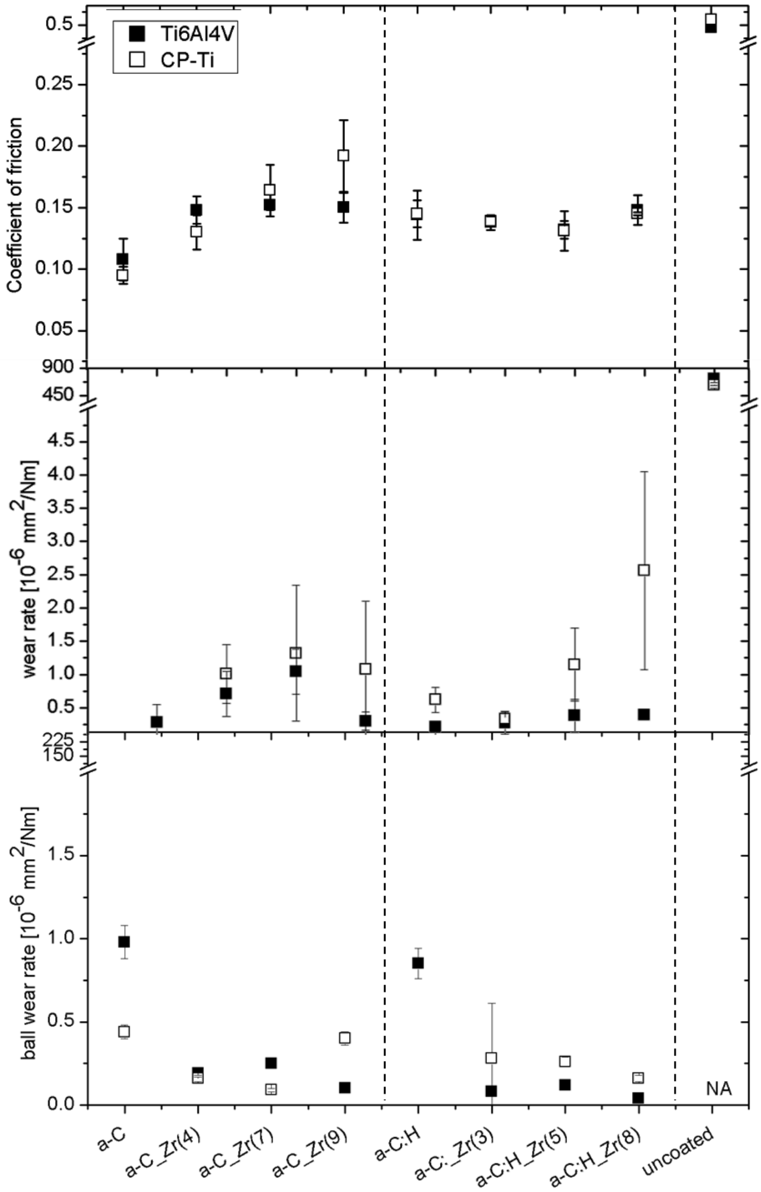

Figure III.9 Tribological properties of non-hydrogenated and hydrogenated coatings deposited on Ti grade 2 and 5, together with the uncoated values in ambient air. (NA stands for not analysed)

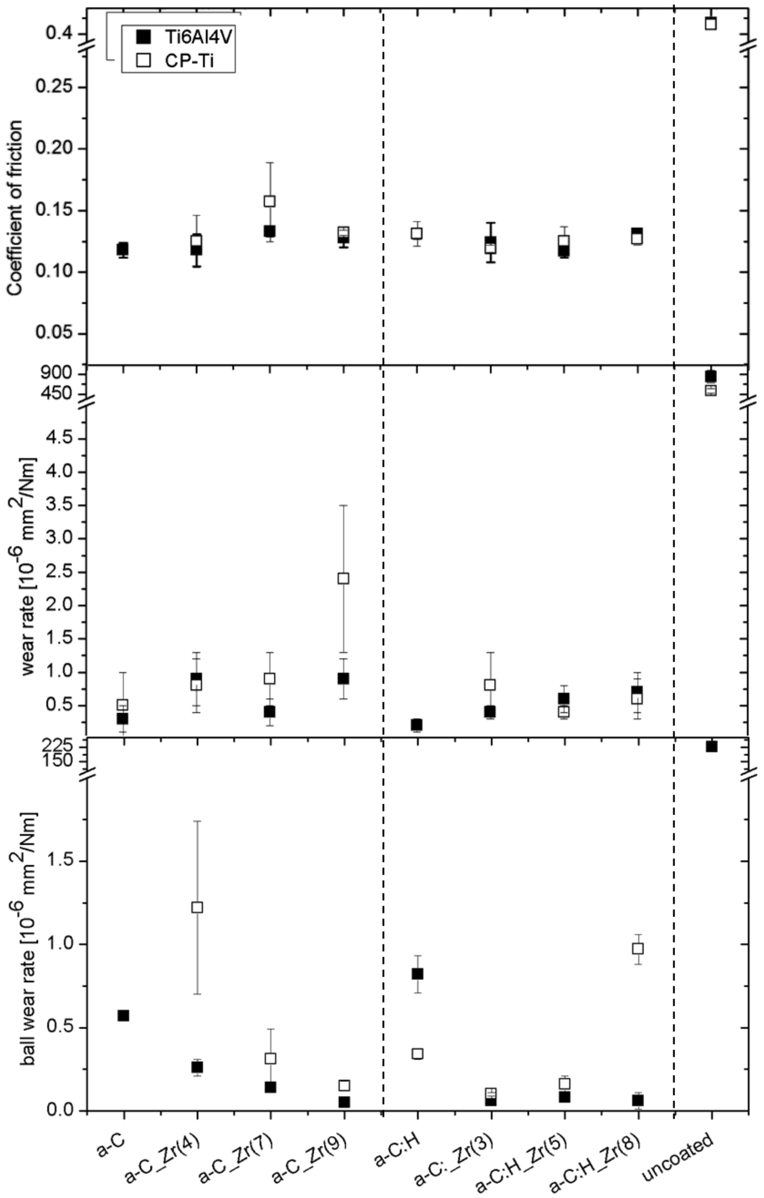

Figure III.10 Tribological properties of non-hydrogenated and hydrogenated coatings deposited on Ti grade 2 and 5, together with the uncoated values in PS.

Although the tribological properties (friction coefficient, wear rate, etc.) were only slightly dependent on the substrate, the wear track was found to be significantly different for the same film deposited on both Ti-based substrates. The use of a softer substrate (CP-Ti) led to a higher plastic deformation inducing large strains in the coating; its insufficient elastic deformation caused its fracture. In case of cyclic loading (pin-on-disc) fatigue cracks and/or blisters can occur, especially under corrosive media [198-200]. In fact, the highest deformation was observed for a-C_Zr(9) (see Figure III.11); such severe deformation could not be accommodated by the coating and cracks parallel to the sliding direction were observed. Besides, the presence of such cracks led to local delamination which might also promote the wear of counterbody. Nonetheless, when using a load carrying capacity substrate (Ti6Al4V), Zr-containing films presented good wear-corrosion behaviour and, in general, lower ball wear rate (see Figure III.9 and III.10). Plastic deformation and its influence on the wear of the coatings is described in Paper II.

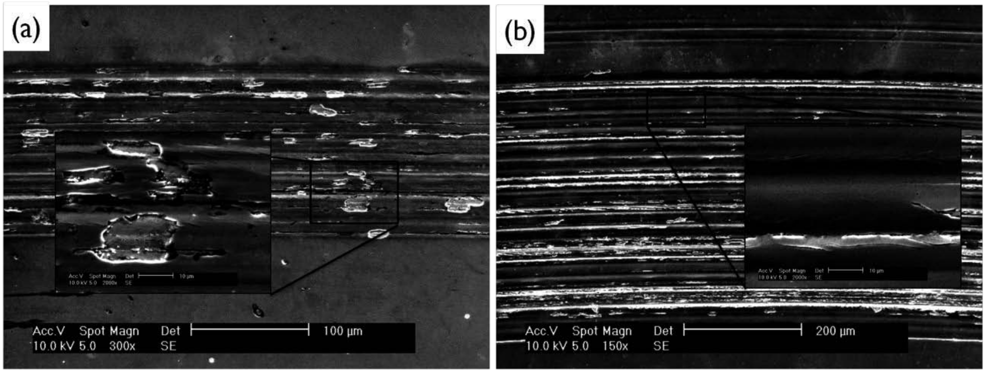

Figure III.11 SEM micrographic pictures from a-C_Zr(9) wear track when deposited on Ti grade 2: (a) ambient air and (b) PS.

When sliding under non-lubricated conditions, DLC films are known to form a graphitic-like tribolayer that works as a solid lubricant. Friction and wear of the coating and counterbody are then dependent on the stability and thickness of such layer [66]. Figure III.12 shows the Raman spectra acquired on the ball wear scars after sliding against a-C and a-C_Zr(9) deposited on Ti6Al4V in room conditions. Even though a-C_Zr(9) wear track did not show any significant structural difference before and after sliding (no graphitization), the ball shows shallow scratches covered by a homogeneous and well-developed graphitic tribolayer (see typical G and D peaks from graphite featuring in the Raman spectrum, Figure III.12). On the contrary, when sliding against pure a-C films such layer could not be identified. The presence of nc-ZrC phase increased carbon structure disorder (see Section 2.2), which may help to develop a stable carbonaceous tribolayer that protected the counterbody from wear. An exhaustive study on the effect of the tribolayer formation under different environments of Zr-containing coatings was developed through a collaborative project with Czech Technical University; for more details see Paper V.

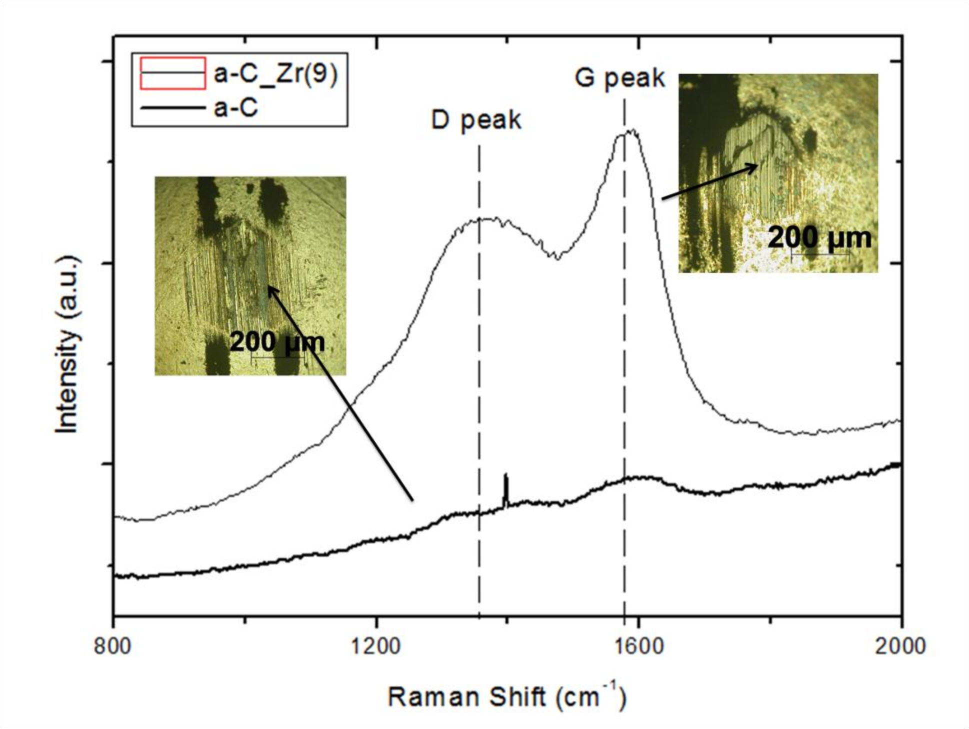

Figure III.12 Raman spectra and micrographs of the ball wear scar that slid against a-C and a-C_Zr(9) films. The arrows show the acquisition zone.

In physiological solution, the formation of a protective transfer layer is typically suppressed [66]. The friction and wear behaviour is then influenced by the properties of the coating surface and the interaction with the environment. It is important to notice that when Zr was added to the C-matrix, the water contact angle increased. Next Chapter is dedicated to the physicochemical properties of the coatings. Nevertheless, lower surface energy is typically related with lower wear rates due to the decrease of the direct solid contacts between surfaces [201-203]. Moreover, it is expected that the interaction with H_2O molecules will be similar with that of moisture (C-H, C-O and C=OOH bonds).

3. Conclusions

The formation of nanocomposite structures consisting in ZrC nanoparticles embedded in an a-C(:H) matrix was achieved when incorporating Zr in contents as low as 3 at.%. The grain size was estimated to be around 1-2.2 nm as a function of the Zr content. Compared to Zr-free, nanocomposite films were denser and smoother. The presence of nc-ZrC relaxed residual stresses in the films both by inducing modification of the C-matrix (graphite-like) and by changing the morphology of the coatings. When deposited in a reactive atmosphere, the films revealed a glassy/compact morphology and exhibited higher compressive residual stresses. In general, increasing Zr content led to higher hardness, higher elastic modulus, lower residual stress and better cohesion/adhesion to the substrate. However, an inverse trend was registered for H/E and H^3/E^2 ratios. This featu re was particularly important when using low load carrying capacity substrates such as Ti-based materials: higher Zr content (more nc-ZrC dispersed in the C-matrix) lowered the adhesion and the tribological properties of the coatings deposited on softer CP-Ti substrates. Substrate plastic deformation resulted in the coatings fracture, cracking and/or blistering, especially when sliding in a corrosive medium. Under these circumstances, CP-Ti should be discarded as a potential substrate since it can increase the risk of either coating degradation or extensive counterbody wear. On the other hand, Ti6Al4V coated with Zr-containing films presented good wear-corrosion behaviour strongly reducing the counterbody wear when if compared with pure films.

CHAPTER IV

The core objective of this chapter is the study of the surface interaction between a-C:(H)_Zr films and biological fluids. The surface chemistry was assessed by means of surface energy and protein adsorption. The tribological properties under BS lubrication are also discussed with the focus on the role of albumin in the sliding process.

The main results of this chapter were presented in **Paper IV**.

1. Introduction

In biomedical field, mechanical and tribological properties are important to assess the potential of materials for their application. Nevertheless, the key parameter is biocompatibility. The prediction of materials biocompatibility and their applicability is hard but not entirely impossible, being strongly dependent on the energy, morphology and chemistry of the biomedical surfaces [204]. Real surfaces are characterized by a certain degree of roughness and/or of chemical heterogeneity, thus inducing deviations from an ideal surface [205]. For instance, smooth surfaces (Ra < 1 µm) are known to limit the thrombogenicity [206] and bacterial adhesion [207] of the biomaterials related to cells flattening out, which prevents their nutrition [208]. The exact interaction between biomaterials and biological fluids is still under extensive study [209]. After implantation, the adsorption of protein is of great importance in understanding the interaction between the material and the human body, since it is one of the first events occurring after implantation and it drives the entire biological response to the implanted material [210-212].

In this Chapter, the physicochemical properties of the coating surface are described. Wettability measurements were used to evaluate the affinity of the coatings with water. Protein-adsorption studies were performed by focusing on albumin adsorption, since it is the most abundant constituent in synovial fluid and it has been recognized as critical for the lubrication mechanism [213,214]. Finally, the tribological behaviour of the coatings was also assessed in the presence of foetal bovine serum (BSA). The tests were performed by using pin-on-disc tests to investigate the wear mechanism, friction, and lubrication under protein containing solutions. The results shown here summarize the results presented in Paper IV.

2. Surface Chemistry – Physicochemical Properties

Immediately after implantation, water and ions are the first adsorbing on the implant surface, since water is the predominant substance in all tissues and fluids in the human body (50-80%) [1]. Thus, the way surfaces interact with water can be considered as one of the most important properties of the surface when it comes to predict its behaviour under biological environments. In fact, numerous physiological events at subcellular and cellular levels, such as cell adhesion and protein adsorption, are greatly affected by such property. Wettability is modulated by surface characteristics, such as chemistry and surface topography [215], and it can be expressed in two different ways: (i) a less wettable surface (hydrophobic surface) which implies high contact angle values; and (ii) on the contrary, low contact angles values present a more wettable surface (hydrophilic surface) [216]. To study such property, water contact angles measurements were performed. Since surface roughness can strongly influence the results, the coatings were deposited on glass substrates. Moreover, the base radius of the drop was chosen bearing in mind that it had to be large enough in proportion to the scale of the sample roughness (larger than three orders of magnitude) to ensure accurate contact angle measurements [205]. Table IV.1 shows the roughness, the water contact angle and the calculated surface energy of the coatings. For non-hydrogenated coatings, the contact angle increased inversely with the surface roughness. However, hydrogenated coatings follow an inverse trend. Typically, the contact angle increases with decreasing surface roughness [217-219]; therefore, little or no correlation between roughness and surface wettability was found in this study. The surface topography cannot then be considered alone to explain the wettability behaviour of the coatings.

Table IV.1 Surface roughness (R_a and Rms), water contact angle (θ) and surface energy (γ_s) of the coatings.

Samples	**Roughness** [nm]		Θ_{water} [°]	**Surface energy** [mJ.m^{-2}]		
	R_a	Rms		γ_s^p	γ_s^d	γ_s
a-C_Zr(14)	4.6	5.8	71±2	4.3	39.1	43.4
a-C_Zr(7)	4.5	6.0	67±1	5.0	40.5	45.5
a-C_Zr(4)	5.8	7.3	66±3	5.1	45.8	50.9
a-C	13.4	16.9	50±7	11.2	51.2	62.3
a-C:H_Zr(8)	6.4	8.0	73±2	3.9	36.7	40.6
a-C:H_Zr(3)	3.6	4.6	65±2	12.8	27.2	40.0
a-C:H	2.5	3.2	57±2	14.2	33.9	48.1

Pure non-hydrogenated and hydrogenated carbon films were characterized as hydrophilic ($\theta < 65°$). When Zr was incorporated, the contact angle increased as a function of Zr content and became similar to uncoated samples. Air stored Ti-based substrates have typically water contact angles around 70° due to the naturally formed passive TiO_2 layer that is responsible for the good biological performance of Ti implants [205, 215]. The exact water-interaction mechanism of alloyed DLC coatings is still not clear and further investigation is needed. Nevertheless, similarly to the well-known influence of hydrogen on the decrease of unsaturated bonds C=C (compare pure a-C and a-C:H), the metallic element can further decrease the dipolar interaction with water, by decreasing the polar component and additionally the surface energy [220].

Protein adsorption is strongly influenced by surface chemistry, namely by surface wettability. For instance, albumin has three homologous domains (comparable amino acid sequences) assembled in a heart-shape structure which are sustained by hydrophobic interactions, hydrogen bonds and disulphide bridges [210, 221]. Once the adsorption is initiated, proteins tend to maximize the surface interaction by exposing either their hydrophobic domain (typically hidden toward the interior) or hydrophilic domains, depending on the surface wettability. Nevertheless, hydrophobic surfaces enhance a protein-surface interaction, when compared to hydrophilic due to the fact that they promote hydrophobic interactions. Actually, the adsorption on hydrophilic surfaces is thermodynamically unfavourable [216, 222]. On the other hand, proteins can undergo reversible/irreversible conformational changes when adsorbed on hydrophobic surfaces that may lead to unfavourable cell response if the proper binding domains are disrupted [204, 211]. Figure IV.1 shows the estimated amount of proteins adsorbed in relation to surface contact angles. As expected, Zr-containing coatings (hydrophobic surfaces) adsorbed more than pure films (hydrophilic surfaces). In fact, the incorporation of small Zr content (4 at.%) was able to increase 10 times the adsorption ratio of the films if compared to pure carbon films.

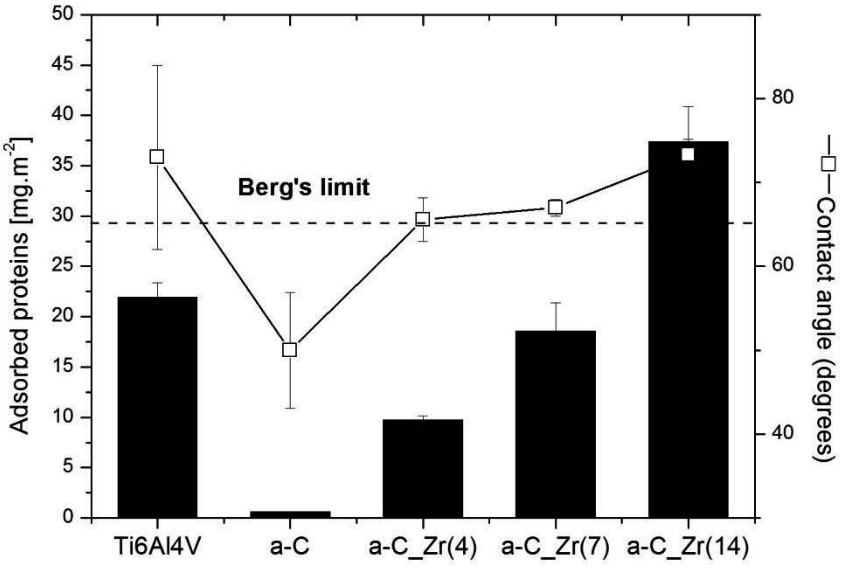

Figure IV.1 BSA adsorption vs contact angle measurements. The dash line represents the Berg's limit[4] (θ = 65°).

---

[4] Berg's limit stands to the minimum detectable hydrophobic forces suggested by Berg et al. [216, 223].

Taking the albumin size, its molecular weight [224] and the surface area into account, there should be a maximum protein concentration allowed to be adsorbed; it is approximately 4 mg.m^{-2} for monolayer adsorption (side-on and/or end-on) [225, 226]. However, it has been reported that multilayer adsorption is likely to occur on metallic substrates, especially for high concentration solutions [213, 225, 227]. Zr-containing samples revealed to have multilayer adsorption since the maximum amount for monolayer adsorption was highly exceeded. Moreover, after rinsing with water to remove any non-chemically bonded (chemisorbed) proteins on the surface, the amount of protein removed from the a-C surfaces was around 46% whereas no evidence of desorbed proteins was detected for Zr-alloyed samples. This may be attributed to the different conformation of the adsorbed layer that influences protein-protein and/or protein-surface interaction [213, 227]. After all, Zr-containing coatings (hydrophobic surfaces) showed not only a higher amount of adsorbed protein but also that they were more tightly bound than on a-C films.

In order to prove the existence of such adsorbed layer, XPS analyses were performed on the surfaces of the samples. Figure IV.2 shows the XPS survey spectra for uncoated substrate (Ti6Al4V) and non-hydrogenated coatings after immersion in BSA. The first main difference observed, when compared to as-deposited spectrum (Figure IV.2f), was the appearance of a well defined N 1s peak (N 1s 400 eV), usually assigned to the amino-acid of the protein [228, 229]. For the Zr-containing samples the intensity of Zr 3d peak decreased after immersion, meaning that the adsorbed protein layer is rather discontinued, leaving bare areas of the film/substrate surface. In fact, many authors [213, 227, 230] have reported that protein monomers preferably aggregate to surface clusters if compared to adsorbed on empty surfaces sites forming an island-like structure, whose thickness corresponds to several layers. Moreover, the S weak band can only belong to S-containing amino acids, i.e., methionine (Met) and cysteine (Cys) [231], which corroborates the presence of such layer (see the inset of Figure IV.2). Although XPS did not provide quantitative information about the total amount of adsorbed proteins, it was possible to monitor such tendency by analysing the N 1s core level before and after immersion: the higher the adsorbed ratio, the higher the intensity [213]. Figure IV.3 shows the N 1s core level spectra for uncoated and coated samples. The high intensity peak of a-C_Zr(14) corroborated the adsorption results. A complete analysis of the XPS data (deconvolution of the peaks, bonding identification, etc.) is given in Paper IV.

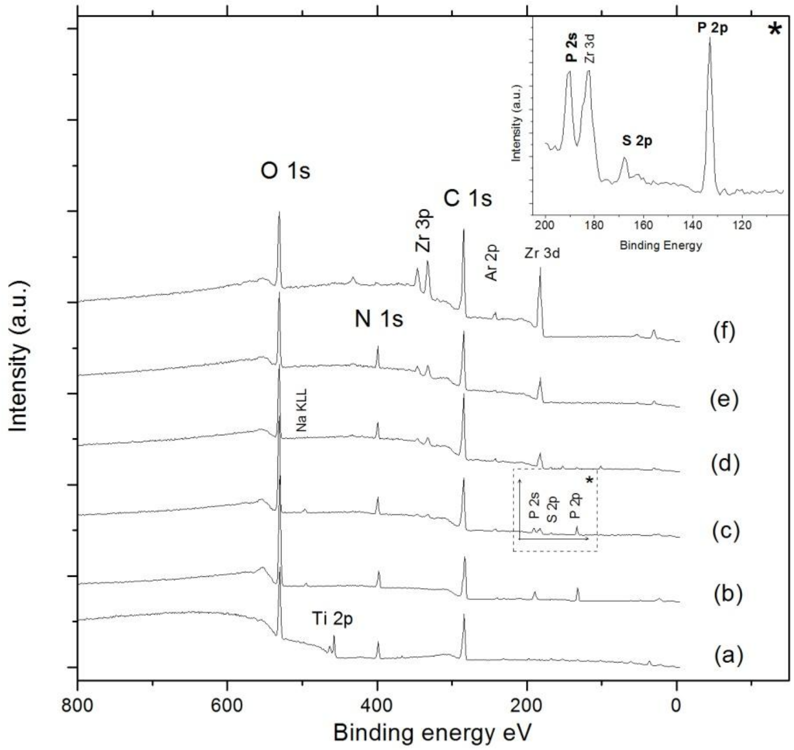

Figure IV.2 XPS spectra of the uncoated and coatings after immersion in BSA for 24h: (a) Ti6Al4V, (b) a-C, (c) a-C_Zr(4), (d) a-C_Zr(7) and (e) a-C_Zr(14). a-C_Zr(14) before immersion was also add for comparison (f). The inset (*) shows a zoom in of the 200-400 eV region of the a-C_Zr(4) film XPS spectra revealing the S 2p photo-peak.

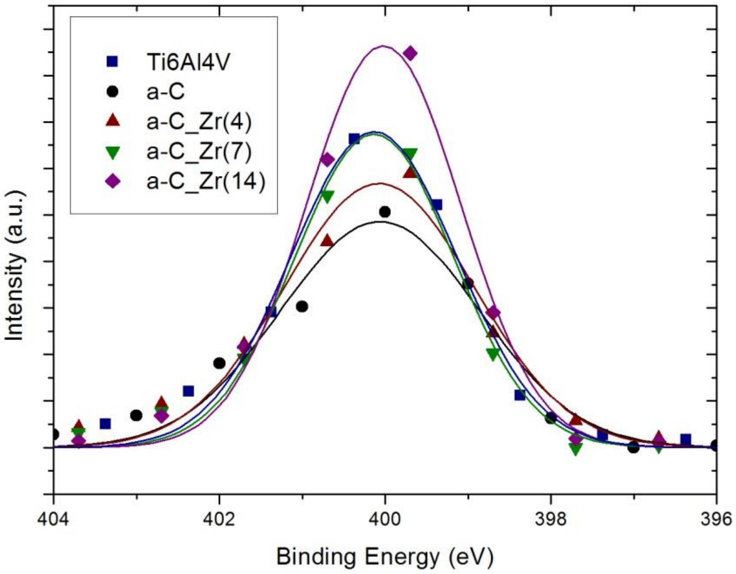

Figure IV.3 N 1s core level spectra for coated and uncoated samples after immersion.

3. Tribological properties under BSA

The natural lubricant present in the contact after arthroplasty is a complex mixture containing proteins. However, the research studies concerned with natural lubrication have focused on single-component fluid rather than on mixtures as the synovial fluid, mostly for reasons of availability and convenience. As albumin is by far the most abundant protein and readily adsorbs onto artificial materials, it has been widely considered the most important protein in lubrication studies. Thus, to identify a promising coating composition, pin-on-disc friction tests were performed under protein-containing solution (BSA). Figure IV.4 shows the COF and the ball wear rate of coated and uncoated samples. The presence of proteins in the lubricant protected the coatings from wear, since in all cases the worn surface did not show any measurable wear. Moreover, sliding against Zr-alloyed films resulted in a decrease of the wear of the Ti-alloy ball. On the other hand, despite the mechanical and structural differences all coated samples presented similar COF (~0.16).

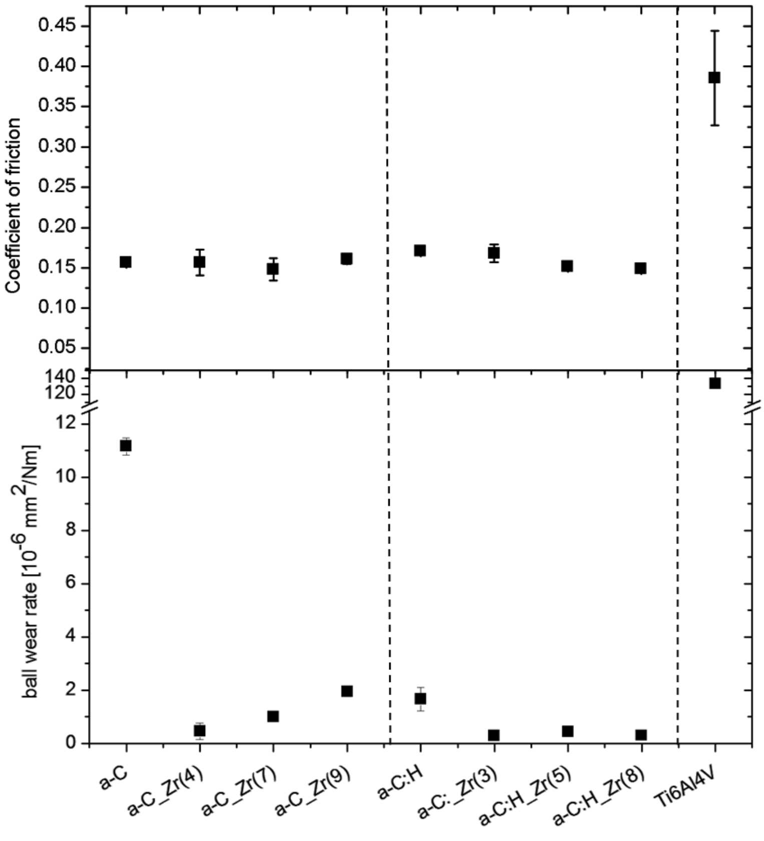

Figure IV.4 Average friction coefficient and ball wear rate of the coated and Ti6Al4V uncoated samples under BSA lubrication.

Upon adsorption, albumin created a layer more or less thick depending on the surface wettability, as mentioned in Section 2. Once adsorbed on hydrophobic surfaces, albumin typically restructures its conformation in order to maximize the inter protein and protein-surface interactions. On the other hand, on hydrophilic surfaces albumin maintains its native conformation being less tightly bound to the surface [227]. The interaction of protein with metallic surfaces is then complex and may play antagonist roles: acting as a lubricant [232] but also interfering with the sliding of the pin and providing resistive forces that lead to higher friction [201]. Thus, the ability to adsorb protein on the surface is of fundamental importance in the wear process: hydrophobic surfaces increase the protein adsorption that restrains the direct contact between mating materials and, consequently, decreases the counterbody wear. Figure IV.5 presents a schematic representation of the general wear process.

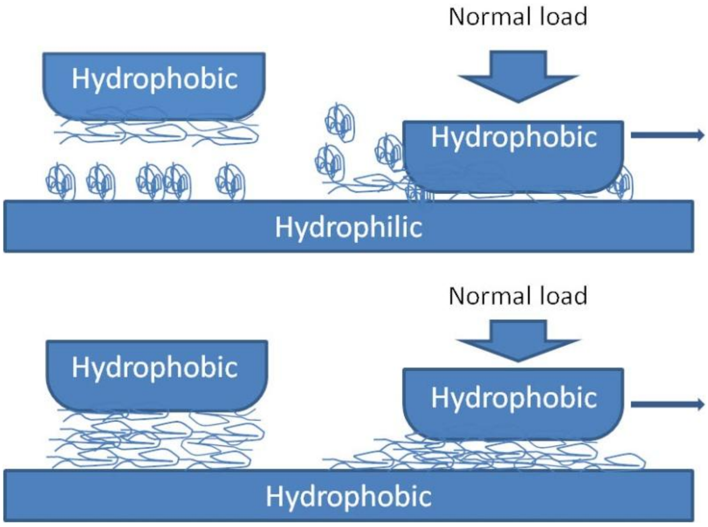

Figure IV.5 Schematic representation of the key mechanism of albumin-mediated lubrication on hydrophilic and hydrophobic DLC films.

Although this may be true, it is also important to notice that the wear of the ball was always higher when compared to tests in ambient air or PS, especially against Zr-free films (see Chapter III, section 2.3). Typically, protein adsorption increases the wear resistance of metallic alloys (ball) [233] but if the top surface of the material is rubbed and the natural passive film is destroyed, albumin plays an important role affecting the tribocorrosion behaviour of the alloy [234]. In fact, TiO_2 produces two types of surface hydroxyl groups when interacting with water: one type derived from a protonated base and another type derived from the acidic hydroxyl groups [17]. When sliding in PS, the anions bind to the titanium ions in exchange reactions with those basic hydroxyl groups, thus forming a new passive layer that protects the surface from rubbing. When proteins are added to the lubricant such process is delayed [234] and it depends on the stability of both the passive and the protein layer [235]. In addition, if a very thin protein layer is formed (such as on a-C films), direct contact between mating materials can still occur, further increasing the wear of the counterpart. The same behaviour was observed for uncoated samples; sliding in protein containing solutions resulted in slightly lower surface wear (5.7×10^{-4} mm^3/Nm) and counterbody wear (1.3×10^{-4} mm^3/Nm) compared to sliding in PS (7.2×10^{-4} mm^3/Nm and 2.2×10^{-4} mm^3/Nm, respectively, see Chapter III, section 2.3). It further confirms the protective effect of the protein layer. A closer look at Figure IV.4 bears it evident that, despite the reduction of wear of the counterbody when sliding against Zr-containing films if compared to pure films, the wear tendentiously increased with the increase of albumin absorption ratio. Such behaviour can be related to the mechanical properties of the coatings. It is expected that the local contact pressure of Zr-containing films is higher than Zr-free films, since they have higher Young modulus (see Chapter III). The protein adherent layer would be then easier squeezed out and contact between mating surfaces would occur [232]. Many authors [236-238] also refer to the thermal and shear induced denaturation and precipitation of proteins under sliding conditions that can change the rheological properties of the lubricant and, consequently, influence the lubrication properties and the wear mechanism. Nevertheless, this phenomenon is usually associated with a higher friction, which was not observed in this study (see Figure IV.4).

4. Conclusions

The physicochemical properties of the coatings were screened by evaluating the water- and protein-surface interactions. The incorporation of Zr decreased the surface energy (hydrophobic character), enhancing the albumin adsorption if compared to pure a-C(:H) films. XPS confirmed the presence of such adsorbed layer onto the surfaces and the adsorption tendency: the higher the Zr content, the higher the contact angle, and the higher the protein adsorption. Moreover, under sliding, the ability to effectively adsorb proteins was fundamental not only for protecting the coating from wear but also for protecting the surfaces from direct contact.

In general, Zr-containing films presented better tribological performance when compared to pure ones, since the wear of the counterbody decreased. Nevertheless, higher Zr content resulted in higher wear of the ball, even with higher protein adsorption rate. A synergetic effect is then expected between mechanical and chemical properties that influence the overall performance of the coating under biological conditions. Despite the excellent protein adsorption of coatings with high Zr content, the coatings that best fitted for further testing were the ones with lower Zr content. a-C_Zr(4) was then selected for further testing as representative of the best Zr-alloyed films.

CHAPTER V

This chapter describes the sliding behaviour of two selected coatings (pure a-C and a-C_Zr(4)) when tested against UHMWPE and PEEK. The tribological tests were carried out in a multidirectional pin-on-disc apparatus that replicated the typical cross-shear motion typical of endoprosthesis.

Paper **VI** fully reviews the results exposed herein.

1. Introduction

One of the most commonly used material combinations in arthroplasty is UHMWPE vs metal (MoP). Despite the good mechanical and tribological properties of this tribopair, there is strong concern related to the production of wear debris *in vivo*, which eventually leads to the failure of the prosthesis. For instance, 10% of the knee implants failures were directly related with UHMWPE wear [57]. As a result, most studies on artificial joint materials concentrate on the wear analyses and the wear-particle characterization, especially when trying to implement new material combinations. This can be assessed in a first attempt by "bench tests" (e.g. linear reciprocating motion, ball-cup wear, delamination wear, etc.) and at the final stage by using joint simulators that replicate the real movement of the natural joints. In Chapter IV, the tribological properties of the coatings were evaluated by pin-on-disc measurements with linear reciprocating motion under physiological conditions in order to pre-select a promising set of coatings that could be tested in conditions closer to reality. To rank materials for polymer wear rates under simulated physiological conditions, the testing conditions should be representative of the wear rates and the mechanisms of those in a TJR [239-241]. More specifically, the wear of certain polymers is highly dependent on "crossing shear" sliding conditions. In fact, it was found that unidirectional motion strain-hardened the polyethylene, gradually increased its integrity along the established path and thus resulting in unreliable polymer wear [240]. Thus, the general requirement to evaluate the wear of the polymer is that the polymer surface must change direction in proportion to the counterface.

Unfortunately, our lab does not provide any other facility to effectively evaluate the wear against polymeric materials. Therefore, Professor Markus A. Wimmer, Head of the Section of Tribology at Rush University Medical Center, was contacted in order to use a multidirectional pin-on-disc (AMTI's Ortho-POD™) equipment based in his laboratory. In this experiment, the pin is rubbed against a plate in an elliptical or square waveform to create the cross-shear motion conditions. This collaboration is summarized in Paper VI that describes in detail the wear behaviour of a-C and a-C_Zr(4) coated Ti alloys against two different polymeric materials (UHMWPE and PEEK).

2. Tribological behaviour against UHMWPE and PEEK counterbodies

Contradictory results have been reported in literature when DLC slides against UHMWPE, ranging from strong improvement to drastically increased wear [103]; only one study, to our knowledge, of DLC against PEEK reported a significant increase in the life span of implants using such a combination [242]. Thus, there is enough space to explore such a combination and its use on load-bearing implant. The tribological properties were assessed by using multidirectional pin-on-disc test. In accordance to ASTM F-732 [174], this technique has been considered as the simplest and the most widely accepted model for the basic biotribological simulation of candidate biomaterials. The exact loading and motion patterns are not replicated with such machines though; the multidirectional motion generates "crossing shear" conditions, which are typical for TJR and strongly influence the polymer wear rate [240, 243-245], being closer to real contact conditions. The tests were performed for a maximum of 2 million cycles (Mc), which represents ~2 years *in service*, under protein-containing solution (BS). The square motion pattern was chosen by taking the typical patient locomotion into account, since the trajectory of relative motion between a femoral head and an acetabular cup takes a general quasi elliptical or rectangular/square shape during a patient gait cycle [245, 246]. Moreover, the contact pressure used in the present study was ~1.5 MPa which is lower than values reported in literature (2 to 5 MPa) [59, 240, 243-245]. However, extremely loud squeaking due to high friction could be noticed when using higher contact pressures. Apart from coated and uncoated Ti6Al4V samples, CoCrMo alloy was also used as reference materials with prosthetic-quality surface finishing ($R_a < 0.05$ μm) to avoid any influence of an abrasive wear mechanism [174].

Although there is no simple relationship between wear and friction, low friction materials can generally be expected to enhance the performance of an artificial hip; therefore, the friction is an important parameter to consider [247, 248]. Figure V.1 shows the average coefficient of friction measured for all testing samples against both polymeric materials. The friction behaviour was strongly dependent on the polymer type. When testing against PEEK, the friction coefficient (COF) was almost 2 times higher than against UHMWPE. In fact, PEEK is known to present a relatively high friction coefficient ~0.3 against metals [243, 249]. The CoCr/polymer combination has always showed lower COF when compared to the other tribopairs. Moreover, statistically ($p < 0.003$), the metal/UHMWPE pairings presented lower COF when compared to coated samples. On the other hand, there was almost no difference in COF for different surfaces tested against PEEK ($p > 0.057$).

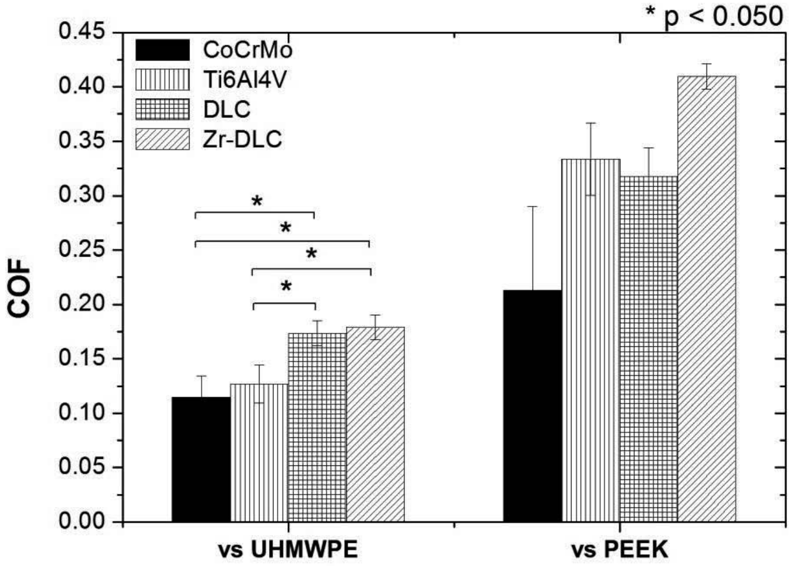

Figure V.1 Average COF for all samples against UHMWPE and PEEK. (*) represents statistically significant differences between samples in the same group ($p < 0.05$, ANOVA test).

Figure V.2 shows the volumetric wear loss versus the number of cycles for both UHMWPE and PEEK pins. The wear factor, calculated from linear regression analysis of the average of three measurements, is shown in Figure V.2 (see insets). Similarly to friction, wear was strongly dependent on the polymer counterbody. In nearly all cases, the wear was correlated with friction: PEEK wore more than UHMWPE ($p < 0.049$). The only exception was found for CoCr, where there were no significant differences in wear factor when sliding against PEEK and UHMWPE ($p > 0.127$). In fact, the wear factor for CoCr/UHMWPE ($2.6 \pm 0.1 \times 10^{-6}$ mm^3/Nm) was at the range of those reported from clinically retrieved TJR couples (10^{-6} mm^3/Nm [240, 250]), which demonstrates the reproduction of the *in vivo* wear mechanism. Thus, the behaviour of new materials combinations could be assessed by this method in a relative cost-effective way.

It is worth noting that the wear of the metallic alloys and the coatings could not be measured: (i) samples were too heavy for the microbalance and/or weight losses too small for the standard laboratory balance; and /or (ii) the wear track depth and shape could not be effectively detected by profilometry analysis to determine the wear rate. Therefore, Figure V.3 shows the discs surfaces for a better understanding of the wear phenomena. Although no significant differences were observed on the UHMWPE wear ($p > 0.66$), the wear mechanism was dependent on the testing surface. Ti6Al4V revealed its poor tribological properties with signs of abrasive wear (grooving) when compared to CoCr (Figure V.3a and 3c). On the other hand, when Ti alloy was coated, no wear was initially observed; the coatings thus successfully protected Ti6Al4V from wear (Figure V.3e). Nevertheless, Zr-containing samples sliding against UHMWPE delaminated after 1.2 million cycles (Mc) (Figure V.3g). When sliding against PEEK, both coatings, a-C and a-C_Zr(4), delaminated after 1.2 Mc and 0.9 Mc, respectively (Figure V.3f and 3h). The test with uncoated Ti6Al4V was also stopped after 300,000 cycles due to severe surface damage (see Figure V3d). Its poor shear strength led to a detachment of the oxide layer, which then acted as an abrasive [105, 158, 251, 252].

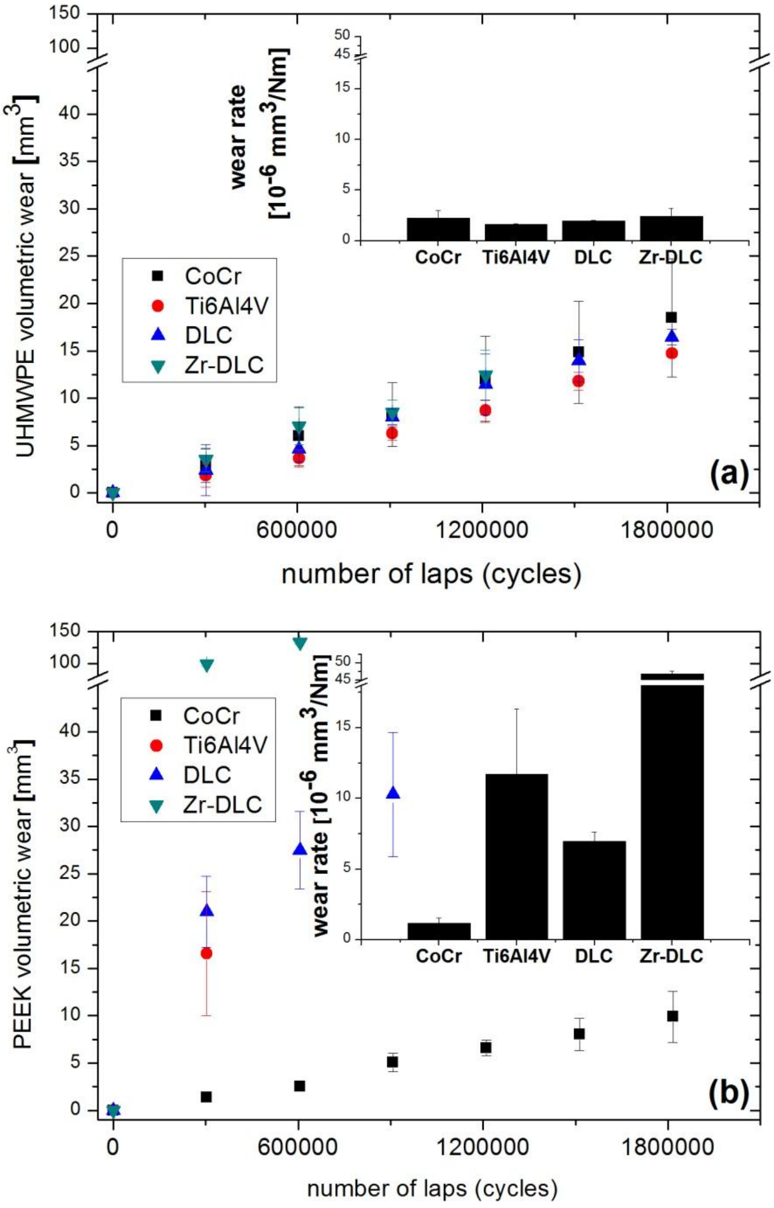

Figure V.2 (a) UHMWPE and (b) PEEK volumetric wear loss and wear rate (in the insets) against the different surfaces.

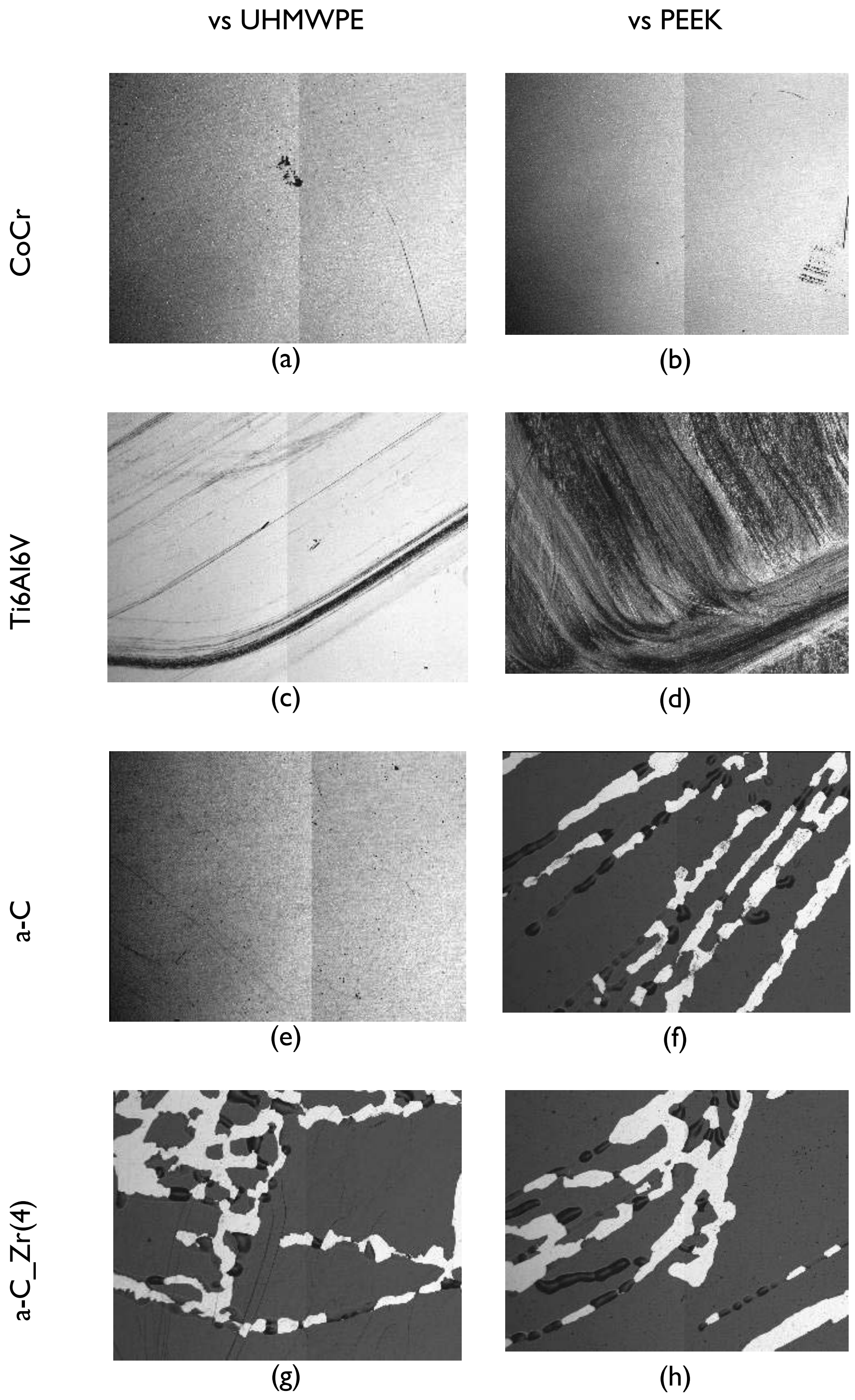

Figure V.3 Images from the wear track of the disc after testing against (a,c,e,g) UHMWPE (a,c,e,g) and (b,d,f,h) PEEK.

As seen in Chapter III, the incorporation of small amounts of Zr led to changes in the coating microstructure and mechanical properties. In fact, Zr-containing films exhibit higher adhesion strength and lower residual stress when compared to a-C pure films, especially for higher Zr content. However, low Zr content presented better tribological properties under BS solution, showing lower counterbody wear (see Chapter IV). Thus, one may think that a-C_Zr(4)/Polymer would decrease the polymer wear and consequently the *in vivo* wear debris production and release. Instead, the coatings failed catastrophically when tested under multi-directional stress in body fluids.

Surface layer failure is the major concern when using coatings in the biomedical field and has quite frequently been reported *in vivo* and *in vitro* by many authors [103, 106, 253]. A graded interlayer scheme was applied in order to avoid such problem, resulting in a satisfactory composition gradient (see Chapter II). Moreover, such interlayer also resulted in a desired functional gradient of elastic properties at the coating/substrate preventing coating chipping and delamination. Despite the good mechanical adhesion achieved in ambient air, the presence of biological species in the body solution (ions, proteins, etc.) can boost the corrosion of the adhesion-promoting interlayer and consequently lead to the delamination of the coating [254]. In order to evaluate the effect of the body fluids on the adhesion strength of the coatings after testing, R-C indentation test was performed in the wear tracks and, when present, near the delamination zones (Figure V.4). The overall adhesion of the film was maintained (i.e. it was identical to that of the as-deposited samples), even when the film was clearly damaged after testing. Moreover, Raman spectra acquired in the wear tracks did not reveal any significant difference after testing (see Figure V.5).

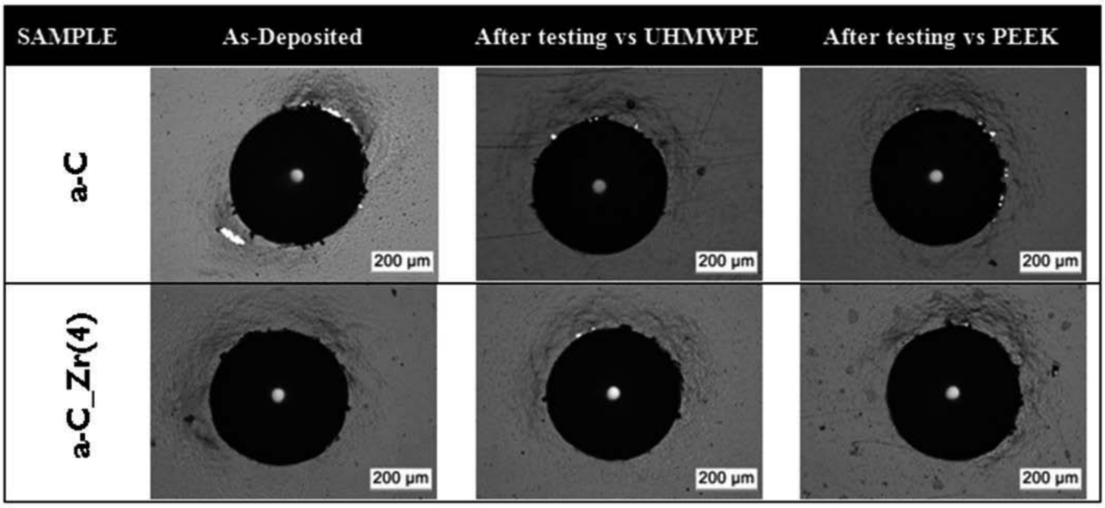

Figure V.4 Optical micrographs of the Rockwell-C indentation of a-C and a-C_Zr(4) films before and after testing against UHMWPE and PEEK.

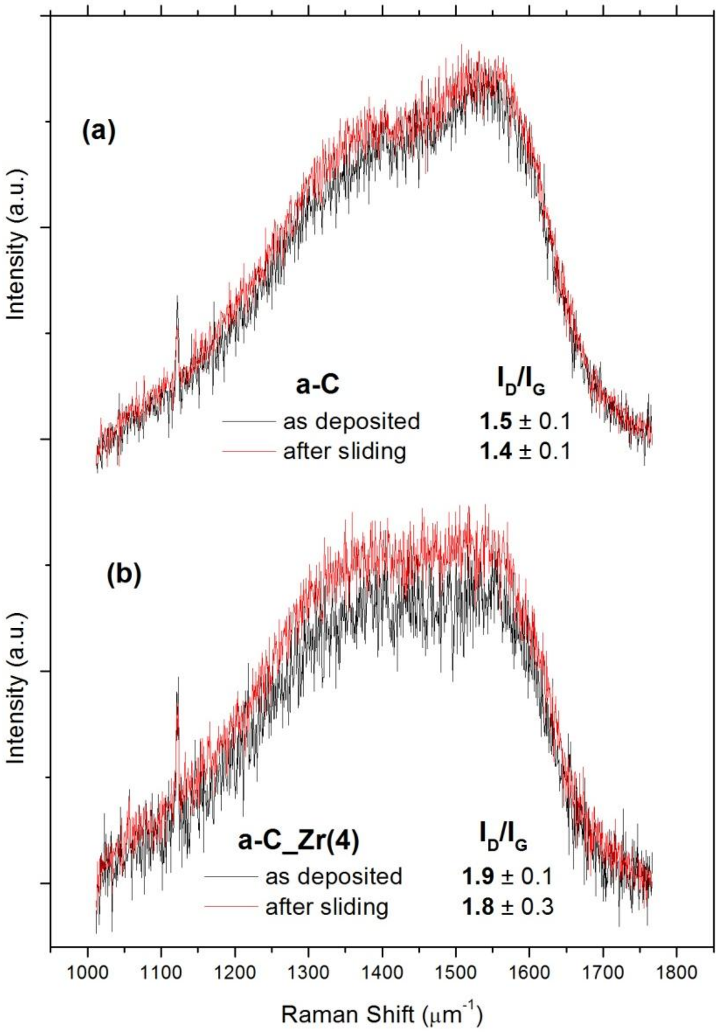

Figure V.5 Raman spectra for (a) a-C and (b) a-C_Zr(4) acquired before and after sliding against UHMWPE under BS. Since a-C_Zr(4) delaminate after 1.2 Mc cycles the acquisition was done near the delaminations zones. The I_D/I_G ratio is also displayed in the insets.

It has been suggested that the most common corrosion mechanisms hindering the cohesion/adhesion of the coatings in contact with body fluids are pitting, crevice corrosion (CC) and stress-corrosion cracking (SCC) [71]. CC and SCC are related to the slow crack advancement or interlayer dissolution resulting in a delayed delamination. On the other hand, pitting is related to surface defects. Since every coating present some surface defects (pinholes, scratches and/or loose grains) [255], the body fluids can penetrate through the coating and act as a corrosive electrolyte forming blisters that, if they exceed a certain dimension, they can enhance the local delamination [122]. Table V.1 shows the defects density on both coatings. The incorporation of Zr decreased the average surface coverage but the defects are larger than on pure a-C films. Thus, it is possible that under body fluid the presence of pinholes may promote SCC and initiate delamination.

Table V.1 Defects density on the coatings.

Sample	Area coverage [%]	Average size [µm]
a-C	7.6±0.7	4.1±0.3
a-C_Zr(4)	2.9±0.4	6.8±1.3

In order to investigate the possibility of SCC further, we followed a complementary method proposed by Hauert and co-workers [198, 254]: by inducing substrate deformation with Rockwell-C indentation and simultaneous immersion of the sample in a protein-containing solution (Figure V.6); SCC should be promoted at the mechanically loaded interface. However, even after 3 days at 37°C (the equivalent of approximately 300,000 testing cycles) the coatings did not reveal any changes in the indentation profile, thus suggesting a more complex failure mechanism than SCC alone. It is also important to point out that the average delamination speed in the body fluid lies on 145 µm.year^{-1} [70], which appears to be very slow to be solely considered as the failure mode. Moreover, frictional induced heating should be also taken into account due to the inevitable thermal unfolding of proteins which led to protein precipitation and rheological changes. In fact, during the test the serum bath changed from translucent reddish-brown tint to creamy yellow color, typical for this type of wear tests [256]. The samples were also immersed at 50°C and 70°C after R-C indentation (see Figure V.6) and again no significant differences were observed as far as the adhesion of the coatings at different temperature was concerned.

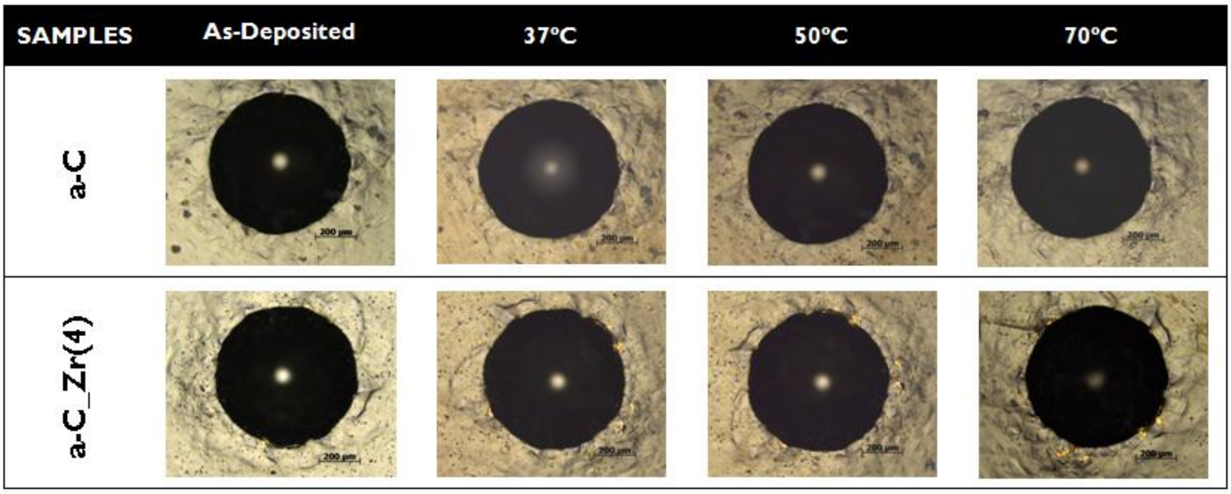

Figure V.6 Optical micrograph top-view of the Rockwell-C indentation test of the a-C and a-C_Zr(4) films after immersion in BS for 72h at 37°C, 50°C and 70°C.

The exact failure mode has not been fully determined. However, it is expected that the presence of protein enhanced the delamination of the coatings [70, 107]. Although protein adsorption can act as a protecting barrier from wear by forming a *compact layer*, especially on Zr-containing films (see Chapter IV), it can entrap the liquid in the crevices. It limits exchange of liquid with the environment and, consequently, lowers the pH, which is known to enhance corrosion [70, 107, 122]. Thus, a less compact protein layer developed on the surface of pure carbon films may be beneficial to prevent the early coating spallation [257]. It is also important to take into account that UHMWPE and PEEK differs in surface energy: UHMWPE is more hydrophobic than PEEK (θ_{UHMWPE} = 87° and θ_{PEEK} = 63°, data from the manufacturers); the adsorption of proteins on UHMWPE will then be favourable (see Chapter IV), and therefore influence the whole frictional and wear behaviours [237]. Finally, a high friction induces an increased shear load in the coating, which reduces the resistance against the coating delamination, particularly in synergy with tribocorrosion. Such phenomena were particularly observed when sliding against PEEK.

3. Conclusions

The use of multidirectional testing was found to be an effective long-term "bench test" for polymer wear evaluation, which was proven by the testing reference materials (UHMWPE/CoCrMo); the results were comparable to those observed *in vivo*. Moreover, the poor tribological properties of Ti6Al4V were also confirmed with such technique and, in an early stage of sliding, the protective role of coatings was demonstrated as well.

Despite the use of an optimized gradient interlayer scheme and an improved adhesion by incorporation of Zr into the C-matrix, the Zr-containing film delaminated when sliding against UHMWPE and PEEK polymers. Moreover, the protein adsorption, which may lead to the decrease of the wear of metallic counterbody, was found to exhibit an opposite trend when sliding against polymers. The presence of proteins in solution plays an important role by acting as a corrosive electrolyte that could enhance the crevice condition in the surface defects. However, this effect could not be solely responsible for coating delamination, since there were no significant differences in the adhesion strength of tested coatings; Hauert's SCC evaluation did not show the decrease in the adhesion as well. The exact mechanism of coating delamination still has to be revealed. However, there is strong evidence that the failure mode is related to the corrosive effect of body fluids in combination with other factors such as cyclic failure.

OUTPUTS AND FUTURE RESEARCH

The main and supporting idea of the research activity carried out in this thesis was that the application of ZrC/a-C(:H) nanocomposite coatings to biomedical implants could increase the life span of joint prosthesis by reducing the level of wear. To the date the use of protective coatings in the biomedical field has been limited due to adhesion problems under the body fluid environment.

In this thesis, hydrogenated and non-hydrogenated Zr-containing nanocomposite and pure carbon coatings were successfully deposited by DC magnetron sputtering onto Ti-based substrates. In light the literature review, several approaches were made to improve the adhesion of the coating to the substrate by introducing metal and/or gradient interlayers. A Ti/TiN/TiNC functional gradient layer was then chosen as an interface adhesive layer, which successfully prevented coating chipping and delamination. Subsequently, the Zr content was optimized in order to deposit nanostructured nc-ZrC/a-C(:H) coatings by co-sputtering a mixed graphite target with embedded Zr pellets. The incorporation of small amount of Zr (as low as 3 at.%) progressively led to the formation of nanocomposite structure consisting of small ZrC nanoparticles randomly dispersed in the a-C matrix. By XRD and TEM investigations, ZrC nanocrystals were found to vary in size in the range of 1 to 2.2 nm as a function of Zr content. The presence of such nanocrystals relaxed the films' stresses by inducing modifications on the C-matrix (graphite-like) and by changing the coatings morphology. When CH_4 was introduced into the chamber, pure carbon films (hydrogenated) revealed a glassy/compact morphology and high stress. The study also revealed that ZrC nanocrystallites strongly influenced the mechanical properties, specially increasing the elastic modulus and lowering the level of residual stress. Coatings with small crystallites revealed a more favourable elastic-plastic response (lower H/E and H^3/E^2), which was particularly important when depositing on low load carrying capacity substrates such as titanium and titanium alloys. Zr alloyed films showed a similar performance in all sliding conditions (ambient air, PS and BSA solutions, sliding against Ti6Al4V), presenting good wear-corrosion behaviour together with strongly reduced wear of counterbody. The physicochemical properties of the coatings were also strongly related to the presence of ZrC nanocrystals and some ZrO_2 that was detected on the surface. In fact, the wettability of the coatings increased with the increase of Zr content, enhancing albumin adsorption. This was particularly important, since the ability to effectively adsorb proteins protected both surfaces from rubbing in direct contact.

Zr alloyed films developed in the frame of this thesis were superior to a-C films as far as the mechanical and tribological properties are concerned. Moreover, their adhesion was improved, by reducing the residual stress, and the wear of the counterbody during sliding test was lower, thanks to increased proteins adsorption. Our findings also indicate that the optimum properties were achieved by incorporation of small amounts of Zr, since smaller crystallites (low Zr content, ~4 at.%) led to better elastic properties and further decreased the counterbody wear. Nevertheless, the a-C_Zr(4) film delaminated when sliding against UHMWPE and PEEK polymers under BSA. Moreover, the protein adsorption, which may lead to the decrease of the wear of metallic counterbody, was found to exhibit an opposite trend when sliding against polymers.

An area that has not been thoroughly explored within our framework is the study of the interface between the adhesion layer and the substrate, as well as the susceptibility of such interface to corrosion in body environment. It is known that an interface material can be formed by cross-contamination of the samples or from residual gas contamination. This interface will have an interfacial material with a different composition, with different mechanical properties and with particularly different corrosion properties, which may influence the overall adhesion of the coatings, especially under liquid media (protein-containing). In this study a rather solid emphasis was given to the optimization of the adhesion layer; however, typical adhesive tests only examine fracture toughness of the interface and do not address any corrosive deterioration. It is then certainly necessary to find an effective method of predicting long-term *in vivo* performance besides the standard adhesion tests and accelerating wear tests such as pin-on-disc or simulators. Therefore, additional investigations of all possible interfaces and interlayer deterioration effects should be done. If all these effects can be measured and predicted, DLC-based coatings could be further improved and coated implants could be eventually successfully applied *in vivo* as long term solution.

REFERENCES

[1] C. L. VanPutte and R. R. Seeley, *Seeley's anatomy & physiology*. New York, NY: McGraw-Hill, 2014.

[2] D. R. Peterson and J. D. Bronzino, *Biomechanics: Principles and Applications, Second Edition*: Taylor & Francis, 2007.

[3] R. Narayan, *Biomedical Materials*: Springer, 2009.

[4] J. A. Buckwalter, T. A. Einhorn, and S. R. Simon, *Orthopaedic Basic Science: Biology and Biomechanics of the Musculoskeletal System*: American Academy of Orthopaedic Surgeons, 2000.

[5] E. N. Marieb and K. Hoehn, *Human Anatomy and Physiology*: Benjamin Cummings, 2010.

[6] R. Kenney, "The synovial joints: a review of the literature" *JAOA: Journal of the American Osteopathic Association,* 65 (1966) 1092.

[7] P. Brinckmann, W. Frobin, and G. Leivseth, *Musculoskeletal Biomechanics*: Thieme, 2002.

[8] N. Palastanga and R. W. Soames, *Anatomy and Human Movement: Structure and function*: Elsevier Health Sciences UK, 2011.

[9] R. Fitzgerald, H. Kaufer, and A. Malkani, *Orthopaedics*. Philadelphia, PA: Mosby, 2002.

[10] "Finer particles allows better coating characterisation with the Calotest," in *Application bulletin*, C. Intruments Ed., 1997.

[11] K. E. Dreinhöfer, P. Dieppe, T. Stürmer, D. Gröber-Grätz, M. Flören, K.-P. Günther*, et al.*, "Indications for total hip replacement: comparison of assessments of orthopaedic surgeons and referring physicians" *Annals of the Rheumatic Diseases,* 65 (2006)1346-1350.

[12] S. M. Kurtz, K. L. Ong, E. Lau, M. Widmer, M. Maravic, E. Gómez-Barrena*, et al.*, "International survey of primary and revision total knee replacement" *International orthopaedics,* 35 (2011) 1783-1789.

[13] *Updated Projections of Total Joint Arthroplasty Demands in America* vol. 96, 2014.

[14] *Impact of the Economic Downturn on Total Joint Replacement Demand in the United States* vol. 96, 2014.

[15] J. H. Dumbleton, *Tribology of Natural and Artificial Joints*: Elsevier Science, 1981.

[16] T. Gluck, "Invaginationsmetode der Osteo- und Arthroplastic" *Klinische Wochenschrift (Berlin),* 33 (1890) 732-757.

[17] *Tribology & Biophysics of Artificial Joints*: Elsevier Science, 2005.

[18] B. D. Ratner, *Biomaterials science: an introduction to materials in medicine*: Academic press, 2004.

[19] S. M. Kurtz, *The UHMWPE handbook: ultra-high molecular weight polyethylene in total joint replacement*: Academic Press, 2004.

[20] B. Wroblewski, "Charnley low-friction arthroplasty: review of the past, present status, and prospects for the future" *Clinical orthopaedics and related research,* 210 (1986) 37-42.

[21] J. Y. Wong and J. D. Bronzino, *Biomaterials*: Taylor & Francis, 2007.

[22] R. W. CRAWFORD and D. W. MURRAY, "Total hip replacement: indications for surgery and risk factors for failure" *Annals of the Rheumatic Diseases,* 56 (1997) 455-457.

[23] D. J. Berry, W. S. Harmsen, M. E. Cabanela, and B. F. Morrey, "Twenty-five-year survivorship of two thousand consecutive primary Charnley total hip replacements factors affecting survivorship of acetabular and femoral components" *The Journal of Bone & Joint Surgery,* 84 (2002) 171-177.

[24] C. S. Ranawat, W. F. Flynn Jr, S. Saddler, K. K. Hansraj, and M. J. Maynard, "Long-term results of the total condylar knee arthroplasty: a 15-year survivorship study" *Clinical orthopaedics and related research,* 286 (1993) 94-102.

[25] S. Ng Man Sun, E. Gillott, J. Bhamra, and T. Briggs, "Implant Use for Primary Hip and Knee Arthroplasty: Are We Getting It Right First Time?" *The Journal of Arthroplasty,* 28 (2013) 908-912.

[26] R. Sonntag, J. Reinders, and J. Kretzer, "What's next? Alternative materials for articulation in total joint replacement" *Acta biomaterialia,* 8 (2012) 2434-2441.

[27] S. Kurtz, E. Lau, K. Ong, K. Zhao, M. Kelly, and K. Bozic, "Future Young Patient Demand for Primary and Revision Joint Replacement: National Projections from 2010 to 2030" *Clinical Orthopaedics and Related Research®,* 467 (2009) 2606-2612.

[28] I. Global Industry Analysts, "Orthopedic Prosthetics - Global Strategic Business Report" 2012.

[29] T. Mallory, *Mallory head hip system*. Cleveland, OH, 1988.

[30] D. F. Dalury, D. L. Pomeroy, R. S. Gorab, and M. J. Adams, "Why are Total Knee Arthroplasties Being Revised?" *The Journal of Arthroplasty,* 28 (2013) 120-121.

[31] W. C. Schroer, K. R. Berend, A. V. Lombardi, C. L. Barnes, M. P. Bolognesi, M. E. Berend, *et al.*, "Why Are Total Knees Failing Today? Etiology of Total Knee Revision in 2010 and 2011" *The Journal of Arthroplasty,* 28 (2013) 116-119.

[32] A. Unsworth, D. Dowson, V. Wright, and D. Koshal, "The frictional Behavior of Human Synovial Joints—Part II: Artificial Joints" *Journal of Tribology,* 97 (1975) 377-381.

[33] I. Catelas, M. Wimmer, and S. Utzschneider, "Polyethylene and metal wear particles: characteristics and biological effects" *Seminars in Immunopathology,* 33 (2011) 257-271.

[34] J. J. Yue, R. Bertagnoli, P. C. McAfee, and H. S. An, *Motion preservation surgery of the spine: advanced techniques and controversies*: Elsevier Health Sciences, 2008.

[35] U. K. Munzinger, J. G. Boldt, and P. A. Keblish, *Primary Knee Arthroplasty*: Springer, 2004.

[36] M. J. Yaszemski, *Biomaterials in Orthopedics*: Taylor & Francis, 2003.

[37] D. M. Brunette, *Titanium in Medicine: Material Science, Surface Science, Engineering, Biological Responses, and Medical Applications*: Springer, 2001.

[38] S. M. Kurtz, *UHMWPE biomaterials handbook: ultra high molecular weight polyethylene in total joint replacement and medical devices*: Academic Press, 2009.

[39] D. L. Wise, *Biomaterials and bioengineering handbook*: Marcel Dekker, 2000.

[40] J. Park, *Bioceramics: Properties, Characterizations, and Applications*: Springer, 2009.

[41] C. N. Kraft, O. Diedrich, B. Burian, O. Schmitt, and M. A. Wimmer, "Microvascular response of striated muscle to metal debris: a comparative in vivo study with titanium and stainless steel" *Journal of Bone & Joint Surgery, British Volume,* 85-B (2003) 133-141.

[42] B. S. Bal, J. Garino, M. Ries, and M. N. Rahaman, "Ceramic Materials in Total Joint Arthroplasty" *Seminars in Arthroplasty,* 17 (2006) 94-101.

[43] T. N. Castillo, D. Kaufman, and W. J. Maloney Iii, "Ceramic-on-Ceramic Total Hip Arthroplasty: Not A New Standard" *Seminars in Arthroplasty* 25 (2014) 116-119.

[44] Y.-S. Park, S.-K. Hwang, W.-S. Choy, Y.-S. Kim, Y.-W. Moon, and S.-J. Lim, "Ceramic failure after total hip arthroplasty with an alumina-on-alumina bearing" *The Journal of Bone & Joint Surgery,* 88 (2006) 780-787.

[45] E. Sariali, S. Klouche, and P. Mamoudy, "Ceramic-on-ceramic total hip arthroplasty: Is squeaking related to an inaccurate three-dimensional hip anatomy reconstruction?" *Orthopaedics & Traumatology: Surgery & Research,* 100 (2014) 437-440.

[46] T. Kiyama, T. L. Kinsey, and O. M. Mahoney, "Can Squeaking With Ceramic-On-Ceramic Hip Articulations In Total Hip Arthroplasty Be Avoided?" *The Journal of Arthroplasty,* 28 (2013) 1015-1020.

[47] J. Olofsson, T. M. Grehk, T. Berlind, C. Persson, S. Jacobson, and H. Engqvist, "Evaluation of silicon nitride as a wear resistant and resorbable alternative for total hip joint replacement" *Biomatter,* 2 (2012) 94-102.

[48] B. S. Bal and M. N. Rahaman, "Orthopedic applications of silicon nitride ceramics," *Acta Biomaterialia,* 8 (2012) 2889-2898.

[49] M. Mazzocchi, D. Gardini, P. L. Traverso, M. G. Faga, and A. Bellosi, "On the possibility of silicon nitride as a ceramic for structural orthopaedic implants. Part II: chemical stability and wear resistance in body environment" *Journal of Materials Science: Materials in Medicine,* 19 (2008) 2889-2901.

[50] C. Howlett, E. McCartney, and W. Ching, "The effect of silicon nitride ceramic on rabbit skeletal cells and tissue: An in vitro and in vivo investigation" *Clinical orthopaedics and related research,* 244 (1989) 293-304.

[51] H. Klemm, "Silicon Nitride for High-Temperature Applications," *Journal of the American Ceramic Society,* 93 (2010) 1501-1522.

[52] M. N. Rahaman, A. Yao, B. S. Bal, J. P. Garino, and M. D. Ries, "Ceramics for prosthetic hip and knee joint replacement" *Journal of the American Ceramic Society,* 90 (2007) 1965-1988.

[53] J.-D. Chang, "Future Bearing Surfaces in Total Hip Arthroplasty" *Clinicas in Orthopedic Surgery,* 6 (2014) 110-116.

[54] A. Mamalis, J. J. Ramsden, A. Grabchenko, L. Lytvynov, V. Filipenko, and S. Lavrynenko, "A novel concept for the manufacture of individual sapphire-metallic hip joint endoprostheses" *Journal of Biological Physics and Chemistry,* 6 (2006) 113-117.

[55] G. Pezzotti and K. Yamamoto, "Artificial hip joints: The biomaterials challenge" *Journal of the Mechanical Behavior of Biomedical Materials,* 31 (2014) 3-20.

[56] O. K. Muratoglu, A. Mark, D. A. Vittetoe, W. H. Harris, and H. E. Rubash, "Polyethylene damage in total knees and use of highly crosslinked polyethylene," *The Journal of Bone & Joint Surgery,* 85 (2003) S7-S13.

[57] S. Scholes and A. Unsworth, "Wear studies on the likely performance of CFR-PEEK/CoCrMo for use as artificial joint bearing materials" *Journal of Materials Science: Materials in Medicine,* 20 (2009)163-170.

[58] S. M. Kurtz and J. N. Devine, "PEEK biomaterials in trauma, orthopedic, and spinal implants," *Biomaterials,* 28 (2007) 4845-4869.

[59] A. Wang, R. Lin, C. Stark, and J. H. Dumbleton, "Suitability and limitations of carbon fiber reinforced PEEK composites as bearing surfaces for total joint replacements" *Wear,* 225–229 (1999) 724-727.

[60] P. Werner, V. Altstädt, R. Jaskulka, O. Jacobs, J. K. W. Sandler, M. S. P. Shaffer, *et al.*, "Tribological behaviour of carbon-nanofibre-reinforced poly(ether ether ketone)" *Wear,* 257 (2004) 1006-1014.

[61] Z. Rasheva, G. Zhang, and T. Burkhart, "A correlation between the tribological and mechanical properties of short carbon fibers reinforced PEEK materials with different fiber orientations" *Tribology International,* 43 (2010) 1430-1437.

[62] N. Hallab, Q.-B. Bao, and T. Brown, "Assessment of epidural versus intradiscal biocompatibility of PEEK implant debris: an in vivo rabbit model" *European Spine Journal,* 22 (2013) 2740-2751.

[63] N. Pace, M. Marinelli, and S. Spurio, "Technical and Histologic Analysis of a Retrieved Carbon Fiber–Reinforced Poly-Ether-Ether-Ketone Composite Alumina-Bearing Liner 28 Months After Implantation" *The Journal of Arthroplasty,* 23 (2008) 151-155.

[64] V. Lorber, A. C. Paulus, A. Buschmann, B. Schmitt, T. M. Grupp, V. Jansson, *et al.*, "Elevated cytokine expression of different PEEK wear particles compared to

UHMWPE in vivo" *Journal of Materials Science: Materials in Medicine,* 25 (2014) 141-149.

[65] S. B. Goodman, Z. Yao, M. Keeney, and F. Yang, "The future of biologic coatings for orthopaedic implants" *Biomaterials,* 34 (2013) 3174-3183.

[66] C. Donnet and A. Erdemir, *Tribology of diamond-like carbon films: fundamentals and applications*: Springer, 2007.

[67] P. Panigrahi, N. Durig, E. Alvarez, and M. K. Harman, "Failure Mechanisms from Unintentional Metal-Metal Articulation After Polyethylene Wear-Through: Analysis of Explanted Knee Prostheses" 2nd International Conference on BioTribology in Toronto, ON, Canada (May 2014).

[68] J. Robertson, "Diamond-like amorphous carbon" *Materials Science and Engineering: R: Reports,* 37 (2002) 129-281.

[69] C. Hinuber, C. Kleemann, R. J. Friederichs, L. Haubold, H. J. Scheibe, T. Schuelke, *et al.*, "Biocompatibility and mechanical properties of diamond-like coatings on cobalt-chromium-molybdenum steel and titanium-aluminum-vanadium biomedical alloys" *Journal* of *Biomedical* Materials Research Part A, 95 (2010) 388-400.

[70] R. Hauert, C. V. Falub, G. Thorwarth, K. Thorwarth, C. Affolter, M. Stiefel, *et al.*, "Retrospective lifetime estimation of failed and explanted diamond-like carbon coated hip joint balls" *Acta Biomaterialia,* 8, (2012) 3170-3176.

[71] R. Hauert, K. Thorwarth, and G. Thorwarth, "An overview on diamond-like carbon coatings in medical applications" *Surface and Coatings Technology,* 233 (2013) 119-130.

[72] M. Amaral, C. Abreu, F. Oliveira, J. Gomes, and R. Silva, "Tribological characterization of NCD in physiological fluids" *Diamond and Related Materials, 17* (2008) 848-852.

[73] M. J. Papo, S. A. Catledge, Y. K. Vohra, and C. Machado, "Mechanical wear behavior of nanocrystalline and multilayer diamond coatings on temporomandibular joint implants" *Journal of Materials Science: Materials in Medicine,* 15 (2004) 773-777.

[74] M. Vila, M. Amaral, F. Oliveira, R. Silva, A. Fernandes, and M. Soares, "Residual stress minimum in nanocrystalline diamond films" *Applied physics letters,* 89 (2006) 093109-093109-3.

[75] M. Ross, C. James, G. Couzens, and J. Klawitter, "19 - Pyrocarbon small joint arthroplasty of the extremities" in *Joint Replacement Technology (Second Edition)*, P. A. Revell, Ed., ed: Woodhead Publishing, 2014, 628-673.

[76] P. A. Revell, *Joint Replacement Technology*: Elsevier Science, 2014.

[77] C. J. Bravo, M. Rizzo, K. B. Hormel, and R. D. Beckenbaugh, "Pyrolytic Carbon Proximal Interphalangeal Joint Arthroplasty: Results With Minimum Two-Year Follow-Up Evaluation" *The Journal of Hand Surgery,* 32 (2007) 1-11.

[78] V. A. Nuñez and N. D. Citron, "Short-term results of the Ascension™ pyrolytic carbon metacarpophalangeal Joint replacement arthroplasty for osteoarthritis" *Chirurgie de la Main,* 24 (2005) 161-164.

[79] L. B. Wall and P. J. Stern, "Clinical and Radiographic Outcomes of Metacarpophalangeal Joint Pyrolytic Carbon Arthroplasty for Osteoarthritis" *The Journal of Hand Surgery,* 38 (2013) 537-543.

[80] M. D. Ries, "Oxidized Zirconium in Total Joint Arthroplasty" *Seminars in Arthroplasty,* 17 (2006) 161-164.

[81] W. L. Jaffe, E. J. Strauss, M. Cardinale, L. Herrera, and F. J. Kummer, "Surface Oxidized Zirconium Total Hip Arthroplasty Head Damage Due to Closed Reduction: Effects on Polyethylene Wear" *The Journal of Arthroplasty,* 24 (2009) 898-902.

[82] K. Holmberg, H. Ronkainen, and A. Matthews, "Tribology of thin coatings" *Ceramics International,* 26 (2000) 787-795.

[83] T. Röstlund, B. Albrektsson, T. Albrektsson, and H. McKellop, "Wear of ion-implanted pure titanium against UHMWPE" *Biomaterials,* 10 (1989) 176-181.

[84] I. J. Leslie, S. Williams, C. Brown, J. Anderson, G. Isaac, P. Hatto, *et al.*, "Surface engineering: a low wearing solution for metal-on-metal hip surface replacements" *Journal of Biomedical Materials Research Part B: Applied Biomaterials,* 90 (2009) 558-65.

[85] M. Pettersson, T. Berlind, S. Schmidt, S. Jacobson, L. Hultman, C. Persson, *et al.*, "Structure and composition of silicon nitride and silicon carbon nitride coatings for joint replacements" *Surface and Coatings Technology,* 235 (2013) 827-834.

[86] M. Pettersson, S. Tkachenko, S. Schmidt, T. Berlind, S. Jacobson, L. Hultman, *et al.*, "Mechanical and tribological behavior of silicon nitride and silicon carbon nitride coatings for total joint replacements" *Journal of the Mechanical Behavior of Biomedical Materials,* 25 (2013) 41-47.

[87] V. Braic, M. Braic, M. Balaceanu, A. Vladescu, C. N. Zoita, I. Titorencu, *et al.*, "(Zr,Ti)CN coatings as potential candidates for biomedical applications" *Surface and Coatings Technology,* 206 (2011) 604-609.

[88] S. Calderon V, R. E. Galindo, J. C. Oliveira, A. Cavaleiro, and S. Carvalho, "Ag^+ release and corrosion behavior of zirconium carbonitride coatings with silver nanoparticles for biomedical devices" *Surface and Coatings Technology,* 222 (2013) 104-111.

[89] I. Ferreri, V. Lopes, S. Calderon V, C. J. Tavares, A. Cavaleiro, and S. Carvalho, "Study of the effect of the silver content on the structural and mechanical behavior of Ag–ZrCN coatings for orthopedic prostheses" *Materials Science and Engineering: C* 42 (2014) 782-790.

[90] S. Calderon V, V. Lopez, C. F. Almeida Alves, A. Cavaleiro, and S. Carvalho, "Structural and electrochemical characterization of Zr–C–N–Ag coatings deposited by DC dual magnetron sputtering" *Corrosion Science,* 80 (2014)229-236.

[91] M. T. Raimondi and R. Pietrabissa, "The in-vivo wear performance of prosthetic femoral heads with titanium nitride coating" *Biomaterials,* 21 (2000) 907-913.

[92] S.-W. Park, H. Kim, and Y. In, "Fracture of titanium nitride-coated femoral component after total knee arthroplasty" *The Knee,* 21 (2014) 871-874.

[93] C. Donnet and A. Erdemir, "Solid lubricant coatings: recent developments and future trends" *Tribology Letters,* 17 (2004) 389-397.

[94] A. Erdemir and C. Donnet, "Tribology of diamond-like carbon films: recent progress and future prospects" *Journal of Physics D: Applied Physics,* 39 (2006) R311.

[95] C. A. Charitidis, "Nanomechanical and nanotribological properties of carbon-based thin films: A review" *International Journal of Refractory Metals and Hard Materials,* 28 (2010) 51-70.

[96] R. Hauert, "A review of modified DLC coatings for biological applications" *Diamond and Related Materials,* 12 (2003) 583-589.

[97] V.-M. Tiainen, "Amorphous carbon as a bio-mechanical coating — mechanical properties and biological applications" *Diamond and Related Materials,* 10 (2001) 153-160.

[98] R. Hauert and U. Müller, "An overview on tailored tribological and biological behavior of diamond-like carbon" *Diamond and Related Materials,* 12 (2003) 171-177.

[99] A. Grill, "Diamond-like carbon coatings as biocompatible materials—an overview" *Diamond and Related Materials,* 12 (2003) 166-170.

[100] G. Dearnaley and J. H. Arps, "Biomedical applications of diamond-like carbon (DLC) coatings: A review" *Surface and Coatings Technology,* 200 (2005) 2518-2524.

[101] R. K. Roy and K. R. Lee, "Biomedical applications of diamond-like carbon coatings: A review" *Journal of Biomedical Materials Research Part B: Applied Biomaterials,* 83 (2007) 72-84.

[102] Y. Ohgoe, K. K. Hirakuri, H. Saitoh, T. Nakahigashi, N. Ohtake, A. Hirata, *et al.*, "Classification of DLC films in terms of biological response" *Surface and Coatings Technology,* 207 (2012) 350-354.

[103] C. A. Love, R. B. Cook, T. J. Harvey, P. A. Dearnley, and R. J. K. Wood, "Diamond like carbon coatings for potential application in biological implants—a review" *Tribology International,* 63 (2013) 141-150.

[104] C. Hee Ay, C. Dipankar, N. Md Julker, and O. Noor Azuan Abu, "Effects of surface coating on reducing friction and wear of orthopaedic implants" *Science and Technology of Advanced Materials,* 15 (2014) 014402.

[105] T. J. Joyce, "Examination of failed ex vivo metal-on-metal metatarsophalangeal prosthesis and comparison with theoretically determined lubrication regimes" *Wear,* 263 (2007) 1050-1054.

[106] G. Taeger, L. E. Podleska, B. Schmidt, M. Ziegler, and D. Nast-Kolb, "Comparison of Diamond-Like-Carbon and Alumina-Oxide articulating with Polyethylene in Total Hip Arthroplasty" *Materialwissenschaft und Werkstofftechnik,* 34 (2003) 1094-1100.

[107] R. Hauert, G. Thorwarth, U. Müller, M. Stiefel, C. V. Falub, K. Thorwarth, *et al.*, "Analysis of the in-vivo failure of the adhesive interlayer for a DLC coated

articulating metatarsophalangeal joint" *Diamond and Related Materials,* 25 (2012) 34-39.

[108] X. L. Peng and T. W. Clyne, "Residual stress and debonding of DLC films on metallic substrates" *Diamond and Related Materials,* 7 (1998) 944-950.

[109] P. Dearnley, A. Neville, S. Turner, H.-J. Scheibe, R. Tietema, R. Tap, *et al.*, "Coatings tribology drivers for high density plasma technologies," *Surface Engineering,* 26 (2010) 80-96.

[110] H. Ronkainen, J. Koskinen, S. Varjus, and K. Holmberg, "Load-carrying capacity evaluation of coating/substrate systems for hydrogen-free and hydrogenated diamond-like carbon films" *Tribology Letters,* 6 (1999) 63-73.

[111] G. Thorwarth, C. V. Falub, U. Müller, B. Weisse, C. Voisard, M. Tobler, *et al.*, "Tribological behavior of DLC-coated articulating joint implants," *Acta Biomaterialia,* 6 (2010) 2335-2341.

[112] C. Wei, Y.-S. Wang, and F.-C. Tai, "The role of metal interlayer on thermal stress, film structure, wettability and hydrogen content for diamond like carbon films on different substrate" *Diamond and Related Materials,* 18 (2009) 407-412.

[113] C. Wei and J.-Y. Yen, "Effect of film thickness and interlayer on the adhesion strength of diamond like carbon films on different substrates" *Diamond and related materials,* 16 (2007) 1325-1330.

[114] K. Thorwarth, G. Thorwarth, R. Figi, B. Weisse, M. Stiefel, and R. Hauert, "On Interlayer Stability and High-Cycle Simulator Performance of Diamond-Like Carbon Layers for Articulating Joint Replacements" *International Journal of Molecular Sciences,* 15 (2014) 10527-10540.

[115] A. Voevodin, M. Capano, S. Laube, M. Donley, and J. Zabinski, "Design of a Ti/TiC/DLC functionally gradient coating based on studies of structural transitions in Ti–C thin films" *Thin Solid Films,* 298 (1997) 107-115.

[116] D.-Y. Wang, Y.-Y. Chang, C.-L. Chang, and Y.-W. Huang, "Deposition of diamond-like carbon films containing metal elements on biomedical Ti alloys" *Surface and Coatings Technology,* 200 (2005) 2175-2180.

[117] K.-L. Choy and E. Felix, "Functionally graded diamond-like carbon coatings on metallic substrates" *Materials Science and Engineering: A,* 278 (2000) 162-169.

[118] B. Tay, Y. Cheng, X. Ding, S. Lau, X. Shi, G. You, *et al.*, "Hard carbon nanocomposite films with low stress" *Diamond and related materials,* 10 (2001) 1082-1087.

[119] A. Voevodin, S. Prasad, and J. Zabinski, "Nanocrystalline carbide/amorphous carbon composites" *Journal of Applied Physics,* 82 (1997) 855-858.

[120] Y. T. Pei, D. Galvan, and J. T. M. De Hosson, "Nanostructure and properties of TiC/a-C:H composite coatings" *Acta Materialia,* 53 (2005) 4505-4521.

[121] M. Morshed, D. Cameron, B. McNamara, and M. Hashmi, "Pre-treatment of substrates for improved adhesion of diamond-like carbon films on surgically implantable metals deposited by saddle field neutral beam source" *Surface and Coatings technology,* 174 (2003) 579-583.

[122] L. Chandra, M. Allen, R. Butter, N. Rushton, A. H. Lettington, and T. W. Clyne, "The effect of exposure to biological fluids on the spallation resistance of diamond-like carbon coatings on metallic substrates" *Journal of Materials Science: Materials in Medicine,* 6 (1995) 581-589.

[123] C. W. Zou, H. J. Wang, L. Feng, and S. W. Xue, "Effects of Cr concentrations on the microstructure, hardness, and temperature-dependent tribological properties of Cr-DLC coatings" *Applied Surface Science,* 286 (2013) 137-141.

[124] C. W. Moura e Silva, J. R. T. Branco, and A. Cavaleiro, "How can H content influence the tribological behaviour of W-containing DLC coatings" *Solid State Sciences,* 11 (2009) 1778-1782.

[125] E. Alakoski, V. M. Tiainen, A. Soininen, and Y. T. Konttinen, "Load-bearing biomedical applications of diamond-like carbon coatings - current status" *The Open Orthopaedics Journal,* 2 (2008) 43-50.

[126] B. Feng, D. M. Cao, W. J. Meng, J. Xu, R. C. Tittsworth, L. E. Rehn, *et al.*, "Characterization of microstructure and mechanical behavior of sputter deposited Ti-containing amorphous carbon coatings" *Surface and Coatings Technology,* 148 (2001) 153-162.

[127] W. J. Meng, R. C. Tittsworth, and L. E. Rehn, "Mechanical properties and microstructure of TiC/amorphous hydrocarbon nanocomposite coatings" *Thin Solid Films,* 377–378 (2000) 222-232.

[128] T. Zehnder and J. Patscheider, "Nanocomposite TiC/a–C:H hard coatings deposited by reactive PVD" *Surface and Coatings Technology,* 133–134 (2000) 138-144.

[129] P. M. Martin, *Handbook of Deposition Technologies for Films and Coatings: Science, Applications and Technology*: Elsevier Science, 2009.

[130] Y. T. Pei, D. Galvan, J. T. M. De Hosson, and C. Strondl, "Advanced TiC/a-C:H nanocomposite coatings deposited by magnetron sputtering" *Journal of the European Ceramic Society,* 26 (2006) 565-570.

[131] Y. T. Pei, C. Q. Chen, K. P. Shaha, J. T. M. De Hosson, J. W. Bradley, S. A. Voronin, *et al.*, "Microstructural control of TiC/a-C nanocomposite coatings with pulsed magnetron sputtering" *Acta Materialia,* 56 (2008) 696-709.

[132] Y. T. Pei, D. Galvan, J. T. M. De Hosson, and A. Cavaleiro, "Nanostructured TiC/a-C coatings for low friction and wear resistant applications" *Surface and Coatings Technology,* 198 (2005) 44-50.

[133] D. Galvan, *Nanocomposite Coatings: Processing, Structure and Tribological Performance*: University Library Groningen, 2007.

[134] K. N. Pandiyaraj, J. Heeg, A. Lampka, F. Junge, T. Barfels, M. Wienecke, *et al.*, "In vitro Cyto and Blood Compatibility of Titanium Containing Diamond-Like Carbon Prepared by Hybrid Sputtering Method" *Plasma Science and Technology,* 14 (2012) 829.

[135] R. Hauert, U. Müller, G. Francz, F. Birchler, A. Schroeder, J. Mayer, *et al.*, "Surface analysis and bioreactions of F and Si containing a-C:H" *Thin Solid Films,* 308–309 (1997) 191-194.

[136] W.-H. Liao, C.-R. Lin, D.-H. Wei, Y.-R. Shen, Y.-C. Li, J.-A. Lee, *et al.*, "Concurrent improvement in biocompatibility and bioinertness of diamond-like carbon films with nitrogen doping" *Journal of Biomedical Materials Research Part A,* 100A (2012) 3151-3156.

[137] M. Cloutier, R. Tolouei, O. Lesage, L. Levesque, S. Turgeon, M. Tatoulian, *et al.*, "On the long term antibacterial features of silver-doped diamondlike carbon coatings deposited via a hybrid plasma process" *Biointerphases,* 9 (2014)029013.

[138] P. Kumar, P. D. Babu, L. Mohan, C. Anandan, and V. K. W. Grips, "Wear and Corrosion Behavior of Zr-Doped DLC on Ti-13Zr-13Nb Biomedical Alloy" *Journal of Materials Engineering and Performance,* 22 (2013) 283-293.

[139] M.-T. Tsai, Y.-Y. Chang, H.-L. Huang, Y.-C. Chen, S.-P. Wang, and C.-H. Lai, "Biological characteristics of human fetal skin fibroblasts and MG-63 human osteosarcoma cells on tantalum-doped carbon films" *Surface and Coatings Technology,* 245 (2014) 16-21.

[140] G. Francz, A. Schroeder, and R. Hauert, "Surface analysis and bioreactions of Ti-and V-containing a-C: H" *Surface and interface analysis,* 28 (1999) 3-7.

[141] R. Hauert, L. Knoblauch-Meyer, G. Francz, A. Schroeder, and E. Wintermantel, "Tailored a-C:H coatings by nanostructuring and alloying" *Surface and Coatings Technology,* 120–121 (1999) 291-296.

[142] P. V. Bharathy, D. Nataraj, P. K. Chu, H. Wang, Q. Yang, M. S. R. N. Kiran, *et al.*, "Effect of titanium incorporation on the structural, mechanical and biocompatible properties of DLC thin films prepared by reactive-biased target ion beam deposition method" *Applied Surface Science,* 257 (2010) 143-150.

[143] A. Bruinink, A. Schroeder, G. Francz, and R. Hauert, "In vitro studies on the effect of delaminated a-C:H film fragments on bone marrow cell cultures" *Biomaterials,* 26 (2005) 3487-3494.

[144] D. B. Lee, M. Roberts, C. G. Bluchel, and R. A. Odell, "Zirconium: biomedical and nephrological applications," *ASAIO Journal,* 56 (2010) 550-556.

[145] N. Stojilovic, E. Bender, and R. Ramsier, "Surface chemistry of zirconium," *Progress in surface science,* vol. 78, pp. 101-184, 2005.

[146] M. Balden, "Characterization of nano-structured W-, Ti-, V-, and Zr-doped carbon films," *Thin Solid Films,* 519 (2011) 4032-4036.

[147] M. Balden, B. Cieciwa, I. Quintana, E. de Juan Pardo, F. Koch, M. Sikora, *et al.*, "Metal-doped carbon films obtained by magnetron sputtering" *Surface and Coatings Technology,* 200 (2005) 413-417.

[148] Y.-Y. Chang, D.-Y. Wang, and W. Wu, "Catalysis effect of metal doping on wear properties of diamond-like carbon films deposited by a cathodic-arc activated deposition process" *Thin Solid Films,* 420–421 (2002) 241-247.

[149] C.-M. Sung and M.-F. Tai, "Reactivities of transition metals with carbon: Implications to the mechanism of diamond synthesis under high pressure" *International Journal of Refractory Metals and Hard Materials,* 15 (1997) 237-256.

[150] W. Kao, "Optimized aC coatings by doping with zirconium for tribological properties and machining performance" *Diamond and Related Materials,* 16 (2007) 1896-1904.

[151] L. Mohan, P. Dilli Babu, P. Kumar, and C. Anandan, "Influence of zirconium doping on the growth of apatite and corrosion behavior of DLC-coated titanium alloy Ti–13Nb–13Zr" *Surface and Interface Analysis,* 45 (2013) 1785-1791.

[152] A. Scarano, M. Piattelli, S. Caputi, G. A. Favero, and A. Piattelli, "Bacterial adhesion on commercially pure titanium and zirconium oxide disks: an in vivo human study" *Journal of Periodontology,* 75 (2004) 292-296.

[153] Y. Tsutsumi, D. Nishimura, H. Doi, N. Nomura, and T. Hanawa, "Difference in surface reactions between titanium and zirconium in Hanks' solution to elucidate mechanism of calcium phosphate formation on titanium using XPS and cathodic polarization" *Materials Science and Engineering: C,* 29 (2009) 1702-1708.

[154] G. Manivasagam, D. Dhinasekaran, and A. Rajamanickam, "Biomedical implants: Corrosion and its prevention-a review" *Recent Patents on Corrosion Science,* 2 (2010) 40-54.

[155] D. Q. Martins, W. R. Osório, M. E. P. Souza, R. Caram, and A. Garcia, "Effects of Zr content on microstructure and corrosion resistance of Ti–30Nb–Zr casting alloys for biomedical applications" *Electrochimica Acta,* 53 (2008) 2809-2817.

[156] L. A. Allen, A. V. Ambardekar, K. M. Devaraj, J. J. Maleszewski, and E. E. Wolfel, "Clinical problem-solving. Missing elements of the history" *The New England Journal of Medicine,* 370 (2014) 559-66.

[157] H. J. Rack and J. I. Qazi, "Titanium alloys for biomedical applications" *Materials Science and Engineering: C,* 26 (2006) 1269-1277.

[158] A. L. Zaitsev, "Mechanisms of hard alloy wear in frictional processes with polymers and composite materials" *Wear,* 162-164 (1999) 40-46.

[159] J. Jiang, R. D. Arnell, and J. Tong, "Some special tribological features of DLC coatings deposited on soft substrates" *Wear,* 211 (1997) 254-264.

[160] Q. Zeng, O. Eryilmaz, and A. Erdemir, "Analysis of plastic deformation in diamond like carbon films–steel substrate system with tribological tests" *Thin Solid Films,* 519 (2011) 3203-3212.

[161] N. P. Barradas and C. Jeynes, "Advanced physics and algorithms in the IBA DataFurnace" *Nuclear Instruments and Methods in Physics Research Section B: Beam Interactions with Materials and Atoms,* 266 (2008) 1875-1879.

[162] Project SPIRIT, avaiable from http://www.spirit-ion.eu/ (Jully 2014).

[163] Joint Committee on ower Diffraction Standards, *Index (inorganic) to the powder diffraction file* Philadelphia, Pa.: American Society for Testing and Materials (ASTM), 2000.

[164] M. Birkholz, *Thin Film Analysis by X-Ray Scattering*: Wiley, 2006.

[165] ESTEEM 2 stems from the successful FP6 project ESTEEM, avaiable from *http://esteem2.eu/* (Jully 2014).

[166] A. Ferrari and J. Robertson, "Interpretation of Raman spectra of disordered and amorphous carbon" *Physical Review B,* 61 (2000) 14095-14107.

[167] M. Żenkiewicz, "Methods for the calculation of surface free energy of solids" *Journal of Achievements in Materials and Manufacturing Engineering,* 24 (2007) 137-145.

[168] C. Jie-Rong and T. Wakida, "Studies on the surface free energy and surface structure of PTFE film treated with low temperature plasma" *Journal of Applied Polymer Science,* 63 (1997) 1733-1739.

[169] G. G. Stoney, "The Tension of Metallic Films Deposited by Electrolysis" *Proceedings of the Royal Society of London. Series A,* 82 (1909)172-175.

[170] W. C. Oliver and G. M. Pharr, "An improved technique for determining hardness and elastic modulus using load and displacement sensing indentation experiments" *Journal of Materials Research,* 7 (1992) 1564-1583.

[171] DIN EN 1071-3, "Advanced technical ceramics - Methods of test for ceramic coatings - Part 3: Determination of adhesion and other mechanical failure modes by a scratch test", European Standard (EN) 2005.

[172] DIN EN 1071-8" Advanced technical ceramics - Methods of test for ceramic coatings - Part 8: Rockwell indentation test for evaluation of adhesion", European Standard (EN), 2002.

[173] T. Arai, H. Fujita, and M. Watanabe, "Evaluation of adhesion strength of thin hard coatings" *Thin Solid Films,* 154 (1987) 387-401.

[174] ASTM F732-00, "Standard test method for wear testing of polymeric materials used in total joint protheses" ASTM International, 2006.

[175] ASTM F2025-00, "Standard practice for gravimetric measurement of polymeric components for wear assessment" ASTM International, 2000.

[176] D. A. Glocker and S. I. Shah, *Handbook of Thin Film Process Technology*: Institute of Physics Publishing, 1995.

[177] K. Bewilogua, R. Wittorf, H. Thomsen, and M. Weber, "DLC based coatings prepared by reactive d.c. magnetron sputtering," *Thin Solid Films,* 447–448 (2004) 142-147.

[178] L. Joska, J. Fojt, O. Mestek, L. Cvrcek, and V. Brezina, "The effect of a DLC coating adhesion layer on the corrosion behavior of titanium and the Ti6Al4V alloy for dental implants" *Surface and Coatings Technology,* 206 (2012) 4899-4906.

[179] G. Welsch, R. Boyer, and E. Collings, *Materials properties handbook: titanium alloys*: ASM international, 1993.

[180] Sputerring Yield Rates, avaiable from http://www.semicore.com/reference/sputtering-yields-reference (Jully 2014)

[181] O. A. Fouad, A. K. Rumaiz, and S. I. Shah, "Reactive sputtering of titanium in Ar/CH4 gas mixture: Target poisoning and film characteristics" *Thin Solid Films,* 517 (2009) 5689-5694.

[182] M. Ban and T. Hasegawa, "Internal stress reduction by incorporation of silicon in diamond-like carbon films" *Surface and Coatings Technology,* 162 (2003) 1-5.

[183] A. Kaloyeros, M. Hoffman, and W. S. Williams, "Amorphous transition metal carbides" *Thin Solid Films,* 141, (1986) 237-250.

[184] M. Andersson, S. Urbonaite, E. Lewin, and U. Jansson, "Magnetron sputtering of Zr–Si–C thin films," *Thin Solid Films,* 520 (2012) 6375-6381.

[185] W. Gulbiński, S. Mathur, H. Shen, T. Suszko, A. Gilewicz, and B. Warcholiński, "Evaluation of phase, composition, microstructure and properties in TiC/a-C:H thin films deposited by magnetron sputtering" *Applied Surface Science,* 239 (2005) 302-310.

[186] U. Jansson and E. Lewin, "Sputter deposition of transition-metal carbide films — A critical review from a chemical perspective" *Thin Solid Films,* 536 (2013) 1-24.

[187] E. Lewin, P. O. Å. Persson, M. Lattemann, M. Stüber, M. Gorgoi, A. Sandell, *et al.*, "On the origin of a third spectral component of C1s XPS-spectra for nc-TiC/aC nanocomposite thin films" *Surface and Coatings Technology,* 202 (2008) 3563-3570.

[188] M. Magnuson, E. Lewin, L. Hultman, and U. Jansson, "Electronic structure and chemical bonding of nanocrystalline-TiC/amorphous-C nanocomposites" *Physical Review B,* 80 (2009) 235108.

[189] Q. N. Meng, M. Wen, F. Mao, N. Nedfors, U. Jansson, and W. T. Zheng, "Deposition and characterization of reactive magnetron sputtered zirconium carbide films" *Surface and Coatings Technology,* 232 (2013) 876-883.

[190] E. Lewin, M. Råsander, M. Klintenberg, A. Bergman, O. Eriksson, and U. Jansson, "Design of the lattice parameter of embedded nanoparticles" *Chemical Physics Letters,* 496 (2010) 95-99.

[191] C. Adelhelm, M. Balden, M. Rinke, and M. Stueber, "Influence of doping (Ti, V, Zr, W) and annealing on the sp2 carbon structure of amorphous carbon films" *Journal of Applied Physics,* 105 (2009) 033522.

[192] T. Polcar, T. Vitu, L. Cvrcek, R. Novak, J. Vyskocil, and A. Cavaleiro, "Tribological behaviour of nanostructured Ti-C:H coatings for biomedical applications" *Solid State Sciences,* 11 (2009) 1757-1761.

[193] W. Lengauer and A. Eder, "Carbides: Transition Metal Solid-State Chemistry" in *Encyclopedia of Inorganic Chemistry*, ed: John Wiley & Sons, Ltd, 2006.

[194] A. Leyland and A. Matthews, "On the significance of the H/E ratio in wear control: a nanocomposite coating approach to optimised tribological behaviour" *Wear,* 246 (2000) 1-11.

[195] Y. Liu and E. I. Meletis, "Tribological behavior of DLC coatings with functionally gradient interfaces" *Surface and Coatings Technology,* 153 (2002) 178-183.

[196] A. P. Zhilyaev and T. G. Langdon, "Using high-pressure torsion for metal processing: Fundamentals and applications" *Progress in Materials Science,* 53 (2008) 893-979.

[197] J.-G. Kim, K.-R. Lee, and S.-J. Yang, "Wear-corrosion performance of Si-DLC coatings on Ti-6Al-4V substrate" *Journal of Biomedical Materials Research Part A,* 86A (2008) 41-47.

[198] C. V. Falub, G. Thorwarth, C. Affolter, U. Müller, C. Voisard, and R. Hauert, "A quantitative in vitro method to predict the adhesion lifetime of diamond-like carbon thin films on biomedical implants" *Acta Biomaterialia,* 5 (2009) 3086-3097.

[199] M. D. Drory and J. W. Hutchinson, "Measurement of the Adhesion of a Brittle Film on a Ductile Substrate by Indentation," *Proceedings of The Royal Society A: Mathematical, Physical and Engineering Sciences,* 452 (1996) 2319-2341.

[200] R. H. Dauskardt, Q. Ma, and N. Krishna, "Adhesion and debonding of multi-layer thin film structures" *Engineering Fracture Mechanics,* 61 (1998) 141-162.

[201] R. Hang and Y. Qi, "A study of biotribological behavior of DLC coatings and its influence to human serum albumin" *Diamond and Related Materials,* 19 (2010) 62-66, 2010.

[202] H. Ronkainen, S. Varjus, and K. Holmberg, "Friction and wear properties in dry, water- and oil-lubricated DLC against alumina and DLC against steel contacts" *Wear,* 222 (1998) 120-128.

[203] E. Rabinowicz, "Practical uses of the surface energy criterion," *Wear,* 7 (1964) 9-22.

[204] J. Ramsden, *Biomedical Surfaces*, Artech House Incorporated, 2008.

[205] F. Rupp, R. A. Gittens, L. Scheideler, A. Marmur, B. D. Boyan, Z. Schwartz*, et al.*, "A review on the wettability of dental implant surfaces I: Theoretical and experimental aspects" *Acta Biomaterialia,* 10 (2014) 2894-2906.

[206] G. Tepe, J. Schmehl, H. P. Wendel, S. Schaffner, S. Heller, M. Gianotti*, et al.*, "Reduced thrombogenicity of nitinol stents--in vitro evaluation of different surface modifications and coatings" *Biomaterials,* 27 (2006) 643-650.

[207] C. Desrousseaux, V. Sautou, S. Descamps, and O. Traoré, "Modification of the surfaces of medical devices to prevent microbial adhesion and biofilm formation" *Journal of Hospital Infection,* 85 (2013) 87-93.

[208] A. Wennerberg and T. Albrektsson, "Effects of titanium surface topography on bone integration: a systematic review" *Clinical Oral Implants Research,* 20 S4 (2009) 172-84.

[209] S. Bauer, P. Schmuki, K. von der Mark, and J. Park, "Engineering biocompatible implant surfaces: Part I: Materials and surfaces," *Progress in Materials Science,* 58 (2013) 261-326.

[210] P. Roach, D. Farrar, and C. C. Perry, "Interpretation of Protein Adsorption: Surface-Induced Conformational Changes" *Journal of The American Chemical Society,* 127 (2005) 8168-8173.

[211] J. D. Andrade and V. Hlady, "Protein adsorption and materials biocompatibility: A tutorial review and suggested hypotheses" in *Biopolymers/Non-Exclusion HPLC.* 79, ed: Springer Berlin Heidelberg, 1986, 1-63.

[212] K. Nakanishi, T. Sakiyama, and K. Imamura, "On the adsorption of proteins on solid surfaces, a common but very complicated phenomenon" *Journal of Bioscience and Bioengineering,* 91 (2001) 233-244.

[213] A. P. Serro, M. P. Gispert, M. C. L. Martins, P. Brogueira, R. Colaço, and B. Saramago, "Adsorption of albumin on prosthetic materials: Implication for tribological behavior" *Journal of Biomedical Materials Research Part A,* 78A (2006) 581-589.

[214] T. Horbett, L. Brash John, and W. Norde, Eds., *Proteins at Interfaces III State of the Art* (ACS Symposium Series 1120). American Chemical Society, 2012.

[215] R. A. Gittens, L. Scheideler, F. Rupp, S. L. Hyzy, J. Geis-Gerstorfer, Z. Schwartz, *et al.*, "A review on the wettability of dental implant surfaces II: Biological and clinical aspects" *Acta Biomaterialia,* 10 (2014) 2907-2918.

[216] E. A. Vogler, "Structure and reactivity of water at biomaterial surfaces" *Advances in Colloid and Interface Science,* 74 (1998) 69-117.

[217] E. M. Christenson, K. S. Anseth, J. J. J. P. van den Beucken, C. K. Chan, B. Ercan, J. A. Jansen, *et al.*, "Nanobiomaterial applications in orthopedics" *Journal of Orthopaedic Research,* 25 (2007) 11-22.

[218] C. Wei, W.-J. Pan, and M.-S. Hung, "The effects of substrate roughness and associated surface properties on the biocompatibility of diamond-like carbon films" *Surface and Coatings Technology,* 224 (2013) 8-17.

[219] M. Stüber, L. Niederberger, F. Danneil, H. Leiste, S. Ulrich, A. Welle, *et al.*, "Surface Topography, Surface Energy and Wettability of Magnetron-Sputtered Amorphous Carbon (a-C) Films and Their Relevance for Platelet Adhesion" *Advanced Engineering Materials,* 9 (2007) 1114-1122.

[220] J. S. Chen, S. P. Lau, Z. Sun, G. Y. Chen, Y. J. Li, B. K. Tay, *et al.*, "Metal-containing amorphous carbon films for hydrophobic application" *Thin Solid Films,* 398–399 (2001) 110-115.

[221] G. Fanali, A. di Masi, V. Trezza, M. Marino, M. Fasano, and P. Ascenzi, "Human serum albumin: From bench to bedside," *Molecular Aspects of Medicine,* 33 (2012) 209-290.

[222] L. Paul and C. P. Sharma, "Preferential adsorption of albumin onto a polymer surface: An understanding," *Journal of Colloid and Interface Science,* 84 (1981) 546-549.

[223] J. M. Berg, L. G. T. Eriksson, P. M. Claesson, and K. G. N. Borve, "Three-Component Langmuir-Blodgett Films with a Controllable Degree of Polarity" *Langmuir,* 10 (1994) 1225-1234.

[224] J. E. Puskas, Y. Dahman, A. Margaritis, and M. Cunningham, "Novel Thymine-Functionalized Polystyrenes for Applications in Biotechnology. 2. Adsorption of Model Proteins" *Biomacromolecules,* 5 (2004) 1412-1421.

[225] S. R. Sousa, P. Moradas-Ferreira, B. Saramago, L. V. Melo, and M. A. Barbosa, "Human serum albumin adsorption on TiO2 from single protein solutions and from plasma," *Langmuir,* 20 (2004) 9745-54.

[226] M. Soderquist and A. Walton, "Structural changes in proteins adsorbed on polymer surfaces," *Journal of Colloid and Interface Science,* 75 (1980) 386-397.

[227] M. Rabe, D. Verdes, and S. Seeger, "Understanding protein adsorption phenomena at solid surfaces" *Advances in Colloid and Interface Science,* 162 (2011) 87-106.

[228] C. Gruian, E. Vanea, S. Simon, and V. Simon, "FTIR and XPS studies of protein adsorption onto functionalized bioactive glass" *Biochimica et Biophysica Acta (BBA) - Proteins and Proteomics,* 1824 (21012) 873-881.

[229] E. Vanea and V. Simon, "XPS study of protein adsorption onto nanocrystalline aluminosilicate microparticles" *Applied Surface Science,* 257 (2011) 2346-2352.

[230] R. W. Paynter, B. D. Ratner, T. A. Horbett, and H. R. Thomas, "XPS studies on the organization of adsorbed protein films on fluoropolymers" *Journal of Colloid and Interface Science,* 101 (1984) 233-245.

[231] K. Hirayama, S. Akashi, M. Furuya, and K.-i. Fukuhara, "Rapid confirmation and revision of the primary structure of bovine serum albumin by ESIMS and frit-FAB LC/MS" *Biochemical and Biophysical Research Communications,* 173 (1990) 639-646.

[232] C. Myant, R. Underwood, J. Fan, and P. M. Cann, "Lubrication of metal-on-metal hip joints: The effect of protein content and load on film formation and wear" *Journal of the Mechanical Behavior of Biomedical Materials,* 6 (2012) 30-40.

[233] M. A. Wimmer, A. Fischer, R. Büscher, R. Pourzal, C. Sprecher, R. Hauert, *et al.*, "Wear mechanisms in metal-on-metal bearings: The importance of tribochemical reaction layers" *Journal of Orthopaedic Research,* 28 (2010) 436-443.

[234] M. J. Runa, M. T. Mathew, and L. A. Rocha, "Tribocorrosion response of the Ti6Al4V alloys commonly used in femoral stems" *Tribology International,* 68 (2013) 85-93.

[235] S. Karimi, T. Nickchi, and A. Alfantazi, "Effects of bovine serum albumin on the corrosion behaviour of AISI 316L, Co–28Cr–6Mo, and Ti–6Al–4V alloys in phosphate buffered saline solutions" *Corrosion Science,* 53 (2011) 3262-3272.

[236] C. Myant and P. Cann, "On the matter of synovial fluid lubrication: Implications for Metal-on-Metal hip tribology" *Journal of the Mechanical Behavior of Biomedical Materials,* 34 (2014) 338-348.

[237] M. P. Heuberger, M. R. Widmer, E. Zobeley, R. Glockshuber, and N. D. Spencer, "Protein-mediated boundary lubrication in arthroplasty," *Biomaterials,* 26 (2005) 1165-1173.

[238] H. Mishina and M. Kojima, "Changes in human serum albumin on arthroplasty frictional surfaces" *Wear,* 265 (2008) 655-663.

[239] C. R. Bragdon, D. O. O'Connor, J. D. Lowenstein, M. Jasty, and W. D. Syniuta, "The importance of multidirectional motion on the wear of polyethylene" *Proceedings of the Instition of Mechanical Engineers Part H,* 210 (1996) 157-65.

[240] V. Saikko, "A multidirectional motion pin-on-disk wear test method for prosthetic joint materials" *Journal of Biomedical Materials Research,* 41 (1998) 58-64.

[241] A. Wang, C. Stark, and J. H. Dumbleton, "Mechanistic and morphological origins of ultra-high molecular weight polyethylene wear debris in total joint

replacement prostheses" *Proceedings of the Instition of Mechanical Engineers Part H,* 210 (1996) 141-55.

[242] L. Franta, J. Fojt, L. Joska, J. Kronek, L. Cvrcek, J. Vyskocil, *et al.*, "Hinge-type knee prosthesis wear tests with a mechanical load and corrosion properties monitoring" *Tribology International,* 63 (2013) 61-65.

[243] K. A. Laux and C. J. Schwartz, "Influence of linear reciprocating and multi-directional sliding on PEEK wear performance and transfer film formation" *Wear,* 301 (2013) 727-734.

[244] S. Ge, S. Wang, N. Gitis, M. Vinogradov, and J. Xiao, "Wear behavior and wear debris distribution of UHMWPE against Si3N4 ball in bi-directional sliding," *Wear,* 264 (2008) 571-578.

[245] M. E. Turell, G. E. Friedlaender, A. Wang, T. S. Thornhill, and A. Bellare, "The effect of counterface roughness on the wear of UHMWPE for rectangular wear paths" *Wear,* 259 (2005) 984-991.

[246] A. Wang, "A unified theory of wear for ultra-high molecular weight polyethylene in multi-directional sliding" *Wear,* 248 (2001) 38-47.

[247] J. P. Davim and N. Marques, "Evaluation of Tribological Behaviour of Polymeric Materials for Hip Prostheses Application" *Tribology Letters,* 11 (2001) 91-94.

[248] J. P. Davim, N. Marques, and A. M. Baptista, "Effect of carbon fibre reinforcement in the frictional behaviour of Peek in a water lubricated environment" *Wear,* 251 (2001) 1100-1104.

[249] J. Geringer, W. Tatkiewicz, and G. Rouchouse, "Wear behavior of PAEK, poly(aryl-ether-ketone), under physiological conditions, outlooks for performing these materials in the field of hip prosthesis" *Wear,* 271 (2011) 2793-2803.

[250] J. R. Atkinson, D. Dowson, J. H. Isaac, and B. M. Wroblewski, "Laboratory wear tests and clinical observations of the penetration of femoral heads into acetabular cups in total replacement hip joints: III: The measurement of internal volume changes in explanted Charnley sockets after 2–16 years in vivo and the determination of wear factors" *Wear,* 104 (1985) 225-244.

[251] K. H. Fitzgerald RH, Malkani AL, *Orthopaedics*. Philadelphia: Mosby, 2002.

[252] W. Y. Li, H. Dong, and W. Shi, "New insights into wear of Ti6Al4V by ultra-high molecular weight polyethylene under water lubricated conditions" *Wear,* 250 (2001) 553-560.

[253] T. Xu and L. Pruitt, "Diamond-like carbon coatings for orthopaedic applications: an evaluation of tribological performance" *Journal of Materials Science: Materials in Medicine,* 10 (1999) 83-90.

[254] C. V. Falub, U. Müller, G. Thorwarth, M. Parlinska-Wojtan, C. Voisard, and R. Hauert, "In vitro studies of the adhesion of diamond-like carbon thin films on CoCrMo biomedical implant alloy" *Acta Materialia,* 59 (2011) 4678-4689.

[255] J. Vetter, M. Stüber, and S. Ulrich, "Growth effects in carbon coatings deposited by magnetron sputtering" *Surface and Coatings Technology,* 168 (2003) 169-178.

[256] M. R. Hill, S. A. Catledge, V. Konovalov, W. C. Clem, S. A. Chowdhury, B. S. Etheridge, *et al.*, "Tribological Evaluation of Nanostructured Diamond Coatings and CoCr against Ultra-High Molecular Weight Polyethylene" *Journal of Biomedical Materials Research Part B, Applied Biomaterials,* 85 (2008) 140-148.

[257] R. Crockett, M. Roba, M. Naka, B. Gasser, D. Delfosse, V. Frauchiger, *et al.*, "Friction, lubrication, and polymer transfer between UHMWPE and CoCrMo hip-implant materials: A fluorescence microscopy study" *Journal of Biomedical Materials Research Part A,* 89A (2009) 1011-1018.

PAPER I

DLC(H) Doped with Zr Coatings for Orthopaedics Applications: Adhesion Properties

A. Escudeiro, T. Polcar and A. Cavaleiro

55th Annual Technical Conference Proceedings, ed: Society of Vaccum Coaters, **2012**

DLC(H) Doped With Zr Coatings for Orthopaedics Applications: Adhesion Properties

A. Escudeiro, SEG-CEMUC – Department of Mechanical Engineering, University of Coimbra, Coimbra, Portugal; T. Polcar, National Centre for Advanced Tribology (nCATS), School of Engineering Sciences, University of Southampton, Highfield, Southampton, United Kingdom and Department of Control Engineering, Czech Technical University in Prague, Prague, Czech Republic; and A. Cavaleiro, SEG-CEMUC – Department of Mechanical Engineering, University of Coimbra, Coimbra, Portugal

ABSTRACT

DLC coatings doped with Zr were deposited by dc unbalanced magnetron sputtering in Ar (non-hydrogenated) and Ar+CH_4 (hydrogenated) atmosphere onto two different substrates: Ti grade 2 (pure titanium) and Ti grade 5 (Ti6Al4V). To improve adhesion between the films and substrates a functional Ti-based gradient layer was deposited (~300nm). Fundamental properties of coating were measured, such as chemical composition, structure, and mechanical properties. The main attention was paid to the adhesion testing evaluated using both Rockwell indentation and scratch test. It was shown that doping with Zr increased the adhesion between the coating and the substrate.

INTRODUCTION

The production of wear particles from metal-on-metal (MoM) and metal-on-polyethylene (MoP) knee joint replacement and their adverse effects on the body has been a continual problem since the first implants were applied. Surface modification of the metallic bearing surfaces is expected to have the potential to reduce the generation of wear particles and, subsequently, to minimize aseptic loosening of the prosthesis. DLC ("diamond-like" carbon) coatings have been subject to a number of studies over the past years due to their excellent properties, such as wear, corrosion resistance, and biocompatibility. However, despite promising lab testing, these films have so far limited success *in vivo*. The major issue associated to these coatings is poor adhesion to the metallic substrates as a result of high residual stresses and poor chemical bonding between the film and substrate. Thus, partial delamination and consequent failure of the film cause failure of the implant [1, 2].

Among the metallic materials use for implants, Co-Cr alloy has been the standard material for hard bearing joint replacement components due to the superior tribological performances. However, it has been shown that Co- and Cr-ions released during wear and tribocorrosion processes are toxic or even carcinogenic [3, 4]. Compared to Co-Cr alloys, Ti grade 2 and 5 ELI show higher fatigue resistance and particularly excellent *in vivo* corrosion resistance [5, 6]. On the other hand, Ti-alloys exhibit low wear resistance due to low hardness (Ti grade 2 – 145 HV; Ti grade 5 ELI – 349 HV) and Young modulus (103-120 GPa) [7, 8]. Thus, to use Ti-alloys in demanding implant applications, surface modification is required to enhance the surface hardness and thus wear resistance. Obviously the low friction coefficient is one of the requirements. The core objective of this work is the evaluation of the adhesion strength of zirconium-doped DLC coatings deposited by magnetron sputtering on two different Ti-based substrates.

MATERIALS AND METHODS

The coatings were deposited using dc dual magnetron sputtering in an Ar atmosphere (non-reactive process) and Ar+CH_4 to produce non-hydrogenated and hydrogenated coatings, respectively. Two targets were used: Ti, to deposit an interface layer, and graphite, to prepare functional film. Zirconium was introduced using pellets embedded into the erosion zone of graphite target. The substrates (Ti grade 2 and Ti grade 5 ELI) were polished to a roughness of Ra≤50 nm and cleaned in an ultrasonic bath in acetone, ethanol and distilled water for 15 min each. The substrates were then etched via Ar ion bombardment at a substrate bias voltage of -650V. Table 1 summarizes the deposition parameters. The work pressure was kept constant at approximately 0.38 Pa; a pulsed bias voltage of -50V and frequency of 250 kHz was applied. A pure Ti/TiN bilayer and a grade TiNC layer, with a total thickness of about 550 nm, were deposited in order to improve the adhesion. The thickness of the coating was set to approximately 1.4 µm by adjusting the deposition time. To facilitate the reading, the coatings are denominated as DLC-Zr(X) and DLC:H-Zr(X) for doped films (X is the Zr content) and DLC and DLC:H the pure ones, the H is related to the hydrogenated films.

Table 1: Deposition parameters of DLC-Zr(X) and DLC-Zr:H(X) coatings.

Parameters	DLC-Zr(X)	DLC-Zr:H(X)
Reactive gas flow (sccm)	---	5
Ar flow (sccm)	45	40
Chamber pressure (Pa)	1.48×10^{-3}	
Working Pressure (Pa)	0.38	
Substrate bias (V)	-50	
Graphite doped target (W/mm^2)	0.075	

The chemical composition and structure of the coatings were evaluated by electron probe microanalysis (EPMA) and X-ray diffraction (XRD), respectively. The molecular structure characterization was carried out by Raman spectroscopy with a laser wavelength of 532 nm. The hardness and Young modulus were measured by a depth-sensing nanoindentation test using a Berkovich indenter. The compressive stress of the films was calculated from Stoney's equation using the curvature of the substrate (SS 304), measured by an optical profilometer.

The coatings adhesion was evaluated using both Rockwell C indentation and scratch test, standard techniques commonly used to quantify the interfacial strength of coating-substrate systems. During Rockwell C adhesion test, a cone-shaped diamond 120° tip was perpendicularly indented into the coating causing layer damage at the boundary of the indentation. The results of the test were qualitatively evaluated by comparing the optical microscope images of the crack network and the degree of delamination to an adhesion quality chart and classifying the images into six categories from HF1-HF6 [9]. The coating adhesion was also evaluated using scratch test using a spherical diamond 120° tip with a diameter of 0.2 mm. The indentations were performed perpendicularly to the coating surface at 10 N/mm with a range of 2-50N.

RESULTS AND DISCUSSION

Deposition Process, Film Structure and Composition

The coatings were produced by reactive (Ar+CH_4) and non reactive sputtering (Ar) deposition in order to obtain hydrogenated and non-hydrogenated films, respectively. By increasing the number of Zr pellets embedded into carbon target, the zirconium content increased to a maximum of 9 at.% (Table 2). Due to higher deposition rate of Zr pellets compared to C target, the deposition rate of non-hydrogenated films increased with number of zirconium pellets. The deposition rate of DLC(H) film was almost two times higher than that of DLC due to additional source of carbon in the chamber. However, the deposition rate was almost independent of the pellets number when the sputtering was carried out in a reactive atmosphere. In the presence of methane a compound layer is formed on the pellets surface significantly decreasing deposition rate (so-called 'poisoning effect'). Moreover, direct deposition of hydrocarbon from the plasma [10-12] could be expected. The deposition rate increased only for the highest number of pellets probably due to higher Zr surface area; CH_4 flow is then not sufficient to completely switch the sputtering from metallic to compound regime.

Table 2: Summary of structural, chemical and mechanical properties of the coatings.

Sample		**DLC**	**DLC_ Zr(3)**	**DLC_ Zr(7)**	**DLC_ Zr(9)**	**DLC:H**	**DLC:H_ Zr(4)**	**DLC:H_ Zr(5)**	**DLC:H_ Zr(8)**
Zr Content (at.%)		-	3	7	9	-	4	5	8
Dep. Rate (nm/min)		4.6	5.0	7.3	8.3	8.8	8.5	10.0	12.0
Hardness (GPa)		10.9±0.5	10.4±0.4	11.9±0.6	10.7±0.5	8.9±0.3	10.0±1.6	11.4±0.4	12.2±0.5
Young Modulus (GPa)		94.0±01	109.9±3.1	126.0±2.6	133.3±2.2	69.9±0.3	87.3±2.6	103.1±1.2	114.1±3.4
D peak (cm^{-1})		1374	1373	1371	1374	1378	1384	1389	1379
G peak (cm^{-1})		1560	1558	1551	1554	1549	1550	1551	1548
I_D/I_G		1.6	1.9	2.3	2.3	0.7	0.8	1.0	1.0
Ti Grade 2	Lc_1 (N)	4.5±0.2	4.4±0.4	4.4±0.4	5.1±0.6	4.8±1.6	4.4±1.2	4.6±0.2	4.8±0.5
	Lc_2 (N)	7.9±2.5	8.0±1.8	9.3±0.9	7.5±2.4	6.3±2.5	8.4±0.1	10.2±0.1	5.7±0.6
	Lc3 (N)	41.9±11.5	35.5±3.2	>50	13.5±2.1	12.0±6.3	38.9±8.4	35.7±1.1	14.4±1.4
	R-C test	HF3	HF3	HF2	HF2	HF5	HF3	HF3	HF5
Ti Grade 5 ELI	Lc_1 (N)	7.9±2.1	6.0±0.8	7.4±0.7	11.4±0.7	5.6±1.6	7.9±0.5	6.7±0.7	6.3±0.6
	Lc_2 (N)	13.7±1.8	13.2±1.4	10.7±1.1	13.2±2.4	12.1±3.3	10.9±1.3	12.2±1.6	12.8±1.3
	Lc3 (N)	>50	37.1±7.1	>50	19.0±8.0	>50	38.7±1.5	37.8±0.6	>50
	R-C test	HF3	HF3	HF3	HF2	HF3	HF3	HF3	HF3

[a] *Lc_1, lower critical load is defined as the load where the first cracks occur (cohesive failure) and Lc_2, upper critical load, is defined as the load where the first spallation/flaking on the film is observed (adhesive failure). L_{c3} is then defined as the load where the coating is penetrated in the scratch [13].*

[b] *HF1-HF4 is typically considered as an acceptable failure, whereasHF5-*

XRD diffractograms clearly show the amorphous structure of the Zr-free coatings, where the only visible peaks were from the interlayer/gradient layer (Figure 1). High Zr content films showed broad peak identified as ZrC and thus indicating the presence of ZrC nanocrystalline structures embedded into the C-matrix.

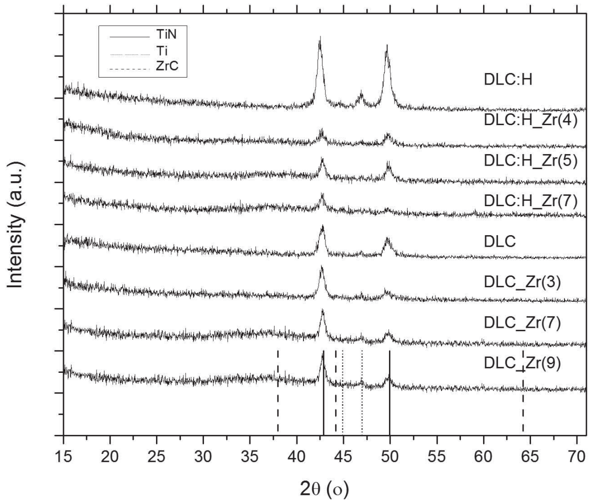

Figure 1: XRD diffractograms and phase labelling of the pure DLC and Zr-doped hydrogenated and non-hydrogenated films.

The deconvoluted positions of G (Graphite) and D (Disorder) peaks from the Raman spectra are shown in Table 2. The peaks were fitted using two Gaussian peaks [14]. For both hydrogenated and non-hydrogenated coatings the co-sputtering with Zr significantly influenced the structure of the carbon matrix. I_D/I_G ratio increased with the Zr content indication an increase of the carbon clustering (Table 2). XRD diffractograms showed a very broad peak at approx. 37 2 theta, i.e. close to the position of ZrC (111) (ICCD card n. 74-1221), as seen by Kao [15]. Coatings with high zirconium content are thus composed of nanocrystalline ZrC embedded into the C-amorphous matrix. Bewilogua et al [12] reported the similar structures for several metal-doped DLC films. Furthermore, the injection of CH4 into the chamber resulted in saturation of sp^2-C bonds with H converting than into sp^3 C-H sites, which could eventually form soft polymeric chains [16].

Measured Raman spectra were used to estimate hydrogen content in the coatings. The typical signature of hydrogen in visible Raman spectra is the presence of the photoluminescence background (PL); it increases with the H content. A good estimate of H content could be obtained from the ratio between the slope, m, of the fitted linear background and the intensity of the G peak, m/I(G) [17]. The analysis gave hydrogen content of metal-free hydrogenated coating (DLC:H) close to 28 at.%. We validate the method using similar films [18]; the H obtained from Raman spectra, ~34 at.%, was almost identical with direct measurements of H content by ERDA (~33 at.%).

Coating Adhesion and Cohesion

Table 2 summarizes the main results of both adhesion tests performed. As expected the adhesion results were significant sensitive to the substrate used (Ti grade 2 and Ti grade 5 ELI).

Rockwell C indentation test is a qualitative adhesion method widely used in industry. The contact geometry in combination with the intense load transfer induces extreme shear stresses at the interface. Figure 2 shows the Rockwell indentations of the coatings (hydrogenated and non-hydrogenated). The adhesion decreased when H was incorporated into the C matrix. The compressive residual stress was similar for all coatings, about 2 GPa; therefore, the residual stress cannot be a key factor influencing coating adhesion. It is important to notice that hydrogenated films presented lower hardness, Young modulus and lower I_D/I_G ratio, which results in an inadequate load support of the coating particularly on soft

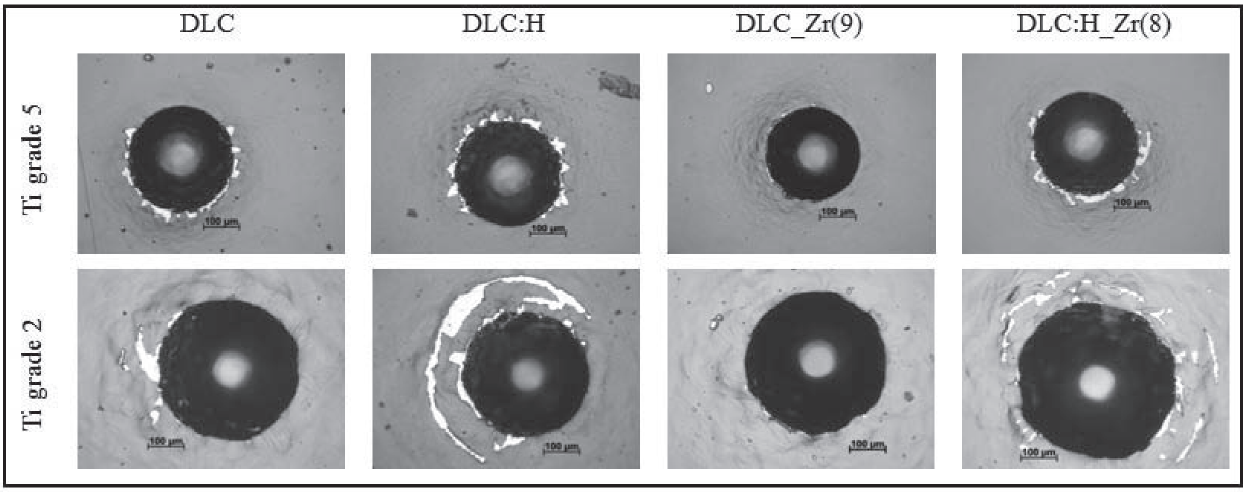

Figure 2: Coating Rockwell indentation.

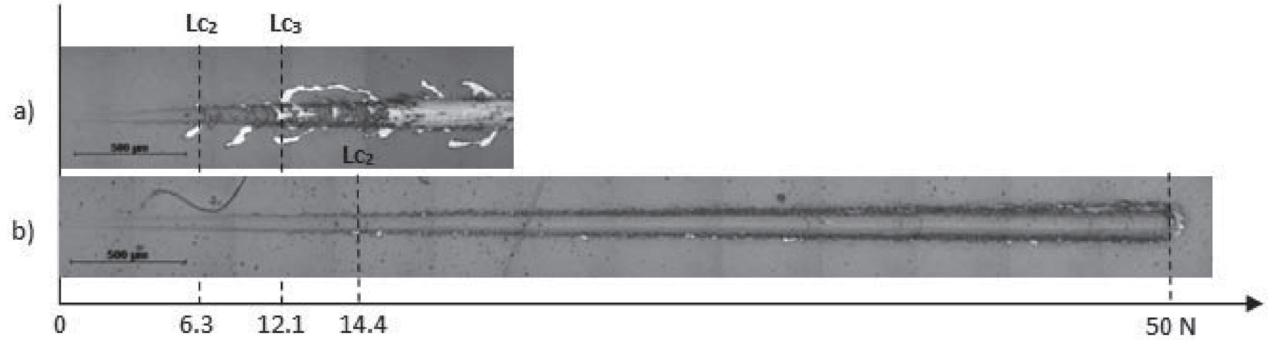

Figure 3: Scratching test at increasing load on DLC:H coated on both a) Ti grade 2 and b) Ti grade 5. The inset indicates the adhesion critical loads.

substrates [19]. Non-hydrogenated coatings doped with Zr showed sufficient adhesion increasing with Zr content. Moreover, there was no indication of delamination. Hydrogenated films exhibited large-scale delamination at the indentation edges (see Figure 2). Delamination and radial cracking could be related to substrate plastic deformation [20, 21]. HF6 is not accepted as a sufficient adhesion [9].

Scratch test, also known as 'short time tribological test' [22], is the only test method capable of generating stresses which exceed the interfacial bond strength of thin, well-adherent coatings [23]. Moreover, it has been considered as an adhesion assessment of new biocompatible materials [24]. As expected, the coatings deposited on Ti grade 2 exhibited lower adhesion than those on Ti grade 5; the adhesion is in general higher for non-hydrogenated films. Figure 3 demonstrates the influence of the substrate on the coating adhesion.

Cohesive failure of DLC:H coating occurred at the beginning of the test (Lc1) although with only few smooth cracks. However, the coating damage close to Lc2 depended on the substrate: (i) conformal cracks/chipping on Ti grade 5 and (ii) spallation/debonding on Ti grade 2. Moreover, Lc_3 was only observed when using Ti grade 2 as substrate, in such case a complete failure of the coating was observed. Doping with Zr improved the adhesion measured by Rockwell indentation on both substrates; metal doping typically leads to higher adhesion [25]. In general, the adhesion estimation obtained by both methods clearly showed the advantage of using harder Ti grade 5 as substrate. This finding corroborates the results shown by Kim et al, [26], where plastic deformation of CP Ti strongly influenced the fracture/fatigue cracks destroying the DLC layer and thus, limiting their tribological properties compared to Ti6Al4V/DLC combination

CONCLUSION

DLC thin films doped by Zr were deposited by magnetron sputtering under reactive and non-reactive atmosphere. Increasing Zr content changed coating microstructure from amorphous (pure DLC film) to nanocomposite with ZrC nano-crystalline phase embedded into the amorphous carbon matrix. Pure DLC films show a very low adhesion; however, doping with Zr led to much higher critical load values obtained by scratch test and better qualitative adhesion estimated from Rockwell indents. When compared the two substrates, Ti grate 2 and Ti grade 5, it is clear that the later offer much better support for the coating.

ACKNOWLEDGEMENT

The authors would like to thank the Czech Science Foundation for financial support through the project 108/10/1782 by national funds through FCT – Fundação para a Ciência e a Tecnologia, under the grant SFRH/BD/75071/2010.

REFERENCES

1. G. Thorwarth, C.V. Falub, U. Müller, B. Weisse, C. Voisard, M. Tobler and R. Hauert, "Tribological behavior of DLC-coated articulating joint implants", Acta Biomater. 6(2010) 2335.

2. T.J. Joyce, "Examination of failed ex vivo metal-on-metal metatarsophalangeal prosthesis and comparison with theoretically determined lubrication regimes", Wear 263(2007) 1050.

3. A. Dorner-Reisel, C. Schürer and E. Müller, "The wear resistance of diamond-like carbon coated and uncoated Co28Cr6Mo knee prostheses", Diamond Relat. Mater. 13(2004) 823.

4. J.O. Galante, J. Lemons, M. Spector, P.D. Wilson and T.M. Wright, "The biologic effects of implant materials", J. Orthop. Res. 9(1991) 760.

5. H. Matsuno, A. Yokoyama, F. Watari, M. Uo and T. Kawasaki, "Biocompatibility and osteogenesis of refractory metal implants, titanium, hafnium, niobium, tantalum and rhenium", Biomaterials 22(2001) 1253.

6. Biomedical Materials, edited by R. Narayan, pp. 40-81, Springer, 2009.

7. Materials Properties Handbook: Titanium Alloys, edited by R. Boyer, G. Welsch, and E.W. Collings, ASM International, Materials Park, OH 1994.

8. ASM Handbook, Volume 18 - Friction, Lubrication, and Wear Technology, edited by P.J. Blau, ASM International, 1992.

9. N. Vidakis, A. Antoniadis and N. Bilalis, "The VDI 3198 indentation test evaluation of a reliable qualitive control for layered compounds", J. Mater. Process. Technol. 143-144 (2003) 481.

10. Handbook of thin film process and technology edited by D. Glocker and S.I. Shah, Institute of physics publishing, 1995.

11. O.A. Fouad, A.K. Rumaiz, and S.I. Shah, "Reactive sputtering of titanium in Ar/CH_4 gax mixture: Target poisoning and film characteristics", Thin Solid Films, 517 (2009) 5689.

12. K. Bewilogua, R. Wittorf, H. Thomsen and W. Weber, "DLC based coatings prepared by reactive d.c. magnetron sputtering", Thin Solid Films 447-448 (2004) 142.

13. European Committee for standardization, European Stardard DIN ENV 1071-3 (1994), draft European Standard prEN 1071-3 (2002).

14. F.C. Tai, S.C. Lee, J. Chen, C. Wei and S.H. Chang, "Multipeak fitting analysis of Raman spectra on DLCH film", J. Raman Spectrosc. 40 (2009) 1055.

15. W.-H Kao, "The tribological properties of Zr-C:H coatings deposited on AISI M2 substrate", Wear 264 (2008) 368.

16. A.C. Ferrari and J. Robertson, "Interpretation of Raman spectra of disordered and amorphous carbon" Phys. Rev. B, vol 61, **20** (2000) 14095.

17. C. Casiraghi, F. Piazza, A.C. Ferrari, D. Grambole, J. Robertson, "Bonding in hydrogenated diamond-like carbon by Raman spectroscopy", Diamond Relat. Mater. 14 (2005) 1098.

18. A. Escudeiro, T. Polcar and A. Cavaleiro, "Tribolofical behaviour a-C and a-C:H films doped with Ti in biological solutions", Vacuum 85 (2011) 1144.

19. H.Ronkainen, J. Koskinen, S. Verjus, and K. Holmberg, "Load-carrying capacity of coating/substrate systems for hydrogen-free and hydrogenated diamond-like carbon films", Tribol. Lett. 6 (1999) 63.

20. N.B. Thomsen, A.C. Fisher-Cripps and M.V. Swain, "Crack formation mechanisms during micro indetnation of diamond-like carbon coating on elastic-plastic substrates", Thin Solid films 332 (1998) 180.

21. M.D. Drory and J.W. Hutchinson, Proceedings: Mathematical, Physical and Engineering Sciences, Vol. 452, No. 1953 (1996) 2319-2341.

22. C. Berg, C. Friedrich, E. Broszeit, C. Berger, "Scratch test measurement of tribological hard coatings in practice", Fresenius J. Anal. Chem. 358 (1997) 281.

23. D.M Drory, D.B Bogy, M.S Donley, J.E Field, "Mechanical Behaviour of Diamond and other Forms of Carbon", Mater. Res. Soc. Symp. Proc., PA 1995.

24. P. Kutilek, and J. Miksovsky, "The procedure of evaluating the practical adhesion strength of new biocompatible nano- and micro-thin films in accordance with international standards", Acta Bioeng. Biomech, vol. 13, 3 (2011) 87.

25. D.-Y Wang, Y.-Y. Chang, C.-L. Chang, Y.-W. Huang, "Deposition of diamond-like carbon containing metal elements on biomedical Ti alloys", Surf. Coat. Technol. 200 (2005) 2175-2180.

26. D.-H. Kim, H.-E Kim, K.-R. Lee, C.-N. Whang, and I.-S Lee, "Characterization of diamond-like carbon films deposited on comercially pure Ti and Ti-6Al-4V", Mater. Sci. Eng., C 22 (2002) 9-14.

PAPER II

a-C(:H) and a-C(:H)_Zr coatings deposited on biomedical Ti-based substrates: Tribological properties

A. Escudeiro, T. Polcar and A. Cavaleiro

Thin Solid Films 538 **(2013)** 89-9

Thin Solid Films 538 (2013) 89–96

Contents lists available at SciVerse ScienceDirect

Thin Solid Films

journal homepage: www.elsevier.com/locate/tsf

a-C(:H) and a-C(:H)_Zr coatings deposited on biomedical Ti-based substrates: Tribological properties

A. Escudeiro [a,*], T. Polcar [b,c], A. Cavaleiro [a]

[a] SEG-CEMUC, Department of Mechanical Engineering, University of Coimbra, 3030-788 Coimbra, Portugal
[b] National Centre for Advanced Tribology (nCATS), School of Engineering Sciences, University of Southampton, Highfield, Southampton, SO17 1BJ, UK
[c] Department of Control Engineering, Czech Technical University in Prague, Technicka 2, Prague 6, Czech Republic

ARTICLE INFO

Available online 6 January 2013

Keywords:
a-C(:H) coating
Zirconium
Biocompatible
Wear
Sputtering

ABSTRACT

Amorphous carbon (a-C) based coatings are possible candidates as a surface treatment for various biocompatible materials used in medicine. In this study, the carbon coatings co-sputtered with Zr, deposited by dc unbalanced magnetron sputtering in Ar (non-hydrogenated, i.e. a-C/Zr) and Ar + CH_4 (hydrogenated, i.e. a-C:H/Zr) discharges, were investigated and compared with pure carbon films. Polished pure commercial Ti grade 2 and Ti grade 5 ELI (Ti6Al4V) discs were used as substrates. To improve the coating/substrate adhesion, a gradient Ti-based interlayer was deposited (~450 nm). The coating structure was characterized by X-ray diffraction, X-ray photoelectron spectroscopy and Raman spectroscopy; the chemical composition was measured by electron probe microanalysis. The adhesion was evaluated by scratch-test and the hardness was measured by nanoindentation. Tribological testing of the coatings was carried out using unidirectional pin-on-disc experiments; pure titanium balls were used as counterparts. The wear rate of the coatings was negligible except for the films with the highest Zr content deposited on Ti grade 2 substrates.

1. Introduction

Ti grades 2 and 5 ELI are among the most suitable metallic materials used for hard tissue replacement. These materials are an ideal choice due to the combination of low density, high strength to weight ratio, elastic modulus, sufficient failure resistance, corrosion resistance and excellent biocompatibility, particularly when compared to Co–Cr alloys [1,2]. However, Ti-based alloys are soft, their wear resistance is limited, particularly when adhesion or abrasion wear occurs, and they show high friction coefficients [3–5].

Amorphous (a-C) or hydrogenated amorphous (a-C:H) carbon has been considered as a potential protective layer of artificial joint materials due to excellent mechanical and tribological properties, corrosion resistance, chemical inertness, and biocompatibility [6–8]. The deposition of a-C films on soft substrates, such as Ti or Ti-based alloys, is a continuous challenge due to substrate plastic deformation, which could cause fracture and delamination [9–11]. Moreover, a-C films typically exhibit high internal compressive stress which significantly limits the adhesion of the coating and contributes to its tribological failure. The adhesion could be significantly improved by substrate surface pretreatments, such as nitriding or etching [2,12], by optimizing the deposition parameters, such as the substrate bias and Ar pressure [13–15], or by deposition of an adhesion improving interlayer [8]. The latter could be prepared as a gradient layer (Me/MeC, Me/MeN, or Me/MeN/MeNC, where Me is a metallic element) in order to avoid sharp interfaces with large mismatch of mechanical properties [9,16]. Co-sputtering of carbon films by metals (e.g. Ti, W, Cr) might improve the adhesion as well; however, these coatings then significantly differ from the pure carbon films [17–20].

Similar to titanium, zirconium is biocompatible and exhibits excellent tribological properties together with high corrosion resistance [21,22]. Therefore, zirconium is a potential candidate to improve properties of carbon-based films. The structure of carbon films co-sputtered with Zr is typically described as a nanocomposite, i.e., zirconium carbide nanograins embedded into an amorphous carbon matrix [23–25]. The core objective of this study is to evaluate the fundamental structural, mechanical and tribological properties of a-C and a-C:(H) coatings containing different zirconium contents deposited on soft Ti-based substrates.

2. Experimental details

2.1. Coating deposition

The coatings were deposited using dc dual magnetron sputtering in Ar (non-reactive) and Ar/CH_4 (reactive) atmospheres to produce non-hydrogenated and hydrogenated films, respectively. Two targets were used: titanium, to deposit the adhesion improving interlayer, and graphite to deposit the functional coating. To produce the Zr containing

---

[*] Corresponding author. Tel.: +351 239790745.
E-mail address: ana.escudeiro@dem.uc.pt (A. Escudeiro).

0040-6090/$ – see front matter © 2013 Elsevier B.V. All rights reserved.
http://dx.doi.org/10.1016/j.tsf.2012.12.086

films, different numbers of Zr pellets (diameter 5 mm) were embedded into the erosion zone of the graphite target; thus, the Zr content could be controlled by the number of Zr pellets. Commercial pure Ti (Ti grade 2) and Ti6Al4V alloy (Ti grade 5 ELI) discs (diameter 50 mm; thickness 4 mm) were polished down to a roughness of $R_a \leq 50$ nm and cleaned in an ultrasonic bath in acetone, ethanol, and distilled water for 15 min each. To measure residual stress and hardness, thin discs of 304 stainless steel and Si wafer were used, respectively. The substrates were mounted on the rotating sample holder (18 rpm) in the deposition chamber; the target-to-substrate distance was approximately 170 mm. The samples were etched via Ar ion bombardment for 1 h to remove all surface contaminants and oxides (bias voltage of −650 V). After etching, a Ti/TiN/TiNC(Zr) composite gradient layer with a total thickness of 450 nm was deposited to enhance the functional film adhesion, see scheme in Fig. 1. Ti target was first sputtered in pure Ar atmosphere (Ar flow 35 sccm); then, nitrogen was introduced (17 sccm) and, finally, the power of the graphite target (with or without embedded Zr pellets) was gradually increased. The top layer, approximately 1 μm thick, was deposited by sputtering the graphite (with or without Zr pellets) target in Ar or Ar/CH_4 atmosphere using a power density close to 7.5 W cm^{-2}. The number of Zr pellets used in this study was 0 (referential coating), 8, 14, and 20 which corresponds to a relative erosion area (A_{Zr}/A_C) between 0 and 6%. The total pressure was kept constant at approx. 0.4 Pa by adjusting the gas flow and a pulsed substrate bias was applied (−50 V; frequency 250 kHz). The coating thickness was kept around 1.4 μm by adjusting the deposition time. The thickness was measured by 2D optical profilometer (Perthometer S4P) using a substrate/coating step.

2.2. Coating characterization

The chemical composition of the coatings was determined by electron probe microanalysis (EPMA) with a CAMECA Camebax SX 50 model. The applied voltage was 10 keV corresponding to a maximum penetration depth below 2 μm for carbon-based coatings. It should be noted that EPMA cannot detect hydrogen; therefore, it gives only Zr/C ratio in the case of hydrogenated coatings. The microstructure was analysed by X-ray diffraction (XRD) with a Philips, X′Pert diffractometer operating with Co Kα radiation. To increase the signal from the film in relation to the substrate, grazing incidence with an angle of 2° was used. Chemical bonding was characterized by X-ray photoelectron spectroscopy (XPS) (ESCAprobe P, Omicron Ltd., Al Kα, binding energy calibrated with Au 4f (84.1 eV)). The peak decomposition of C1s and Zr 3d were carried out using a GL(30) line shape, which stand for Gaussian/Lorentzian product formulas with 30% Lorentzian weight, and the contribution of the background was approximated by the Shirley method. The spin-orbital splitting in Zr 3d was assumed to be the same for all the phases and equal to 2.4 eV [26,27] and the integrated intensity of the Zr $3d_{5/2}$ peak relative to that of the Zr $3d_{3/2}$ peak was considered equal to the spin-orbital multiplicity of 2/3. Moreover, to remove surface contamination, the samples were bombarded during 30 min by Ar^+ ions before analysis (beam energy 5 keV). Raman spectroscopy (Xplora, Horiba, DPSS laser with a wavelength of 532 nm) was used to analyse the carbon structure. The Raman spectra were fitted using two Gaussian peaks following the procedure described in Ref. [28]. The hardness was measured by depth-sensing indentation (Micromaterials Nanotest) using a Berkovich indenter. The normal stylus load was 5 mN (indentation depth approx. 150 nm); 32 independent indentations from two distinct areas on the sample were used to analyse the hardness data. Moreover, the reduced Young modulus was derived from the indentation measurements by the standard Oliver and Pharr method [29].

2.3. Adhesion and tribological properties

The coating cohesion and adhesion to the substrates were evaluated by scratch testing (CSM Instruments; spherical diamond 120° tip with a diameter of 200 μm). The load was increased from 2 to 50 N (loading speed 10 N mm^{-1}) and three critical loads were reported. Lc_1, the lower critical load, is the load corresponding to the first cracks that occur (cohesive failure). Lc_2, the upper critical load, is defined as the load where the first spallation/flaking of the film is observed (adhesive failure). Finally, Lc_3 corresponds to the load where penetration of the coating is detected in the centre of the scratch. The tribological tests were carried out using a pin-on-disc set-up (CSM Instruments) in relative air humidity 30%; a normal load of 1 N, a linear speed of 20 cm s^{-1} and test duration of 10,000 laps were used in this study. All coatings were tested with Ti6Al4V ELI counterbody machined as a ball with a diameter of 8 mm. The friction coefficient was measured during the sliding tests, whereas the wear rate was calculated as the worn volume per sliding distance per load. The worn volume was measured by 3D profilometer (Zygo NewView 7200); the wear of the ball was evaluated as well. Optical microscope and scanning electron microscopy (SEM) were used for the wear track evaluation. The influence of the plastic deformation of the substrate on the measured coating worn volume is discussed below. The mechanical properties of Ti grade 2 and Ti grade 5 ELI shown in Table 1 [4,5] differ significantly. However, the initial and mean Hertzian pressures for the ball-on-plate contact are almost identical.

3. Results and discussion

3.1. Coating deposition and chemical composition

Table 2 shows the zirconium content together with the mechanical properties of the deposited coatings. Low amounts of Ti and N originated from the interface were observed. The oxygen contamination arising from the residual atmosphere was lower than 3 at.%. Due to the higher sputtering yield of zirconium compared to the graphite target, the deposition rate increased with the number of Zr pellets. To keep the coating thickness constant, the deposition time was decreased when Zr

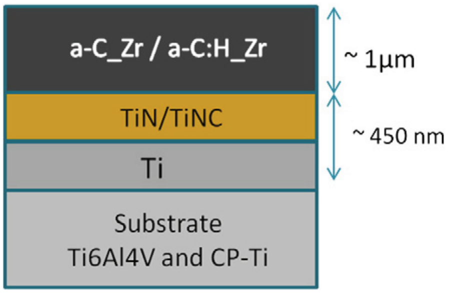

Fig. 1. Schematic design of a-C(:H)_Zr coatings.

Table 1
Summary of the mechanical properties (hardness, H, Young modulus, E, elastic strain to failure, H/E, resistance to plastic deformation, H^3/E^2, and yield strength, Y) and the Hertzian contact conditions (maximum and medium contact pressure, P_0 and P_m, and maximum shear stress, τ_{max}) for both substrates.

	H (GPa)	E (GPa)	H/E	H^3/E^2 (GPa)	Y (MPa)	P_{0max} (MPa)	P_m (MPa)	τ_{max} (MPa)
Ti grade 5	3.1	114	0.034	0.0023	793	360	240	110
Ti grade 2	1.5	103	0.026	0.0003	276	360	240	110

Table 2
Deposition rate, chemical composition and mechanical properties (hardness, H, Young modulus, E, elastic strain to failure, H/E, resistance to plastic deformation, H^3/E^2, and elastic recovery, R) of the coatings.

	Sample	Dep. rate (nn/min)	Zr (at.%)	H (GPa)	E (GPa)	H/E	H^3/E^2 (GPa)	R (%)
Non-hydrogenated	a-C	4.6	0	10.9 ± 0.5	94.0 ± 0.1	0.116	0.147	71
	a-C_Zr(3)	5.0	3	10.4 ± 0.4	109.9 ± 3.1	0.094	0.092	62
	a-C_Zr(7)	7.3	7	11.9 ± 0.6	126.0 ± 2.6	0.094	0.105	68
	a-C_Zr(9)	8.3	9	10.7 ± 0.5	133.3 ± 2.2	0.080	0.069	59
Hydrogenated	a-C:H	8.8	0	8.9 ± 0.3	69.9 ± 0.3	0.128	0.146	74
	a-C:H_Zr(4)	8.5	4	10.0 ± 1.6	87.3 ± 2.6	0.115	0.132	71
	a-C:H_Zr(5)	10.0	5	11.4 ± 0.4	103.1 ± 1.2	0.111	0.140	73
	a-C:H_Zr(8)	12.0	8	12.2 ± 0.5	114.1 ± 3.4	0.107	0.140	67

pellets were added. The maximum Zr content was 9 at.%. When methane was introduced into the chamber, the deposition rate increased. Since Zr content was only slightly lower for hydrogenated films, it was probable that the poisoning of Zr pellets surface was negligible, since additional carbon was added through reactive gas [30,31].

To facilitate reading, the coatings are hereinafter denominated as a-C_Zr(X) and a-C:H_Zr(X), where X is the Zr content and H indicates hydrogenated films.

3.2. Structure and chemical bonding

XRD diffractograms clearly show the amorphous structure of the carbon coatings, since the only visible peaks were originated from the gradient interlayer (Fig. 2). When Zr was added, it was possible to detect a very broad peak near 37.9° which was identified as the ZrC phase (111) (ICDD card n. 74-1221).

Fig. 3 shows XPS C1s and Zr 3d spectra of a-C:H_Zr(8) coating after 30 min of sputter-etching. Three peaks were detected in C 1s spectrum; C – C bond, C – O bond, and a peak positioned at 283.2 eV. The binding energy of ZrC phase is typically in the range (281.8–282.3 eV) [25,26,32,33]. However, Smith et al. [34] reported the presence of such a peak near 283.6 eV, together with the typical ZrC peak deposited from single source organometallic precursors. The presence of such peak may correspond to the organometallic: Zr═C – , Zr – CH_n – , or Zr═CH – bonds. Anderson et al. [25] also studied thin Zr containing carbon films. They observed a Zr–C peak in the standard position typical for bulk ZrC; however, their spectra revealed an additional peak at higher binding energy (282.7 eV). This peak was attributed to atoms at the matrix–carbide interface. Lewin [35,36] has previously found a similar peak in a nc-TiC/a-C nanocomposite; this peak was attributed to metal atoms in an interfacial state at the carbide/matrix interface. These works referred above showed significantly higher Zr(Ti) contents compared to the present work (close to 40 at.%). In our case, the Zr content is much lower and the presence of a broad peak in the XRD diffractograms may indicate the presence of a ZrC nanophase. Therefore, almost all Zr atoms in the Zr-C grains are positioned at the interface with the amorphous carbon matrix, which should give rise almost exclusively to the peak at higher binding energy. Zr 3d spectrum was deconvoluted considering the spin-orbit splitting equal to 2.4 eV [26] (Fig. 3). Two bonds were identified: Zr – O (probably from oxygen contamination from residual atmosphere) and Zr – C. The latter is positioned at ~180.4 eV, i.e. close to Zr – C (179.1–181.1 eV (Zr $3d_{5/2}$) [26,34,37]). The Zr metallic phase peak (178.7 eV $Zr3d_{5/2}$ [27]) was not observed.

Thus, XRD and XPS results could be considered as an indication of a nanocomposite structure with ZrC nanograins embedded in an amorphous carbon matrix. Similar results were reported by Adelhelm et al. [38] in the case of carbon films with approximately 7 at.% of Zr. Nevertheless, further analysis, namely transmission electron microscopy, is planned for future study.

The typical Raman spectra of the deposited coatings shown in Fig. 4 are composed of two broad bands: the G (Graphite) peak and the D (Disorder) peak centred at around 1580 cm^{-1} and 1350 cm^{-1}, respectively [28]. Fig. 5 summarizes the I_D/I_G ratio (i.e. the ratio of integrated

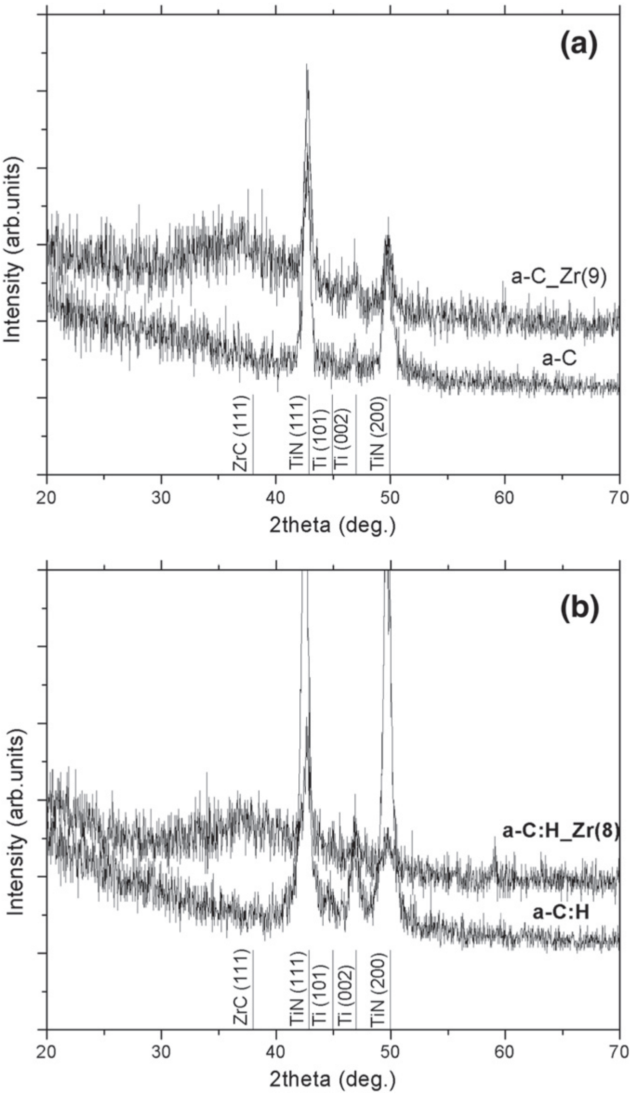

Fig. 2. XRD diffractograms of (a) a-C and a-C_Zr(9) and (b) a-C:H and a-C:H_Zr(8) with indexation patterns.

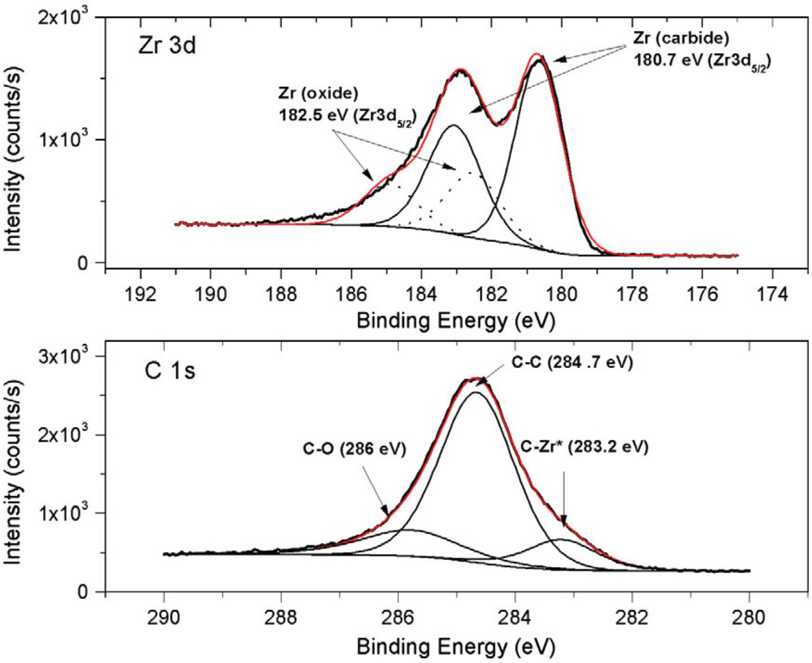

Fig. 3. XPS Zr 3d and C 1s spectra of a-C:H_Zr(8) coating.

intensities of D and G band) and G peak position as a function of Zr content. Simultaneous, the presence of Zr and H in carbon films played an important role in promoting both the formation of aromatic rings and the increase of the organization of C clusters, as documented by the increase of either the D peak intensity (i.e. growing of I_D/I_G ratio) or the G peak position [28]. Although I_D/I_G ratio was also increasing with Zr content in the case of non-hydrogenated coatings, G peak position shifted to lower values (Fig. 5). These results corroborate those presented by Adelhelm et al. [23], who found a similar G peak shift for a-C:Me (Me = Ti or Zr). It can thus be concluded that: (i) there was higher bond disorder even if sp^2 clustering is higher and/or (ii) the presence of heavy metals can influence the vibration modes of adjacent C═C bond due to the slowing of the relative sp^2 movement, which is responsible for the G peak. Moreover, the presence of ZrC phase could act as a catalyst and promote the graphitization of the adjacent carbon matrix leading to higher sp^2 content in the films [23,31] and a slight increase of the G peak position for higher Zr contents. Nevertheless, further investigation will be carried out in order to better understand the influence of heavy atoms on the C-matrix structure.

3.3. Mechanical properties

The hardness and the Young modulus of the films are shown in Table 2. One of the main objectives of coating titanium-based substrates with Zr containing carbon-coatings was to improve the wear resistance. According to Archard model [39], there is a linear relationship between the volume worn during the sliding and the inverse of the hardness. Thus, a higher hardness should lead to a higher wear resistance. In general, the hardness of the deposited coatings was significantly higher than that of the substrates. Non-hydrogenated a-C_Zr films showed a comparable hardness with that of pure a-C (~11 GPa). The lowest hardness value was observed in the case of pure hydrogenated carbon film (8.9 GPa); however, it progressively increased with Zr content. The Young modulus was calculated using the following parameters: $E_i =$ 1140 GPa and $\nu_i = 0.07$ for the diamond indenter [29] and $\nu = 0.3$ for the coating (ν is the Poisson ratio) [40]. Co-sputtering with Zr decreased the elastic strain to failure (H/E) and the resistance to plastic deformation (H^3/E^2) of the coatings; the effect was more pronounced for the non-hydrogenated coatings. Moreover, a higher Young modulus of hydrogen-free films implied that the elastic recovery (R) also decreased (Table 2). The slope of the linear section of the unload curve was higher for the pure film than that of a-C_Zr(9); thus, the pure films presented a higher elasticity compared to the Zr containing films. The same trend was found in carbon films co-sputtered with Cr, where brittle CrC phase decreases the film toughness and elastic recovery [41]. In general, the elastic recovery of the hydrogenated films was higher compared to non-hydrogenated ones. In contrast to bulk Ti-based substrates (see Table 1), the H/E and the (H^3/E^2) values of the coatings were about one to two orders of magnitude higher.

Typical scratches produced by the adhesion test are shown in Fig. 6. Piling-up along the edges of the scratch track, which is clearly observed in both substrate materials, indicated plastic deformation (Fig. 6a and c). As expected, the plastic deformation was much more evident in the case of Ti grade 2 substrates, i.e. it was visible for lower loads. Fig. 6b and d shows the scratches of a-C:H coatings deposited on Ti grade 2 and Ti grade 5 ELI, respectively. The scratch tracks are much wider for the softer Ti grade 2 substrates when an identical load was applied. Fig. 7 shows the critical loads Lc_1, Lc_2, and Lc_3 as a function of Zr content. As expected, the critical loads of the coatings deposited on Ti grade 2 were in general inferior compared to those prepared on Ti grade 5 ELI substrates. This finding agrees with the results shown by Kim et al. [42], where the plastic deformation of pure titanium substrates strongly promoted the formation of cracks, leading to the destruction of a-C films; a harder substrate (Ti6Al4V/a-C(:H)) showed improved coating adhesion and wear resistance. All coatings presented in this study showed similar compressive residual stress, approx. 2 GPa, calculated by the Stoney's equation [43]. Thus, the residual stress was not expected to be a key factor determining the adhesion behaviour. a-C_Zr(7) coating presented the best scratch behaviour for both substrates and delamination were not observed (i.e. $Lc_3 > 50$ N). Although the pure carbon coatings showed higher plastic deformation resistance (H^3/E^2 ratio) than the films containing Zr, there was no significant

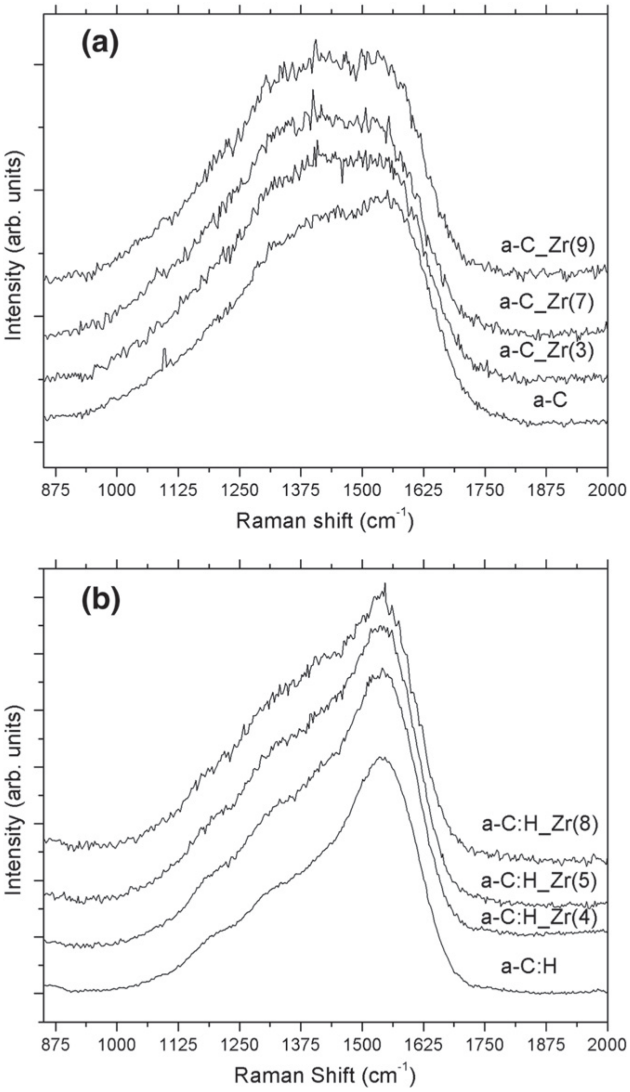

Fig. 4. Raman spectra of (a) non-hydrogenated films and (b) hydrogenated films.

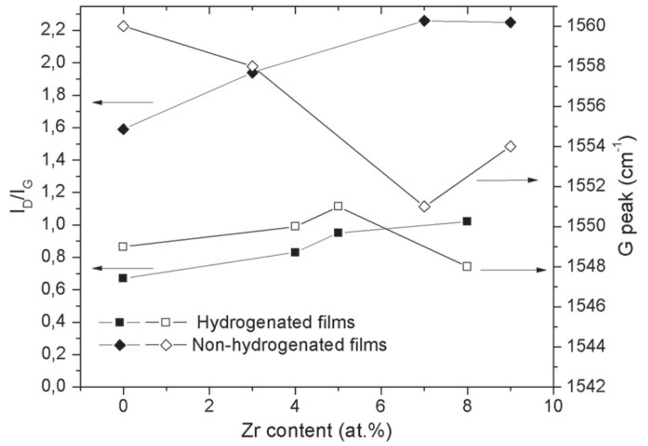

Fig. 5. I_D/I_G ratio and G peak position as a function of Zr content.

differences in the measured critical loads. Thus, the substrate mechanical properties were much more important than the difference among coatings. High pile-up could lead to higher wear of the counterbody; again, the Ti grade 2 substrates were inferior with increased risk of counterbody damage during the sliding tests.

3.4. Friction and wear properties

Table 3 summarizes the tribological results of the coatings; the values for the uncoated substrates are shown as a reference. As expected, the friction coefficient dropped significantly when pure carbon-based coatings (i.e. a-C and a-C:H) were applied. The friction, then, slightly increased when Zr was added. The wear rate of the films was about three orders of magnitude lower than that of uncoated substrates. Although the tribological parameters, such as the maximum depth of the wear track and the coating wear rate, were similar for both substrates (see Table 3), the appearance of the wear track was significantly different (Fig. 8). Fig. 9 shows a SEM micrograph from the wear track on softer Ti grade 2 substrates. Even though, the presence of areas lifted above the surface is a typical feature of the material transfer from the ball material onto the coating surface, there were traces neither from such transfer nor accumulation of the wear debris in the wear tracks. Therefore, only the plastic deformation of the substrate could lead to the formation of the wear tracks shown in Fig. 8. The highest deformation was observed in the coating a-C_Zr(9), where the depth of the wear track oscillated between −1 (i.e. above the surface) and 2 μm. Such severe deformation could not be accommodated by the coating and cracks parallel to the sliding direction were observed. Moreover, the presence of cracks led to local coating delamination (Fig. 9). It should be pointed out that a-C_Zr(9) was the only coating which failed during the sliding tests. The failure of the film corresponded to the results of scratch test (the lowest critical force Lc_3); moreover, this film also exhibited the lowest elastic recovery (Table 2).

Since significant plastic deformation was observed, we had to consider it in the calculation of the wear rate. The wear rate calculated as the worn volume per sliding distance per load, which could be given in our case as the area of the wear track cross-section per number of cycles per load, would give misleading results. Therefore, we report here the worn volume as the difference between the volume of the wear track (i.e. missing material below original coating surface) and the volume of the material above the surface [44]. The wear rate calculated in this way is almost independent of the substrate material, although the maximum depth of the wear track was significantly higher for Ti grade 2 substrates. The wear of the counterbody calculated as the worn volume per sliding distance per load was the highest for pure carbon coatings; we can thus conclude that co-sputtering with Zr slightly increased the friction, but significantly diminished the wear of the counterpart.

Although the sliding tests were performed in humid air (relative humidity 30%) and the contact pressure was much higher than that in real biomedical applications, this study could indicate either the potential or the risks of applying a-C(:H)_Zr coatings deposited on Ti-based substrates. Commercial pure titanium and Ti6Al4V alloy typically present abrasive and adhesive wear due to plastic deformation and material transfer [3]. Ti grade 2 is more likely to deform plastically than Ti grade 5 ELI. According to Tresca criterion, under normal load axisymmetric contact condition, the plastic yield occurs when the maximum contact pressure, P_o, exceeds 1.6 the yield strength, Y, of the contacting material:

$$P_o^{\ Y} = 1.6Y_{\text{Ti grade 5 ELI}} = 1270\,\text{MPa and}\,P_o^{\ Y} = 1.6Y_{\text{Ti grade 2}} = 442\,\text{MPa}.$$

Table 1 shows that the maximum contact pressure for both substrates was lower than the onset of plastic deformation. Moreover, the required load to initiate yield is related to the maximum contact

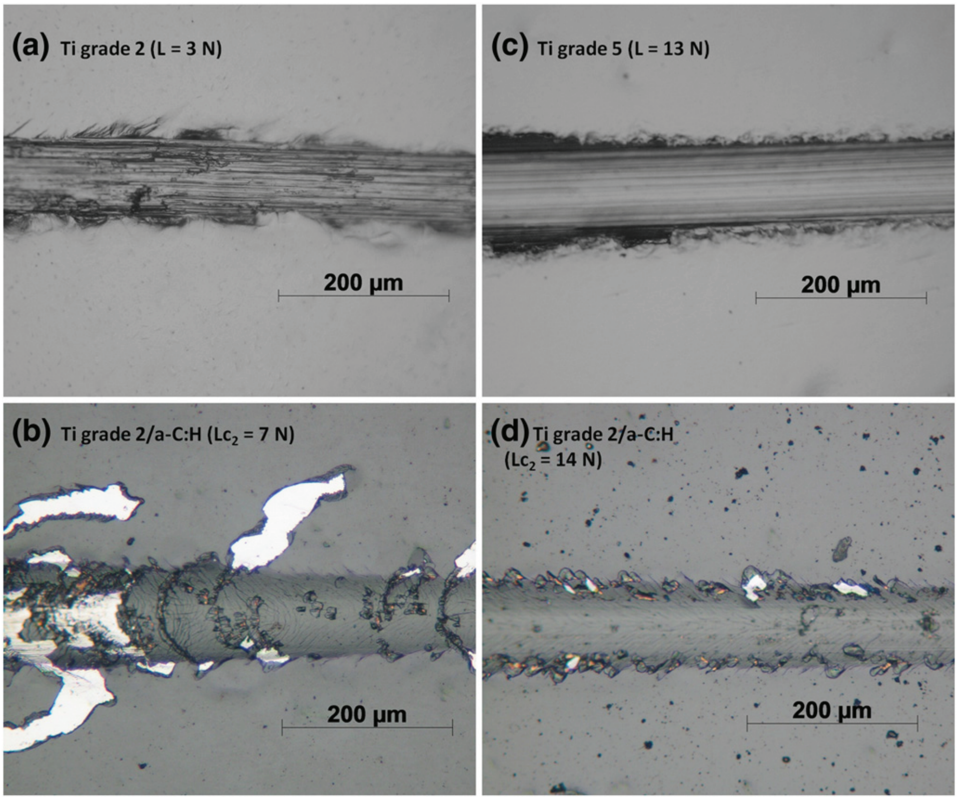

Fig. 6. Optical images of typical scratch tracks performed on (a) uncoated Ti grade 2 and (c) Ti grade 5 ELI and (b) a-C:H deposited on Ti grade 2 and (d) Ti grade 5 ELI. Scratch direction is from right to left. The arrows show the adhesive critical load Lc$_2$ and coating delamination (Lc$_3$).

load [44]; it was 1.35 N for Ti grade 2, i.e. slightly higher than 1 N load used in this study. However, it is important to point out that the calculation was based on ideal smooth ball and disc surfaces. Since real surfaces in contact are rough the local contact pressure between asperities is much higher. Thus, plastic deformation can occur at lower loads [45].

4. Conclusions

Zr doped a-C hydrogenated and non-hydrogenated coatings have been deposited by magnetron sputtering onto soft Ti-based biomaterials (pure titanium and Ti6Al4V alloy) in order to enhance their tribological properties. The coatings with the highest Zr content exhibited a

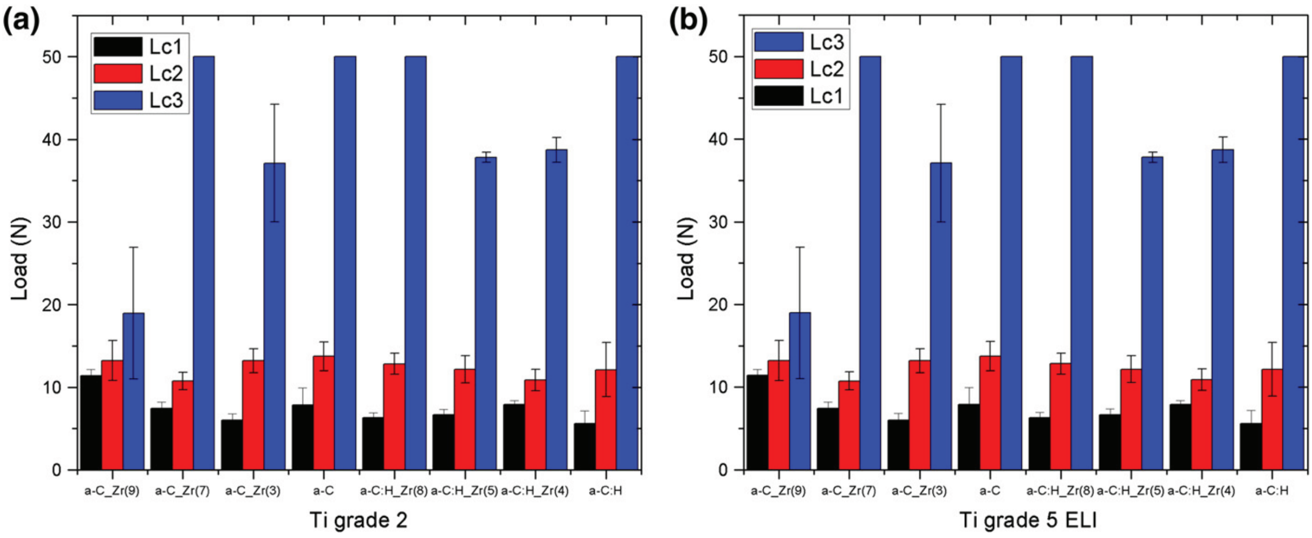

Fig. 7. Critical loads for the coating deposited on (a) Ti grade 2 and (b) Ti grade 5 ELI. Symbol (*) is used when the delamination was not observed even at the highest applied load.

Table 3
Wear test results from pin-on-disc experiments. Symbol (*) represents not measurable wear.

	Samples	Ti grade 2					Ti grade 5 ELI				
		R_a (μm)	Depth (μm)	Disc wear rate (10^{-6} mm^3/Nm)	Ball wear rate (10^{-6} mm^3/Nm)	COF	R_a (μm)	Depth (μm)	Disc wear rate (10^{-6} mm^3/Nm)	Ball wear rate (10^{-6} mm^3/Nm)	COF
Non-hydrogenated	a-C	0.086	0.4 ± 0.2	0.6 ± 0.4	0.44 ± 0.04	0.09	0.055	0.2 ± 0.1	0.4 ± 0.3	0.98 ± 0.10	0.10
	a-C_Zr(3)	0.086	1.1 ± 0.2	1.3 ± 0.7	0.16 ± 0.02	0.12	0.085	0.5 ± 0.1	0.8 ± 0.2	0.19 ± 0.02	0.16
	a-C_Zr(7)	0.086	0.8 ± 0.3	0.5 ± 0.4	0.09 ± 0.01	0.15	0.088	0.2 ± 0.1	0.6 ± 0.4	0.25 ± 0.03	0.15
	a-C_Zr(9)	0.085	1.4 ± 0.1	2.4 ± 1.1	0.40 ± 0.04	0.19	0.103	0.7 ± 0.2	1.0 ± 0.4	0.10 ± 0.01	0.14
Hydrogenated	a-C:H	0.101	*	*	0.33 ± 0.03	0.14	0.076	0.2 ± 0.1	0.2 ± 0.1	0.85 ± 0.09	0.16
	a-C:H_Zr(4)	0.064	0.4 ± 0.1	0.6 ± 0.5	0.28 ± 0.03	0.14	0.051	0.3 ± 0.1	0.5 ± 0.2	0.08 ± 0.01	0.13
	a-C:H_Zr(5)	0.083	0.8 ± 0.2	0.4 ± 0.1	0.26 ± 0.03	0.13	0.055	0.6 ± 0.2	0.6 ± 0.2	0.12 ± 0.01	0.13
	a-C:H_Zr(7)	0.073	0.7 ± 0.2	0.7 ± 0.3	0.16 ± 0.02	0.15	0.076	0.6 ± 0.1	0.8 ± 0.3	0.04 ± 0.01	0.16
Uncoated		<0.050	13.5 ± 3.3	528.2 ± 54.6	–	0.52	<0.050	10.6 ± 1.1	843.7 ± 139.2	–	0.49

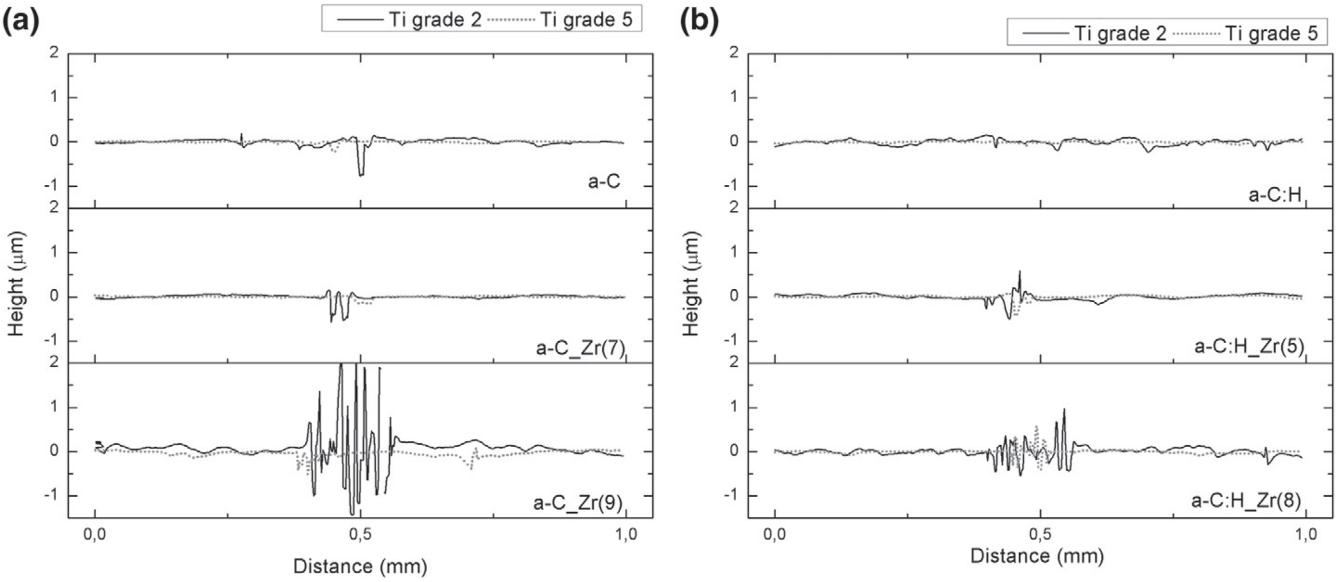

Fig. 8. Comparison of the wear track profiles (cross-section): (a) non-hydrogenated and (b) hydrogenated coatings.

nanocomposite structure with ZrC nanograins embedded into an amorphous carbon matrix. The incorporation of Zr into hydrogenated coatings increased the film hardness; however, such effect was not observed in the case of non-hydrogenated films. The adhesion of the carbon coatings on the substrates was improved by co-sputtering with Zr. Protection of Ti-based substrates against the wear, lower friction and significantly lower wear rates of the counterpart could be considered as major benefits of Zr containing a-C(:H) coatings.

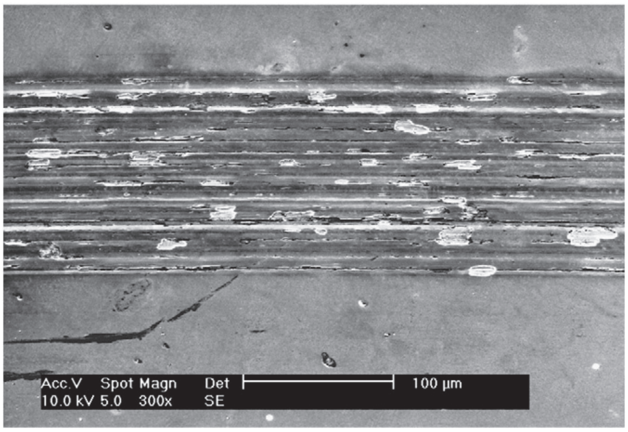

Fig. 9. SEM micrograph of the wear track, a-C_Zr(9) coating deposited on Ti grade 2.

Acknowledgement

This work was supported by the Czech Science Foundation through the project 108/10/1782 and by national funds through FCT — Fundação para a Ciência e a Tecnologia (QREN-POPH), under the grant SFRH/BD/75071/2010 and co-funding by FSE and MSTES. The authors would like to thank Amilcar Ramalho (CEMUC, Mechanical Engineering Department, University of Coimbra) for suggestions concerning tribological testing.

References

[1] I. Cvijović-Alagić, Z. Cvijović, C. Mitrović, M. Rakin, D. Veljović, M. Badić, Tribol. Lett. 40 (2010) 59.
[2] C. Martini, L. Ceschini, B. Casadei, I. Boromei, J.B. Guion, Wear 271 (2011) 2025.
[3] K.G. Budinski, Wear 151 (1991) 203.
[4] R. Boyer, G. Welsch, E.W. Collings, Materials Properties Handbook: Titanium Alloys, ASM International, Materials Park, OH, 1994.
[5] P.J. Blau, ASM Handbook, Friction, Lubrication, and Wear Technology, volume 18, ASM International, 1992.
[6] C. Donnet, A. Erdemir, in: C. Donnet, A. Erdemir (Eds.), Tribology of Diamond-like Carbon Films, Springer, New York, 2008, p. 1.
[7] L.A. Thompson, F.C. Law, N. Rushton, Biomaterials 12 (1991) 37.
[8] G. Thorwarth, C.V. Falub, U. Müller, B. Weisse, C. Voisard, M. Tobler, R. Hauert, Acta Biomater. 6 (2010) 2335.
[9] J. Jiang, R.D. Arnell, J. Tong, Tribol. Int. 30 (8) (1997) 613.
[10] Q. Zeng, O. Eryilmaz, A. Erdemir, Thin Solid Films 519 (2011) 3203.
[11] H. Ronkainen, J. Koskinen, S. Varjus, K. Holmberg, Tribol. Let. 6 (1999) 63.
[12] Y. Lui, E.I. Meletis, Surf. Coat. Technol. 153 (2002) 178.
[13] C. Jin, W. Wei, in: R. Narayan (Ed.), Biomedical Materials, Springer, New York, 2009, p. 183.

[14] Y. Pauleau, in: C. Donnet, A. Erdemir (Eds.), Tribologyof Diamond-like Carbon Films, Springer, New York, 2008, p. 102.
[15] M.M. Morshed, D.C. Cameron, B.P. McNamara, M.S.J. Hashmi, Surf. Coat. Technol. 174–175 (2003) 579.
[16] Y.F. Zheng, X.L. Lui, H.F. Zhang, Surf. Coat. Technol. 202 (2008) 3011.
[17] D.-Y. Wang, Y.-Y. Chang, C.-L. Chang, Y.-W. Huang, Surf. Coat. Technol. 200 (2005) 2175.
[18] B.K. Tay, Y.H. Cheng, X.Z. Ding, S.P. Lau, X. Shi, G.F. You, D. Sheeja, Diamond Relat. Mater. 10 (2001) 1082.
[19] J.C. Sánchez-López, A. Férnandez, in: C. Donnet, A. Erdemir (Eds.), Tribology of Diamond-like Carbon Films, Springer, New York, 2008, p. 311.
[20] C.W. Moura, Solid State Sci. 11 (2009) 1778.
[21] D.B. Lee, M. Roberts, C.G. Bluchel, R.A. Odell, ASAIO J. (2010) 550.
[22] N. Stojilovis, E.T. Bender, R.D. Ramsier, Prog. Surf. Sci. 78 (2005) 101.
[23] C. Adelhem, M. Balden, M. Rinke, M. Stueber, J. Appl. Phys. 105 (2009) 033522.
[24] M. Sazaki, Y. Kozukue, K. Hashimoto, K. Takayama, I. Nakamura, I. Takano, Y. Sawada, Surf. Coat. Technol. 196 (2005) 236.
[25] M. Andersson, S. Urbonaite, E. Lewin, U. Jansson, Thin Solid Films 520 (2012) 6375.
[26] M. Matsuoka, S. Isotani, W. Sucasaire, N. Kuratani, K. Ogata, Surf. Coat. Technol. 202 (2008) 3129.
[27] In: C.D. Wagner, W.M. Riggs, L.E. Davis, J.F. Moulder, G.E. Muilenberg (Eds.), Handbook of X-ray Photoelectron Spectroscopy, Perkin-Elmer Corporation, Minnesota, 1979.
[28] A.C. Ferrari, J. Robertson, Phys. Rev. B 61 (20) (2000) 14095.
[29] W.C. Oliver, G.M. Pharr, J. Mater. Res. 7 (1992) 1564.
[30] O.A. Fouad, A.K. Rumaiz, S.I. Shah, Thin Solid Films 517 (2009) 5689.
[31] K. Bewilogua, R. Wittorf, H. Thomsen, W. Weber, Thin Solid Films 447–448 (2004) 142.
[32] C.L. Chu, H.L. Ji, L.H. Yin, Y.P. Pu, P.H. Lin, P.K. Chu, Mater. Sci. Eng. C31 (2011) 423.
[33] Y.F. Zheng, X.L. Liu, H.F. Zhang, Surf. Coat. Technol. 202 (2008) 3011.
[34] D.C. Smith, R.R. Rubiano, M.D. Healy, R.W. Springer, MRS Proc. 282 (1992) 643.
[35] E. Lewin, P.O.Å. Persson, M. Lattemann, M. Stüber, M. Gorgoi, A. Sandell, C. Ziebert, F. Schäfers, W. Braun, J. Halbritter, S. Ulrich, W. Eberhardt, L. Hultman, H. Siegbahn, S. Svensson, U. Jansson, Surf. Coat. Technol. 202 (2008) 3563.
[36] E. Lewin, M. Råsander, M. Klintenberg, A. Bergman, O. Eriksson, U. Jansson, Chem. Phys. Lett. 496 (2010) 95.
[37] Y.S. Won, Y.S. Kim, V.G. Varasi, O. Kryliouk, T.J. Anderson, C.T. Sirimanne, L. MacElwee-White, J. Cryst. Growth 304 (2007) 324.
[38] C. Adelhem, M. Balden, M. Rasinski, M. Linding, T. Plocinski, E. Welter, M. Sikora, Surf. Coat. Technol. 205 (2011) 4335.
[39] K. Holmberg, A. Matthews, Coatings tribology: properties, mechanisms, techniques and applications in surface engineering, Tribology and Interface Engineering Series, vol. 56, Elsevier, Amesterdam, 1994.
[40] A.C. Ferrari, in: C. Donnet, A. Erdemir (Eds.), Tribology of Diamond-like Carbon: Fundamentals and Applications, Springer, New York, 2008, p. 74.
[41] W. Dai, G. Wu, A. Wang, Appl. Surf. Sci. 257 (2010) 244.
[42] D.-H. Kim, H.-E. Kim, K.-R. Lee, C.-N. Whang, I.-S. Lee, Mater. Sci. Eng. C 22 (2002) 9.
[43] ENV1071-11, Advanced Technical Ceramics — Methods of Test for Ceramic Coatings — Part 11: Measurement of Internal Stress with the Stoney Formula, 2004.
[44] B. Bhushan, Modern Tribology Handbook, CRC Press LLC, Florida, 2000.
[45] J. Jiang, R.D. Arnell, Wear 239 (2000) 1.

Thin Solid Films 548 (2013) 661

Contents lists available at ScienceDirect

Thin Solid Films

journal homepage: www.elsevier.com/locate/tsf

Corrigendum

Corrigendum to “a-C(:H) and a-C(:H)_Zr coatings deposited on biomedical Ti-based substrates: Tribological properties” [Thin Solid Films 538 (2013) 89–96]

A. Escudeiro[a,*], T. Polcar[b,c], A. Cavaleiro[a]

[a] SEG-CEMUC, Department of Mechanical Engineering, University of Coimbra, 3030-788 Coimbra, Portugal
[b] National Centre for Advanced Tribology (nCATS), School of Engineering Sciences, University of Southampton, Highfield, Southampton SO17 1BJ, UK
[c] Department of Control Engineering, Czech Technical University in Prague, Technicka 2, Prague 6, Czech Republic

The authors regret that the two plots in Fig. 7 are the same. Fig. 7a should be referred to the following plot.

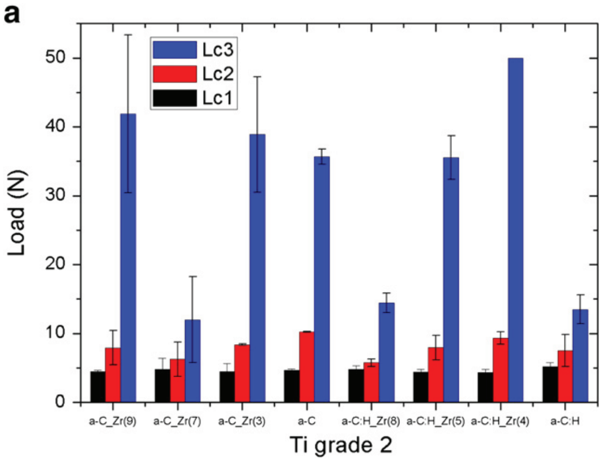

Fig. 7. a. Critical loads for the coating deposited on (a) Ti grade 2.

These corrections do not affect the conclusions in this paper. The authors would like to apologise for any inconvenience caused.

DOI of original article: http://dx.doi.org/10.1016/j.tsf.2012.12.086.

* Corresponding author. Tel.: +351 239790745.
E-mail address: ana.escudeiro@dem.uc.pt (A. Escudeiro).

http://dx.doi.org/10.1016/j.tsf.2013.10.130

PAPER III

Indentation and scratch testing of DLC-Zr coatings on ultrafine-grained titanium processed by high-pressure torsion

C.T. Wang, A. Escudeiro, T. Polcar, A. Cavaleiro, R.J.K. Wood, N. Gao and T.G. Langdon

Wear, 306, 1-2 **(2013)** 304-310

Wear 306 (2013) 304–310

Contents lists available at ScienceDirect

Wear

journal homepage: www.elsevier.com/locate/wear

Indentation and scratch testing of DLC-Zr coatings on ultrafine-grained titanium processed by high-pressure torsion

Chuan Ting Wang [a,b], Ana Escudeiro [c], Tomas Polcar [a], Albano Cavaleiro [c], Robert J.K. Wood [a], Nong Gao [b,*], Terence G. Langdon [b,d]

[a] National Centre for Advanced Tribology at Southampton, Faculty of Engineering and the Environment, University of Southampton, Southampton SO17 1BJ, UK
[b] Materials Research Group, Faculty of Engineering and the Environment, University of Southampton, Southampton SO17 1BJ, UK
[c] SEG-CEMUC – Department of Mechanical Engineering, University of Coimbra, 3030-788 Coimbra, Portugal
[d] Departments of Aerospace & Mechanical Engineering and Materials Science, University of Southern California, Los Angeles, CA 90089-1453, USA

ARTICLE INFO

Article history:
Received 17 October 2012
Received in revised form
18 December 2012
Accepted 20 December 2012
Available online 11 January 2013

Keywords:
High-pressure torsion
Titanium
DLC-Zr coatings
Adhesion
Bio-implants

ABSTRACT

High-pressure torsion was employed to refine the microstructure of grade 2 Ti under an imposed pressure of 3.0 GPa at room temperature. The microhardness of grade 2 Ti increased from 1.82 GPa for the coarse grain state to 3.05 GPa after high-pressure torsion processing, where this value is very close to the hardness of the Ti–6Al–4V alloy. Subsequently, several diamond-like carbon (DLC) coatings with thicknesses of ~1.4 μm were deposited on as-received Ti, high-pressure torsion processed Ti and Ti–6Al–4V samples via physical vapour deposition. Both indentation and scratch tests showed a much improved adhesion of DLC-7Zr, DLC:H-7Zr and DLC-9Zr coatings with high-pressure torsion processed Ti as the substrate by comparison with the same coatings on coarse-grained Ti. The results suggest that commercial pure Ti processed by high-pressure torsion and coated with a diamond-like carbon coating provides a potential candidate material for bio-implant applications.

1. Introduction

Human joints might suffer from pain and functional loss due to degenerative diseases, aging and accidents. A total joint replacement is regarded as an effective procedure for treating joint diseases and fractures [1]. A technical survey reported that there is an increasing demand for new and improved implants because of a rapidly growing patient population and increasing numbers of younger patients [2]. The Ti–6Al–4V alloy was designed originally for the aerospace industry but it has been used widely for biomedical applications due to its high strength, good fatigue characteristics, bio-tolerance and excellent corrosion resistance [1]. Despite these attractive qualities, Ti–6Al–4V has significant drawbacks which limit its further capacity to be used as an orthopaedic and dental implant material. For example, the toxic Al and V ions released from Ti–6Al–4V may cause long-term health problems and adverse reactions with body tissues [3,4]. Therefore, there is now an urgent need for exploring the potential for developing other bio-metals.

Pure titanium has excellent properties including high corrosion resistance, low electronic conductivity, a low ion-formation tendency and very good biocompatibility. All these characteristics make it a very good candidate as an implant material. Nevertheless, pure titanium has a relatively low strength and a very poor wear resistance when it is subjected to sliding and abrasion. Thus, it is generally not suitable for use in artificial joints which seek materials with high strength and good tribological properties. Recently, pure titanium with ultra-fine grain sizes, processed through the application of severe plastic deformation (SPD), appears to offer an alternative possibility for the production of implant materials [5,6]. In severe plastic deformation processing, a high level of straining is imposed on a metal using an extensive hydrostatic pressure and the strain is achieved without changing the overall dimensions of the material [7,8]. Thus, a very large strain may be imposed on materials via repeated severe plastic deformation processing. The ultrafine-grained (UFG) materials produced by severe plastic deformation often possess extraordinary properties, including both high strength and toughness [9], long fatigue life [10,11] and reasonable wear resistance [12,13]. To date, various severe plastic deformation processing methods have been applied successfully for the production of high strength pure Ti [6,14–17]. However, the evidence suggests that severe plastic deformation processing may lead to only a relatively minor improvement in the wear resistance of Ti [5,18]. As an alternative approach, it appears that surface treatments or coatings may be necessary to enhance the service durability of titanium as implant components [19].

The idea of improving wear resistance of Ti alloys via surface treatment has been reported extensively. Surface engineering technologies such as thermal oxidation, ion implantation and

---

[*] Corresponding author. Tel.: +44238 0593396; fax: +44238 0593016.
E-mail address: n.gao@soton.ac.uk (N. Gao).

0043-1648/$ - see front matter © 2012 Elsevier B.V. All rights reserved.
http://dx.doi.org/10.1016/j.wear.2012.12.033

thin coatings can significantly improve the tribological properties of Ti alloys. The high strength of coatings were favourable to maintain the low surface roughness during sliding motion, which also led to less wear loss of the polyethylene counterpart [20,21].

In recent years, attention has moved to surface engineering of ultrafine-grained Ti. High-current-density nitrogen ion implantation was used to enhance the wear resistance of ultrafine-grained Ti and the results demonstrated the potential for forming a hard layer with good wear and corrosion resistance on the surface of ultrafine-grained Ti via ion implantation [22]. However, this method required that the samples were held at the relatively high temperature of 820 K and there is evidence this may be recrystallisation of the ultrafine-grained structure of Ti when the temperature is above ~620 K [23]. It appears, therefore, that chemical vapour deposition (CVD) and physical vapour deposition (PVD) may be better approaches for this purpose because this permits the use of a lower processing temperature and easier control over the surface roughness. It is important to note that PVD methods such as magnetron sputtering can be controlled at room temperature leading to a much lower internal stress at the interface. For example, a thin and hard TiN coating was deposited on both coarse-grained and ultrafine-grained Ti substrates using PVD at a temperature below 420 K in a recent study [19]. The subsequent wear tests showed that the TiN coating improved the wear resistance of Ti by nearly two orders of magnitude and the ultrafine-grained Ti was a better substrate than coarse-grained Ti due to its higher strength. Therefore, a PVD coating on ultrafine-grained Ti shows significant promise for further exploration in future bio-implant applications.

Diamond-like carbon (DLC) coatings are regarded as other good candidates for the purpose of wear protection because of their excellent mechanical and tribological properties such as high hardness, good wear and corrosion resistance. Moreover, DLC coatings also have a much lower coefficient of friction (COF) which can also reduce the wear of the counter surface during sliding [24]. To date, several studies have explored DLC coatings for bio-implant use [25–27]. Despite the excellent tribological properties of DLC coatings, delamination of the coatings was a major problem which appeared to limit their application as articulating joints [25]. It is reasonable to anticipate that, once removed from the substrate, these DLC coating particles would act as a third body causing severe damage to the substrate or even severe reactions with the tissue. In order to solve these issues, studies have been reported exploring the use of new interlayers to improve the bonding of DLC coatings [28]. Doping with metallic elements, such as Cr [21,29], Ti [30] and W [31], may also improve the adhesion and wear resistance. Recently, zirconium was used as a dopant metal to provide low-toxicity, good tribological behaviour and high corrosion resistance [32–34].

The present investigation was therefore initiated in order to explore the effect of substrate microstructure on the adhesion behaviour and scratch resistance of DLC-7Zr, DLC:H-7Zr and DLC-9Zr coatings deposited on grade 2 pure titanium substrates both with and without high-pressure torsion processing and, in addition, to make a direct comparison with deposition on a Ti–6Al–4V substrate.

2. Experimental materials and procedures

2.1. Materials and processing

The experiments were conducted using grade 2 pure titanium having a composition of 0.015 H, 0.1C, 0.25 O, 0.03 N, 0.3 Fe and balance Ti (wt%) and the Ti–6Al–4V alloy with extra low interstitials. Initially, some of the grade 2 Ti samples were subjected to high-pressure torsion processing. The samples for high-pressure torsion were machined into disks with a diameter of 10 mm and thicknesses between 0.80 and 0.85 mm. During high-pressure torsion, the disk samples were held in shallow depressions on the faces of two massive anvils, a load was applied and then torsional straining was achieved through rotation of the lower anvil. In high-pressure torsion, the shear strain, γ, at different position of the disk can be estimated using the relationship [35]

$$\gamma = \frac{2\pi NR}{h} \tag{1}$$

where N is the number of rotation revolutions, R is the distance from the centre of the disk and h is the height (or thickness) of the sample. In this study, high-pressure torsion processing was conducted using an imposed pressure of 3.0 GPa for 10 revolutions under quasi-constrained conditions in which there is some restricted outflow of material around the periphery of the disk during the processing operation [36,37]. Additional details on the principles of high-pressure torsion processing are given in earlier reports [38–40].

Microhardness testing of the samples was performed under an indentation load of 1 kg for 15 s. As described earlier [19], tensile testing was conducted at room temperature after high-pressure torsion processing using an initial tensile strain rate of $1.0 \times 10^{-2}\ \mathrm{s}^{-1}$. The microstructures of the materials were examined using a JEM 3010 transmission electron microscope (TEM) operating under an accelerating voltage of 200 kV. A detailed description of these analytical procedures was given in earlier reports [5,19].

2.2. Coating deposition and characterisation

Prior to deposition, the substrates were polished to a roughness less than 50 nm, cleaned in an ultrasonic bath in acetone, ethanol and distilled water for 15 min, and then etched using Ar^+ bombardment for 1 h at a substrate bias voltage of −650 V in order to remove all contaminants and oxides on the substrate surface. The coatings were deposited using dc dual magnetron sputtering in an Ar atmosphere (non-reactive process) and $\mathrm{Ar}+\mathrm{CH}_4$ (reactive process) to produce non-hydrogenated and hydrogenated coatings, respectively. Two targets were used: titanium was used to deposit an interface layer and a graphite target was used with embedded Zr pellets to prepare functional film. Table 1 summarises the deposition parameters. The work pressure was maintained constant for both reactive and non-reactive sputtering by adjusting the gas flow. A pulsed bias voltage of −50 V and a frequency of 250 kHz were applied. A TiN/TiCN interlayer with a varying composite gradient and a thickness of 450 nm was deposited in order to improve adhesion. The thickness of the functional coating was approximately 1 μm so that the total film thickness was of the order of ~1.4 μm. To facilitate a detailed description of the results, the coatings were denoted as DLC-XZr and DLC:H-XZr, where X represents the zirconium content.

Table 1
Deposition parameters of DLC-XZr and DLC:H-XZr coatings.

Parameters	DLC-XZr	DLC:H-XZr
Reactive gas flow (%)	–	5
Ar flow (%)	45	40
Base pressure (Pa)	1.5×10^{-3}	
Work pressure (Pa)	0.4	
Substrate bias (V)	−50	
Graphite doped target (W/mm^2)	0.075	

The chemical composition was determined by electron probe microanalysis (EPMA) applying a 10 keV voltage. The coating hardness was measured by depth-sensing indentation using a Berkovich indenter and a load of 5 mN. A series of 32 indentations from two distinct areas were carried out in order to critically evaluate the hardness of the coatings. In addition, the reduced Young modulus was derived from the indentation measurements using the standard method [41]. The Young modulus was calculated using the following parameters: $E_i = 1140$ GPa and $\nu_i = 0.07$ for the diamond indenter and $\nu = 0.3$ for the coating [41].

2.3. Rockwell C indentation and scratch test

The coating adhesion to the Ti substrates was evaluated using Rockwell C indentation and scratch testing where these are standard techniques commonly used to quantify the interfacial strength of coating-substrate systems. During the Rockwell C indentation test, a cone-shaped diamond 120° tip (200 μm in radius) was indented perpendicularly onto the coating applying a normal load of 200 N, thereby causing layer damage to the boundary of the indentation. The results of the test were qualitatively evaluated by comparing the optical microscope images of the crack network and the degree of delamination with an adhesion quality chart which classifies the images into six levels from HF1-HF6 [42]. In this classification, HF1 is featured with only a few minor cracks after indentation which indicates a good bonding while at the other extreme HF6 denotes extensive delamination of the coating and very poor adhesion. Adhesion levels from HF1 to HF4 are typically considered as acceptable coating adhesions for use in commercial applications.

The scratch test was performed by using a spherical Rockwell C diamond indenter (200 μm radius) according to standard testing methods [43]. The indenter was slid over the coating surface and the load increased from 2 to 50 N at a speed of 10 N/mm. The lower critical load, L_{c1}, was defined as the load where the first cracks occurred (representing cohesive failure) and the upper critical load, L_{c2}, was defined as the load associated with the first delamination at the edge of the scratch track (representing adhesive failure). In addition, a load L_{c3} was defined as the load under which the coating was totally removed from the substrate. The scratch tests were repeated for three times in order to obtain reliable results. After scratch testing, the cracking or delamination of the coating was observed using optical microscopy along the scratch track. The cross-section profiles of the DLC coatings at the critical load were measured using an ultimate focus optical microscope operating in the line scanning mode.

3. Experimental results

3.1. Mechanical properties of Ti substrates

The results of optical microscopy and TEM showed that high-pressure torsion processing significantly refined the grain size of pure Ti from ~8.6 μm in the as-received state to ~130 nm after high-pressure torsion processing. Due to this grain refinement, the microhardness of pure Ti increased from an initial value of ~1.82 GPa in the coarse-grained state to ~3.05 GPa after high-pressure torsion processing. This latter value for the ultrafine-grained pure Ti is comparable with the hardness of 3.09 GPa for the Ti–6Al–4V alloy used in this study [5].

The tensile testing demonstrated that the ultimate tensile strength (UTS) of Ti increased from ~660 MPa in the coarse-grained state to ~940 MPa after high-pressure torsion with some associated reduction in ductility [19]. This high strength and reasonable ductility of ultrafine-grained pure Ti is compatible with the Ti–6Al–4V alloy where the UTS is ~980 MPa and the elongation to failure is ~14%.

3.2. Coating characterisation

Table 2 shows the zirconium content, the hardness and the values of the Young modulus of the deposited coatings. It should be noted that the low indentation depth for the indenter (approximately 10% of the coating thickness) made it difficult to ascertain the effect from the substrate material when obtaining these mechanical properties. Details of the coating structure were studied by X-ray diffraction, Raman spectroscopy and X-ray photoelectron spectroscopy and these results were reported elsewhere [33,44]. All of the coatings investigated in this study (with Zr contents of 7–9 at%) exhibited a nanocomposite structure with very small ZrC nanograins (up to ~2 nm) embedded within an amorphous carbon matrix.

3.3. Adhesion performance of the DLC coatings

Table 3 summaries the adhesion results of DLC coating on all three substrates. The Rockwell C indentation tests showed HF3 and HF4 for all samples with only minor delamination and microcracking observed around the indentation marks, thereby demonstrating an acceptable adhesion for all tested coatings. The scratch test results showed that the DLC coatings with UFG Ti and Ti–6Al–4V substrates had similar critical loads and these loads were much higher than with the coarse-grained Ti as substrates. Thus, the UFG Ti and Ti–6Al–4V substrates provided better support with their higher hardness and this produced a higher critical load of the DLC coating. These results demonstrate again the important role of substrates for the adhesion of thin DLC coatings.

Optical images of the Rockwell indentations are shown in Fig. 1. It can be seen that the load of 200 N led to radial plastic deformation of the coating which caused circumferential cracking of the film outside the indentation area. Through-thickness cracks were observed on all coatings which may be related to the elastic-plastic boundary of the substrates. The indentation marks had a diameter of ~380 μm on the DLC/coarse-grained Ti samples

Table 2
Summary of coatings chemical composition and mechanical properties.

System	Zr content (at%)	Hardness (GPa)	*E* (GPa)
DLC-7Zr	7 ± 1	11 ± 2	120 ± 3
DLC:H-7Zr	8 ± 1	13 ± 1	117 ± 4
DLC-9Zr	10 ± 1	12 ± 2	131 ± 3

Table 3
Summary of adhesion results.

Substrate	Coating	Rockwell C		Scratch			
		Ø (μm)	Adhesion	L_{c1} (N)	L_{c2} (N)	L_{c3} (N)	Track width at L_{c3} (μm)
CG Ti	DLC-7Zr	375	HF3	7 ± 2	8 ± 1	13 ± 2	149.7
	DLC:H-7Zr	391	HF4	5 ± 1	7 ± 2	13 ± 1	130.1
	DLC-9Zr	384	HF4	7 ± 1	9 ± 1	15 ± 1	130.7
UFG Ti	DLC-7Zr	282	HF3	8 ± 1	12 ± 1	22 ± 2	113.3
	DLC:H-7Zr	286	HF3	7 ± 2	10 ± 1	20 ± 1	120.9
	DLC-9Zr	287	HF3	10 ± 2	14 ± 1	24 ± 1	123.8
Ti–6Al–4V	DLC-7Zr	277	HF3	9 ± 2	11 ± 1	23 ± 2	139.7
	DLC:H-7Zr	274	HF4	5 ± 1	10 ± 2	19 ± 2	132.1
	DLC-9Zr	282	HF3	11 ± 2	15 ± 1	25 ± 2	126.2

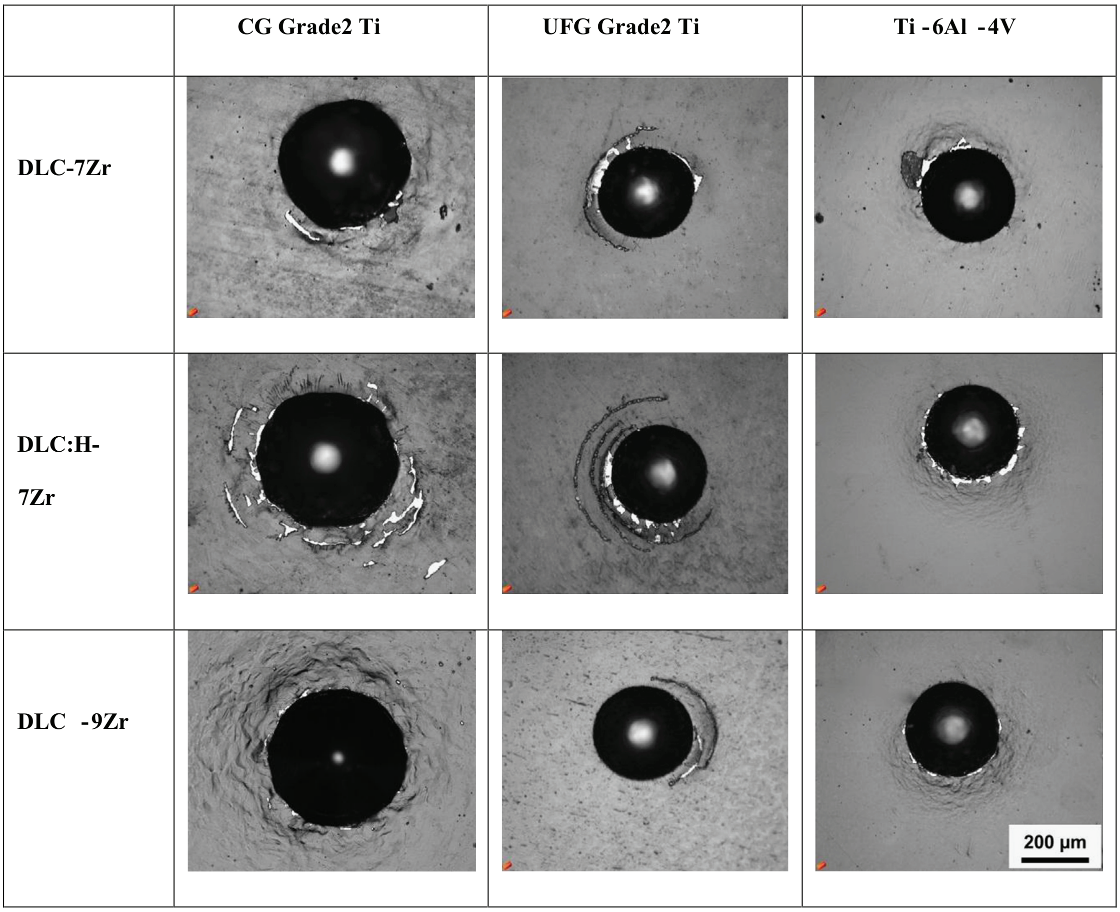

Fig. 1. Rockwell indentation of DLC on different Ti substrates.

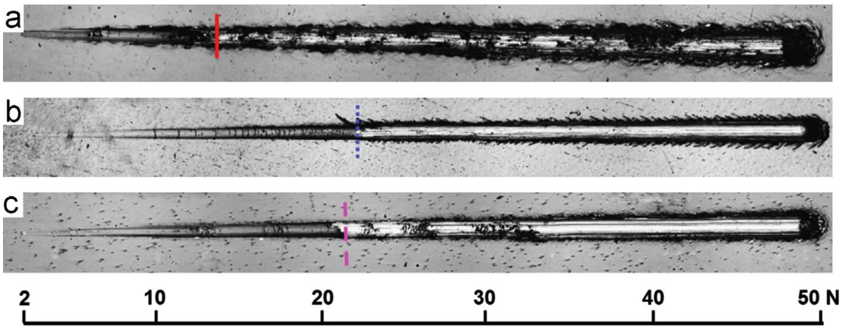

Fig. 2. Scratch tracks of DLC-7Zr coatings on (a) coarse-grained Ti, (b) ultrafine-grained Ti, and (c) Ti–6Al–4V substrates.

which would cause more deformation at the edge and more delamination compared to the DLC/ultrafine-grained Ti and DLC/Ti–6Al–4V samples. This effect was mainly caused by the different hardness of the Ti substrates. Furthermore, the doping of H content led to a decrease in the adhesion strength because all the indents of the DLC:H-7Zr coating showed a higher delamination than DLC-7Zr. It is obvious that the DLC-9Zr coatings with higher Zr content presented the best adhesion behaviour with only small cracks and minor coating delamination. Therefore, it may be possible to further enhance the coating adhesion by increasing the zirconium content. A more comprehensive study of the adhesion of DLC coatings with different Zr content is given elsewhere [44].

The scratch test results matched well with observation from the Rockwell indentations. Fig. 2 shows the scratch tracks of the DLC-7Zr coating on the Ti substrates with increasing loads from 2 to 50 N. Generally, the plastic deformation of the Ti substrates was the main cause for the coating failure. As the diamond stylus was sliding with increasing normal load on the coating surface, the coating followed the deformation of the Ti substrate. The tensile stress both inside the coating and at the interface led to cracking and delamination of the coatings. As shown in Fig. 2(a), the DLC-7Zr coating on coarse-grained Ti failed at an early stage during the scratch test and the indenter caused extensive deformation of the substrate. On the other hand, the DLC-7Zr coatings deposited on ultrafine-grained Ti and Ti–6Al–4V failed at a higher

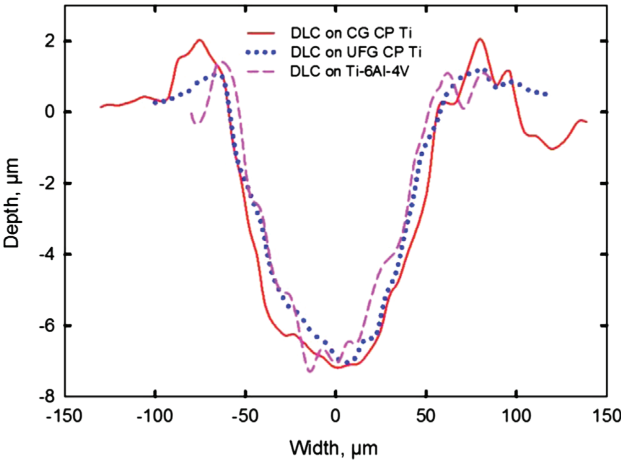

Fig. 3. Cross-section of the scratch tracks in the positions indicated in Fig. 2.

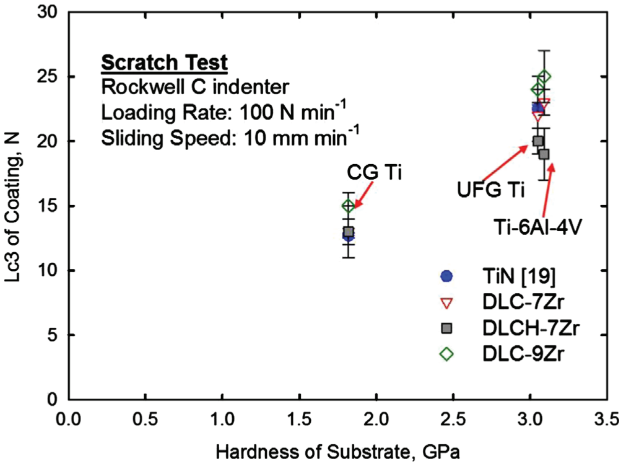

Fig. 4. Critical load of coatings versus the hardness of substrates.

load and the adhesion of the films deposited on both substrates was almost identical (Fig. 2(b) and (c)). The cross-section of the scratch tracks where the substrate was revealed in the scratch track (see the short vertical lines in Fig. 2(a)–(c)) was measured using an ultimate focus optical microscope. Although the coating was deposited onto different substrates, these measurements showed that it always failed when the scratch track was approximately 7 μm deep and 130 μm wide as illustrated in Fig. 3.

4. Discussion

In this study, a grade 2 pure Ti was processed using high-pressure torsion to achieve significant grain refinement and then DLC coatings were successfully deposited on the different Ti substrates and their scratch behaviour was studied. In terms of future bio-medical applications, the results provide a clear demonstration that it is possible to replace the conventional Ti–6Al–4V alloy with ultrafine-grained pure Ti having preferable mechanical properties which may be achieved through high-pressure torsion processing.

Various coating technologies are now available to provide wear resistance for bio-implants. Technologies such as plasma electrolytic oxidation (PEO) and internal oxidation (IO) have been used extensively to process Ti–6Al–4V and other bio-metals but these methods often involve a high processing temperature which may lead to recrystallisation of ultrafine-grained structures [45,46]. When ultrafine-grained materials are chosen as the substrates, the post processing temperature must not exceed the recrystallisation temperature in order to restrict any grain growth of the ultrafine-grained structures. Moreover, the oxidation layers produced through these methods are often very rough and this will entail additional polishing before their use in implants. Thus, PVD methods are regarded as one of the best choices for surface modifying ultrafine-grained materials.

A good adhesion between the thin coating and the substrate is essential for the coating/substrate system. The interposition of a gradient layer (Ti/TiN/TiCN) improves the interface shear strength and the load bearing capacity of the coating [28]. It was observed in this study that, when using ultrafine-grained Ti as the substrate, the load bearing capacity of DLC coatings was improved extensively compared to those with coarse-grained Ti as substrates. A similar trend was observed also on TiN thin coatings on different Ti substrates [19]. The TiN on ultrafine-grained Ti also had a higher critical failure load as it prevented the thin coating from undergoing deformation. Fig. 4 shows the critical load of the DLC coatings and TiN coating on Ti substrates plotted against the hardness of the substrate. The trend is clear because a harder substrate after high-pressure torsion leads to a higher critical load for the coatings. Therefore, on one hand it is very important to explore better coating parameters such as new interlayer designs and coating compositions in order to achieve a good performance of the coatings. On the other hand, it is also very important to enhance the properties of substrates through surface hardening or grain refinement (i.e. increase the H/E ratio) and thereby give a better support to the thin coatings.

The results from this research showed that the DLC coating failures occurred at the same depth and width of penetration for all three substrates, as is clearly observed in Fig. 3. As the UFG Ti and Ti–6Al–4V had very similar hardness, therefore, the datum points were very close to each other. As shown in Fig. 3, the critical load of all coatings increased with increasing hardness of the substrates. A similar trend was also observed on various TiN coated substrates including stainless steel, high speed steel and WC [47]. An explanation was given by assuming the TiN coating adjusted to the elastic–plastic deformation of the substrates therefore the coating underwent a cohesive–adhesive failure that leads to film delamination. A critical indentation width of 60 μm was observed in that study, where the coating failed whenever it was bent to this width regardless of the substrate material.

By simplifying the coating-substrate system as a two-layer composite, the overall hardness of the coating-substrate system may be represented by the following relationship according to the Burnett–Rickerby model which is based on a volume law of mixtures [47–50]

$$H_{C,S} = \frac{V_C}{V_{total}} H_C + \frac{\chi^3 V_S}{V_{total}} H_S \tag{2}$$

where $H_{C,S}$ is the apparent hardness of the coating-substrate system, H_S is the hardness of the substrate, H_C is the hardness of the coating, χ is a factor by which the plastic zone changes, and the V_C, V_S and V_{total} are the deformation volumes of the coating, substrate and total deformation volume, respectively.

The volumes of the deformation zones are expressed by the following equations:

$$V_C \approx \pi R_C^2 t \tag{3}$$

$$V_S \approx \chi^3 \frac{2}{3} \pi R_S^3 \tag{4}$$

where R_C and R_S are the radii of deformation zone of coating and substrate, respectively. The factor, χ was determined via fitting experimental results by Burnett and Rickerby [48] and addressed as

$$\chi=\left(\frac{E_C H_S}{E_S H_C}\right)^{1/2} \tag{5}$$

where E_C and H_C are the Young's Modulus and hardness of the coating, and E_S and H_S are the Young's Modulus and hardness of the substrate, respectively. R_C and R_S can be obtained through the equation

$$R=r\left(\frac{E}{H}\right)^{1/2} \tag{6}$$

where r is the geometrical length of the indentation volume.

As observed in Fig. 3, the indentation depths of all samples were only around 7 μm, and this depth was obtained after the diamond indenter was removed. In this case, the measured indentation depth was underestimated due to the elastic recovery of materials. Therefore, it is more accurate to recalculate the indentation depth using the measured indentation width considering the sphere shape of the indenter, according to the equation

$$r=\left[\pi\left(R_{ind}^2-\frac{W^2}{4}\right)\left(R_{ind}-\frac{\sqrt{R_{ind}^2-\frac{W^2}{4}}}{3}\right)\right]^{1/3} \tag{7}$$

where R_{ind} is the radius of diamond indenter and W is the track width at the critical load point.

Therefore, the overall hardness of this coating-substrate is achieved by rewriting Eqs. (2)–(6)

$$H_{C,S}=\frac{E_C t+\frac{2}{3} r H_S\left(\frac{E_C}{H_C}\right)^{3/2}}{\left(\frac{E_C}{H_C}\right)t+\left(\frac{2}{3}\right)r\left(\frac{E_C}{H_C}\right)^{3/2}} \tag{8}$$

During the scratch testing, the indenter was travelling with an increasing normal load and it was always the front half of the spherical cap in the coating-substrate system. Therefore, the critical load, L_{C3}, is expressed as

$$L_{C3}=H_{C,S}\pi R_{ind}\sqrt{R_{ind}^2-\frac{W^2}{4}} \tag{9}$$

Thus, Eqs. (8) and (9) clearly emphasise the effect of substrate strength on the scratch behaviour of thin coatings. It further explains that the DLC coatings, with thicknesses around 1 μm, often exhibit high critical loads with hard materials as substrates, such as more than 100 N on Si or glass [51].

The track width of each sample is listed in Table 3 and this can be applied to Eqs. (8) and (9). The comparison between experimental results and the Burnett–Rickerby model is plotted in Fig. 5. It worth noting that as the interlayers had varying compositions and properties and were much thinner than the coatings, thus this analysis simply neglects the properties of the interlayers although in practice the interlayer is important in improving the bonding. This may lead to an underestimation of the model. Moreover, errors may also be introduced due to the ridges formed at the edge of the scratch tracks which made it difficult to measure the track widths.

In this study, the strength and hardness of pure Ti were successfully improved by high-pressure torsion processing. Firstly, this improves the mechanical durability of pure Ti as the main body of bio-implants when they suffer fatigue and shear loadings. Secondly, ultrafine-grained pure Ti is a good substrate for thin coatings and provides improved load bearing capacity of the coating. Therefore, with good strength, fatigue life, excellent biocompatibility and no toxic release tendency of ultrafine-grained pure Ti, and with good wear resistance and an extremely low coefficient of friction of the DLC coatings, the DLC/ultrafine-grained Ti system appears to be an exceptionally strong candidate material for future bio-implant applications.

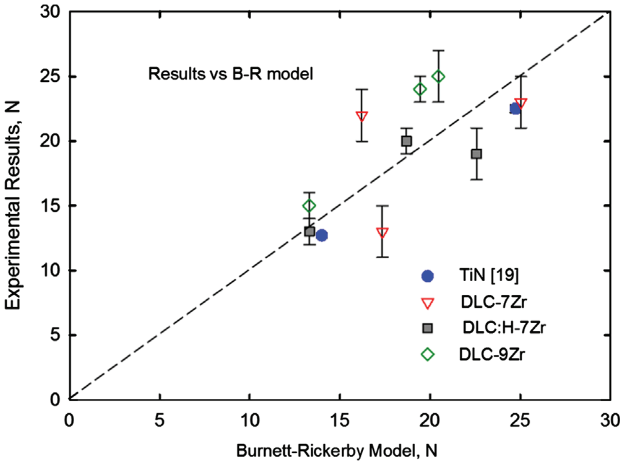

Fig. 5. Comparison of critical load between experimental results and calculation from Burnett and Rickerby model.

5. Conclusions

The adhesion behaviour and scratch resistance of three diamond-like carbon coatings deposited on grade 2 pure Ti substrates before and after high-pressure torsion processing were investigated and a comparison was made with a Ti–6Al–4Vsubstrate. The following conclusions are reached:

1. DLC coatings with a gradient TiN/TiCN interlayer show good adhesion on Ti substrates.
2. Hydrogen-free DLC-Zr coatings have better adhesion than hydrogen-doped DLC-Zr coatings, and increase in the percentage of Zr increases the adhesion.
3. The effect of substrate on the performance of the DLC coating under high load was highlighted, showing that coatings with ultrafine-grained pure Ti and Ti–6Al–4V substrates have similar scratch and indentation behaviour. Both are significantly better than the results obtained with coarse-grained Ti substrates.

Acknowledgements

The authors are grateful for support from the University of Southampton together with a scholarship from the China Scholarship Council (CTW). This work was partially supported by EPSRC under Grant No. EP/D00313X/1 and by the National Science Foundation of the United States under Grant No. DMR-1160966 (TGL). The authors also acknowledge FCT-Fundação para a Ciência e a Tecnologia (QREN-POPH) for funding support under Grant SFRH/BD/75071/2010 which was co-funded by FSE and MSTES.

References

[1] M. Geetha, A.K. Singh, R. Asokamani, A.K. Gogia, Ti based biomaterials, the ultimate choice for orthopaedic implants – a review, Progress in Materials Science 54 (2009) 397–425.
[2] S.S. Leopold, Numbers for breakfast: summary of hip arthroplasty outcomes from the national joint registry for England and wales 8th annual report (2011), Journal of Bone and Joint Surgery 93 (2011) 1–3.

[3] Y. Li, C. Wong, J. Xiong, P. Hodgson, C. Wen, Cytotoxicity of Titanium and Titanium Alloying Elements, Journal of Dental Research 89 (2010) 493–497.

[4] S. Makihira, Y. Mine, H. Nikawa, T. Shuto, S. Iwata, R. Hosokawa, K. Kamoi, S. Okazaki, Y. Yamaguchi, Titanium ion induces necrosis and sensitivity to lipopolysaccharide in gingival epithelial-like cells, Toxicology in Vitro 24 (2010) 1905–1910.

[5] C.T. Wang, N. Gao, M.G. Gee, R.J.K. Wood, T.G. Langdon, Effect of grain size on the micro-tribological behavior of pure titanium processed by high-pressure torsion, Wear 280 (2012) 28–35.

[6] V.L. Sordi, M. Ferrante, M. Kawasaki, T.G. Langdon, Microstructure and tensile strength of grade 2 titanium processed by equal-channel angular pressing and by rolling, Journal of Materials Science 47 (2012) 7870–7876.

[7] R.Z. Valiev, T.G. Langdon, Principles of equal-channel angular pressing as a processing tool for grain refinement, Progress in Materials Science 51 (2006) 881–981.

[8] A.P. Zhilyaev, T.G. Langdon, Using high-pressure torsion for metal processing: fundamentals and applications, Progress in Materials Science 53 (2008) 893–979.

[9] R.Z. Valiev, I.V. Alexandrov, Y.T. Zhu, T.C. Lowe, Paradox of strength and ductility in metals processed by severe plastic deformation, Journal of Materials Research 17 (2002) 5–8.

[10] M. Kautz, H.W. Höppel, C. Xu, M. Murashkin, T.G. Langdon, R.Z. Valiev, H. Mughrabi, An overview: fatigue behaviour of ultrafine-grained metals and alloys, International Journal of Fatigue 28 (2006) 1001–1010.

[11] I.P. Semenova, R.Z. Valiev, E.B. Yakushina, G.H. Salimgareeva, T.C. Lowe, Strength and fatigue properties enhancement in ultrafine-grained Ti produced by severe plastic deformation, Journal of Material Science 43 (2008) 7354–7359.

[12] C.T. Wang, N. Gao, R.J.K. Wood, T.G. Langdon, Wear behavior of an aluminum alloy processed by equal-channel angular pressing, Journal of Materials Science 46 (2011) 123–130.

[13] N. Gao, C.T. Wang, R.J.K. Wood, T.G. Langdon, Tribological properties of ultrafine-grained materials processed by severe plastic deformation, Journal of Materials Science 47 (2012) 4779–4797.

[14] X. Zhao, W. Fu, X. Yang, T.G. Langdon, Microstructure and properties of pure titanium processed by equal-channel angular pressing at room temperature, Scripta Materialia 59 (2008) 542–545.

[15] X. Zhao, X. Yang, C. Wang, X. Wang, T.G. Langdon, The processing of pure titanium through multiple passes of ECAP at room temperature, Materials Science and Engineering A527 (2010) 6335–6339.

[16] I. Sabirov, R.Z. Valiev, I.P. Semenova, R. Pippan, Effect of equal channel angular pressing on the fracture behavior of commercially pure titanium, Metallurgical and Materials Transactions A 41 A (2010) 727–733.

[17] Y. Zhang, R.B. Figueiredo, S.N. Alhajeri, J.T. Wang, N. Gao, T.G. Langdon, Structure and mechanical properties of commercial purity titanium processed by ECAP at room temperature, Materials Science and Engineering A 528 (2011) 7708–7714.

[18] P. La, J. Ma, Y.T. Zhu, J. Yang, W. Liu, Q. Xue, R.Z. Valiev, Dry-sliding tribological properties of ultrafine-grained Ti prepared by severe plastic deformation, Acta Materialia 53 (2005) 5167–5173.

[19] C.T. Wang, N. Gao, M.G. Gee, R.J. Wood, T.G. Langdon, Processing of an ultrafine-grained titanium by high-pressure torsion: an evaluation of the wear properties with and without a TiN coating, Journal of the Mechanical Behavior of Biomedical Materials 17 (2013) 166–175.

[20] A.V. Byeli, V.A. Kukareko, A.G. Kononov, Titanium and zirconium based alloys modified by intensive plastic deformation and nitrogen ion implantation for biocompatible implants, Journal of the Mechanical Behavior of Biomedical Materials 6 (2012) 89–94.

[21] H. Dong, W. Shi, T. Bell, Potential of improving tribological performance of UHMWPE by engineering the Ti6Al4V counterfaces, Wear 225–229 (1999) 146–153.

[22] Z.X. Zhang, H. Dong, T. Bell, The load bearing capacity of hydrogen-free Cr-DLC coatings on deep-case oxygen hardened Ti6Al4V, Surface and Coatings Technology 200 (2006) 5237–5244.

[23] R.Z. Valiev, A.V. Sergueeva, A.K. Mukherjee, The effect of annealing on tensile deformation behavior of nanostructured SPD titanium, Scripta Materialia 49 (2003) 669–674.

[24] V.M. Tiainen, Amorphous carbon as a bio-mechanical coating-mechanical properties and biological applications, Diamond and Related Materials 10 (2001) 153–160.

[25] T.J. Joyce, Examination of failed ex vivo metal-on-metal metatarsophalangeal prosthesis and comparison with theoretically determined lubrication regimes, Wear 263 (2007) 1050–1054.

[26] C.V. Falub, U. Mueller, G. Thorwarth, M. Parlinska-Wojtan, C. Voisard, R. Hauert, In vitro studies of the adhesion of diamond-like carbon thin films on CoCrMo biomedical implant alloy, Acta Materialia 59 (2011) 4678–4689.

[27] R. Hauert, G. Thorwarth, U. Mueller, M. Stiefel, C.V. Falub, K. Thorwarth, T.J. Joyce, Analysis of the in-vivo failure of the adhesive interlayer for a DLC coated articulating metatarsophalangeal joint, Diamond and Related Materials 25 (2012) 34–39.

[28] J. Chen, G.A. Bell, B.D. Beake, H. Dong, Low temperature nano-tribological study on a functionally graded tribological coating using nanoscratch tests, Tribology Letters 43 (2011) 351–360.

[29] A. Pardo, C. Gomez-Aleixandre, J.O. Orwa, A. Cimmino, S. Prawer, Modification of characteristics of diamond-like carbon thin films by low chromium content addition, Diamond and Related Materials 26 (2012) 39–44.

[30] F. Zhao, H. Li, L. Ji, Y. Wang, H. Zhou, J. Chen, Ti-DLC films with superior friction performance, Diamond and Related Materials 19 (2010) 342–349.

[31] A. Czyzniewski, Optimising deposition parameters of W-DLC coatings for tool materials of high speed steel and cemented carbide, Vacuum 86 (2012) 2140–2147.

[32] D.B.N. Lee, M. Roberts, C.G. Bluchel, R.A. Odell, Zirconium: Biomedical and Nephrological Applications, ASAIO Journal 56 (2010) 550–556.

[33] A. Escudeiro, T. Polcar, A. Cavaleiro, a-C(:H) and a-C(:H)-Zr coatings deposited on biomedical Ti-based substrates: tribological properties, Thin Solid Films, http://dx.doi.org/10.1016/j.tsf.2012.12.086, in press.

[34] P. Kumar, P. Dilli Badu, L. Moham, C. Anandan, V.K. William Grips, Wear and corrosion resistance of Zr doped DLC on Ti–13Zr–13Nb biomedical alloy, Journal of Materials Engineering and Performance 22 (2013) 283–293.

[35] R.Z. Valiev, V. Ivanisenko, E.F. Rauch, B. Baudelet, Structure and deformation behaviour of Armco iron subjected to severe plastic deformation, Acta Materialia 44 (1996) 4705–4712.

[36] R.B. Figueiredo, P.R. Cetlin, T.G. Langdon, Using finite element modeling to examine flow processes in quasi-constrained high-pressure torsion, Materials Science and Engineering A528 (2011) 8198–8204.

[37] R.B. Figueiredo, P.H.R. Pereira, M.T.P. Aguilar, P.R. Cetlin, T.G. Langdon, Using finite element modeling to examine the temperature distribution in quasi-constrained high-pressure torsion, Acta Materialia 60 (2012) 3190–3198.

[38] A.P. Zhilyaev, G.V. Nurislamova, B.K. Kim, M.D. Baró, J.A. Szpunar, T.G. Langdon, Experimental parameters influencing grain refinement and microstructural evolution during high-pressure torsion, Acta Materialia 51 (2003) 753–765.

[39] M. Kawasaki, T.G. Langdon, The significance of strain reversals during processing by high-pressure torsion, Materials Science and Engineering A498 (2008) 341–348.

[40] C.T. Wang, N. Gao, R.J.K. Wood, T.G. Langdon, Wear behaviour of Al-1050 alloy processed by severe plastic deformation, Materials Science Forum 667–669 (2011) 1101–1106.

[41] W.C. Oliver, G.M. Pharr, An improved technique for determining hardness and elastic-modulus using load and displacement sensing indentation experiments, Journal of Materials Research 7 (1992) 1564–1583.

[42] N. Vidakis, A. Antoniadis, N. Bilalis, The VDI 3198 indentation test evaluation of a reliable qualitative control for layered compounds, Journal of Materials Processing Technology 143 (2003) 481–485.

[43] J. Stallard, S. Poulat, D.G. Teer, The study of the adhesion of a TiN coating on steel and titanium alloy substrates using a multi-mode scratch tester, Tribology International 39 (2006) 159–166.

[44] A. Escudeiro, T. Polcar, A. Cavaleiro, DLC(H) doped with Zr coatings for orthopaedics applications: adhesion properties, SVC Spring 2013 Bulletin.

[45] J.M. Wheeler, C.A. Collier, J.M. Paillard, J.A. Curran, Evaluation of micromechanical behaviour of plasma electrolytic oxidation (PEO) coatings on Ti–6Al–4V, Surface and Coatings Technology 204 (2010) 3399–3409.

[46] G. Purcek, O. Saray, F. Rubitschek, T. Niendorf, H.J. Maier, I. Karaman, Effect of internal oxidation on wear behavior of ultrafine-grained Nb–Zr, Acta Materialia 59 (2011) 7683–7694.

[47] A. Rodrigo, P. Perillo, H. Ichimura, On the correlation of substrate microhardness with the critical load of scratch adherence for hard coatings, Surface and Coatings Technology 124 (2000) 87–92.

[48] P.J. Burnett, D.S. Rickerby, The mechanical properties of wear resistant coatings.1. modelling of hardness behaviour, Thin Solid Films 148 (1987) 41–50.

[49] P.J. Burnett, D.S. Rickerby, The relationship between hardness and scratch adhesion, Thin Solid Films 154 (1987) 403–416.

[50] A. Rodrigo, H. Ichimura, Analytical correlation of hardness and scratch adhesion for hard films, Surface and Coatings Technology 148 (2001) 8–17.

[51] Y. Huang, Q. Wang, M. Wang, Z. Fei, M. Li, Characterization and analysis of DLC films with different thickness deposited by RF magnetron PECVD, Rare Metals 31 (2012) 198–203.

PAPER IV

Adsorption of bovine serum albumin on Zr co-sputtered a-C(:H) films: implication on wear behavior

A. Escudeiro, T. Polcar and A. Cavaleiro

Journal of Mechanical Behavior of Biomedical Materials 39 **(2014)** 316-327

JOURNAL OF THE MECHANICAL BEHAVIOR OF BIOMEDICAL MATERIALS 39 (2014) 316–327

Available online at www.sciencedirect.com

ScienceDirect

www.elsevier.com/locate/jmbbm

Research Paper

Adsorption of bovine serum albumin on Zr co-sputtered a-C(:H) films: Implication on wear behaviour

A. Escudeiro[a,*], *T. Polcar*[b,c], *A. Cavaleiro*[a]

[a]*SEG-CEMUC DEM University of Coimbra, Coimbra, Portugal*
[b]*Engineering Materials, University of Southampton, Highfield, Southampton, United Kingdom*
[c]*Department of Control Engineering, Czech Technical University in Prague, Technicka 2, Prague 6, Czech Republic*

ARTICLE INFO

Article history:
Received 15 May 2014
Received in revised form
30 July 2014
Accepted 3 August 2014
Available online 11 August 2014

Keywords:
DLC-Zr
H content
Wettability
Protein adsorption
Biotribology

ABSTRACT

The use of protective coatings in biomedical field is an ongoing scientific challenge. Among different materials, carbon-based coatings are considered a potential surface treatment for orthopaedic implants. In this study, the effect of Zr incorporation in amorphous carbon coatings on the wear behaviour under protein containing lubrication was investigated. The coatings were deposited by dc unbalanced magnetron sputtering in Ar (non-hydrogenated) and Ar+CH_4 (hydrogenated) discharges onto Ti based biomedical substrate. To improve the adhesion between the film and substrate a functional gradient Ti based layer was deposited (~550 nm). The surface wettability was evaluated to assess the effect of the Zr and hydrogen content. The films with Zr were found to be hydrophobic enhancing the protein adsorption onto the surface; no significant differences were found when H was incorporated in the films. The adsorption layer characterized by X-ray photoelectron spectroscopy showed a well defined nitrogen peak originating from the organic layer. The tribological properties of the film were evaluated by unidirectional pin-on-disc testing with diluted bovine serum lubrication and physiological solution at 37 ± 3 C°. The friction and the wear of the coatings were very low compared to uncoated substrates in both lubrication conditions. The ability of the surfaces to adsorb proteins was considered as the driving force for wear resistance acting as a protecting layer. In addition, the incorporation of Zr decreased the wear of the counterbody (Ti alloy) due to higher albumin adsorption.

1. Introduction

Fatigue fracture and wear have been identified as the major problems associated with implant loosening, stress-shielding and ultimate implant failure. Demanding contact conditions coupled with the aggressive body environment lead to fatigue failure of almost all implant materials. The fatigue wear process causes the generation of wear debris which, by acute host-tissue reactions, tend to aggravate and speed up the failure of the biomaterial. Wear is a critical issue for prostheses, implants

---

*Corresponding author.
E-mail address: ana.escudeiro@dem.uc.pt (A. Escudeiro).

http://dx.doi.org/10.1016/j.jmbbm.2014.08.001
1751-6161/

and other medical devices and its reduction is still an ongoing scientific and technological challenge. Diamond-like carbon (DLC) coatings have been widely studied to enhance implant performance due to its inertness, wear and corrosion resistance, hardness and excellent bio- and hemo-compatibility (Hauert 2003, 2004; Dearnaley and Arp, 2005; Love et al., 2013). In fact, DLC was already implanted as an artificial joint (Taeger et al., 2003; Joyce, 2007; Hauert et al., 2012a,b), surviving just 2–10 years due to delamination problems in-vivo. It is well known that DLC exhibits high internal stress which significantly limits the adhesion of the coating to metallic substrates. Thus, in order to overcome this problem, a metallic interlayer (Cr, Ti, Zr, Si, etc.) and/or functionally graded layers (Me/MeN/MeNC or Me/MeC, Me corresponds to the metallic element) have been deposited between the metallic substrate and the DLC coatings avoiding abrupt changes in composition and diminishing the stress concentration (Choy and Felix, 2000; Thorwarth et al., 2010). The use of transition metal (Zr, Ti, Cr, etc.) co-sputtered amorphous carbon (a-C) films has also been widely studied as one possible solution to improve DLC performance (Chang et al., 2002; Corbella et al., 2005; Adelhelm et al., 2011). Moreover, the incorporation of hydrogen can further enhance structural changes by stabilizing the covalent bonding network (sp^3) and playing a key role in the mechanical and tribological behaviour of the coating (Robertson, 2002). Even thought, under the highly corrosive human body environment the degeneration problem still persists promoting the failure of the coating (Hauert et al., 2012b). Actually, Hauert et al., (2012a) found that the main problem of DLC coatings is that, after some time in the body environment, the interface between substrate and functional coating can suffer a corrosion process by the penetration of body liquid through defects such as pinholes.

The exact interaction between biomaterials and natural fluids is still under extensive studies (Bauer et al., 2013). Immediately after implantation, water and ions from the body fluid are adsorbed and then a protein layer is formed onto the surface. Protein adsorption is indeed the first event which signalizes the overall biological response of the body to the implanted material (Andrade and Hlady, 1986; Roach et al., 2005; Rabe et al., 2011). A number of factors (surface chemistry, charge, topography, wetting behaviour, etc.) can alter protein conformation and/or orientation and consequently directly influence the cell response. For the joint implant point of view, proteins were also found to enhance lubrication through the adsorption of a protein layer on the joint materials surfaces (Heuberger et al., 2005; Serro et al., 2006). The natural lubrication typically minimizes the shearing damage and decreases the friction energy loss. However, when using artificial joint, the synovial fluid lubrication ability depends on many factors, such as surface treatment and the sliding conditions which could provoke catastrophic failure of the implant with partial or complete loss of functionality The effect of the synovial proteins on friction and lubrication is still unclear (Karimi et al., 2011; Runa et al., 2013; Myant and Cann, 2014), particularly when considering realistic surface engineering solutions. In fact, only few papers dealing with the influence of protein on (tribo)corrosion properties of DLC coatings (Hang et al., 2010; Liu et al., 2013; Wang et al., 2005) and even less for metal-containing DLC coatings (Maguire et al., 2005; Escudeiro et al., 2011) can be found in literature. In the present study the effects of H and Zr incorporation in the a-C-matrix were analysed tribologicaly using physiological lubricants (0.9% NaCl and diluted foetal bovine serum) in order to predict its behaviour under such adverse environments. Additionally, the interaction of albumin with the surfaces was also accessed using X-ray photoelectron spectroscopy (XPS) together with wettability tests for surface chemistry characterization.

2. Materials and methods

2.1. *Coatings deposition*

The coatings were deposited onto Ti grade 5 (Ti6Al4V) substrates and Si (111) wafers for the tribological testing and for coatings characterization, respectively. The Ti grade 5 substrates were mechanically polished with SiC paper (500, 600, 800, 1200 grits), and then finished by using diamond suspensions (6, 3 and 1 μm) and a colloidal silica suspension in order to obtain a mean substrate surface roughness (Ra) lower than 50 nm. Prior to deposition, the substrates were then cleaned in an ultrasonic bath in acetone, ethanol and deionised water for 15 min, and mounted on the rotating sample holder (18 rpm) in the deposition chamber. The coatings were deposited with a DC dual magnetron sputtering machine. A pure graphite target was used for the production of the a-C films in reactive (Ar/CH_4) and non-reactive atmosphere (Ar), in order to produce hydrogenated and non-hydrogenated films, respectively. Zr pellets were added to the erosion zone of the graphite target (relative erosion area, A_{Zr}/A_C, between 0 and 6%) to produce Zr containing films. All coatings were deposited with a constant applied bias voltage of -50 V and graphite target power density close to 7.5 W cm^{-2}. Moreover, a pure Ti target was also sputtered for the deposition of a composite gradient interlayer (Ti/TiN/TiCN) to improve the film adhesion on the metallic substrates. For each deposition conditions, the deposition time was calculated to obtain films ~1.4 μm thick. Further detailed deposition specification can be found elsewhere (Escudeiro et al., 2013). To facilitate reading, the coatings will be denominated as a-C_Zr(X) and a-C:H_Zr(X) for the non-hydrogenated and hydrogenated, respectively, where X is the Zr content.

2.2. *Coating characterization*

The chemical composition of the coatings was analysed by a full “Total Ion Beam Analysis (IBA)” (Jeynes et al., 2012) – Rutherford backscattering (RBS), non-Rutherford elastic backscattering (EBS), elastic recoil detection (ERD) and particle-induced X-ray emission (PIXE) self-consistently – used by the DataFurnace code (NDFv9.4f (Barradas and Jeynes, 2008)). This work was carried out at Surrey Ion Beam Centre, University of Surrey, UK. The analysis used an alpha particle beam of energies 3045 keV and 4315 keV with normal and tilted beam geometries, two backscattered particle detectors with different geometries, together with a forward recoil and an X-ray detector. Evaluated non-Rutherford particle scattering cross-sections (Gurbich, 2010) were used for H, C, N, O; those for H using the R-matrix parameters of the very

Table 1 – Liquid's surface energy and their polar and dispersive components (Jie-Rong and Wakida, 1997; Żenkiewicz, 2007).

Liquid	γ_{LV} (mJ m^{-2})	γ_l^d (mJ m^{-2})	γ_l ^{p}(mJ m^{-2})
Water	72.8	29.1	43.7
Glycerine ($C_3H_8O_2$)	63.4	37.4	26.0
Formamide (CH_3NO)	58.2	35.1	23.1
Diiodomethane (CH_3I_2)	50.8	50.8	–

thorough treatment of Dodder et al. (1977) and those for C and N are described, respectively, by Gai and Gurbich (2013) and Gurbich et al. (2011). The He-PIXE used the LibCPIXE code of Pascual-Izarra et al. (2006) and the ionization cross-sections of Taborda et al. (2011). SRIM2003 stopping (energy loss) cross-sections were used (Ziegler, 2004). For these samples all the information was in the 4315 keV data at 15° incidence angle, at which energy the 4263 keV $^{12}C(\alpha,\alpha)^{12}C$ resonance is excited giving high sensitivity at the surface to C in the presence of Zr. The ERD detector was at 30° scattering angle, and all four spectra (backscattering at 170° and 150°, ERD and PIXE at 120°) were interpreted self-consistently. The ERD detector relative solid angle was calibrated using a Kapton sample; the range foil thickness was 34 μm Kapton. The X-ray detector had a 146 μm Be filter to exclude backscattered particles. The PIXE showed the presence of Hf (assumed to be a contaminant at 0.85 at% relative to Zr), and of Ar (from the sputtering process: <5 at% relative to C).

The structure of the coatings was analysed by X-ray diffraction (XRD) (Philips, X'Pert diffractometer, Co Kα radiation) whereas X-ray photoelectron spectroscopy (XPS) (ESCAprobe P, Omicron Ltd., Al Kα, binding energy calibrated with Au 4f (84.1 eV)) was used to identify chemical bonding. The hardness was measured by depth-sensing indentation (Micromaterials Nanotest) using a Berkovich indenter. The normal stylus load was 5 mN (indentation depth approx. 150 nm); 32 independent indentations from two distinct areas on the sample were used to analyse the hardness data. Additional information is given in Escudeiro et al. (2013).

2.3. Contact angle and surface free energy

The contact angle measurements were performed through the sessile drop method. Drops were generated with a Krüs GmbH G-23 goniometer at ~20 °C and room humidity (50%). A minimum of 5 drops were deposited on the surface and a sequence of images were acquired for the contact angle calculation. The surface energy was calculated by measuring the contact angle of various liquid solutions: water, glycerine ($C_3H_8O_2$), formamide (CH_3NO) and diiodomethane (CH_3I_2), see Table 1.

The surface free energy (SFE) was calculated using the Owens equation (Żenkiewicz, 2007). Wetting behaviour is governed by the Young equation:

$$\gamma_{LV}\ \cos\ \theta = \gamma_S - \gamma_{SL}, \tag{1}$$

where θ is the measured solid–liquid contact angle and γ_S and γ_{SL} are the solid–liquid and liquid SFE. The surface energy (γ_S) can be expressed as polar (γ^p) and dispersive (γ^d) components. The dispersive component is related to London interaction, arising from electron dipole fluctuation. Thus,

$$\gamma_{SL} = \gamma_{SV} - \gamma_{LV} - 2\sqrt{\gamma_S^d \gamma_l^d} - 2\sqrt{\gamma_S^p \gamma_l^p}. \tag{2}$$

Combining Eq. (1) with (2) we obtain:

$$\gamma_{LV}(\cos\ \theta + 1) = 2\sqrt{\gamma_S^d \gamma_l^d} + 2\sqrt{\gamma_S^p \gamma_l^p}. \tag{3}$$

Thus, the polar and dispersive component of the film surface energy can be calculated and, as a result, the total surface energy (γ_S) is obtained.

2.4. Protein adsorption

The interaction with bovine serum albumin (BSA) was studied by immersion of the samples in a 2 ml BSA containing solution (4 mg ml^{-1}) diluted with a basic solution (NaCl: 9 (g/l); EDTA: 0.2 (g/l); Tris: 27 (g/l); sodium azide: 0.3%, pH 7.6) for 24 h at 4 °C. The incubation time was chosen in order to take into account the Vroman effect and the tendency of the proteins to adjust its conformation with the surface (Andrade and Hlady, 1986). The amount of total immobilized protein was calculated using the Bradford reagent against a standard BSA calibration curve. This technique is a powerful technique to study protein-to-protein variability. However, it is influenced by the presence of interfering substances such as detergent and different ionic compounds (such as metallic ions) which prevents the precise quantification of proteins. Thus, a reliable qualitative result can be obtained by comparison between samples as soon as the experimental uncertainties are considered constant. After immersion, all the samples were washed with water Mili-Q for eventual detachment of non-chemisorbed proteins. The detached proteins were also taken into account for the protein quantification using the same method described above. The samples were then air-dried for 24 h before the XPS spectra were recorded. The XPS analysis was performed using a Kratos AXIS Ultra with VISION software for data acquisition and CASAXPS software for data analysis. The analysis was carried out with a monochromatic Al Kα X-ray source (1486.7 eV), operating at 15 kV (90 W), in FAT mode (Fixed Analyser Transmission), with a pass energy of 40 eV for regions ROI and 80 eV for survey. Data acquisition was performed with a pressure lower than 10^{-6} Pa, and a charge neutralisation system was used. To take into account shifts caused by charging of the sample surface, all spectra were adjusted taking the C 1s peak at 285.0 eV as a reference for the carbon contamination. The binding energy scale was charge referenced to the C 1s at 285 eV. The deconvolution of the spectra was performed using the CasaXPS programme, in which an adjustment of the peaks was performed using peak fitting with Gaussian–Lorentzian peak shape and Shirley type background subtraction. The spin-orbital splitting in Zr 3d was assumed to be the same for all phases and equal to 2.4 and the integrated intensity of the Zr $3d_{5/2}$ peak relative to that of the Zr $3d_{3/2}$ was considered equal to the spin-orbital multiplicity of 2/3 (Matsuoka et al., 2008).

2.5. *Tribological tests*

The tribological tests were carried out using a pin-on-disc CSM tribometer in two different lubrication conditions: physiological solution (PS; 0.9% NaCl water solution), and foetal bovine serum (FBS), prepared according to the ASTM F732-00, (2006) standard test method. The temperature was maintained constant at 37±3 °C. A Ti6Al4V ball of 8 mm diameter was used as counterbody. An applied normal force of 1 N, linear speed of 20 cm s^{-1}, and 10,000 cycles were employed. Tests on non-coated substrates were also performed under the same testing conditions for comparison purposes. The tribological behaviour was examined with respect to the friction coefficient and the wear rate; the latter was evaluated on the basis of 3D profile measurements on the wear track, whereas the wear rates of the balls were calculated from measurements of the spherical wear cap using optical microscopy.

3. Results and discussion

3.1. *Coatings characterization*

Table 2 shows the chemical composition obtained by IBA. The use of reactive (Ar+CH_4) and non-reactive (Ar) sputtering led to the production of hydrogenated and non-hydrogenated coatings, respectively. The use of the reactive atmosphere promoted the incorporation of hydrogen in the coating in a range from 23 to 38 at% and almost doubled the deposition rate compared to non-hydrogenated coatings. The increase of the number of Zr pellets led to an increase of the Zr content and higher deposition rate, particularly for the non-hydrogenated coatings. The H content diminished with the increase of the Zr content. The density of the coatings was determined by IBA in μg/cm^2; using the thickness of the coating measured by optical profilometer, it was possible to calculate the density of the coatings in g/cm^3. The density varied from 2.6 to 3.9 for the non-hydrogenated coatings and from 1.9 to 3.1 for the hydrogenated coatings. The density is strongly related to the coordination defect content, H content, sp^3 bonding and lattice disorder, and, obviously, zirconium content (Charitidis, 2010). In general, the incorporation of H into the C-matrix led to the decrease of density compared to the non-hydrogenated films. Moreover, Zr co-sputtered films were harder and denser than pure films. Zr is a transition metal which present electrons at the outer shell loosely bound to their nuclei. Thus, the substitution of carbon atoms by Zr metal dopant in the rigid C–C and C–H network may distort the electron density distribution (Corbella et al., 2005) and, thus, decrease the coordination defect and increase the density. However, for Zr contents higher than 5 at% the density decreased. XRD diffractograms presented a weak and very broad peak close to ZrC (111) phase which indicates a nanocrystalline material with a grain size in the order of a few nanometres. Moreover, a nc-ZrC phase was also identified by XPS where the C 1s spectra showed a peak located at higher biding energy (~283.2 eV) compared to the typical Zr–C (281.8–282.3 eV) which is typical coatings with nanometric grain size. We can summarize here that, the increase

Table 2 – Chemical and mechanical properties of the coatings.

Name	Chemical composition				Dep. rate (nm/min)	Density (g/cm^3)	Ra (nm)	H (GPa)	E (GPa)
	C (at%)	Ar (at%)	Zr (at%)	H (at%)					
a-C_Zr(9)	90.3	0.6	**9.0**	0.2	8.3	3.1	103	10.7±0.5	133±2
a-C_Zr(8)	88.1	3.0	**7.5**	1.5	7.3	3.9	88	11.9±0.6	126±3
a-C_Zr(4)	91.4	3.8	**3.8**	0.9	5.0	3.3	85	10.4±0.4	110±3
a-C	94.0	4.4	–	1.6	4.6	2.6	55	10.7±0.5	94±1
a-C:H_Zr(6)	67.6	1.9	**5.7**	24.8	12.0	2.8	76	12.2±0.5	114±3
a-C:H_Zr(5)	71.3	1.0	**4.8**	22.9	10.0	2.3	55	11.4±0.4	103±1
a-C:H_Zr(3)	64.1	1.1	**3.3**	31.5	8.5	3.1	51	10.0±1.6	87±3
a-C:H	61.3	0.6	–	38.1	8.8	1.9	76	8.9±0.3	70±1

of Zr content led to the formation of nanostructure with ZrC nanocrystals embedded in the C-matrix. A detail study of the structural characterization of the Zr co-sputtered a-C films by XPS can be found in Escudeiro et al. (2013). The coordination number of C network can be then reduced by binding C atoms into carbide and, in accordance with thermodynamical models of DLC formation, resulting in the decrease of the local atom density in DLC film (Li et al., 2004; Wang et al., 2007).

3.2. *Contact angle and surface free energy*

The interaction of the films with water is very important from the biomedical point of view. Numerous physiological events at subcellular and cellular levels, such as cell adhesion and protein adsorption, are greatly affected by such a property. The surface energy has been related to the adsorption ratio of diverse proteins and, consequently, cell spreading. Albumin is considered as a multifunctional transporter protein and the most abundant protein found in the plasma (approx. 50 mg ml^{-1}) (Roach et al., 2005; Fanali et al., 2012). Moreover, its adsorption has been found to be related to the inhibition of the coagulation cascade and, consequently, platelet adsorption (Vogler, 1998; Lackner and Waldhauser, 2010). Albumin has three homologous domains (comparable amino acid sequences) assembled in a heart-shape structure which are sustained by mainly hydrophobic interactions, hydrogen bonds and disulphide bridges (Fanali et al., 2012). Thus, surface–protein interaction should be strongly related to surface chemistry. Table 3 shows the wettability characteristics assessed by contact angle measurements for selected coated samples. The wetting character of a surface can be obtained using water. Thus, high contact angle values imply a less wettable surface (hydrophobic surface) and, on the contrary, low contact angles values indicate a more wettable surface (hydrophilic surface). Pure non-hydrogenated and hydrogenated carbon films were characterized as hydrophilic coatings ($\theta < 65^\circ$), which was in good agreement with the proposed contact angles found in literature (Robertson, 2002; Zhou et al., 2006). When zirconium was added into the C-matrix in increasing contents, the water contact angle increased suggesting hydrophobic surfaces. The exact water-interaction mechanism of alloyed DLC coatings is still not clear and further investigation is needed. However, albumin is known to have a higher binding affinity to hydrophobic surfaces due to hydrophobic interactions between the protein and the surface (Roach et al., 2005). Hence, Zr containing samples are expected to bond more proteins compared to pure films.

As expected, pure hydrogenated and non-hydrogenated coatings presented higher surface energy than the respective co-sputtered films. The incorporation of Zr led to a decrease of the surface energy due mainly to the reduction of the polar component. The metallic element can decrease the presence of unsaturated bonds and consequently decrease the dipolar interaction with water (Chen et al., 2001). Additionally, the presence of non-polar C–H bonds on the surface of hydrogenated coatings further decreased the interaction of the surface with polar molecules such as water and thus, for the same Zr content, the SFE was found to be lower compared to non-hydrogenated films. This fact is highlighted by the low polar component found in the Zr co-sputtered films, which strongly contributes to the hydrophilic functional chemical groups on the surface (Table 3). Each protein has a hydrophobic peptide backbone where the basis of polarity of R group emphasizes the possibility of functional role. The protein interfacial tension, γ_{BSA}, was calculated by the following equation (Paul and Sharma, 1981):

$$\gamma_{\mathrm{BSA}} = \left(\sqrt{\gamma^{d}_{\mathrm{BSA}}} - \sqrt{\gamma^{d}_{\mathrm{s}}}\right)^2 + \left(\sqrt{\gamma^{p}_{\mathrm{BSA}}} - \sqrt{\gamma^{p}_{\mathrm{s}}}\right)^2 + \Delta_{\mathrm{BSAs}}, \qquad (4)$$

where the value Δ_{BSAs} describes the interdiffusion of ionic–covalent interactions which can be considered negligible. Further, if the interfacial tension approaches zero the interactions protein-surface are supposed to be lower. Albumin interfacial energy parameters are $\gamma^{d}_{\mathrm{BSA}} = 31.4\ \mathrm{mJ\ m^{-2}}$ and $\gamma^{p}_{\mathrm{BSA}} = 33.6\ \mathrm{mJ\ m^{-2}}$ (Paul and Sharma, 1981). Table 2 shows the calculated values for the coated surfaces. Low polar component and low polar/dispersive ratio presented higher interfacial tensions. In fact, many authors related a low ratio of polar to dispersive components with plasma protein adsorption (Baszkin and Lyman, 1980; Birdi, 1981). Additionally, Vogler (1998) found that the water adhesion tension, τ_0, was the key parameter for biological reactivity of a biomaterial. The wettability is then measured by τ_0 and calculated as a product of water tension by the cosine of the measured water contact angle. Hydrophobic and hydrophilic surfaces are separated by Berg's limit ($\tau_0 = 30\ \mathrm{mJ\ m^{-2}}$) which also limits the protein attraction/repulsion characteristic, respectively. Actually, the adsorption on hydrophilic surfaces was found to be thermodynamically unfavourable, i.e., the competition between water and proteins adsorption is an endothermic process (Paul and

Table 3 – Water contact angle (θ), surface energy (γ_s), water adhesion tension values (τ_0) and BSA interfacial tension (γ_{BSA}) of the deposited films and uncoated substrate (Azevedo et al., 2005; Pacha-Olivenza et al., 2008; Braic et al., 2011).

Samples	Θ_{water} (°)	Surface energy (mJ m^{-2})			τ_0 (mJ m^{-2})	γ_{BSA} (mJ m^{-2})
		γ_{sp}	γ_{sd}	γ_s		
a-C_Zr(8)	67±1	5.0	40.5	45.5	28.0	13.3
a-C_Zr(4)	66±3	5.1	45.8	50.9	30.1	13.8
a-C	50±7	11.2	51.2	62.4	46.8	8.4
a-C:H_Zr(6)	73±2	3.9	36.7	40.6	20.9	14.7
a-C:H_Zr(3)	65±2	12.8	27.2	40.0	31.0	5.1
a-C:H	57±2	14.2	33.9	48.1	40.2	4.2
Ti6Al4V	73±11	8.1	31.1	39.2	21.3	8.7

Sharma, 1981; Vogler, 1998). Once the adsorption is initiated, proteins tend maximize the surface interaction by exposure either hydrophobic domain (typically hidden toward the interior) or hydrophilic domains trough the surface. Therefore, the exclusion of water from the hydrophobic surface potentiates protein–surface interaction and, consequently, the hydrophobic interactions (except for the case when the protein in question has hydrophobic regions on its surface). Thus, the incorporation of Zr content led to lower τ_0. Besides, the films with higher Zr content were found to have $\tau_0 < 30\,\mathrm{mJ\,m^{-2}}$ further highlighting the ability to adsorb protein. On the other hand, the adsorbed molecules through hydrophobic interaction can undergo reversible/irreversible conformational changes which may lead to unfavourable cell response if the proper binding domain is disrupted.

3.3. *Protein adsorption*

In order to confirm the wettability results, the protein adsorption phenomenon was evaluated for the non-hydrogenated samples. Coated and un-coated samples were immersed for 24 h in a BSA containing solution and rinsed several times with ultra pure water in order to leave only the irreversibly bound proteins on top of the surfaces. The amount of protein absorbed was estimated using the Bradford protein assay and is shown in Fig. 1. As expected, pure amorphous coatings showed lower protein affinity compared to co-sputtered and uncoated surfaces. Although, Ti6Al4V presented the highest affinity to protein adsorption, the incorporation of Zr co-sputtered films significantly improved protein affinity when compared to “inert” a-C surface. Even though proteins often adsorbed as monolayers on metallic substrates (side-on and/or end-on), multilayer adsorption is not uncommon, particularly for high concentration solutions (Sousa et al., 2004; Serro et al., 2006). Taking into account the albumin size and molecular weight (Puskas et al., 2004), a close pack monolayer can be formed by approximately $4\,\mathrm{mg/m^{-2}}$ (Soderquist and Walton, 1980; Sousa et al., 2004). Thus, it is expected that in the case of Zr-containing samples albumin adsorbed as a multilayer coverage. This result corroborates the observation shown above: hydrophobic surfaces tend to bind more protein through “hydrophobic interactions” (Fig. 1). In general, the driving force for protein adsorption is the entropy gain resulting from dehydration of parts of the sorbent and the protein surface. a-C coating presented the highest surface energy together with the highest dispersive component; then, it should be expected to bond less protein compared to Zr co-sputtered films (hydrophobic surfaces). Moreover, the amount of protein desorbed after washing (i.e. not chemically adsorbed on the surface) was around 46% compared to 4% found for uncoated samples. It shows that the proteins are less tightly bound to the hydrophilic surface (Rabe et al., 2011).

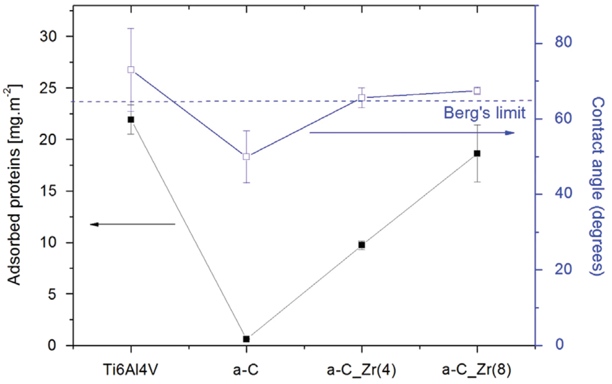

Fig. 1 – BSA adsorption vs contact angle measurements.

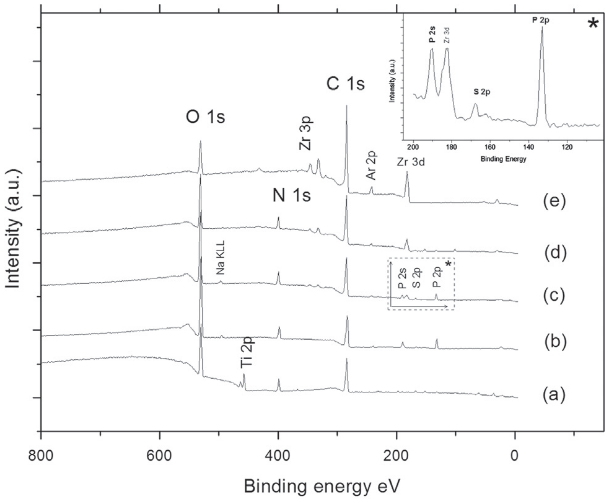

Fig. 2 – XPS spectra of the uncoated and coatings after immersion in BSA: (a) Ti6Al4V, (b) a-C, (c) a-C_Zr(4), and (d) a-C_Zr(8). a-C_Zr(8) spectrum (e) before immersion was also added for comparison. The inset (*) shows a zoom in of the 200–100 eV region of the a-C_Zr(4) film XPS spectra revealing the S 2p photo-peak.

XPS analysis was performed in order to prove the presence of the adsorbed albumin layer. Fig. 2 shows the XPS survey spectra for uncoated samples and non-hydrogenated coatings after immersion in BSA. In order to take into account the typical contamination layer, a-C_Zr(7) XPS spectrum before immersion is also shown as a representative of all the samples in as-deposited conditions. In fact, after removing such contamination layer by argon sputtering (spectrum not shown here) the only visible changes were an increase in carbide bonds (for the Zr-containing samples) and a decrease in O-containing bonds, confirming the presence of a thin contamination oxide layer. The spectra show the peaks corresponding to oxygen (O 1s 532 eV), nitrogen (N 1s 400 eV), carbon (C 1s 285 eV) and sulphour (S 2p 164 eV, see Fig. 2 inset). The appearance of the well defined N 1s peak for all samples after immersion is usually attributed to the amino acids of the protein (Vanea and Simon, 2011; Gruian et al., 2012). However, it can be also related to the basic solution used for dilution. On the other hand, the presence of the S weak band can only belong to S-containing amino acids, i.e., methionine (Met) and cysteine (Cys). Indeed such amino acids correspond to around 7% of the total 538 amino acids residues that compose BSA (Hirayama et al., 1990). For Zr-containing films another important feature was observed; the

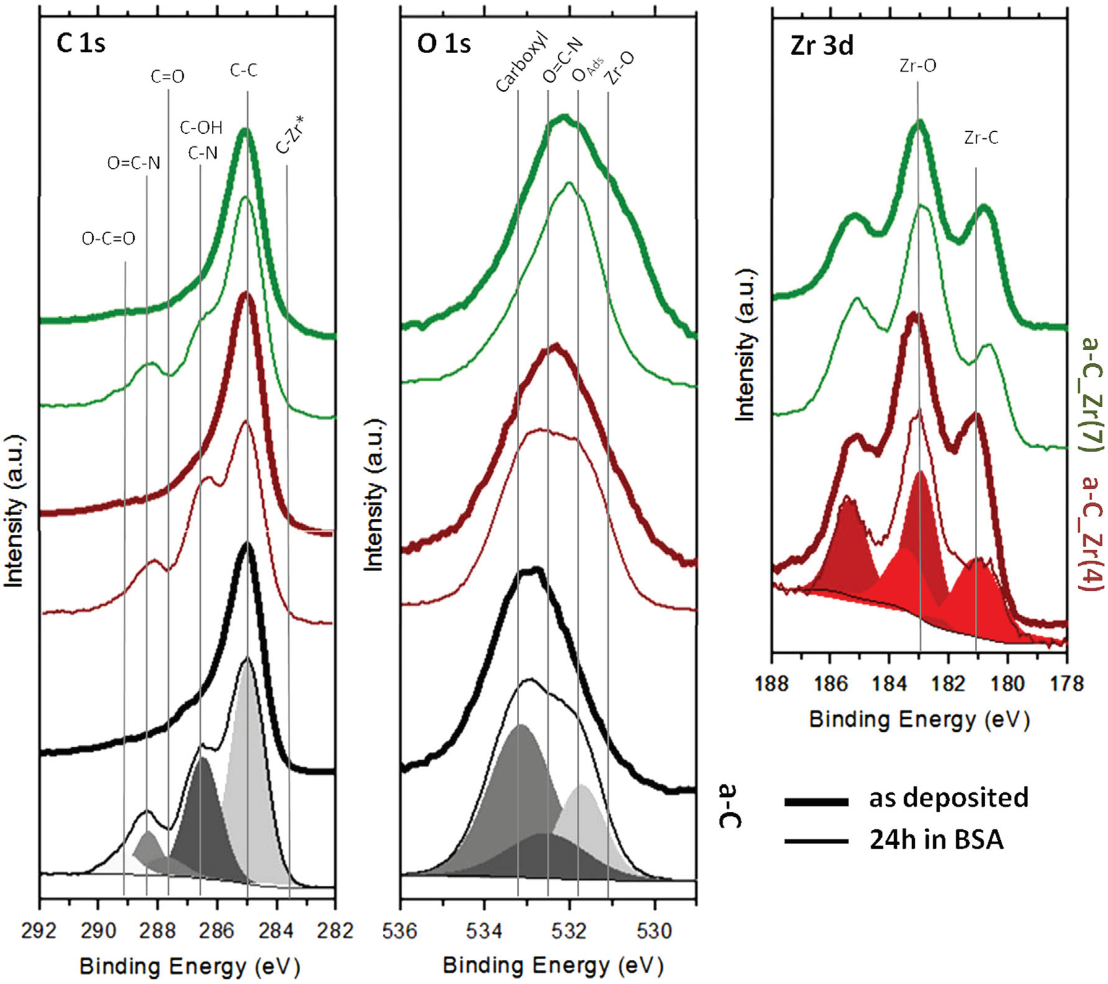

Fig. 3 – Deconvolution of C 1s, O 1s and Zr 3d core level spectra of the coatings before and after immersion for 24 h in BSA.

decrease in the intensity of the Zr 3d core level peak due to the presence of the organic adherent layer on the top of the sample (compare Fig. 2(d and e)). Sodium and phosphorus were also detected and considered as contamination from the basic solution used to dilute BSA.

The deconvolution of the peaks in C 1s, O 1s and Zr 3d core level spectra of the films, before and after BSA immersion, is shown in Fig. 3. Before immersion, all C 1s spectra were fitted using the alkyl type carbon (C–C, C–H) at 285 eV as charge reference; a second peak at 286.5 eV was added with the same FWHM as the main peak, indicating the alcohol (C–OH) and/or ester (C–O–C) functionality. Two other components can also be detected corresponding to the C═O and O–C═O at 2.8–3.0 eV and 3.6–4.3 eV, respectively (Kaufmann et al., 1988). When Zr was incorporated in the matrix an extra peak was also observed close to 283.4±0.2 eV attributed to C–Zr*, i.e. Zr–C bond in the nanocrystal as referred to above (Escudeiro et al., 2013; Meng et al., 2013). After immersion in BSA an additional peak appeared at 288.3±0.1 eV attributed to the O═C–N groups from the peptide backbone (Serro et al., 2006; Premathilaka et al., 2007; Vanea and Simon, 2011; Gruian et al., 2012). O 1s band also revealed an extra peak at 532.6 eV after protein adsorption confirming the presence of such bond together with two other peaks revealing oxygen contamination (531.7 eV) and carboxyl groups (533.1 eV) on the film surface (Premathilaka et al., 2007). Again, for Zr-containing films a shoulder around 532.1 eV is observed and identified as Zr-O bond. The Zr 3d spectra show the presence of both Zr–C (181.2 eV) and Zr–O (183 eV) bonds typically found for Zr-conatining DLC films (Escudeiro et al., 2013; Meng et al., 2013). After immersion in BSA, a decrease in intensity of the Zr–C bonding component is well visible indirectly supporting existence of protein layer.

Although XPS does not provide quantitative information about the total amount of adsorbed protein, it is commonly monitored by the intensity of N peak before and after protein adsorption (Serro et al., 2006). The presence of N was imperceptible before the immersion in BSA. Fig. 4 shows the N 1s core-level spectra for all measured samples after 24 h immersion in BSA. As expected, the intensity of the N 1s peak varies in a similar way as protein adsorption. The deconvolution of the peaks (not shown) revealed one component close to 400.2 eV characteristic of O═C–N groups from the peptide bonds (Serro et al., 2006; Gispert et al., 2006; Premathilaka et al., 2007; Vanea and Simon, 2011; Gruian et al., 2012) and an additional peak near to 401.8 eV which can be attributed to a protonate amine group (–NH$^+$) of the terminal amino groups (Auditore et al., 2002; Ahmed et al., 2013; Lubambo et al.,

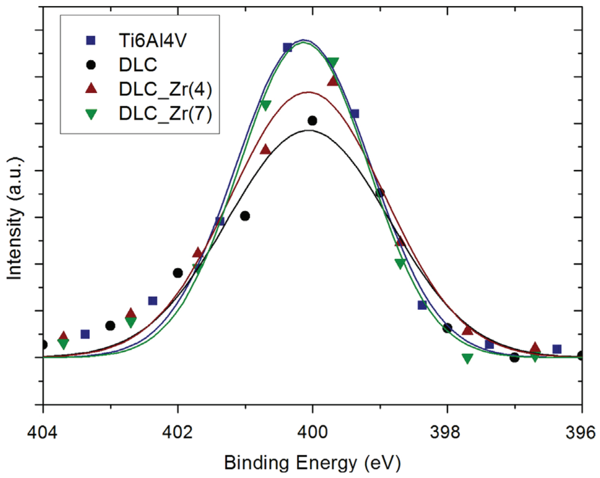

Fig. 4 – N 1s core level spectra of Ti6Al4V and non-hydrogenated coatings after immersion in BSA.

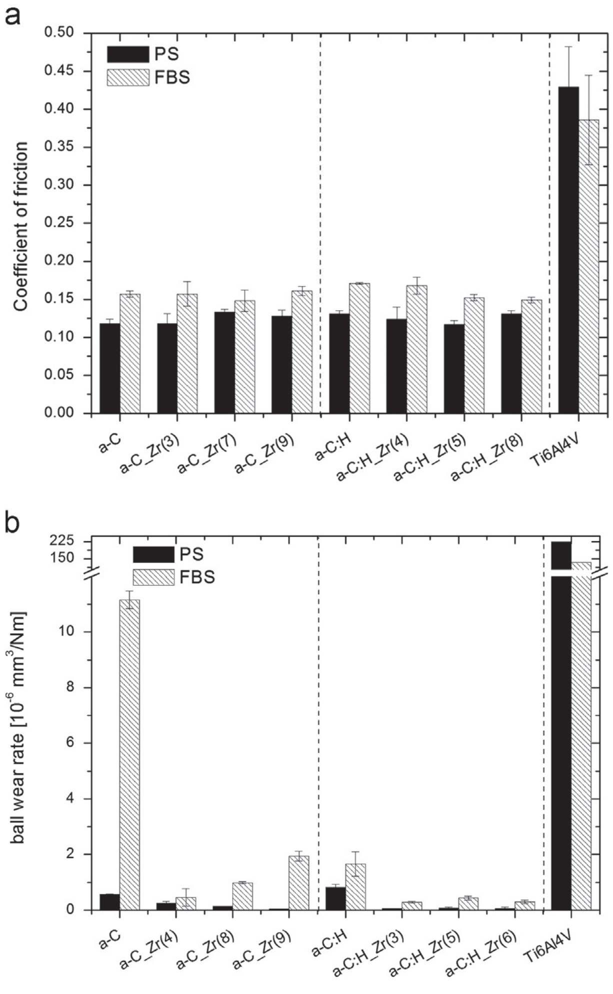

Fig. 5 – Average friction coefficients (a) and ball wear rate (b) of the coated and uncoated samples under both lubrication conditions.

2013). This may indicate that the BSA will bind through carboxyl acid group rather than amino group (Ueda et al., 1976).

3.4. *Friction and wear*

To identify a promising coating composition for the articulating joints, forensic tribological screening tests (unidirectional pin-on-disc tests) were performed using a corrosive lubricants (0.9% NaCl, physiological solution – PS) and a protein containing lubricant (Fetal Bovine Serum – FBS). The use of physiological solution was chosen in order to create a synergistic effect between the wear and the corrosion due to the presence of water and ions that may accelerate material degradation (Wang et al., 2005; Kim et al., 2008). On the other hand, FBS was used in order to approach the physiological conditions.

Fig. 5 presents the friction data from the tribological tests in PS and FBS. Surprisingly, the friction coefficient of coated samples tested in PS was found to be similar to that of dry sliding (Escudeiro et al., 2013) and lower than that measured in FBS. Moreover, the incorporation of Zr did not lead to any statistically significant difference in friction among the coatings. In all cases, the worn surface did not show any signs of film failure (Fig. 6). In general, all coatings present very low wear rate ($\sim 0.5\times10^{-6}$ mm^3/Nm) compared to the uncoated surface under both lubrication conditions (7.2×10^{-4} mm^3/Nm

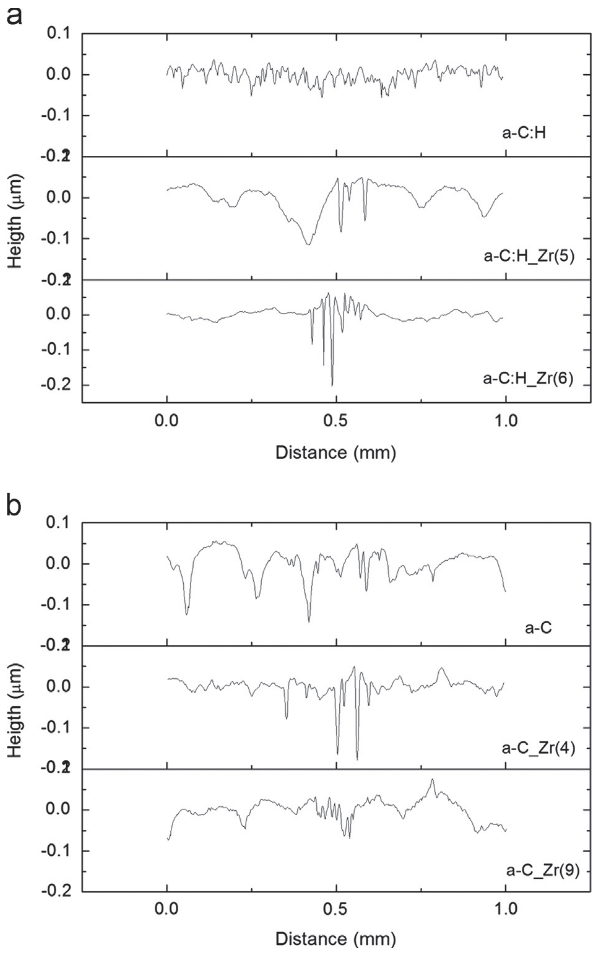

Fig. 6 – Comparison between the wear tracks (cross-section) of hydrogenated and nonhydrogenated films under PS lubrication.

and 5.7×10^{-4} mm^3/Nm) for PS and FBS, respectively, see Fig. 7). The incorporation of Zr did not significantly improve the wear compared to pure carbon coatings. Nevertheless, the wear of the counterbody was strongly reduced when testing against doped films (Fig. 5).

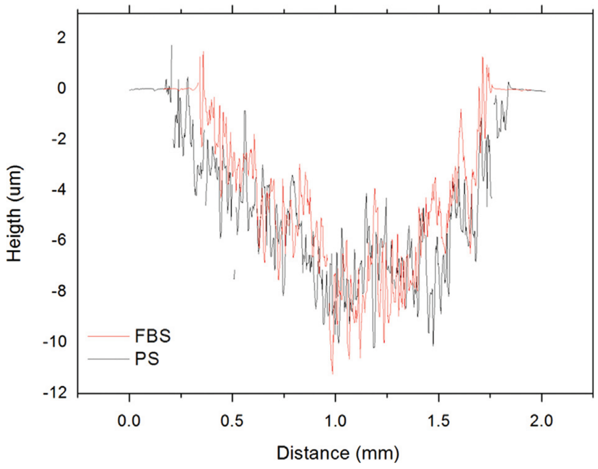

Fig. 7 – Wear profile of Ti6Al4V sample tested under PS and FBS.

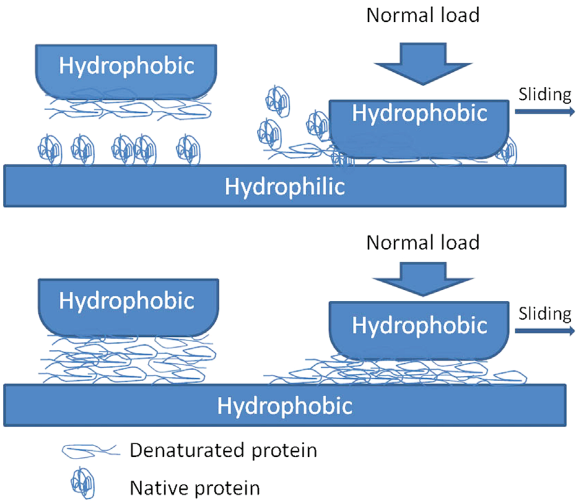

Fig. 8 – Schematic representation of the key mechanisms of the albumin-mediated lubrication on DLC films.

When tested in highly corrosive medium (PS), it is expected that the production of the wear products and their accumulation in the wear track precipitate abrasion wear and delay the repassivation (Kim et al., 2008). The co-sputtered Zr films are known to present good wear-corrosion behaviour. Kumar et al. (2013) showed similar or better corrosion properties of Zr-doped DLC coatings tested in Hank's solution compared to the Ti alloy substrate. Also, Wang et al. (2005) reported an excellent crevice and pitting corrosion resistance of Zr-DLC films. It is thus expected that the incorporation of Zr enhances the corrosion resistance compared to unalloyed films due to its ability to form an oxide layer as observed for Ti and Cr by Wang et al. (2013). The decrease of both wear debris amount and accumulation of corrosion products between the mating materials can consequently decrease the wear of the counterpart. On the other hand, when testing under FBS, the presence of proteins can play two roles in the sliding systems: (i) they act as a lubricant and (ii) they decrease the degradation process by forming a complex adsorbed film (Wimmer et al., 2010). Moreover, protein also can interact with the metallic debris/ions forming metalloprotein complexes that may be processed or eliminated in vivo (Hallab et al., 2001). Protein-rich lubricants are known to improve the stability of the passive film on metallic substrates (SS 316L, Ti6Al4V alloy and CoCrMo alloy) acting as a corrosion barrier layer and minimizing the surface degradation (Karimi et al., 2011; Runa et al., 2013). The presence of adsorbed proteins protected not only the coated surface, decreasing significantly its wear rate (negligible worn volume, see Fig. 9), but also the counterbody (Fig. 5), particularly when rubbing against Zr-containg coatings. Adding a metallic element to the C-matrix led to higher protein adsorption compared to a-C pure films (see Section 3.3), which could increase (tribo) corrosion resistance of coating–substrate system (Karimi et al., 2011; Runa et al., 2013).

For all coatings the friction coefficient using FBS as lubricant was higher compared to PS; nevertheless, it was still significantly lower compared to that of uncoated substrates (~0.38). The friction coefficient increased up to ~2000 cycles and then oscillated around an average value (~0.16). The same tendency was observed for DLC films co-sputtered with Ti (Escudeiro et al., 2011) and Si (Anil et al., 2010). Fig. 8 shows a schematic representation of the albumin-mediate lubrication on DLC-based films. Although albumin can undergo conformational change due to adsorption on hydrophobic surfaces, the adsorbed layer is more tightly bound

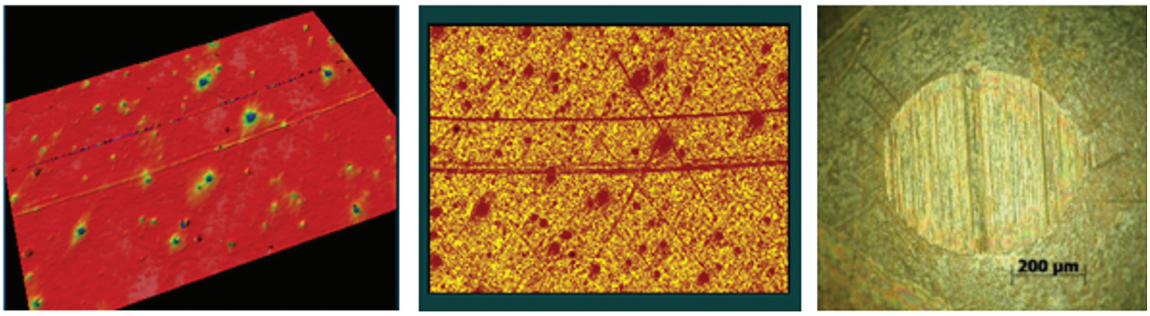

Fig. 9 – Wear track profile and ball micrograph of a-C:H film where only few scratches on the surface could be observed, which contrasted with the wear damage of the ball counterparts showing clear abrasive marks.

compared to hydrophilic surfaces (Hang and Qi, 2010). Thus the wear of the counterbody was particularly decreased by application of Zr co-sputtered coatings. The hydrophobic character of such films led to the adsorption of a robust protein layer onto the surface (high adsorption rate), which prevented the surfaces to rub in direct contact. However, it was also noticed from the wear scars inspection (Fig. 9) that higher surface roughness (Table 2) can be disruptive for such layer resulting in accelerated wear of the counterbody.

4. Conclusions

Zr co-sputtered amorphous films were deposited by DC magnetron sputtering under reactive ($Ar+CH_4$) and non-reactive (Ar) atmosphere and tested in lubricated contact. Zr was added in small amounts (3–9 at.%) forming dense nanostructured coatings composed of ZrC nanocrystalls embedded into an amorphous C-matrix. The incorporation of H did not show any significant differences compared to non-hydrogenated coatings. Zr-alloyed coatings showed higher contact angle (and therefore lower surface free energy) than a-C(:H) ones which enhanced protein adsorption onto the surface. XPS measurements further indicated that albumin adsorbs better on the surface of Zr-doped coatings. When tribologically tested in PS, Zr-doped films behaved similarly to pure carbon films. However, the wear behaviour in FBS lubrication clearly indicated strong dependence on the ability of the surface to adsorb proteins. Although the wear of all coatings was negligible, higher protein adsorption rate of hydrophobic surfaces led to lower counterbody wear due to the presence of a robust protein layer.

Acknowledgement

This research was sponsored by FEDER funds through the program COMPETE – Programa Operacional Factores de Competitividade and by national funds through FCT – Fundação para a Ciência e a Tecnologia, under the Project PEst-C/EME/UI0285/2011, and QREN-POPH for funding support under the Grant SFRH/BD/75071/2010 which was co-funded by FSE and MSTES. This work has been also supported by the European Community as an Integrating Activity “Support of Public and Industrial Research Using Ion Beam Technology (SPIRIT)” under EC Contract no. 227012. The authors would like to thank C. Jeynes from Survey University and Eduardo Alves and N. P Barradas from Instituto Superior Técnico as well for the fruitful discussion and help in analysing IBA results and also A.P. Piedade from the University of Coimbra and S. Calderon, from University of Minho for the help and suggestions concerning wettability tests and protein adsorption results.

REFERENCES

Adelhelm, C., et al., 2011. Investigation of metal distribution and carbide crystallite formation in metal-doped carbon films (a-C:Me, Me = Ti, V, Zr, W) with low metal content. Surf. Coat. Technol. 205, 4335–4342.

Ahmed, M.H., et al., 2013. Comparison between FTIR and XPS characterization of amino acid glycine adsorption onto diamond-like carbon (DLC) and silicon doped DLC. Appl. Surf. Sci. 273, 507–514.

Andrade, J.D., Hlady, V., 1986. Protein adsorption and materials biocompatibility: a tutorial review and suggested hypotheses. Biopolymers/Non-Exclusion HPLC, 79. Springer, Berlin Heidelberg 1–63.

Anil, M., et al., 2010. Tribological performance of hydrophilic diamond-like carbon coatings on Ti-6Al-4V in biological environment. Diam. Relat. Mater. 19, 300–304.

ASTM F732-00, 2006. Standard test method for wear testing of polymeric materials used in total joint protheses. ASTM International.

Auditore, A., et al., 2002. Human serum albumin adsorption onto a-SiC:H and a-C:H thin films deposited by plasma enhanced chemical vapor deposition. Biomol. Eng. 19, 85–90.

Azevedo, A.F., et al., 2005. Wettability and corrosion tests of diamond films grown on Ti6Al4V alloy. Surf. Coat. Technol. 194, 271–275.

Barradas, N.P., Jeynes, C., 2008. Advanced physics and algorithms in the IBA datafurnace. Nucl. Instrum. Methods B 266, 1875–1879.

Baszkin, A., Lyman, D.J., 1980. The interaction of plasma proteins with polymers. I. Relationship between polymer surface energy and protein adsorption/desorption. J. Biomed. Mater. Res. 14, 393–403.

Bauer, S., et al., 2013. Engineering biocompatible implant surfaces: Part I: materials and surfaces. Prog. Mater. Sci. 58, 261–326.

Birdi, K.S., 1981. Cell adhesion on solids and the role of surface forces. J. Theor. Biol. 93, 1–5.

Braic, V., et al., 2011. Zr,Ti)CN coatings as potential candidates for biomedical applications. Surf. Coat. Technol. 206, 604–609.

Chang, Y.-Y., et al., 2002. Catalysis effect of metal doping on wear properties of diamond-like carbon films deposited by a cathodic-arc activated deposition process. Thin Solid Films 420–421, 241–247.

Charitidis, C.A., 2010. Nanomechanical and nanotribological properties of carbon-based thin films: a review. Int. J. Refract. Met. H 28, 51–70.

Chen, J.S., et al., 2001. Metal-containing amorphous carbon films for hydrophobic application. Thin Solid Films 398–399 (0), 110–115.

Choy, K.-L., Felix, E., 2000. Functionally graded diamond-like carbon coatings on metallic substrates. Mater. Sci. Eng. A: Struct. 278, 162–169.

Corbella, C., et al., 2005. Structure of diamond-like carbon films containing transition metals deposited by reactive magnetron sputtering. Diam. Relat. Mater. 14, 1103–1107.

Dearnaley, G., Arp, J.H., 2005. Biomedical applications of diamond-like carbon (DLC) coatings: a review. Surf. Coat. Technol. 200, 2518–2524.

Dodder, D.C., et al., 1977. Elastic scattering of protons by helium 4: new experiments and analysis. Phys. Rev. C 15, 518–530.

Escudeiro, A., et al., 2011. Tribological behaviour a-C and a-C:H films doped with Ti in biological solutions. Vacuum 85, 1144–1148.

Escudeiro, A., et al., 2013. a-C(:H) and a-C(:H)_Zr coatings deposited on biomedical Ti-based substrates: tribological properties. Thin Solid Films 538, 89–96.

Fanali, G., et al., 2012. Human serum albumin: from bench to bedside. Mol. Asp. Med. 33, 209–290.

Gai, E.V., Gurbich, A.F., 2013. Evaluated 12C(4He,4He)12C cross-section and its uncertainty. Nucl. Instrum. Methods B 296, 87–91.

Gruian, C., et al., 2012. FTIR and XPS studies of protein adsorption onto functionalized bioactive glass. BBA Protein Proteomics 1824, 873–881.

Gurbich, A.F., 2010. Evaluated differential cross-sections for IBA. Nucl. Instrum. Methods B 268, 1703–1710.

Gurbich, A.F., et al., 2011. Measurements and evaluation of the cross-section for helium elastic scattering from nitrogen. Nucl. Instrum. Methods B 269, 40–44.

Hallab, N.J., et al., 2001. Differential lymphocyte reactivity to serum-derived metal–protein complexes produced from cobalt-based and titanium-based implant alloy degradation. J. Biomed. Mater. Res. 56, 427–436.

Hang, R., et al., 2010. Corrosion behavior of DLC-coated NiTi alloy in the presence of serum proteins. Diam. Relat. Mater. 19, 1230–1234.

Hang, R., Qi, Y., 2010. A study of biotribological behavior of DLC coatings and its influence to human serum albumin. Diam. Relat. Mater. 19, 62–66.

Hauert, R., 2003. A review of modified DLC coatings for biological applications. Diam. Relat. Mater. 12, 583–589.

Hauert, R., 2004. An overview on the tribological behavior of diamond-like carbon in technical and medical applications. Tribol. Int. 37, 991–1003.

Hauert, R., et al., 2012a. Retrospective lifetime estimation of failed and explanted diamond-like carbon coated hip joint balls. Acta Biomater. 8, 3170–3176.

Hauert, R., et al., 2012b. Analysis of the in-vivo failure of the adhesive interlayer for a DLC coated articulating metatarsophalangeal joint. Diam. Relat. Mater. 25, 34–39.

Heuberger, M.P., et al., 2005. Protein-mediated boundary lubrication in arthroplasty. Biomaterials 26, 1165–1173.

Hirayama, K., et al., 1990. Rapid confirmation and revision of the primary structure of bovine serum albumin by ESIMS and frit-FAB LC/MS. Biochem. Biophys. Res. Commun. 173, 639–646.

Jeynes, C., et al., 2012. Total IBA – where are we?. Nucl. Instrum. Methods B 271, 107–118.

Jie-Rong, C., Wakida, T., 1997. Studies on the surface free energy and surface structure of PTFE film treated with low temperature plasma. J. Appl. Polym. Sci. 63, 1733–1739.

Joyce, T.J., 2007. Examination of failed ex vivo metal-on-metal metatarsophalangeal prosthesis and comparison with theoretically determined lubrication regimes. Wear 263, 1050–1054.

Karimi, S., et al., 2011. Effects of bovine serum albumin on the corrosion behaviour of AISI 316L, Co-28Cr-6Mo, and Ti-6Al-4V alloys in phosphate buffered saline solutions. Corros. Sci. 53, 3262–3272.

Kaufmann, R., et al., 1988. XPS studies of the thermal behaviour of passivated zircaloy-4 surfaces. Surf. Interface Anal. 11, 502–509.

Kim, J.-G., et al., 2008. Wear-corrosion performance of Si-DLC coatings on Ti-6Al-4V substrate. J. Biomed. Mater. Res. A 86A, 41–47.

Kumar, P., et al., 2013. Wear and corrosion behavior of Zr-doped DLC on Ti-13Zr-13Nb biomedical alloy. J. Mater. Eng. Perform. 22, 283–293.

Lackner, J.M., Waldhauser, W., 2010. Inorganic PVD and CVD coatings in medicine – a review of protein and cell adhesion on coated surfaces. J. Adhes. Sci. Technol. 24, 925–961.

Li, H.X., et al., 2004. The effect of applied dc bias voltage on the properties of a-C:H films prepared in a dual dc–rf plasma system. Appl. Surf. Sci. 227, 364–372.

Liu, J., et al., 2013. Tribocorrosion behavior of DLC-coated CoCrMo alloy in simulated biological environment. Vacuum 92, 39–43.

Love, C.A., et al., 2013. Diamond like carbon coatings for potential application in biological implants – a review. Tribol. Int. 63, 141–150.

Lubambo, A.F., et al., 2013. Tuning protein GlnB-Hs surface interaction with silicon: FTIR-ATR, AFM and XPS study. Colloids Surf. B 102, 348–353.

Maguire, P.D., et al., 2005. Mechanical stability, corrosion performance and bioresponse of amorphous diamond-like carbon for medical stents and guidewires. Diam. Relat. Mater. 14, 1277–1288.

Matsuoka, M., et al., 2008. X-ray photoelectron spectroscopy analysis of zirconium nitride-like films prepared on Si(100) substrates by ion beam assisted deposition. Surf. Coat. Technol. 202, 3129–3135.

Meng, Q.N., et al., 2013. Deposition and characterization of reactive magnetron sputtered zirconium carbide films. Surf Coat Tech 232, 876–883.

Myant, C., Cann, P., 2014. On the matter of synovial fluid lubrication: Implications for metal-on-metal hip tribology. J. Mech. Behav. Biomed. 34, 338–348.

Pacha-Olivenza, M.A., et al., 2008. Effect of UV irradiation on the surface Gibbs energy of Ti6Al4V and thermally oxidized Ti6Al4V. J. Colloid Interface Sci. 320, 117–124.

Pascual-Izarra, C., et al., 2006. Simultaneous PIXE and RBS data analysis using Bayesian inference with the datafurnace code. Nucl. Instrum. Methods B 249, 780–783.

Paul, L., Sharma, C.P., 1981. Preferential adsorption of albumin onto a polymer surface: an understanding. J. Colloid Interface Sci. 84, 546–549.

Premathilaka, S.S., et al., 2007. Interaction of whey protein with modified stainless steel surfaces. In: Müller-Steinhagen, M.R. M. Hans, Watkinson, A. Paul (Ed.), Proceedings of the 7th International Conference on Heat Exchanger Fouling and Cleaning – Challenges and Opportunities. Berkeley Electronic Press, Tomar, Portugal, RP5, pp. 150–161.

Puskas, J.E., et al., 2004. Novel thymine-functionalized polystyrenes for applications in biotechnology. 2. Adsorption of model proteins. Biomacromolecules 5, 1412–1421.

Rabe, M., et al., 2011. Understanding protein adsorption phenomena at solid surfaces. Adv. Colloid Interface 162, 87–106.

Roach, P., et al., 2005. Interpretation of protein adsorption: surface-induced conformational changes. J. Am. Chem. Soc. 127, 8168–8173.

Robertson, J., 2002. Diamond-like amorphous carbon. Mater. Sci. Eng. R 37, 129–281.

Runa, M.J., et al., 2013. Tribocorrosion response of the Ti6Al4V alloys commonly used in femoral stems. Tribol. Int. 68, 85–93.

Serro, A.P., et al., 2006. Adsorption of albumin on prosthetic materials: implication for tribological behavior. J. Biomed. Mater. Res. A 78A, 581–589.

Soderquist, M., Walton, A., 1980. Structural changes in proteins adsorbed on polymer surfaces. J. Colloid Interface Sci. 75, 386–397.

Sousa, S.R., et al., 2004. Human serum albumin adsorption on TiO_2 from single protein solutions and from plasma. Langmuir 20, 9745–9754.

Taborda, A., et al., 2011. Polynomial approximation to universal ionization cross-sections of K and L shells induced by H and He ion beams. X-Ray Spectrom. 40, 127–134.

Taeger, G., et al., 2003. Comparison of diamond-like-carbon and alumina-oxide articulating with polyethylene in total hip arthroplasty. Mater. Werkst 34, 1094–1100.

Thorwarth, G., et al., 2010. Tribological behavior of DLC-coated articulating joint implants. Acta Biomater. 6, 2335–2341.

Ueda, I., et al., 1976. Molecular mechanism of inhibition of firefly luminescence by local anesthetics. Proc. Natl. Acad. Sci. U. S. A. 73, 481–485.

Vanea, E., Simon, V., 2011. XPS study of protein adsorption onto nanocrystalline aluminosilicate microparticles. Appl. Surf. Sci. 257, 2346–2352.

Vogler, E.A., 1998. Structure and reactivity of water at biomaterial surfaces. Adv. Colloid Interface 74, 69–117.

Wang, D.-Y., et al., 2005. Deposition of diamond-like carbon films containing metal elements on biomedical Ti alloys. Surf. Coat. Technol. 200, 2175–2180.

Wang, P., et al., 2007. Comparing internal stress in diamond-like carbon films with different structure. Thin Solid Films 515, 6899–6903.
Wang, Q., et al., 2013. Effect of titanium or chromium content on the electrochemical properties of amorphous carbon coathings in simulated body fluid. Electrochim. Acta 112, 603–611.
Wimmer, M.A., et al., 2010. Wear mechanisms in metal-on-metal bearings: the importance of tribochemical reaction layers. J. Orthop. Res. 28, 436–443.
Żenkiewicz, M., 2007. Methods for the calculation of surface free energy of solids. J. Achiev. Mater. Manuf. Eng. 24, 137–145.
Zhou, Y., et al., 2006. Control over the wettability of amorphous carbon films in a large range from hydrophilicity to super-hydrophobicity. Appl. Surf. Sci. 253, 2690–2694.
Ziegler, J.F., 2004. SRIM-2003. Nucl. Instrum. Methods B 219–220, 1027–1036.

PAPER V

Sliding Properties of Zr-DLC Coatings: The effect of Tribolayer Formation

T. Vitù, A. Escudeiro, T. Polcar and A. Cavaleiro
Surface and Coating Technology **(2014)**, in press
DOI: 10.1016/j.surfcoat.2014.08.003

Surface & Coatings Technology 258 (2014) 734–745

Contents lists available at ScienceDirect

Surface & Coatings Technology

journal homepage: www.elsevier.com/locate/surfcoat

Sliding properties of Zr-DLC coatings: The effect of tribolayer formation

T. Vitu [a,*], A. Escudeiro [b], T. Polcar [c,d], A. Cavaleiro [b]

[a] Faculty of Transportation Sciences, Czech Technical University in Prague, Konviktska 20, Prague 1, Czech Republic
[b] SEG-CEMUC — Department of Mechanical Engineering, University of Coimbra, 3030-788 Coimbra, Portugal
[c] Department of Control Engineering, Faculty of Electrical Engineering, Czech Technical University in Prague, Technicka 2, Prague 6, Czech Republic
[d] nCATS, Engineering Sciences, University of Southampton, Highfield, Southampton, United Kingdom

ARTICLE INFO

Article history:
Received 7 November 2013
Accepted in revised form 1 August 2014
Available online 10 August 2014

Keywords:
Zr-DLC
Hydrogenated DLC
Tribology
Tribolayer
Raman spectroscopy

ABSTRACT

Amorphous carbon-based coatings (DLC) exhibit excellent mechanical and tribological properties such as high hardness, high elastic modulus, low friction and low wear. Reduced friction is often related to the formation of a low-friction tribolayer, which is formed during sliding and transferred to the counterpart. Here, we investigate the sliding of hydrogenated and non-hydrogenated DLC coatings alloyed with zirconium; pure DLC films are used as reference. The coatings were deposited by magnetron sputtering in Ar (non-hydrogenated) and Ar/methane atmosphere (hydrogenated) onto steel substrates and silicon wafers. The total thickness of the coatings was around 1.5 μm including a complex Ti/TiN/TiCN adhesion-improving interlayer with a thickness of 450 nm. All deposited coatings were amorphous, Zr/C ratio was approx. 0.05. The hardness was in the range of 9–13 GPa. Tribological tests were carried out in humid air at room temperature, at 100 °C and in nitrogen environment using pin-on-disk. Intermittent tribological test analysis has been performed to understand running-in behaviour. The worn surfaces and wear debris were analysed by Raman spectroscopy. Coatings alloyed with Zr showed lower friction and wear at room temperature compared to pure DLC. In general, Zr-doped hydrogenated coating outperformed the non-hydrogenated one when tested in an inert nitrogen atmosphere or at elevated temperature (100 °C), exhibiting almost super-low friction ($\mu = 0.03$ in the steady-state regime) due to the formation of a homogenous, thick and stable tribolayer.

1. Introduction

It is well known that amorphous carbon-based coatings (typically called as diamond-like coatings, DLC) exhibit unusual mechanical and tribological properties such as high hardness, high elastic modulus, low friction and low wear [1–3]. DLC is used in a wide range of industrial applications in different environmental conditions [4–10]. However, the coating applicability might be limited due to their high level of residual stress. Co-deposition of an appropriate adhesion interlayer, respecting the chemical and mechanical properties of the substrate and coating, and introduction of metallic elements (Cr, Ti, W, etc.) into the C-matrix can successfully reduce the residual stress and enhance the adhesion [3,6,11,12]. Such coatings are often denoted in literature as Me-C(:H) or Me-DLC coatings, where Me stands for the metallic element.

The tribological properties of pure DLC coatings are strongly dependent on their structure and testing environmental conditions. Basically, the DLC coatings deposited on temperature sensitive substrates, such as steel, can be divided into two main groups — hydrogenated films deposited either by PECVD or by reactive magnetron sputtering (a-C:H) [1,2] and non-hydrogenated films prepared by non-reactive magnetron sputtering (a-C). Non-hydrogenated coatings generally perform better in humid environments, while hydrogenated coatings are excellent in dry sliding and inert gas conditions reaching friction values in the range of 0.001–0.2 [3,13,14]. At elevated temperatures (≥300 °C), hydrogenated DLC films may gradually degrade into graphite and hence wear through quickly, while non-hydrogenated coatings are more resistant to oxidation or phase transformation [2,15–17]. The formation of a carbon-rich tribolayer between the surface of DLC coating and the counterpart is a typical product of dry sliding positively affecting the tribological properties [14,18]. A stable tribolayer suppresses friction fluctuations and lowers both the friction and the wear [19]. On the other hand, hard abrasive wear debris particles present in the tribolayer could lead to abrasive wear; consequently, the friction process becomes instable with high fluctuations of the friction coefficient [14,18,20]. The tribolayer composition and mechanisms of generation and growth are a function of the coating and counterpart properties and, particularly, strongly depend on the testing conditions, namely temperature, moisture, and presence of the environmental reactants (ambient air gases or other chemical compounds) [21,22].

The introduction of additional element (e.g. Ti [4,23–28], W [4–6,29], Si [30–34]) into both types of carbon matrix referred to above leads to profound changes of coating properties, such as structure, morphology, surface free energy, and mechanical properties. Doped or alloyed DLC

---

[*] Corresponding author. Tel.: +420 224359918.
E-mail address: vitu@fd.cvut.cz (T. Vitu).

http://dx.doi.org/10.1016/j.surfcoat.2014.08.003

coatings often exhibit improved tribological properties not only by lowering the friction and wear but also by the stabilisation of the tribological properties in different testing environments [35,36]. Scharf and Singer [14] reported that for metal-doped DLC films the tribolayer formation and growth was dependent on the metal dopant and the atmosphere humidity. DLC films co-sputtered with zirconium have been recently studied by several authors [37–39] showing that low content of Zr (<10 at.%) can effectively reduce the friction and wear of the coating compared to un-doped films. In this paper, the structural, mechanical and tribological properties of both non-hydrogenated and hydrogenated Zr-doped DLC coatings were evaluated. The main attention is paid to the mechanisms of surface tribolayer formation, its composition, compactness, and other properties affected by tribological testing conditions. The tribological measurements were carried out at room temperature (RT) and at 100 °C and in nitrogen or humid air atmosphere in order to identify the environment effect on the tribological properties.

2. Experimental details

The Zr-DLC(-H) films were deposited using dc dual magnetron sputtering. Two targets were used for the deposition of pure and co-sputtered Zr films: a titanium target, for the deposition of the adhesion layer, and a graphite target with selected number of Zr pellets embedded in the target erosion zone. The Zr content in the films was controlled by the number of Zr pellets. The Zr content was selected with regard to the results of our previous study [40], where the best mechanical and tribological properties were observed in the range of 3–5 at.% of Zr. All the substrates (mirror polished AISI D2 steel coupons) and targets were sputter-cleaned before the deposition process started. To deposit hydrogenated films, CH_4 was introduced into the chamber. The flows of argon and methane were controlled with the aim of reaching the same total working pressure (0.4 Pa). The deposition parameters are summarized in Table 1. A Ti/TiN/TiCN functional (~450 nm thick) adhesion interlayer was deposited first to improve the adhesion of the coatings to the substrate.

The coating composition was analysed by Electron Probe Microanalysis (EPMA-Cameca SX 50). The structure of the coatings was determined in glancing-mode X-ray diffraction (Phillips diffractometer-Co K_α radiation). The as-deposited carbon matrix bonds as well as the tribology-induced surface changes were studied by Raman spectroscopy (Horiba Jobin Yvon microscope, 532 nm). The Raman spectra have been fitted using Lorentzian peaks; total peak areas have been used to calculate the peak intensity ratio.

The coating hardness was evaluated by Micro Materials nano-test platform. To avoid the influence of both substrate and TiN/TiCN adhesion interlayer a normal load of 5 mN was applied reaching a maximum indentation depth of 130–160 nm. The adhesion of the coatings was determined using a conventional scratch-test (CSEM Revetest); the critical load was assessed by optical-microscope observation.

The surface roughness R_a of the samples was determined using 3D profilometer Zygo NV7200; 20 surface profiles were used and the standard deviation was calculated.

Wettability tests were performed using the sessile drop method. The drops were generated by a micro syringe and deposited on the surface for at least 20 times. A sequence of images was captured using a DMK-41BU02 digital camera mounted horizontally on a robust stand. The tribological measurements were carried out using a pin-on-disk tribometer (CSM Instruments). The coatings were tested at ambient air at room temperature (RT) (25 °C, relative humidity 40 ± 5%), at 100 °C and N_2 environment. The normal load was 5 N, the duration of the test was 1000 cycles (N_2 environment), 5000 (RT and 100 °C) and 30,000 (for lifetime testing), and the relative ball vs. coating velocity was 0.15 $m \cdot s^{-1}$. The testing counterparts were 100Cr6 steel balls with a diameter of 6 mm. The coating wear tracks and the ball wear scars were analysed by 3D non-contacting profilometer Zygo NV7200. The coating wear volumes were calculated from the average of four wear track cross-sections obtained in different positions along the wear track. The difference between the maximum and the minimum measured coating wear volume in one wear track did not exceed 25%, which was in a good agreement with several statistic models in tribology [41,42]. The ball wear volume was calculated from the wear scar 3D analyses using geometrical idealization of the original ball surface. The wear rates were calculated as the worn volume per load per sliding distance [42]. To understand wear mechanisms, particularly running-in stage, the contact pressure evolution was studied by ball contact area determined during the intermittent tribological test. Furthermore, the wear tracks, the ball wear scars and the generated wear debris were analysed by optical microscopy and Raman spectroscopy. The Raman analyses were performed in selected points within and around the coating wear track and counter-part contact area (Fig. 1). During the intermittent testing, Raman inspection was also performed at RT in order to evaluate the running-in behaviour.

3. Results

3.1. Coating characterization

The Zr/C ratio representing the chemical composition of the coatings is shown in Table 1. The oxygen content that originated from residual atmosphere in the deposition chamber was negligible; therefore we report only Zr/C ratio.

Fig. 2 shows the XRD diffractograms of the amorphous carbon films where the only visible peaks were associated to TiN/TiCN adhesion interlayer. The peaks corresponding to the positions of Ti (002), Ti (101), TiN (111), TiN (200) and TiN (220) are clearly visible in Fig. 2.

Table 1

(Zr-)DLC(:H) coating deposition parameters, composition and mechanical properties.

Parameter\sample			DLC	DLC-H	Zr-DLC	Zr-DLC-H
Deposition parameters	Ar flow	(sccm)	45	40	45	40
	CH_4 flow	(sccm)	–	17	–	17
	Bias voltage	(V)	−50	−50	−50	−50
	C/Zr target power	($W \cdot cm^{-3}$)	1500	1500	1500	1500
	A_{Zr}/A_C erosion area	(%)	0	0	3	6
	Deposition rate	(nm/s)	5.8	12.7	7.4	13.1
Composition	Zr/C ratio	(–)	0	0	0.05	0.05
Mechanical properties	Thickness	(μm)	1.1	0.9	1.1	0.9
	Critical load L_{c2}	(N)	43 ± 3	22 ± 2	42 ± 9	35 ± 3
	Hardness	(GPa)	12.3 ± 0.5	10.1 ± 0.3	8.8 ± 0.4	13.3 ± 0.6
	Elastic modulus	(GPa)	120 ± 3	89 ± 1	102 ± 1	116 ± 1
	Surface roughness R_a	(nm)	16.9 ± 3.3	14.3 ± 4.6	18.4 ± 5.6	18.9 ± 4.5
Wettability	Water drop contact angle	(deg)	61.5 ± 3.4	70.3 ± 2.5	66.2 ± 2.4	79.3 ± 1.8
Tribological properties	Initial contact pressure	(MPa)	930	810	870	920
	Contact pressure at 5000 cycles	(MPa)	80	140	110	160

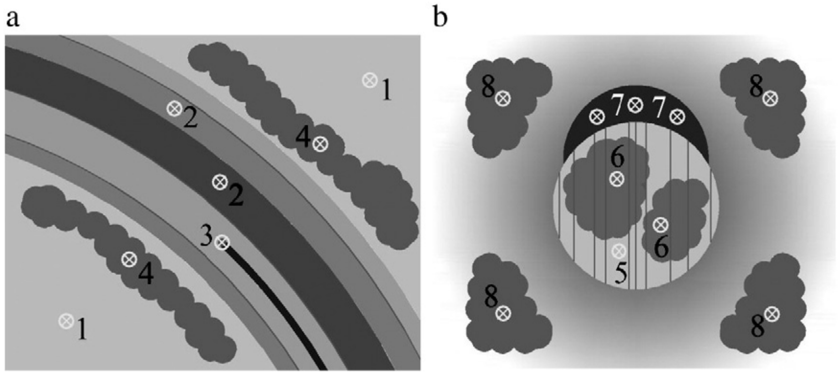

Fig. 1. Schematic plot of the points selected for Raman analyses: a) the wear track, b) the counter-part wear trace. In the text the points are described as: as-deposited surface (1), wear track area (2), wear track embedded particles (3), wear track free wear debris (4), ball contact area (5), tribolayer (6), leading edge wear debris (7), ball free wear debris (8).

As expected for such low Zr content, there was no evidence of ZrC crystalline phase. However, compared to the spectra of non-doped films, the Zr-doped coatings exhibited a very broad peak in the range of 30 to 40°. We have shown recently that the coatings with 9 at.% already contain ZrC nanograins [40], which corroborate the results of Adelhelm et al., who showed existence of ZrC in coatings with approx. 7 at.% of Zr [43]. It is very probable that Zr content presented in this study is close to the limit where the first ZrC nanograins (or sub-nanograins) are formed. Nevertheless, for the purpose of this particular study the structure of Zr-DLC(-H) coatings could be considered as amorphous.

The Raman spectra of as-deposited Zr-DLC(-H) coatings are shown in Fig. 3. The carbon matrix exhibited the typical D and G bands located in the range of 1300–1600 cm^{-1}. When using visible Raman excitation (532 nm), the carbon D and G peaks are results of vibration of sp^2 sites; in other words, the sp2/sp3 ratio cannot be determined. The hydrogenated structures showed a more pronounced G peak corresponding to the prevailing axial vibrations of carbon chains and rings rather than "breathing" mode of the rings that corresponds to the D peak [44,45]. Slight background photoluminescence (PL) effect was also observed. This effect is typical for hydrogenated DLC structures due to the existence of recombination centres in the structure by the presence of hydrogen [46]. The H content can be thus estimated by the ratio between the slope of the linear background and the intensity of the G peak [47]. The calculated H content was approximately 30 at.% which was in a good agreement with the ERDA/RBS analysis of DLC-H coating (not shown). When the Zr-dopant was introduced, the G peak positions decreased in conjunction with the I_D/I_G ratio growth (Fig. 4). Both effects are closely associated with the carbon bond disorder [44,45]. Similar results were obtained by Adelhelm et al. [48] who correlated this behaviour with the presence of heavy Zr atoms.

The Zr-DLC(-H) coating hardness and elastic modulus results are shown in Table 1. The hardness values are placed in a relative narrow range between 9 and 13 GPa and, thus, any significant effects of the coatings composition on the mechanical properties could be hardly defined. Nevertheless, the highest hardness was obtained for the Zr-doped hydrogenated DLC structure suggesting a low proportion of non-bonded hydrogen and a denser carbon matrix [49,50]. Narrow range of the elastic moduli was similar to that of hardness. Apart from the hardness and elastic modulus, the coating surface roughness is considered as one of the important properties from the tribological point of view. Erdemir et al. [13] showed that higher roughness led to more extensive ploughing effect and thus increasing the friction coefficient. In our study there were no significant differences in roughness among the coatings (Table 1). However, higher water contact angle and thus lower surface energy was observed for the hydrogenated DLC surfaces. The same trend was obtained when the Zr atoms were introduced into the carbon structure — the surface energy decreased.

3.2. Tribological performance

3.2.1. Friction and wear

Fig. 5 shows typical friction curves of the deposited coatings tested at RT (Fig. 5a) and 100 °C (Fig. 5b). The friction at RT was relatively stable showing a clearly distinguishable running-in period of about 1500 cycles. The evolution of contact pressure during the tests is shown in Fig. 6. Intermittent tribological test analysis of the wear of the ball contact area clearly proved that the running-in period was closely related with rapid decrease of contact pressure. The shortest

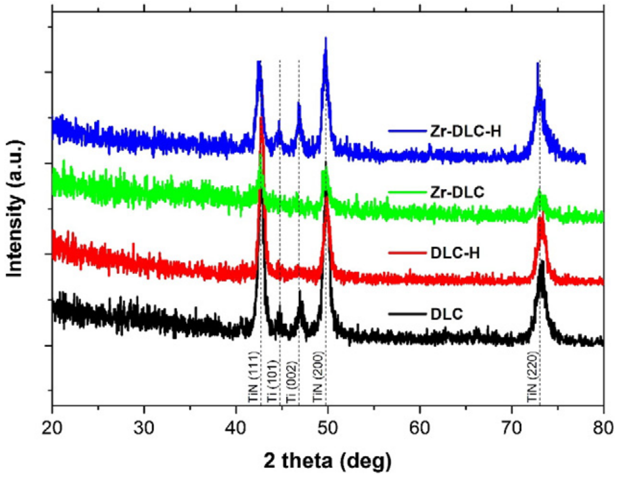

Fig. 2. X-ray diffraction spectra of Zr-DLC(-H) coatings.

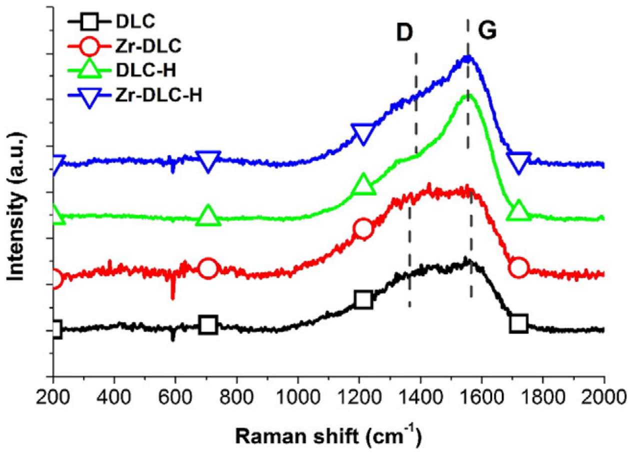

Fig. 3. Raman spectra of as-deposited Zr-DLC(-H) coatings.

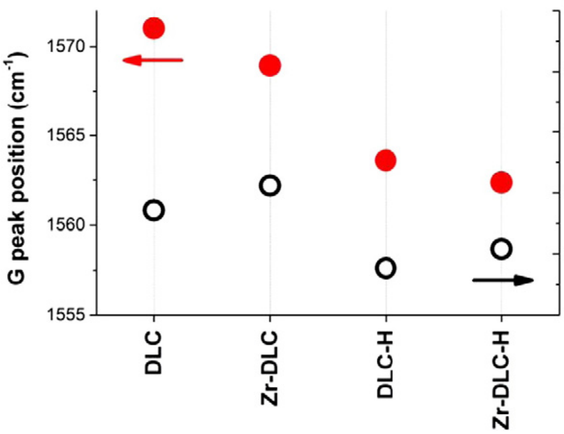

Fig. 4. The Raman carbon peaks analyses — G peak position and I_D/I_G ratio.

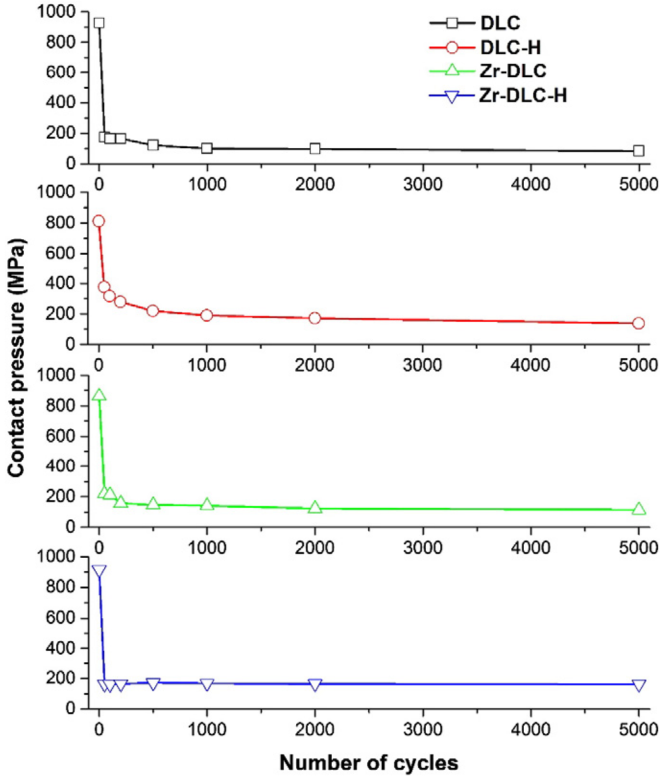

Fig. 6. Evolution of contact pressure with number of cycles calculated according to the ball contacting area — tribology at RT and ambient environment.

running-in phase was observed in the case of Zr-DLC-H coating — about 50 cycles. Then the contact area remained almost constant till the end of the sliding test.

Both hydrogenated and non-hydrogenated Zr-DLC coatings exhibited lower friction coefficients with much lower fluctuations than the coatings without Zr (Fig. 5a). At 100 °C, the friction of the non-hydrogenated coatings was rather instable with high fluctuations. In this case, there was significant difference between the films with and without hydrogen (Fig. 5b). Hydrogenated coatings showed much lower friction at the elevated temperature than at room temperature. Zr-DLC-H coating exhibited remarkably low and stable friction coefficient close to 0.03 in steady-state wear regime (Fig. 5b). For a more precise running-in phase study and determination of the role of the temperature and reaction with atmosphere, the coatings were tested in an inert atmosphere (N_2 environment). The friction evolution is shown in Fig. 7. As expected, the non-hydrogenated coatings did not show any significant difference compared to the tests performed in humid air at room temperature. On the other hand, Zr-DLC-H coating clearly demonstrated the frictional behaviour similar to the test at 100 °C, i.e. very low friction in the steady state regime. However, strong fluctuations were recorded during the Zr-DLC-H running-in phase.

The wear results for both coatings and counter-parts tested in ambient air are shown in Fig. 8. At RT the incorporation of metal and H did not significantly influence the wear performance, although slightly lower coating wear rates were obtained for Zr-doped structures. At elevated temperature the non-hydrogenated Zr coating showed the highest wear rate and the highest effect of testing environment on the wear. It is important to notice here that the depth of the wear tracks did not exceed 500 nm, i.e. less than a half of the total coating thickness. Furthermore, the tests in the N_2 atmosphere did not show any measurable coating wear; only shallow scratches could be observed. The worn surfaces were analysed by Raman spectroscopy; the results are discussed in the following section.

The ball wear scars were characterized by shallow abrasive scratches parallel to the relative movement and a well-adhered surface tribolayer. The ball wear rates exhibited relatively similar results for both temperatures, except when sliding against DLC and Zr-DLC at elevated temperature. The high wear rates of Zr-DLC coating and corresponding counterpart were clearly related to the highest friction, see Fig. 5b.

In order to evaluate the lifetime of the hydrogenated structures, i.e. DLC-H and Zr-DLC-H, test with 30,000 cycles has been performed as well, see friction curves in Fig. 9. It is evident that Zr alloying had a positive effect on the friction coefficient stabilisation compared to

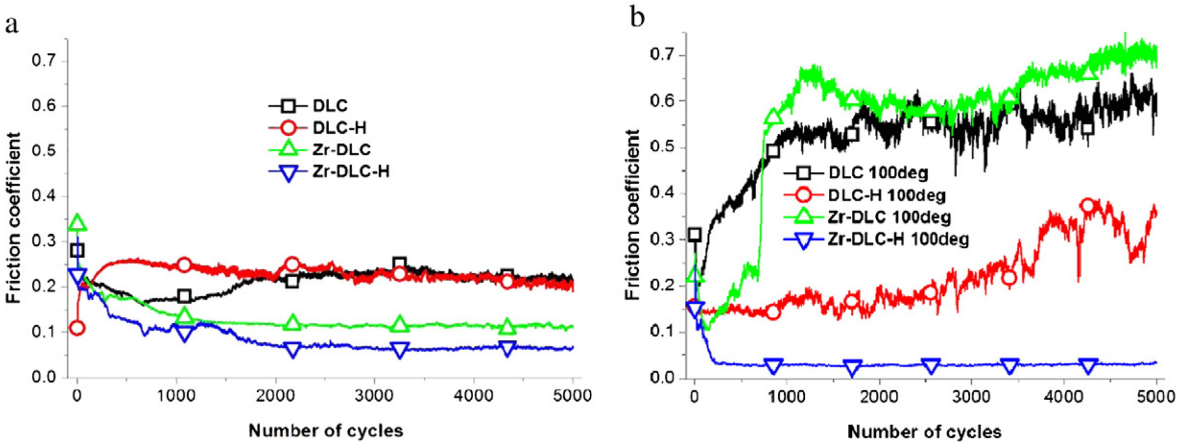

Fig. 5. Friction evolution of Zr-DLC(-H) a) at room temperature and, b) at 100 °C.

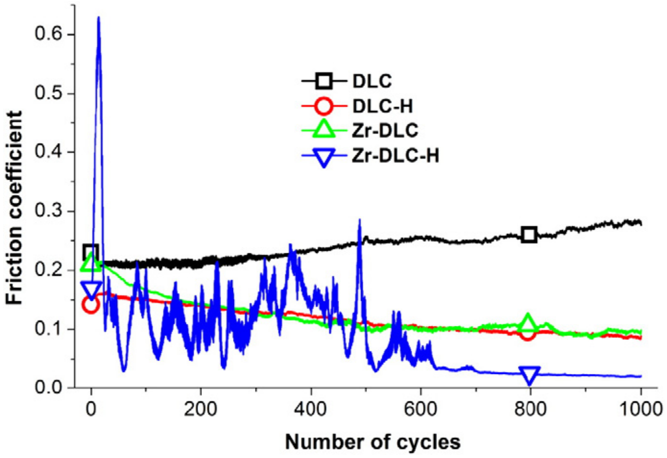

Fig. 7. Friction evolution of the Zr-DLC(-H) coatings in the N_2 atmosphere.

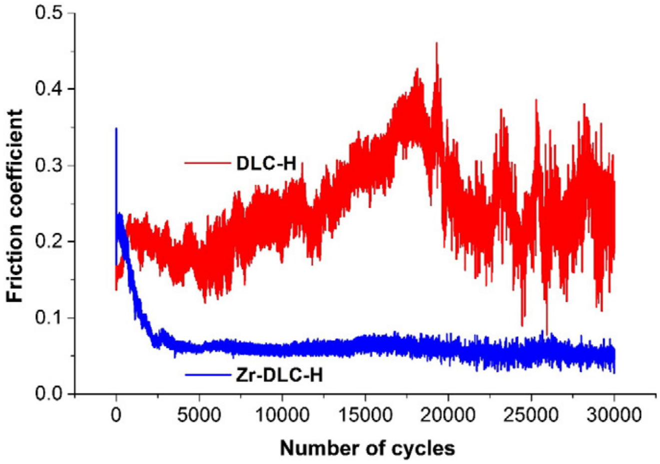

Fig. 9. Friction curves of DLC-H and Zr-DLC-H samples in the lifetime test.

DLC-H coating. We should stress that the coatings were not worn through (maximum wear depth was about 700 nm).

3.2.2. Analysis of worn surfaces

To identify the wear mechanisms of the coatings, optical microscopy, 3D surface analysis and Raman spectroscopy were used to analyse the worn surfaces. The analyses have been predominantly focused on the hydrogenated films, since these coatings represent the majority of DLC-based industrial applications. Nevertheless, the main differences in the hydrogenated and non-hydrogenated coating behaviour are discussed as well.

The running-in behaviour study showed that the surface adaptation (i.e. wear process sufficient to remove asperities from original roughness) was finished at the point when contact pressure steady-state regime was reached. Thus, the balls and coatings were mostly worn during the running-in stage (typically several hundreds to 1500 cycles). The structural changes of the tribolayer adhered on the ball, namely change in carbon structure and iron oxide production, were clearly related to the friction coefficient. The first Raman peaks of iron oxides (if any) appeared within the first 200 cycles. The carbon-related Raman peaks gradually changed positions and intensities till considerably high number of cycles: DLC-H at 500 cycles and all other coatings at 2000 cycles. Thus, the analyses described in the following text are focused on the worn surfaces after 5000 cycle tests when the steady-state regime was fully developed.

The analyses of the wear tracks, ball wear scars and debris adhered on the ball of the hydrogenated DLC coating sliding at room temperature are shown in Fig. 10. The ball wear scar exhibited shallow scratches covered by relatively homogeneous and well-developed tribolayer. The Raman spectra analysis of the tribolayer showed number of peaks in the range of 200–800 cm^{-1} together with the typical carbon bands. The Raman peaks positioned at lower Raman shifts were identified as iron oxides, mainly hematite Fe_2O_3 (peaks at 228 and 294 cm^{-1}) and magnetite Fe_3O_4 (strongest peak at 665 cm^{-1}) [51]. The shape and position of the carbon peaks significantly differed from that of as-deposited coating and the wear track on the coating. The splitting of D and G bands was evident with D band down-ward shift (1391 to 1354 cm^{-1}) and up-ward G band shift (1564 to 1580 cm^{-1}). The Raman spectrum acquired in the centre of the ball wear scar exhibited almost completely separated D and G peaks; the intensity of the latter was very low. In some cases, the α-Fe_2O_3 and Fe_3O_4 phases could exhibit an additional indecisive second harmonic vibration at 1320–1322 cm^{-1} [52,53]. Since we do not have any result indicating the presence of such peak, it was not taken into account during spectra deconvolution. Nevertheless, the existence of a weak additional peak in the position referred to above would not significantly change the shift of carbon peaks. The leading edge and the wear debris attached to the ball scar edges showed carbonaceous material with vestiges of iron oxides (Fig. 10, pos. 7, 8). Finally, a weak background photoluminescence (PL) was observed in all spectra taken from various positions at the ball wear scar, which indicated the presence of hydrogen saturating the recombination centres in the carbon matrix [47].

The coating wear track appeared extremely smooth with only low number of very shallow scratches parallel to the ball-coating relative movement. The maximum wear depth did not exceed 100 nm. Thus, the polishing wear was the predominant wear mechanism. The Raman spectra did not show any vestiges of iron oxides or any other contaminants in the wear track. Moreover, no significant changes in carbon structure were observed when compared to as-deposited coatings (Fig. 10, pos. 1–3). Hence, the friction behaviour is mainly related to properties of the tribolayer.

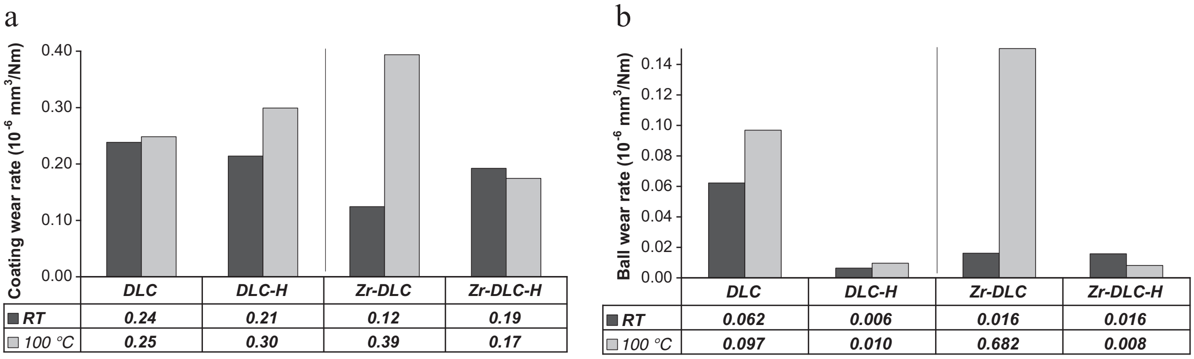

a

	DLC	DLC-H	Zr-DLC	Zr-DLC-H
■ RT	0.24	0.21	0.12	0.19
□ 100 °C	0.25	0.30	0.39	0.17

b

	DLC	DLC-H	Zr-DLC	Zr-DLC-H
■ RT	0.062	0.006	0.016	0.016
□ 100 °C	0.097	0.010	0.682	0.008

Fig. 8. The values of a) Zr-DLC(-H) coating wear rates and b) ball wear rates.

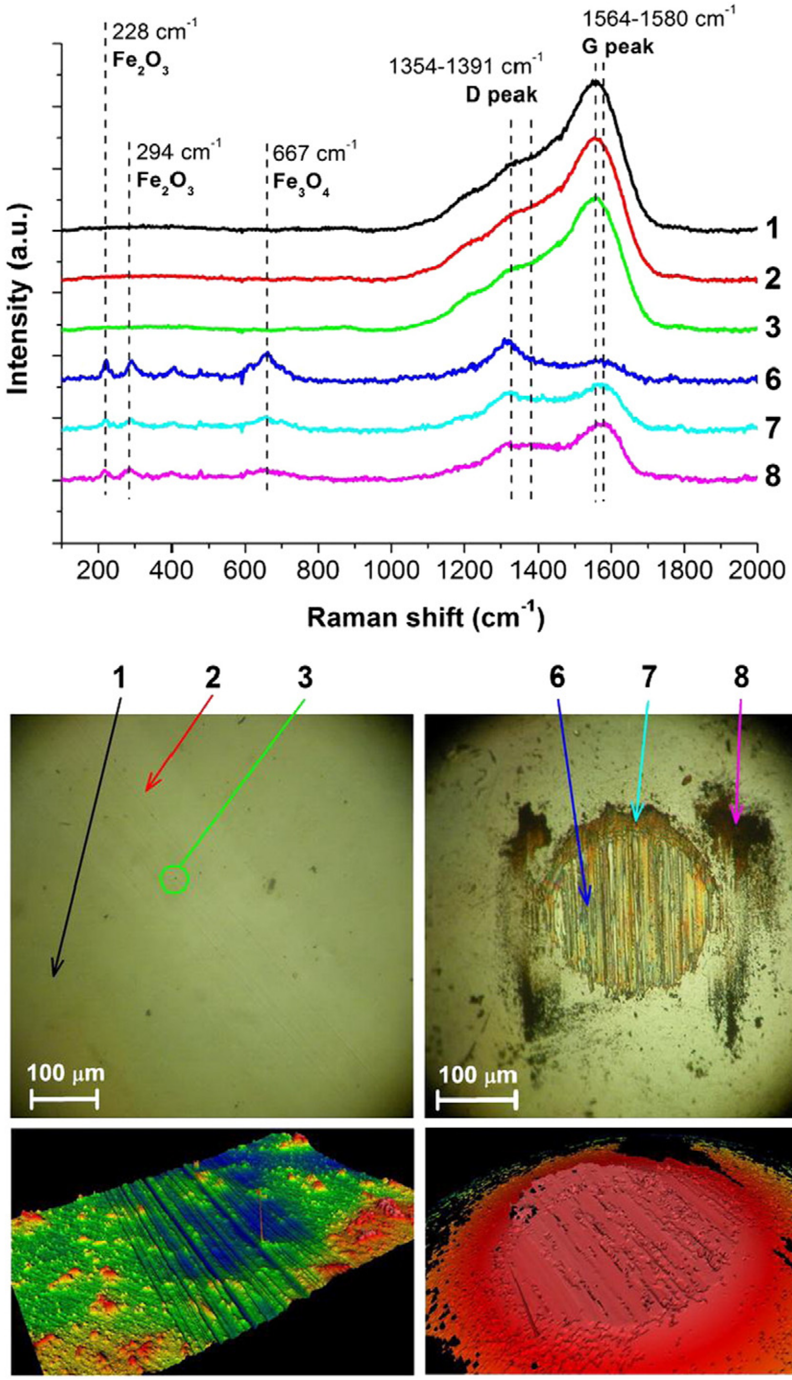

Fig. 10. Raman analysis of the ball wear scar and coating wear track — DLC-H at room temperature. The numbers correspond to the scheme shown in Fig. 1.

Increasing the testing temperature resulted in a higher amount of attached wear debris at the ball leading edge. The tribolayer formed on the ball wear scar was less compact, showing Raman peaks related to iron oxides (magnetite) and carbon (Fig. 11, pos. 6). Interestingly, the peaks of hematite were observed together with those related to magnetite and carbon in the wear debris adhered on the side of the ball wear scar (Fig. 11, pos. 8). As expected, photoluminescence effect was not observed at elevated temperature. The coating surface showed shallow scratches together with a groove in the centre of the wear track (wear depth about 110 nm), which was partially responsible for the increased wear rate when compared with the corresponding test at RT. Again, the Raman spectra from different parts of the wear track were remarkably similar (Fig. 11, pos. 1 - 3).

The results of Raman analyses of the non-hydrogenated coatings sliding at room temperature were comparable with those of hydrogenated films, i.e., the shift of carbon peaks, the decrease of carbon peaks intensities and the presence of iron oxides. At 100 °C, the magnetite and hematite peaks observed on the ball wear scar were more pronounced suggesting a higher steel ball oxidation [51]. Even though the tribolayer was found to be less compact, the production of free wear debris was higher being directly connected to higher friction coefficient [2].

Lower coverage of the ball wear scar by tribolayer was also observed when the hydrogenated Zr-DLC-H coating was tested at room temperature (Fig. 12). The Raman spectra showed sharp separated carbon peaks both shifted in opposite directions (Fig. 12, pos. 3, 6, 7). These shifts were more significantly pronounced than in the case of

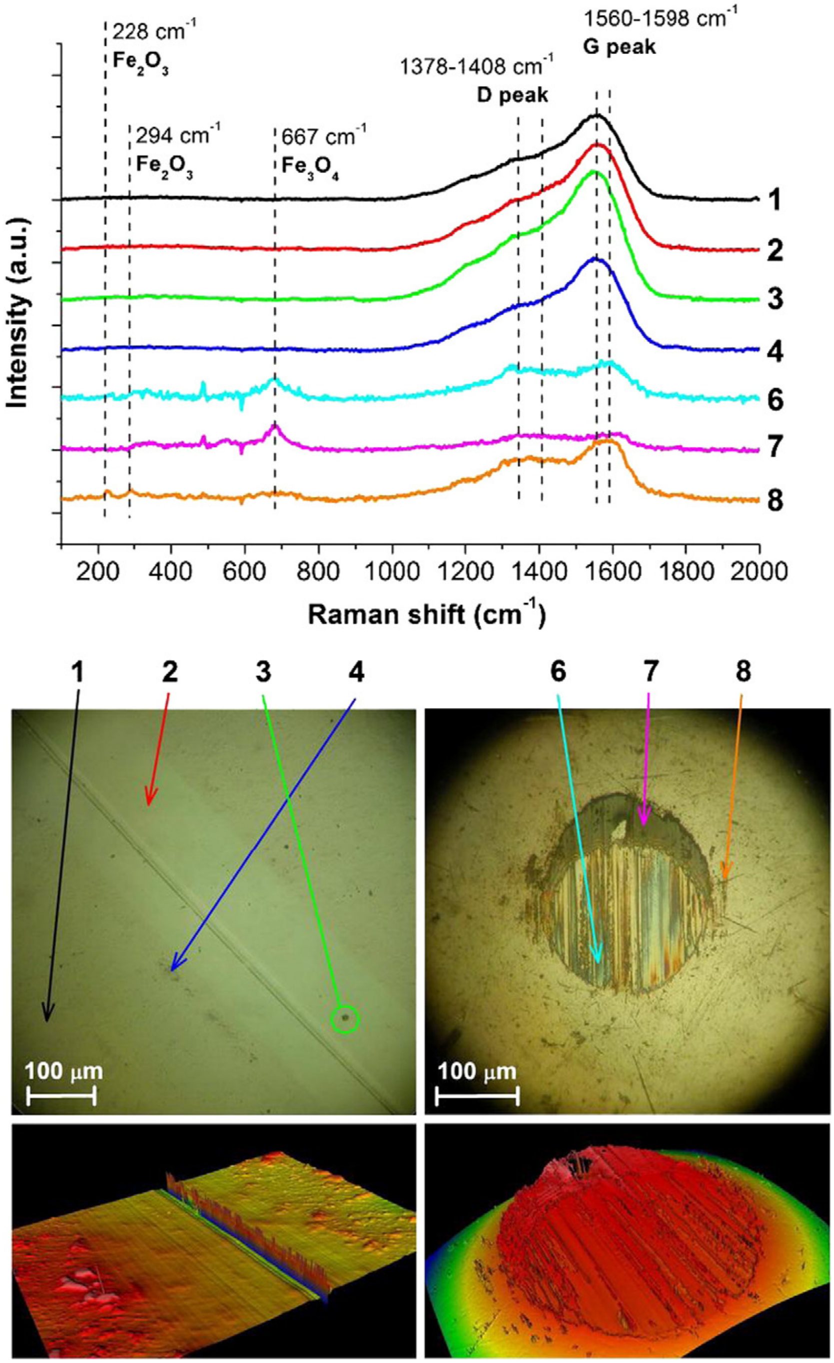

Fig. 11. Raman analysis of the ball wear scar and coating wear track — DLC-H at 100 °C. The numbers correspond to the scheme shown in Fig. 1.

Zr-DLC (not shown) suggesting stronger bond order effects. Slight background photoluminescence was observed indicating the hydrogen presence in the tribolayer. The Raman analysis did not exhibit any vestiges of iron oxides; thus, the formation of the tribolayer inhibited the ball oxidation in the later stages of sliding process due to complete separation of the ball and coating surfaces. The analyses of the wear debris adhered to the ball leading edge and free wear debris produced during the sliding showed again only carbon-related peaks (Fig. 12, pos. 7, 8). The coating wear track was very smooth with shallow scratches (up to 80 nm); no significant changes in the Raman spectra of the wear track and the as-deposited coating were observed. In fact, we identified very small spots covered by the wear debris giving rise to Raman spectra identical to those of the wear debris found at the ball wear scar (Fig. 12, pos. 3). Nevertheless, the area of such spots is negligible compared to the area of the wear track.

Sliding tests at elevated temperature resulted in an almost immeasurable coating wear rate; only few shallow scratches could be observed on the coating surface (maximum wear track depth of 50–70 nm), see Fig. 13. The ball wear scar was fully covered by a tribolayer; the amount of the adhered wear debris at the leading edge of the ball was enormous. The Raman spectra analysis did not show any changes in the wear track when compared to the as-deposited coating (Fig. 13, pos. 1, 2).

The friction coefficient of Zr-DLC and Zr-DLC:H at elevated temperature was 0.7 and 0.03, respectively. Surprisingly, the corresponding Raman spectra of the worn surfaces were similar for both coatings (Figs. 13 and 14). The only difference was the presence of hematite

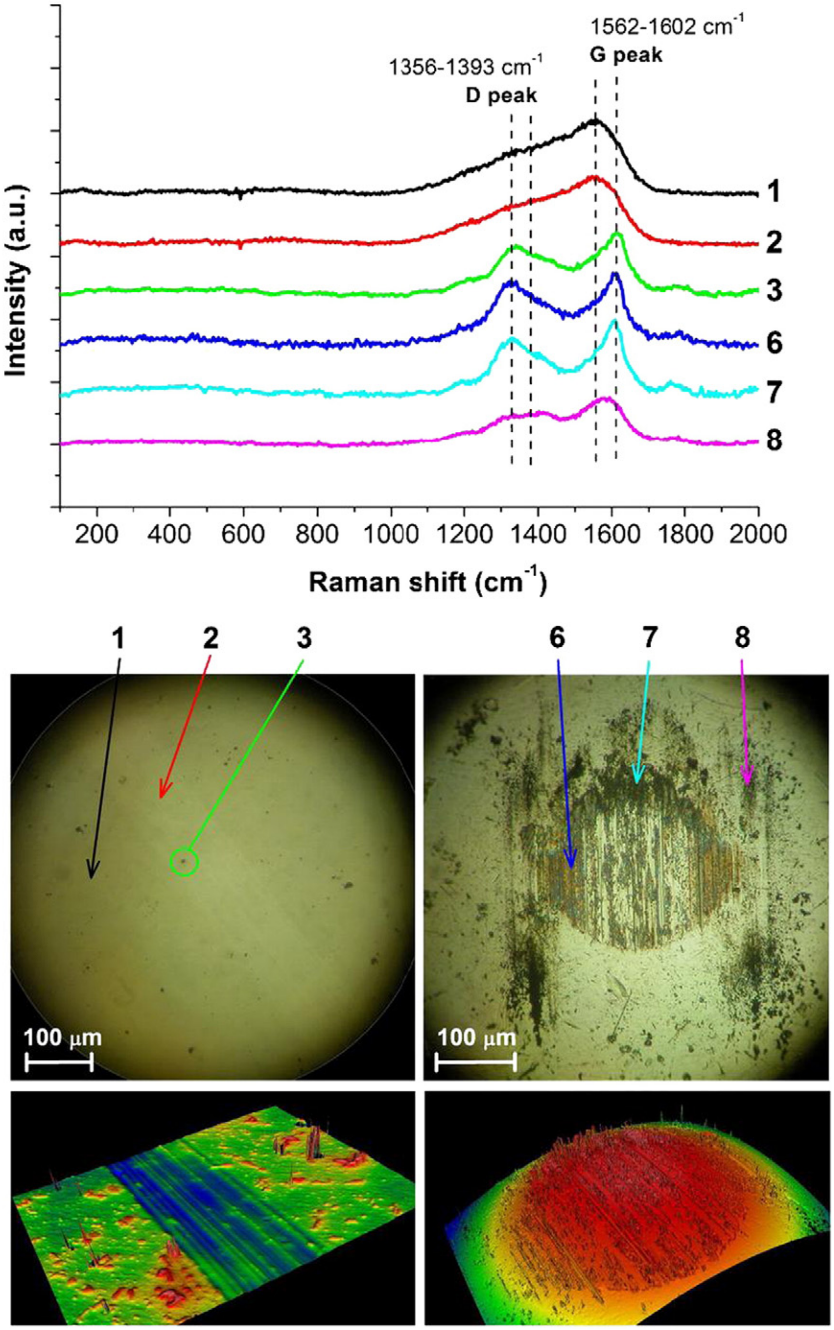

Fig. 12. Raman analysis of the ball wear scar and coating wear track — Zr-DLC-H at RT. The numbers correspond to the scheme shown in Fig. 1.

peaks (228 and 294 cm^{-1}) in the wear debris on the side of the ball wear scar after the test of Zr-DLC (see Fig. 14, pos. 8). Notably lower tribolayer formation on the ball wear scar has been observed for Zr-DLC coating as well.

The coatings were also tested in the N_2 atmosphere to clarify the role of humid air. Iron oxides peaks were not found in corresponding Raman spectra of the ball worn surfaces. Carbon peaks remained at the same positions (when compared to test in humid air); however, the I_D/I_G ratio increased significantly in the case of hydrogenated coatings.

4. Discussion

The effect of environment on sliding properties of DLC coatings is well studied [54]; nevertheless, it is quite complex phenomena depending on sliding conditions and physical and chemical properties of DLC films. Typically we have to consider three mechanisms acting simultaneously: i) friction at nanoscale (passivation of surfaces, adhesion, etc.), ii) tribochemical changes and reactions with atmosphere, and iii) formation of a tribolayer from wear debris.

In order to relate our results – mechanical properties, Raman of as-deposited as well as worn surfaces, and tribology – we will consider the effects of hydrogen and Zr-dopant separately.

The effects of hydrogen in the DLC structure have been described by many authors [1–3,5,11,29]. Increase hydrogen proportion leads to the structural changes of carbon matrix of the DLC that could be observed by Raman spectroscopy. Coatings studied in this study followed the same trend, i.e. I_D/I_G ratio was lower when the hydrogen was present. This is directly proportional to the prevailing axial vibrations of shorter carbon chains and rings [44,45]. Such variations in the structure typically result in lower hardness and improved tribological properties due to

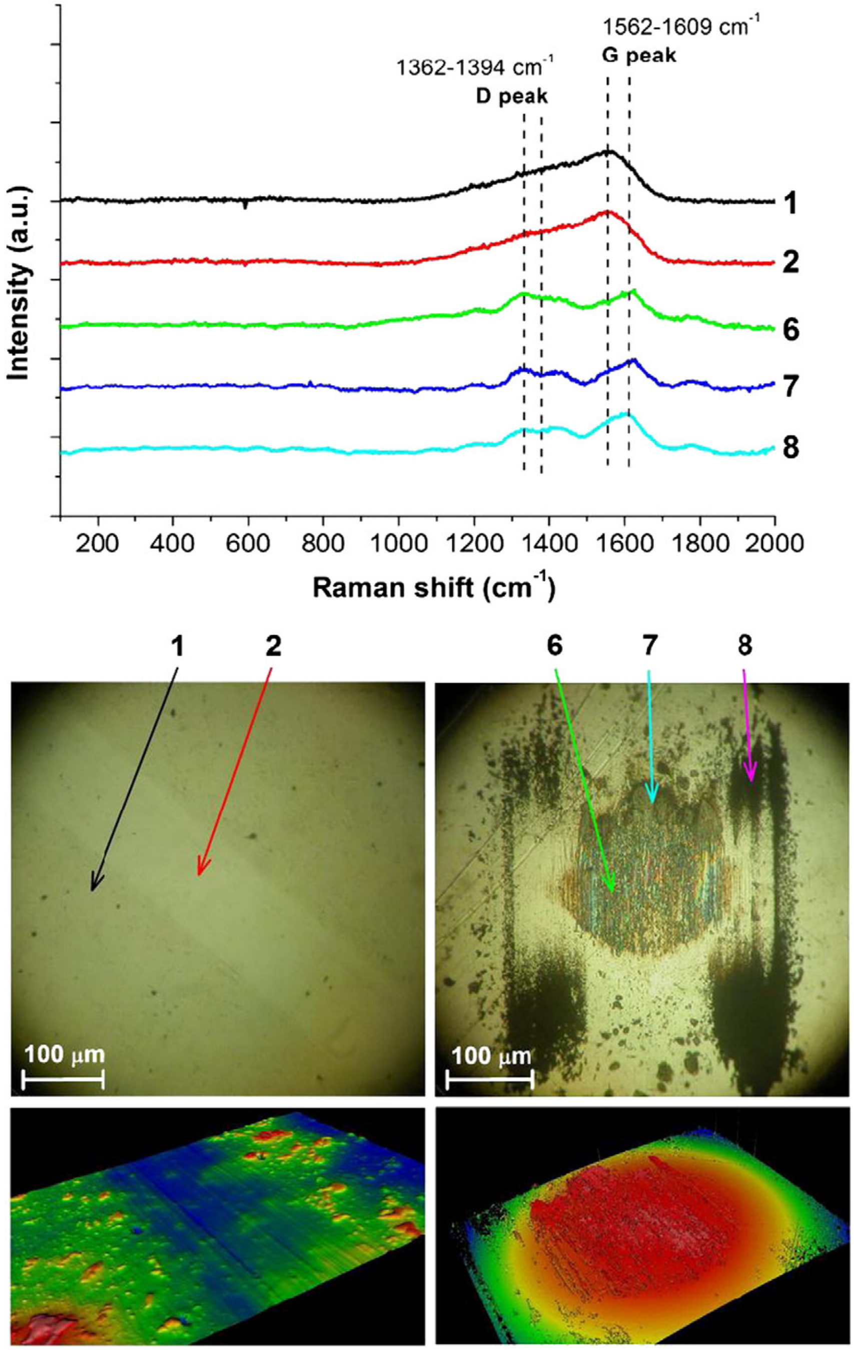

Fig. 13. Raman analysis of the ball wear scar and coating wear track — Zr-DLC-H at 100 °C. The numbers correspond to the scheme shown in Fig. 1.

the formation of low-shear carbonaceous tribolayer. The ability to form low-friction tribolayer depends on the environmental conditions, and proportion of hydrogen in the film [3,8,9,11]. In our case, the effects of hydrogen in the structure in the sliding process could be characterized by three fundamental phenomena - i) higher contact pressure in the steady-state friction regime (due to lower ball wear and narrower wear track), ii) generally lower friction coefficient in the RT ambient environment test and, iii) higher coating sensitivity to the environmental conditions. Hydrogenated DLC coatings are known to exhibit low friction coefficient in vacuum and inert atmospheres due to the formation of low-shear surface tribolayer adhering predominantly onto the counterpart that consequently results in improved coating wear resistance [2,9,11,36,55]. Some authors explained such behaviour by the saturation of the free carbon bonds by hydrogen that predominantly allows formation of weak van der Waals forces between the mating surfaces resulting in low friction [11,48]. The macroscopic effect of this phenomenon could be seen in our results as well, namely in the Zr-DLC-H tests at 100 °C and in the N_2 environment. However, the tribolayer formation in the DLC-H coating test was partially suppressed leading to the increase of friction coefficient and its instability. Deteriorated tribological properties could be an indirect proof of strong bonding established on the surface during sliding [11]. Although there was no significant difference between the Raman spectra of the coatings before and after testing (i.e. no surface graphitization), the presence of iron oxides clearly indicated the detrimental effect on the carbon tribolayer (Fig. 10). It should be also noted that the adhered layer on the leading ball edge contained a mixture of carbon and iron oxides when sliding in humid air, whereas iron oxides were predominantly detected at elevated temperature

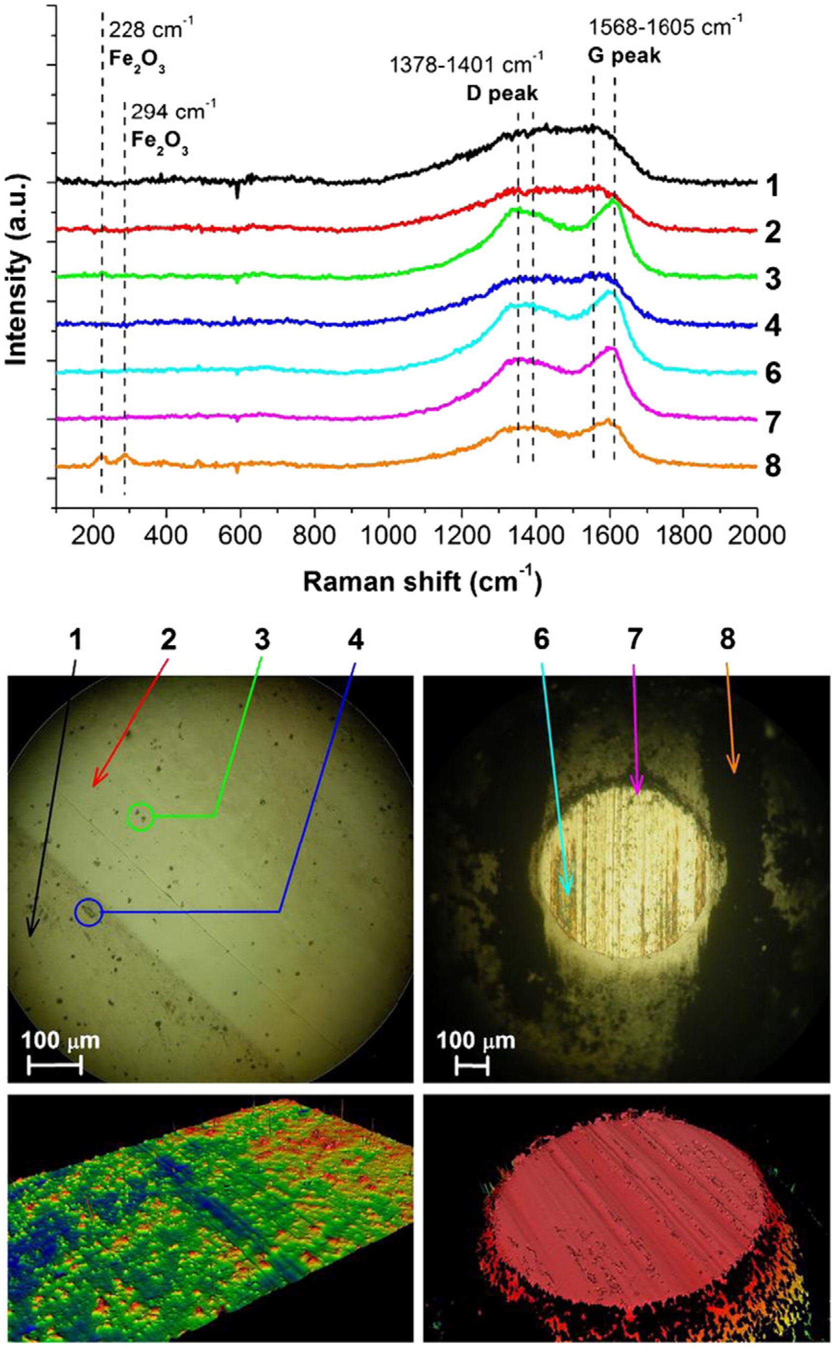

Fig. 14. The Raman analysis of the ball wear scar and coating wear track — Zr-DLC at 100 °C. The numbers correspond to the scheme shown in Fig. 1.

(carbon peaks were very weak). The results of as-deposited surface wettability corroborate the afore-mentioned discussion: the higher the contact angle, the lower the surface chemical activity. Rabinowicz [56] noted that the wear of the surface was directly proportional to surface energy. Moreover, lower surface energy is related to smaller debris formation and thus higher wear, since agglomerated and compacted wear debris acts as a protective layer for both surfaces in the contact [57].

Typically, the non-hydrogenated DLC films exhibit an opposite trend compared to hydrogenated films showing higher friction in inert gases and high temperature [1,3,8,11,15,17]. In our study, the non-hydrogenated coatings reached almost the same mean friction coefficient in N_2 as well as in ambient environment. However, the effect of elevated temperature (suppression of moisture and acceleration of ball oxidation) results in a sharp increase in the friction coefficient (Fig. 5), which is at least partially the result of higher coating surface reactivity and, thus, higher tendency to form contaminant compounds [2,3,9,11].

Zr as doping element was chosen due to its corrosion properties and high chemical stability compared with many other metallic dopants [37,38,43,48]. Alloying the DLC and DLC-H coatings with such element did not significantly change their mechanical properties; nevertheless, the surface energy showed notably lower surface energy for Zr-doped coatings (see Table 1). This is in full agreement with several works dealing with heavy metallic dopants alloying the DLC published in recent years [2,50]. The Raman spectroscopy of our Zr-doped coatings proved growing D peak intensity associated with down-ward G peak shift. Both phenomena are closely connected with carbon structure disorder, which is a typical effect of metallic dopants introduced into DLC [14,29,48]. The tribology of these structures showed significantly shortened running-in phase and stable steady-state friction evolution at RT. However, the non-hydrogenated Zr-DLC coating sliding at 100 °C showed similar features to that of pure DLC coating. We observed a production of enormous amount of the wear debris, a stable carbonaceous tribolayer did not form and severe adhesive wear occurred (note the limited adhered material at the leading edge of the ball wear scar in Fig. 14). Such behaviour indicates the main result of our observations — the protective role of the tribolayer. Basically, we can conclude that the main role of surface third-body tribolayer is the coating surface protection resulting in lower wear and, in most cases, lower friction as well. Moreover, formation of thick and stable tribolayer suppressed the oxidation of the ball surface, which was observed when tribolayer was not well developed. Quick formation of the tribolayer leads to shorter running-in phase and elimination of friction fluctuations. This effect was evident mainly in the case of the Zr-DLC-H coating. The surface low-shear tribolayer was well developed at 100 °C (Fig. 13). The excellent tribological properties achieved by this coating at elevated temperature, as well as in the N_2 environment can be attributed to its low-shear protective tribolayer formation ability that effectively suppresses coating/counterpart oxidation. This result was supported by surface wettability measurements showing the as-deposited coating surface chemical activity. Lower number of active surface bonds should be expected for Zr-DLC-H coating that implicates decreased adherence of contaminants and other products of the tribological process [2,11,58].

Finally, the intermittent tribo-tests at RT shed the light on the running-in process of Zr-DLC(-H) coatings. Initial sliding process is characterized by three interconnected phases: i) initial ball and coating wear leading to surface adaptation and effective contact pressure reduction, ii) production of surface oxides (in case of the non-hydrogenated coatings), and iii) production of carbonaceous surface layer and debris. Our results suggest that the structural changes of the ball-adhered tribolayer closely follow the evolution of friction coefficient, whereas actual wear is more related to the contact pressure. The formation of the carbonaceous layer could effectively act as a protection from surface oxidation at RT decreasing both the friction and the wear.

5. Conclusions

In this study, Zr-DLC(-H) coatings and pure DLC(-H) films were produced by magnetron sputtering and studied in relation to their tribological behaviour in three different environmental conditions: RT, 100 °C and N_2. Doping with Zr was found to be insignificant from the film's mechanical properties point of view. The main results can be divided into three basic aspects:

1. Tribological properties of the coatings are mostly influenced by the formation and composition of tribolayer and the evolution of contact pressure. Although both these properties are related, the analysis of the running-in phase indicated that the friction evolution could be related to tribolayer formation, whereas the wear rate corresponds to actual contact pressure. Our results clearly showed that the most promising tribological behaviour at all tested conditions was achieved for the Zr-DLC-H coating. The other coating structures demonstrated higher sensitivity to the tribological test environment, thus, the applicability of these coatings is limited.
2. Production of dense and homogeneous low-shear carbonaceous tribolayer is the key factor to achieve low friction and avoid counterpart oxidation. The composition and structure of such layer are significantly affected by as-deposited coating properties and friction test conditions.
3. Doping of DLC(-H) coating with Zr led to lowered surface energy together with increased ability to form a stable tribolayer on the ball surface. Consequently, the friction coefficient of Zr containing DLC-H was lower in all tested conditions. The steady state friction process was reached very quickly and the formation of tribolayer was notably accelerated. Consequently, counterpart surface oxidation and production of iron oxide debris particles were limited.

Acknowledgement

This research was sponsored by the Czech Science Foundation (grants Nr. 108/10/P446 and Nr. P108/10/1782) and by FEDER funds through the programme COMPETE – Programa Operacional Factores de Competitividade – and by national funds through FCT – Fundação para a Ciência e a Tecnologia –, under the project PEst-C/EME/UI0285/2011 and SFRH/BD/75071/2010.

References

[1] A. Cavaleiro, J. Th, M. De Hosson, Nanostructured Coatings, Springer Publishing, New York, 2006, ISBN 978-0387-25642-9.
[2] J. Robertson, Mater. Sci. Eng. R 37 (2002) 129–281.
[3] H. Ronkainen, S. Varjus, J. Koskinen, K. Holmberg, Wear 249 (2001) 260–266.
[4] K. Bewilogua, C.V. Cooper, C. Specht, J. Schröder, R. Wittorf, M. Grischke, Surf. Coat. Technol. 127 (2000) 224–232.
[5] K.K. Mistry, A. Morina, A. Neville, Wear 271 (2011) 1739–1744.
[6] B. Kržan, F. Novotny-Farkas, J. Vižintin, Tribol. Int. 42 (2009) 229–235.
[7] D.R. Tallant, J.E. Parmeter, M.P. Siegal, R.L. Simpson, Diam. Relat. Mater. 4 (1995) 191–199.
[8] Y. Liu, A. Erdemir, E.I. Meletis, Surf. Coat. Technol. 94–95 (1997) 463–468.
[9] J. Andersson, R.A. Erck, A. Erdemir, Wear 254 (2003) 1070–1075.
[10] M. Kalin, J. Vižintin, Thin Solid Films 515 (2006) 2734–2747.
[11] A. Erdemir, Surf. Coat. Technol. 146–147 (2001) 292–297.
[12] G.J. van der Kolk, in: C. Donnet, A. Erdemir (Eds.), Tribology of Diamond-like Carbon Films, Springer Publishing, New York, 2008, pp. 484–493.
[13] A. Erdemir, C. Bindal, G.R. Fenske, C. Zuiker, P. Wilbur, Surf. Coat. Technol. 86–87 (1996) 692–697.
[14] T.W. Scharf, I.L. Singer, Tribol. Trans. 45 (2002) 363–371.
[15] H. Ronkainen, J. Koskinen, J. Likonen, S. Varjus, J. Vihersalo, Diam. Relat. Mater. 3 (1994) 1329–1336.
[16] Y.X. Leng, J.Y. Chen, P. Yang, H. Sun, G.J. Wan, N. Huang, Surf. Coat. Technol. 173 (2003) 67–73.
[17] E. Konca, Y.-T. Cheng, A.M. Weiner, J.M. Dasch, A.T. Alpas, Surf. Coat. Technol. 200 (2006) 3996–4005.
[18] I.L. Singer, S.D. Dvorak, K.J. Wahl, T.W. Scharf, J. Vac. Sci. Technol. A 21 (2003) S232–S240.
[19] K. Miyoshi, R.L.C. Wu, A. Garscadden, Surf. Coat. Technol. 54–55 (1992) 428–434.
[20] T.W. Scharf, I.L. Singer, Tribol. Lett. 14 (2003) 3–8.
[21] A. Erdemir, C. Donnet, in: B. Bhushan (Ed.), Modern Tribology Handbook, Materials, Coatings and Industrial Applications, vol. 2, CRC Press, Boca Raton, 2001.
[22] A. Erdemir, C. Donnet, in: G.W. Stachowiak (Ed.), Wear — Materials, Mechanisms and Practice, Wiley, London, 2005.
[23] A.A. Voevodin, M.A. Capano, S.J.P. Laube, M.S. Donley, J.S. Zabinski, Thin Solid Films 298 (1997) 107–115.
[24] W. Dai, P. Ke, M.-W. Moon, K.-R. Lee, A. Wang, Thin Solid Films 520 (2012) 6057–6063.
[25] J. Patscheider, T. Zehnder, M. Diserens, Surf. Coat. Technol. 146–147 (2001) 201–208.
[26] T. Polcar, T. Vitu, L. Cvrcek, R. Novak, J. Vyskocil, A. Cavaleiro, Solid State Sci. 11 (2009) 1757–1761.
[27] T. Vitu, T. Polcar, L. Cvrcek, R. Novak, J. Macak, J. Vyskocil, A. Cavaleiro, Surf. Coat. Technol. 202 (2008) 5790–5793.
[28] L. Joska, J. Fojt, O. Mestek, L. Cvrcek, V. Brezina, Surf. Coat. Technol. 206 (2012) 4899–4906.
[29] C.W.M. e Silva, J.R.T. Branco, A. Cavaleiro, Solid State Sci. 11 (2009) 1778–1782.
[30] D. Hofmann, S. Kunkel, K. Bewilogua, R. Wittorf, Surf. Coat. Technol. 215 (2013) 357–363.
[31] M. Ikeyama, S. Nakao, Y. Miyagawa, S. Miyagawa, Surf. Coat. Technol. 191 (1) (2005) 38–42.
[32] J.R. Gomes, S.S. Camargo Jr., R.A. Simão, J.M. Carrapichano, C.A. Achete, R.F. Silva, Vacuum 81 (11–12) (2007) 1448–1452.
[33] V. Buršíková, V. Navrátil, L. Zajíčková, J. Janča, Mater. Sci. Eng. A 324 (1–2) (2002) 251–254.
[34] B. Vengudusamy, J.H. Green, G.D. Lamb, H.A. Spikes, Tribol. Int. 44 (2011) 165–174.
[35] T. Ohana, T. Nakamura, M. Suzuki, A. Tanaka, Y. Koga, Diam. Relat. Mater. 13 (2004) 1500–1504.
[36] R. Gilmore, R. Hauert, Surf. Coat. Technol. 133–134 (2000) 437–442.
[37] W.H. Kao, Thin Solid Films 529 (2013) 296–300.
[38] W.H. Kao, Diam. Relat. Mater. 16 (2007) 1896–1904.
[39] D. Nilsson, F. Svahn, U. Wiklund, S. Hogmark, Wear 254 (2003) 1084–1091.
[40] A. Escudeiro, T. Polcar, A. Cavaleiro, Thin Solid Films 538 (2013) 89–96.
[41] A. Ramalho, Wear 269 (2010) 213–223.
[42] K. Holmberg, A. Mathews, Coatings Tribology: Properties, Mechanisms, Techniques and Applications in Surface Engineering, 2nd edition Elsevier Science, 2009, ISBN 9780444527509.

[43] C. Adelhelm, M. Balden, M. Rasinski, M. Linding, T. Plocinski, E. Welter, M. Sikora, Surf. Coat. Technol. 205 (2011) 4335–4342.
[44] F. Rabbani, Surf. Coat. Technol. 184 (2004) 194–207.
[45] A.C. Ferrari, Diam. Relat. Mater. 11 (2002) 1053–1061.
[46] N.M.J. Conway, A.C. Ferrari, A.J. Flewitt, J. Robertson, W.I. Milne, A. Tagliaferro, W. Beyer, Diam. Relat. Mater. 9 (2000) 765–770.
[47] C. Casiraghi, F. Piazza, A.C. Ferrari, D. Grambole, J. Robertson, Diam. Relat. Mater. 14 (2005) 1098–1102.
[48] C. Adelhelm, M. Bladen, M. Rinke, M. Stueber, J. Appl. Phys. 105 (2009) 033522.
[49] J.C. Sánchez-López, C. Donnet, J.L. Loubet, M. Belin, A. Grill, V. Patel, C. Jahnes, Diam. Relat. Mater. 10 (2001) 1063–1069.
[50] C. Donnet, Surf. Coat. Technol. 100–101 (1998) 180–186.
[51] R.M. Cornell, U. Schwertmann, The Iron Oxides: Structure, Properties, Reactions, Occurrences and Uses, Wiley-VCH Verlag GmbH, 2003, ISBN 3-527-30274-3.
[52] J.K. Saha, Corrosion of Constructional Steels in Marine and Industrial Environment: Frontier Work in Atmospheric Corrosion, Springer, 2013, ISBN 978-81-322-0720-7.
[53] S.-H. Shim, T.S. Duffy, Am. Mineral. 87 (2001) 318–326.
[54] J. Fontaine, C. Donnet, A. Erdemir, in: C. Donnet, A. Erdemir (Eds.), Tribology of Diamond-like Carbon Films: Fundamentals and Applications, Springer, New York, ISBN: 978-0-387-30264-5, 2008.
[55] F. Gao, A. Erdemir, W.T. Tysoe, Tribol. Lett. 20 (3–4) (2005) 221–227.
[56] E. Rabinowicz, Wear 7 (1) (1964) 9–22.
[57] J. Jiang, S. Zhang, R.D. Arnell, Surf. Coat. Technol. 167 (2–3) (2003) 221–225.
[58] H. Ronkainen, K. Holmberg, in: C. Donnet, A. Erdemir (Eds.), Tribology of Diamond-like Carbon Films: Fundamentals and Applications, Springer, New York, ISBN: 978-0-387-30264-5, 2008.

PAPER VI

Tribological behavior of uncoated and DLC-coated CoCr and Ti-alloy in contact with UHMWPE and PEEK counterbodies

A. Escudeiro, M.A. Wimmer, T. Polcar and A. Cavaleiro

Tribology International, under review

Elsevier Editorial System(tm) for Tribology International
Manuscript Draft

Manuscript Number:

Title: Tribological behavior of uncoated and DLC-coated CoCr and Ti-alloys in contact with UHMWPE and PEEK counterbodies

Article Type: SI: ICOBT2

Keywords: Coating; Slidding; Polymer; Failure physics

Corresponding Author: Ms. Ana Escudeiro,

Corresponding Author's Institution: University of Coimbra

First Author: Ana Escudeiro

Order of Authors: Ana Escudeiro; Markus A. Wimmer; Tomas Polcar; Albano Cavaleiro

Abstract: In this study, DLC and Zr-DLC coatings were deposited by magnetron sputtering onto Ti alloy substrates. Coated and un-coated Ti alloy samples were tribologically tested in multidirectional pin-on-disk equipment. CoCr alloy was also tested as control. Each of the materials was tested against UHMWPE and PEEK for 2 million cycles (Mc) in bovine serum lubricant (37°C). Gravimetrical weight loss and changes in surface profile were similar when tested against UHMWPE. However, Zr-DLC samples delaminated after 1.2 Mc. When tested against PEEK, both coated samples failed, despite that the coatings maintained their integrity. The synergetic effect of stress-induced corrosion through biological fluid and high cyclic shear stress may have caused interface fatigue and subsequent delamination of both coatings.

***Cover Letter**

Ana Escudeiro
SEG-CEMUC - Department of Mechanical Engineering
Rua Luis Reis Santos, 3030-788 Coimbra
Portugal
Telef. 351 239 790745 / 00
FAX 351 239 790701
e-mail -ana.escudeiro@dem.uc.pt

Dear Philippa Cann,

Tribology International, Editor-in-chief

Coimbra, June 28th 2014

The authors would like to state that the paper submitted with the title:

Adsorption of bovine serum albumin on Zr co-sputtered a-C(:H) films: implication on wear Tribological behavior of uncoated and DLC-coated CoCr and Ti-alloys in contact with UHMWPE and PEEK counterbodies

A. Escudeiro, M.A. Wimmer, T. Polcar, A. Cavaleiro

The authors declare that the work submitted has not been published previously, and it is not under consideration for publication elsewhere. Its publication is approved by all authors and, if accepted, it will not be published elsewhere in the same form, in English or in any other language, without the written consent of the Publisher.

Yours sincerely,

Ana Escudeiro

Markus Wimmer

Tomas Polcar

Albano Cavaleiro

***Statement of Originality**

Ana Escudeiro
SEG-CEMUC - Department of Mechanical Engineering
Rua Luis Reis Santos, 3030-788 Coimbra
Portugal
Telef. 351 239 790745 / 00
FAX 351 239 790701
e-mail -ana.escudeiro@dem.uc.pt

Dear Philippa Cann,

Tribology International, Editor-in-chief

Coimbra, June 28th 2014

The authors declare that the work submitted has not been published previously, and it is not under consideration for publication elsewhere. Its publication is approved by all authors and, if accepted, it will not be published elsewhere in the same form, in English or in any other language, without the written consent of the Publisher.

Yours sincerely,

Ana Escudeiro

Markus Wimmer

Tomas Polcar

Albano Cavaleiro

Highlights

- Zr-DLC presented better adhesion and low residual stress compared to DLC coatings.
- No significant differences were found in the wear of UHMWPE for all material combinations
- Zr-DLC and DLC coatings delaminated when tested against PEEK counterbodies
- The presence of biological fluids together with high cyclic shear stress caused interface fatigue

Tribological behavior of uncoated and DLC-coated CoCr and Ti-alloys in contact with UHMWPE and PEEK counterbodies

A. Escudeiro[1], M.A. Wimmer[2], T. Polcar[3], A. Cavaleiro[1]

[1] SEG- CEMUC Department of Mechanical Engineering, University of Coimbra, Portugal

[2] Section of Tribology, Department of Orthopaedic Surgery, Rush University Medical Center, Chicago IL, USA

[3] National Centre for Advanced Tribology, Southampton (nCATS), School of Engineering Sciences, University of Southampton, UK

Abstract

In this study, DLC and Zr-DLC coatings were deposited by magnetron sputtering onto Ti alloy substrates. Coated and un-coated Ti alloy samples were tribologically tested in multidirectional pin-on-disk equipment. CoCr alloy was also tested as control. Each of the materials was tested against UHMWPE and PEEK for 2 million cycles (Mc) in bovine serum lubricant (37°C). Gravimetrical weight loss and changes in surface profile were similar when tested against UHMWPE. However, Zr-DLC samples delaminated after 1.2 Mc. When tested against PEEK, both coated samples failed, despite that the coatings maintained their integrity. The synergetic effect of stress-induced corrosion through biological fluid and high cyclic shear stress may have caused interface fatigue and subsequent delamination of both coatings.

Introduction

The generation of wear particles from metal-on-metal (MoM) and metal-on-polymer (MoP) total joint replacements (TJRs) and related adverse local tissue effects have been an ongoing problem since TJRs were first implanted. In fact, in the case of MoP, 10% of the knee implant failure was directly related to UHMWPE wear [1]. Phagocytosis of wear debris by macrophages induces an inflammatory reaction associated with the release of cytokines and other inflammatory mediators. Once osteolysis has occurred, it tends to progress and may ultimately lead to failure of the implant. On the other hand, despite an overall reduced wear rate, MoM bearings are known to elicit an immune response involving lymphocytes in addition to a macrophage-mediated inflammatory reaction. Nevertheless, the biological effects of metal (nano)particles and ion release is still under investigation and of great clinical concern. Thus, advancements are still desired to improve reliability and long-term implant performance. Among available polymers for *in vivo* application, PEEK and its composites have been used as an alternative bearing surface for UHMWPE due to its biocompatibility, high strength, stiffness, fatigue and wear resistance [2, 3]. Moreover, PEEK particles were found to be less cytotoxic *in vitro* than UHMWPE [4]. However, a recent *in vivo* study found increased cytokine expressions for carbon-fiber reinforced PEEK compared to UHMWPE [5]. PEEK increases the wear of the metallic component (SS 316, Ti6Al4V and CoCr) compared to UHMWPE couples [6-8]. Particularly Ti6Al4V may suffer due to its poor tribological properties which are attributed to the low resistance of the oxide layer to plastic shearing [9-11]. On the other hand, titanium and its alloys are interesting candidate metals for biomedical applications because of the known milder tissue reactions of their degradation products compared with CoCr-alloy or Ni-containing steels [12, 13]. Therefore, surface engineering of titanium bearing surfaces and/or the adoption of new coupling materials could be a promising approach to reduce both metal and polymer wear debris.

Diamond-like carbon (DLC) coatings have been widely studied as a possible solution for implant wear due to their excellent tribological properties and performance in a wide range of industrial applications (e.g. car engines, hard disks, etc.) [14]. DLC is biocompatible [15] and presents low friction and extremely low wear rates [14, 16]. In fact, Hauert [17] tested DLC coatings in an intervertebral spinal disk simulator for 101 million cycles with extremely low material loss being reported. However, contradictory results have been found in literature when testing DLC against UHMWPE, ranging from strong improvement to drastically increased wear [18]. There are few studies of DLC against PEEK. Franta [6] reported a significant increase in the life span of implants using such a combination. In general, one of the main issues of DLC coatings have been associated with the adhesion of the coating to the substrate, especially in a corrosive environment such as the human body [17]. High internal compressive stress imposed by the deposition conditions can further reduce the adhesion strength and promote delamination of the coating. Thus, the interposition of a carefully designed layer between substrate and coating avoiding abrupt compositional changes (Me/MeC, Me/MeN or Me/MeN/MeNC, where Me stands for metallic element), and/or alloying the DLC coating with metallic elements can help to prevent such issues.

In this study, DLC and Zr-DLC coatings were deposited using magnetron sputtering and tested against UHMWPE and PEEK. The incorporation of Zr in the amorphous carbon coating should improve the adhesion of the coating [19, 20] which may beneficially impact its tribological performance. In order to assess the potential of such DLC/polymer combinations for the use in orthopedic implants, the wear behavior of the coatings was studied using a multidirectional pin-on-disc apparatus under physiological load and lubricant conditions. For comparison, CoCr alloy and Ti-alloy were also tested against UHMWPE and PEEK.

Materials and Methods

1. Materials and substrates

UHMWPE (GUR 1050) and PEEK (TECAPEEK natural) wear pins were manufactured and provided by Zimmer, Inc. (Warsaw, IN, USA) and Ensinger (Dobřany, Czech Republic), respectively. The cylindrical pins were 0.375 in. (9.5 mm) in diameter and 0.750 in. (19.1 mm) in length. The metallic counterbodies, disks with a diameter of 40 mm, Ti grade 5 (Ti6Al4V) and CoCr (Co30Cr6Mo) alloy, were mechanically polished with SiC paper (500, 600, 800, 1200 grits), and then finished by using diamond suspensions (6, 3 and 1 µm) and a colloidal silica suspension. Table 1 shows the average and quadratic mean roughness, R_a and R_q, for both metallic and polymeric materials measured by scanning white light interferometry.

2. Coating deposition and characterization

The coatings were deposited onto Ti6Al4V disk substrates and Si(111) wafers for tribological testing and for coating characterization, respectively. Prior to deposition, the substrates were cleaned in an ultrasonic bath containing acetone, ethanol and deionized water for 15 min, and then mounted on the rotating sample holder (18 rpm) in the deposition chamber. The coatings were deposited with a DC dual magnetron sputtering machine. A pure graphite target was used for the production of the a-C films in reactive (Ar/CH_4) and non-reactive atmosphere (Ar), in order to produce hydrogenated and non-hydrogenated films, respectively. Zr pellets were added to the erosion zone of the graphite target (relative erosion area, A_{Zr}/A_C, 1%) to produce Zr containing films. All coatings were deposited with a constant applied bias voltage of -50 V and graphite target power density close to 7.5 W/cm^2. Moreover, a pure Ti target was also sputtered for the deposition of a composite gradient interlayer (Ti/TiN/TiCN) to improve the film adhesion to the metallic substrates. For each deposition condition, the deposition time was calculated to obtain films of ~1.4 µm thickness. Further detailed deposition specification can be found elsewhere [19].

The chemical composition was evaluated by electron probe microanalysis (EPMA, CAMECA Camebax SX 50). The structure of the coatings was analyzed by X-ray diffraction (XRD) (Philips, X'Pert diffractometer, Co Kα radiation) whereas X-ray photoelectron spectroscopy (XPS) (ESCAprobe P, Omicron Ltd., Al Kα, binding energy calibrated with Au 4f (84,1eV)) was used to identify chemical bonding. Raman spectroscopy was used to evaluate the C structure. The analyses were performed at Northwestern University, Evanston, USA with an Acton TriVista CRS Confocal Raman System (Princeton Instruments, Trenton NJ, USA), with excitation radiation of an Ar-Kr gas laser (514.5 nm wavelength). Raman spectra were recorded in the range of 1000-1800 cm^{-1} and fitted using Gaussian fitting following a procedure describe elsewhere [21]. The hardness was measured by depth-sensing indentation (Micromaterials Nanotest) using a Berkovich indenter. The normal stylus load was 5 mN (indentation depth approx. 150 nm); 32 independent indentations from two distinct areas on the sample were used to analyze the hardness data. Rockwell-C indentation and scratch test were used to evaluate coating adhesion and cohesion. Additional information can be found in [19, 20]. In order to quantify any superficial defects in the coatings, optical microscopy analysis was performed for DLC coatings on Ti6Al4V. The quantification was performed by determining the area covered and average size by surface defects. For each coating 6 different areas were analyzed, with a magnification of 50X.

3. Wear test

The wear tests were performed on a six- station pin-on-disc apparatus (OrthoPod® AMTI Inc., Boston MA, USA), with each test containing pins of UHMWPE and/or PEEK. Test and control pins where pre-soaked in the same lubricant used for testing in order to account for any lubricant absorption. The saturation curves were monitored and testing began once equilibrium weight was attained. The pins were subject to a 15 mm x 15 mm square motion pattern in order to generate crossing motion trajectories. All wear tests were conducted at a cycle frequency of 1 Hz and with a constant applied load in order to generate a nominal contact pressure of 1.5 MPa. Each articulation was submersed in a solution containing new born calf serum (NBCS Gibco®) and deionized water with sodium-chloride to achieve 30 g/l protein concentration at physiological salt levels. The pH was adjusted to 7.6. In addition, the solution contained 20mM EDTA (to prevent precipitation of calcium phosphate), Tris-hydroxymethylaminomethane (buffer), and 0.3% sodium azide (anti-microbial agent). The temperature of the lubricant was maintained at 37˚C using a recirculating water bath. A total of up to 2 million cycles (Mc) were conducted. Prior to testing and at regular 0.3 Mc intervals during testing, all metal samples (coated and un-coated) and all polymer components were cleaned in ultrasonic bath with, consecutively, distilled water, Terg-A-Zyme® and propanol for 10 min each and dried with a N_2 gas jet. After cleaning, the pins were weighed to obtain a gravimetric measurement. The gravimetric weight loss per pin was determined by taking the average weight loss of six measurements (according to ASTM 2025 and F732). The total weight loss of each polymer pin was corrected by subtracting the weight increase of soak control specimens during the same test interval. Volumetric wear loss was determined by dividing (corrected) weight loss and density of the polymer (UHMWPE: 0.94 g/cm^2; PEEK: 1.35 g/cm^2, data from the manufacturer). The volumetric wear rates were determined using a linear regression. The tests were then continued with completely fresh lubricant.

Surface topography measurements were performed using a Zygo New Vision 6300 (Middlefield CT, USA) optical 3D profilometer. Ten measurements of R_a and R_q were taken of each pin and plate for every material combination prior and after testing. The surfaces were also inspected by scanning electron microscope (SEM, JSM-5600, JOEL Co., Japan).

4. Statistics

Differences in the wear rates between UHMWPE and PEEK articulating against the same material (i.e. Ti6Al4V, CoCr, DLC, Zr-DLC) were statistically evaluated using independent student's t-tests. Comparisons within each polymer group were performed using one-way analysis of variance (ANOVA) followed by Student-Newman-Keuls (SNK) method to determine pairwise differences. Regression analyses were conducted to determine the correlation between friction and gravimetric wear of each material group. The level of significance was set to $p = 0.05$.

Results

1. Characterization of DLC Coatings

Table 2 shows the coating chemical and mechanical properties. In general, the mechanical properties of the a-C films were maintained when small amounts of Zr (4 at.%) were incorporated. As expected, the residual compressive stress decreased leading to a slight improvement of the adhesion of the coating (see Figure 1). The incorporation of small amounts of a transition metal element into the C-matrix is known to create Me-C or Me-C nanocrystalline phase which has a catalysis effect to the C-matrix, i.e., it breaks the continuity of the carbon network, which results in a decrease of the coordination factor of the C-network [24]. In fact, these films were characterized as ZrC nanocrystalls embedded in an amorphous C-matrix by means of X-ray photoelectron spectroscopy and diffraction analysis [19]. The G position and the I_D/I_G ratio (integrated intensity ratio) can give important clues about the structural (dis)order of the coating [21]. The incorporation of Zr led to an increase of I_D/I_G ratio (see Table 2) suggesting higher organization of the C-clusters within the matrix.

2. Tribological Behavior

2.1. Friction and wear

Figure 2 and 3 show the evolution of the friction coefficient (COF) with respect to the number of cycles. The average friction coefficient for all samples against both polymer materials is presented. The friction behavior was strongly dependent on the polymer type. UHMWPE demonstrated approximately 2 times lower and a more stable COF compared to PEEK. Note that every 300,000 cycles the experiment was stopped to carry out gravimetric measurements and then replenished with new lubricant. In general, the CoCr/Polymer combination had the lowest coefficient of friction. When testing UHMWPE against metal (CoCr and Ti6Al4V) the COF tendentiously increased after the running period (300,000 cycles). The inverse trend was observed for coated samples (DLC and Zr - DLC). However, Zr-containing films did not survive more than 1.2 Mc against UHMWPE due to delamination. Statistically ($p < 0.003$), the metal/UHMWPE pairings presented lower COF compared with coated samples.

All experimental surfaces showed a higher COF for PEEK than for UHMWPE ($p < 0.01$) (Figure 2). In general, the COF was much more variable for PEEK, and particularly for CoCr, showing high periodicity with the cleaning cycles. There were no statistical differences ($p > 0.057$) in the friction coefficient between samples when tested against PEEK. Metal/PEEK showed a tendency for increasing tangential force with increasing number of cycles for the both metal surfaces (from ~0.20 to ~0.35), i.e. not reaching the friction "steady state" during the experiment. Specifically, Ti6Al4V was only tested for 300,000 cycles due to severe surface damage that will be discussed later. Also coated samples failed and delaminated against PEEK after 1.2 Mc and 0.9 Mc for DLC and Zr - DLC, respectively. Only CoCr endured a full 2 Mc testing sequence.

Figure 4 shows the volumetric wear loss versus the number of cycles for both UHMWPE and PEEK pins. The wear factor, calculated from linear regression analysis of the average of three measurements, is shown in Figure 4 (see insets). In general, PEEK wore more than UHMWPE ($p < 0.049$). The only exception was found for CoCr, where the difference was not significant ($p > 0.127$). It is worth noting that the wear of the metallic alloys and the coatings could not be measured (samples were too heavy for the microbalance and/or weight losses too small for the standard laboratory balance). However, extensive abrasive wear patterns (scratches and groves) were found on top of Ti6Al4V after sliding against PEEK. For a better understanding of the wear phenomena, pin and disks surfaces were analyzed and results will be shown in the next section.

2.2 Surface analysis

Figure 5 and 6 show optical images of the disk and pin surfaces after testing. As expected, CoCr did not present signs of wear when sliding against either UHMWPE or PEEK (Figure 5a and 6a). On the contrary, Ti6Al4V showed signs of abrasive wear (grooving), particularly when tested against PEEK (Figure 5c and 6c). Ti6Al4V is known to behave worse than CoCr under tribological stress conditions. In fact, Ti6Al4V can lose its passive (oxide) layer due to sliding and the generated oxide particles may act as a third-bodies aggravating abrasive wear. When a coating (DLC and Zr-DLC) was applied, no wear was observed initially, thus successfully protecting the Ti-alloy from wear. However, Zr-DLC delaminated after a few hundred thousand cycles irrespectively of counterbody material. The exposed areas of the Ti6Al4V surface of DLC-coated samples maintained their integrity though (i.e. no signs of abrasive wear in exposed areas - see Figure 5e and g and 6e and g). Both disc surfaces and pins were analyzed by 3D optical interferometry. There were no significant differences before and after testing for the discs, except for Ti6Al4V. Figure 7 shows the roughness values of the pins for all material combinations. The measurements were taken at the center of pin. In general, UHMWPE pins were found to become randomly scratched during testing. When hard DLC coatings were used, the UHMWPE surface became smoother. The same findings held up for PEEK pins. The Ti6Al4V/PEEK couple showed increased abrasive wear due to released oxide debris (Figure 6d).

Discussion

This study investigated DLC and Zr-containing DLC coatings which were deposited on Ti-based substrates. Both showed beneficial coating characteristics obtained through standard laboratory testing and the incorporation of Zr into the amorphous carbon coating further improved adhesion to the substrate. However, the obtained characteristics did not translate into sustainable biotribological performance. In fact, the novel Zr-DLC coating delaminated already after a few hundred thousand cycles against either UHMWPE or PEEK, which would prohibit its use in patients. This unexpected result highlights the importance of a proper testing sequence to evaluate new materials for TJR. In this section we will discuss the obtained results and make an attempt to elucidate the failure mechanism of the DLC coatings.

Pre-clinical friction and wear measurements are important to assess potentially beneficial combinations of materials for use in TJR. Excessive friction can cause loosening of the prosthetic device at the bone-implant interface and consequently instability and pain. Also wear reduces the prosthesis' life span [25, 26]. Phagocytosis of the wear particles due to macrophages can lead to a cascade of inflammatory reactions that causing osteolysis at the prosthetic interface with subsequent loosening and failure [12]. Multidirectional pin-on-disc machines, that provide both reciprocating and rotational motion, represent the simplest and the most widely accepted model for basic biotribological simulation of candidate biomaterials for joint prosthesis [27]. The exact loading and motion patterns are not replicated with such machines though; the multidirectional motion generates "crossing shear" conditions, which are typical for TJR [28, 29]. In fact, the wear factor found for CoCr/UHMWPE ($k = 2.6\pm0.1\text{x}10^{-6}$ mm^3/Nm) is in the range of those reported from clinically retrieved TJR couples ($k \sim 10^{-6}$ mm^3/Nm [30, 31]). Thus, the behavior of new materials combinations can be assessed in a relatively cost effective way. We will now discuss the results attained for coated and un-coated samples against PEEK and UHMWPE.

For all materials, both friction and wear results were strongly dependent on the polymer counterbody. The friction coefficient was found 2 times higher when tested against PEEK. Also the wear was higher for PEEK, although - in general - the wear mechanism was found to be similar for both polymer types showing typical signs of micro-abrasion [3, 32]. In nearly all cases, wear correlated with the friction coefficient, except for CoCr when tested against PEEK. In fact, PEEK is known to present a relatively high friction coefficient of ~0.3 against metals [8, 33].

There were no significant differences between PEEK and UHMWPE when tested against CoCr. In contrast, in the literature, six to eight times higher wear rates of PEEK compared to UHMWPE have been reported [3, 8, 26]. However, the contact pressure applied in the present study was at the low end (~1.5 MPa) compared to other studies. Davim et al. [25] and Laux and Schwartz [34] have reported that PEEK wear is strongly related to contact pressure. In fact, rising the contact pressure from 1.8 to 3.9 MPa led to a three- to six-fold wear increase of PEEK (dependent on supplier and molecular weight) [34]. The effect between contact pressure and wear is opposite for UHMWPE: both Wang et al. [35] for the hip and Galvin et al. [36] for the knee found that an increase in contact pressure will lead to a decrease in wear. Hence, the relatively low pressure in our study may have diminished PEEK wear but increased UHMWPE wear per load increment, thus causing similar wear factors. Ti6Al4V showed poor tribological properties against polymer surfaces in this study (see Figure 5c and 6c). Its poor shear strength led to disruption of the oxide layer, which then acted as abrasive [7, 10, 11, 37]. The effect was even more pronounced against PEEK. The use of protective coatings was meant to protect the Ti-based substrate from abrasive wear. However, except for DLC against UHMWPE, they all failed catastrophically. In other words, coatings failure was linked to the delamination or spallation of the coating in the sliding region (see Figure 5g, 6e and g).

The incorporation of Zr enhanced the adhesion and reduced the residual stress of the coatings compared to DLC coatings (Table 2). Thus, one would think Zr-DLC should behave superiorly compared to DLC. Despite the good mechanical adhesion that was achieved in ambient air, the coatings failed when tested under multi-directional stress in body fluids. Surface layer failure is the biggest concern for the use of coatings in the biomedical field and has been reported by many other authors for both *in vitro* and *in vivo* [18, 38, 39]. The presence of biological species in solution (ions, proteins, etc.) can encourage corrosion of the adhesion-promoting interlayer and consequently lead to delamination of the coating. The most common corrosion mechanism found in coatings when in contact to body fluids are pitting, crevice corrosion (CC) and stress-induced corrosion (SCC) [17]. CC and SCC are related to slow crack advancement or interlayer dissolution resulting in a delayed delamination. On the other hand, since even a perfect coating will always present some surface defects (pinholes, scratch and/or loose grain that can traverse their entire thickness down to the substrate) pitting may occur. The body fluids can then penetrate through the film and act as a corrosive electrolyte forming coating blisters. If the blister exceeds a certain dimension local delamination can occur [40]. *In vivo*, the average delamination speed lies at 145 µm/year [41]. This process appears too slow to be solely responsible for the observed delamination failure of this study. Also, the incorporation of Zr led to a decrease of surface defect density, with a defect size slightly higher than that of pure carbon films (see Table 3). It might be possible though that these defects promote SCC cracks, which then grow underneath the coating due to the high induced shear stresses at the contact. Figure 8 shows SEM micrograph of Zr-DLC wear track after testing against UHMWPE. The presence of pinholes on the wear track may promote stress-induced corrosion and initiate delamination.

In order to evaluate the effect of body fluids on the adhesion strength of the coatings after testing, Rockwell indentations were performed on the wear track and, when existing, near to the delamination zones. Figure 9 demonstrates that the film adhesion was maintained after testing. Moreover, Raman spectra of the wear track (data not shown) did not reveal any significant changes between pre- and post-testing suggesting that the structural integrity of the coatings was maintained. In order to investigate the possibility of SCC further, we followed a complementary method proposed by Hauert and co-workers [42, 43]: by inducing substrate deformation with Rockwell indentation and simultaneous immersion of the sample in a protein-containing solution, SCC should be promoted at the mechanically loaded interface. However, even after 3 days (the equivalent of approximately 300,000 testing cycles) the coatings did not reveal any differences on the indentation profile, suggesting a more complex failure mechanism than SCC alone.

In summary, the body fluids' corrosive effect cannot be solely responsible but a combination of factors, including cyclic fatigue, boosted by the presence of huge shear stresses, may have caused failure of the coating.

Conclusions

In this study, DLC and Zr-DLC coatings were deposited on Ti-alloy substrates in order to study their tribological behavior against UHMWPE and PEEK for potential *in vivo* applications. Using a multi-directional pin-on-disk wear testing device and a lubricant mimicking body fluids, coated and un-coated samples were tested against the polymers and compared to CoCr-alloy which served as reference. No significant differences were found in the wear of UHMWPE for all material combinations; however, Zr-containing DLC failed early in the test. Although the incorporation of Zr in the C-matrix increased the adhesion strength and reduced the residual stress of the coating, delamination was observed after a few hundred thousand cycles of testing. This study suggests that the presence of surface defects in the presence of body fluids and high shear stress can boost the interface failure and consequently lead to delamination of the coating. Surprisingly the coating integrity was maintained after delamination. In the future, it will be important to understand the synergetic effect between stress-induced corrosion and cyclic fatigue on the interpositional layer and/or substrate in order to eliminate such problems.

Acknowledgment

This research was sponsored by FEDER funds through the program COMPETE – Programa Operacional Factores de Competitividade – and by national funds through FCT – Fundação para a Ciência e a Tecnologia –, under the project PEst-C/EME/UI0285/2011 and QREN-POPH for funding support under the grant

SFRH/BD/75071/2010 which was co-funded by FSE and MSTES. Additional funding was obtained through the Rush Arthritis and Orthopedics Institute. The authors would like to thank Dr. Robin Pourzal Rush University, Chicago for technical assistance with wear testing and imaging, Dr. Yifeng Liao from Northwestern University, Evanston for the Raman spectra acquisitions, and Noora Manninen from University of Coimbra for EPMA analysis.

References

[1] Schroer WC, Berend KR, Lombardi AV, Barnes CL, Bolognesi MP, Berend ME, et al. Why Are Total Knees Failing Today? Etiology of Total Knee Revision in 2010 and 2011. J Arthroplasty. 2013;28:116-9.

[2] Kurtz SM, Devine JN. PEEK biomaterials in trauma, orthopedic, and spinal implants. Biomaterials. 2007;28:4845-69.

[3] Wang A, Lin R, Stark C, Dumbleton JH. Suitability and limitations of carbon fiber reinforced PEEK composites as bearing surfaces for total joint replacements. Wear. 1999;225–229, Part 2:724-7.

[4] Hallab NJ, McAllister K, Brady M, Jarman-Smith M. Macrophage reactivity to different polymers demonstrates particle size- and material-specific reactivity: PEEK-OPTIMA® particles versus UHMWPE particles in the submicron, micron, and 10 micron size ranges. J Biomed Mater Res-B. 2012;100B:480-92.

[5] Lorber V, Paulus AC, Buschmann A, Schmitt B, Grupp TM, Jansson V, et al. Elevated cytokine expression of different PEEK wear particles compared to UHMWPE in vivo. J Mater Sci: Mater Med. 2014;25:141-9.

[6] Franta L, Fojt J, Joska L, Kronek J, Cvrcek L, Vyskocil J, et al. Hinge-type knee prosthesis wear tests with a mechanical load and corrosion properties monitoring. Tribol Int. 2013;63:61-5.

[7] Joyce TJ. Examination of failed ex vivo metal-on-metal metatarsophalangeal prosthesis and comparison with theoretically determined lubrication regimes. Wear. 2007;263:1050-4.

[8] Geringer J, Tatkiewicz W, Rouchouse G. Wear behavior of PAEK, poly(aryl-ether-ketone), under physiological conditions, outlooks for performing these materials in the field of hip prosthesis. Wear. 2011;271:2793-803.

[9] Rack HJ, Qazi JI. Titanium alloys for biomedical applications. Mat Sci Eng C. 2006;26:1269-77.

[10] Fitzgerald RH KH, Malkani AL. Orthopaedics. Philadelphia: Mosby; 2002.

[11] Zaitsev AL. Mechanisms of hard alloy wear in frictional processes with polymers and composite materials. Wear. 1993;162-164:40-6.

[12] Catelas I, Wimmer M, Utzschneider S. Polyethylene and metal wear particles: characteristics and biological effects. Semin Immunopathol. 2011;33:257-71.

[13] Kraft CN, Diedrich O, Burian B, Schmitt O, Wimmer MA. Microvascular response of striated muscle to metal debris: A COMPARATIVE IN VIVO STUDY WITH

TITANIUM AND STAINLESS STEEL. Journal of Bone & Joint Surgery, British Volume. 2003;85-B:133-41.

[14] Robertson J. Classification of Diamond-like Carbons. In: Donnet C, Erdemir A, editors. Tribology of Diamond-Like Carbon Films: Springer US; 2008. p. 13-24.

[15] Anne Thomson L, Law FC, Rushton N, Franks J. Biocompatibility of diamond-like carbon coating. Biomaterials. 1991;12:37-40.

[16] Robertson J. Diamond-like amorphous carbon. Mat Sci Eng R. 2002;37:129-281.

[17] Hauert R, Thorwarth K, Thorwarth G. An overview on diamond-like carbon coatings in medical applications. Surf Coat Tech. 2013;233:119-30.

[18] Love CA, Cook RB, Harvey TJ, Dearnley PA, Wood RJK. Diamond like carbon coatings for potential application in biological implants—a review. Tribol Int. 2013;63:141-50.

[19] Escudeiro A, Polcar T, Cavaleiro A. a-C(:H) and a-C(:H)_Zr coatings deposited on biomedical Ti-based substrates: Tribological properties. Thin Solid Films. 2013;538:89-96.

[20] Escudeiro A, Polcar T, Cavaleiro A. DLC(H) doped with Zr coatings for orthopaedics applications: adhesion properities. 55th Annual Technical Conference Proceedings: Society of Vacuum Coaters; 2012.

[21] Ferrari A, Robertson J. Interpretation of Raman spectra of disordered and amorphous carbon. Phys Rev B. 2000;61:14095-107.

[22] European Committee for standardization, European Stardard DIN ENV 1071-3 (1994), draft European Standard prEN 1071-3 (2002)

[23] Vidakis N, Antoniadis A, Bilalis N. The VDI 3198 indentation test evaluation of a reliable qualitative control for layered compounds. J Mater Process Tech. 2003;143–144:481-5.

[24] Corbella C, Oncins G, Gómez MA, Polo MC, Pascual E, García-Céspedes J, et al. Structure of diamond-like carbon films containing transition metals deposited by reactive magnetron sputtering. Diam Relat Mater. 2005;14:1103-7.

[25] Davim JP, Marques N, Baptista AM. Effect of carbon fibre reinforcement in the frictional behaviour of Peek in a water lubricated environment. Wear. 2001;251:1100-4.

[26] Davim JP, Marques N. Evaluation of Tribological Behaviour of Polymeric Materials for Hip Prostheses Application. Tribol Lett. 2001;11:91-4.

[27] F732-00 AS. Standard test method for wear testing of polymeric materials used in total joint protheses. ASTM International2006.

[28] Ge S, Wang S, Gitis N, Vinogradov M, Xiao J. Wear behavior and wear debris distribution of UHMWPE against Si3N4 ball in bi-directional sliding. Wear. 2008;264:571-8.

[29] Turell ME, Friedlaender GE, Wang A, Thornhill TS, Bellare A. The effect of counterface roughness on the wear of UHMWPE for rectangular wear paths. Wear. 2005;259:984-91.

[30] Atkinson JR, Dowson D, Isaac JH, Wroblewski BM. Laboratory wear tests and clinical observations of the penetration of femoral heads into acetabular cups in total replacement hip joints: III: The measurement of internal volume changes in explanted Charnley sockets after 2–16 years in vivo and the determination of wear factors. Wear. 1985;104:225-44.

[31] Saikko V. A multidirectional motion pin-on-disk wear test method for prosthetic joint materials. J Biomed Mater Res. 1998;41:58-64.

[32] Shi W, Dong H, Bell T. Tribological behaviour and microscopic wear mechanisms of UHMWPE sliding against thermal oxidation-treated Ti6Al4V. Mater Sci Eng A-Struct. 2000;291:27-36.

[33] Laux KA, Schwartz CJ. Influence of linear reciprocating and multi-directional sliding on PEEK wear performance and transfer film formation. Wear. 2013;301:727-34.

[34] Laux KA, Schwartz CJ. Effects of contact pressure, molecular weight, and supplier on the wear behavior and transfer film of polyetheretherketone (PEEK). Wear. 2013;297:919-25.

[35] Wang A, Essner A, Klein R. Effect of contact stress on friction and wear of ultra-high molecular weight polyethylene in total hip replacement. P I Mech Eng H. 2001;215:133-9.

[36] Galvin AL, Kang L, Udofia I, Jennings LM, McEwen HMJ, Jin Z, et al. Effect of conformity and contact stress on wear in fixed-bearing total knee prostheses. J Biomech. 2009;42:1898-902.

[37] Li WY, Dong H, Shi W. New insights into wear of Ti6Al4V by ultra-high molecular weight polyethylene under water lubricated conditions. Wear. 2001;250:553-60.

[38] Xu T, Pruitt L. Diamond-like carbon coatings for orthopaedic applications: an evaluation of tribological performance. J Mater Sci: Mater Med. 1999;10:83-90.

[39] Taeger G, Podleska LE, Schmidt B, Ziegler M, Nast-Kolb D. Comparison of Diamond-Like-Carbon and Alumina-Oxide articulating with Polyethylene in Total Hip Arthroplasty. Materialwissenschaft und Werkstofftechnik. 2003;34:1094-100.

[40] Chandra L, Allen M, Butter R, Rushton N, Lettington AH, Clyne TW. The effect of exposure to biological fluids on the spallation resistance of diamond-like carbon coatings on metallic substrates. J Mater Sci: Mater Med. 1995;6:581-9.

[41] Hauert R, Falub CV, Thorwarth G, Thorwarth K, Affolter C, Stiefel M, et al. Retrospective lifetime estimation of failed and explanted diamond-like carbon coated hip joint balls. Acta Biomater. 2012;8:3170-6.

[42] Falub CV, Thorwarth G, Affolter C, Müller U, Voisard C, Hauert R. A quantitative in vitro method to predict the adhesion lifetime of diamond-like carbon thin films on biomedical implants. Acta Biomater. 2009;5:3086-97.

[43] Falub CV, Müller U, Thorwarth G, Parlinska-Wojtan M, Voisard C, Hauert R. In vitro studies of the adhesion of diamond-like carbon thin films on CoCrMo biomedical implant alloy. Acta Mater. 2011;59:4678-89.

List of Figures

Figure 1 Scratch test with increasing load on a) DLC and b) Zr - DLC coated Ti grade 5. The inset indicates critical coating adhesion loads as described in Table 2.

Figure 2 Friction coefficient vs number of cycles for all experimental surfaces against UHMWPE and PEEK.

Figure 3 Average coefficient of friction (COF) for all surfaces against UHMWPE and PEEK. (*) represents statistically significant differences between samples in the same group ($p < 0.05$ ANOVA test).

Figure 4 (a) UHMWPE and (b) PEEK volumetric wear loss and wear rate (in the inserts) against the different surfaces.

Figure 5 Images from the wear track on the disc and corresponding UHMWPE pin surface after testing: (a,b) CoCr, (c,d) Ti6Al4V, (e,f) DLC and (g,h) Zr-DLC.

Figure 6 Images from the wear track of the disc after testing against PEEK: (a,b) CoCr, (c,d) Ti6Al4V, (e,f) DLC and (g,h) Zr-DLC.

Figure 7 Average roughness measured at the centre of each polymer pin after sliding.

Figure 8 (a) DLC and (b) Zr-DLC SEM image of the wear track after testing against UHMWPE.

Figure 9 Rockwell-C indentation test of the coated films before and after testing against UHMWPE and PEEK.

List of Tables

Table 1 Roughness values [µm] for uncoated discs and polymeric pins.

Table 2 Summary of DLC coating properties: Zr/C ratio, I_D/I_G ratio, G peak position, hardness (H), Young modulus (E), Residual Stress (σ), adhesion critical loads ($Lc_x{}^a$) and Rockwell-C^b adhesion test label.

Table 3 Defects density on the coatings.

Figure1

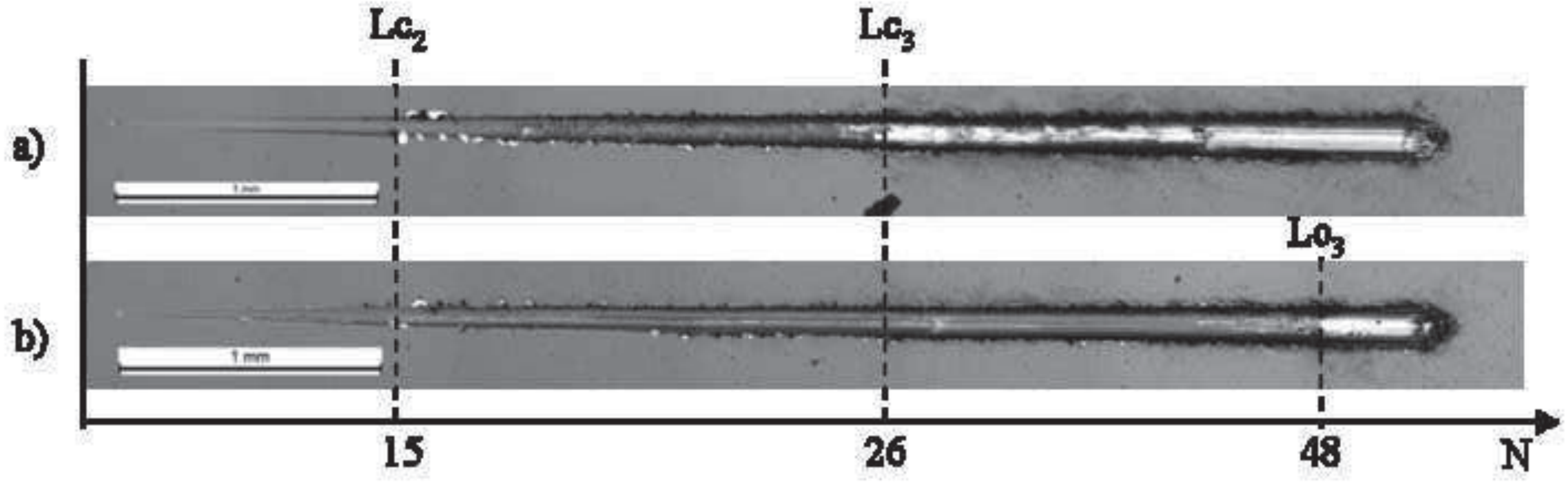

Figure2a

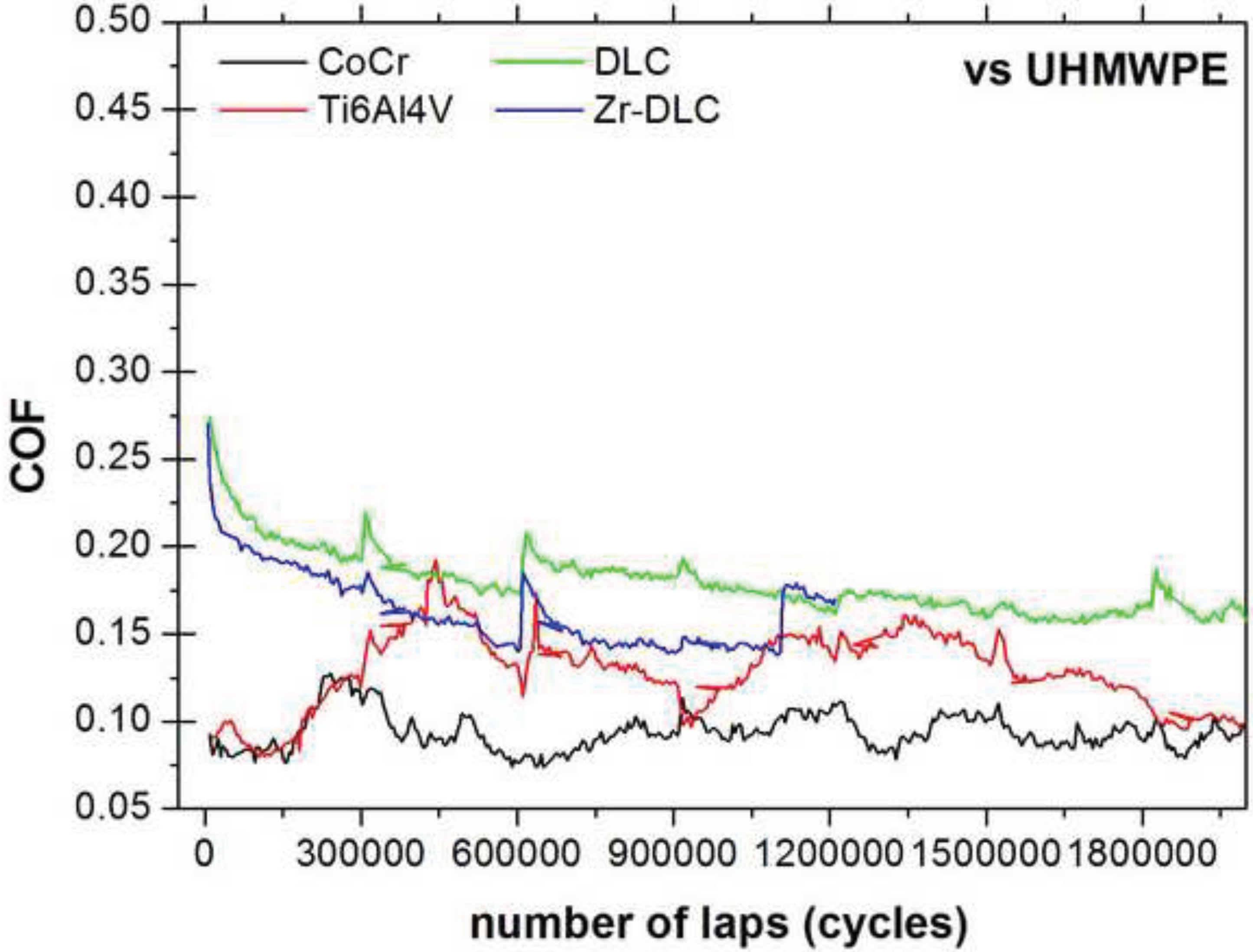
COF
0.50
0.45
0.40
0.35
0.30
0.25
0.20
0.15
0.10
0.05
0
300000
600000
900000
1200000
1500000
1800000
number of laps (cycles)
CoCr
DLC
Ti6Al4V
Zr-DLC
vs UHMWPE

Figure2b

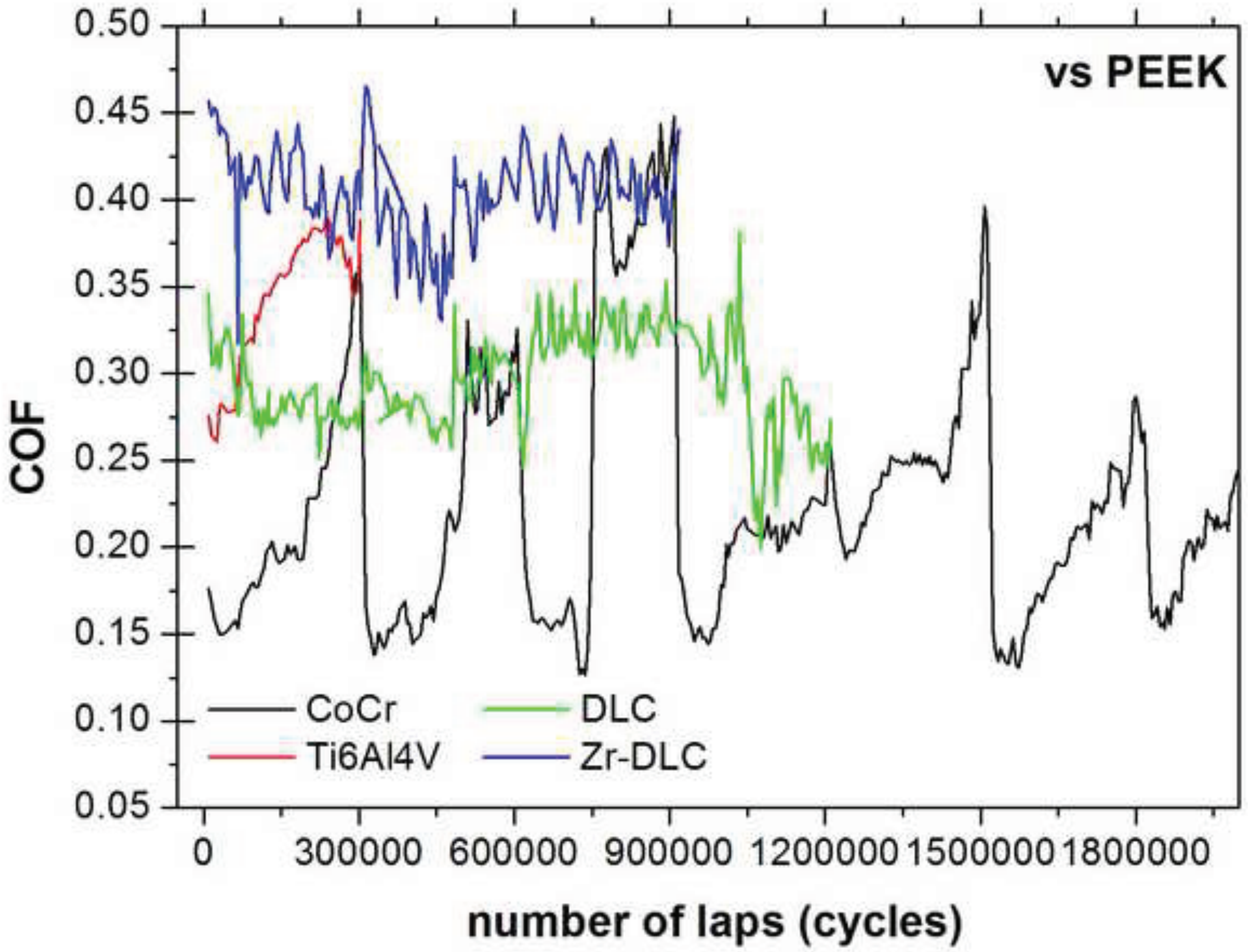
vs PEEK
COF
0.50
0.45
0.40
0.35
0.30
0.25
0.20
0.15
0.10
0.05
0
300000
600000
900000
1200000
1500000
1800000
number of laps (cycles)
CoCr
Ti6Al4V
DLC
Zr-DLC

Figure3

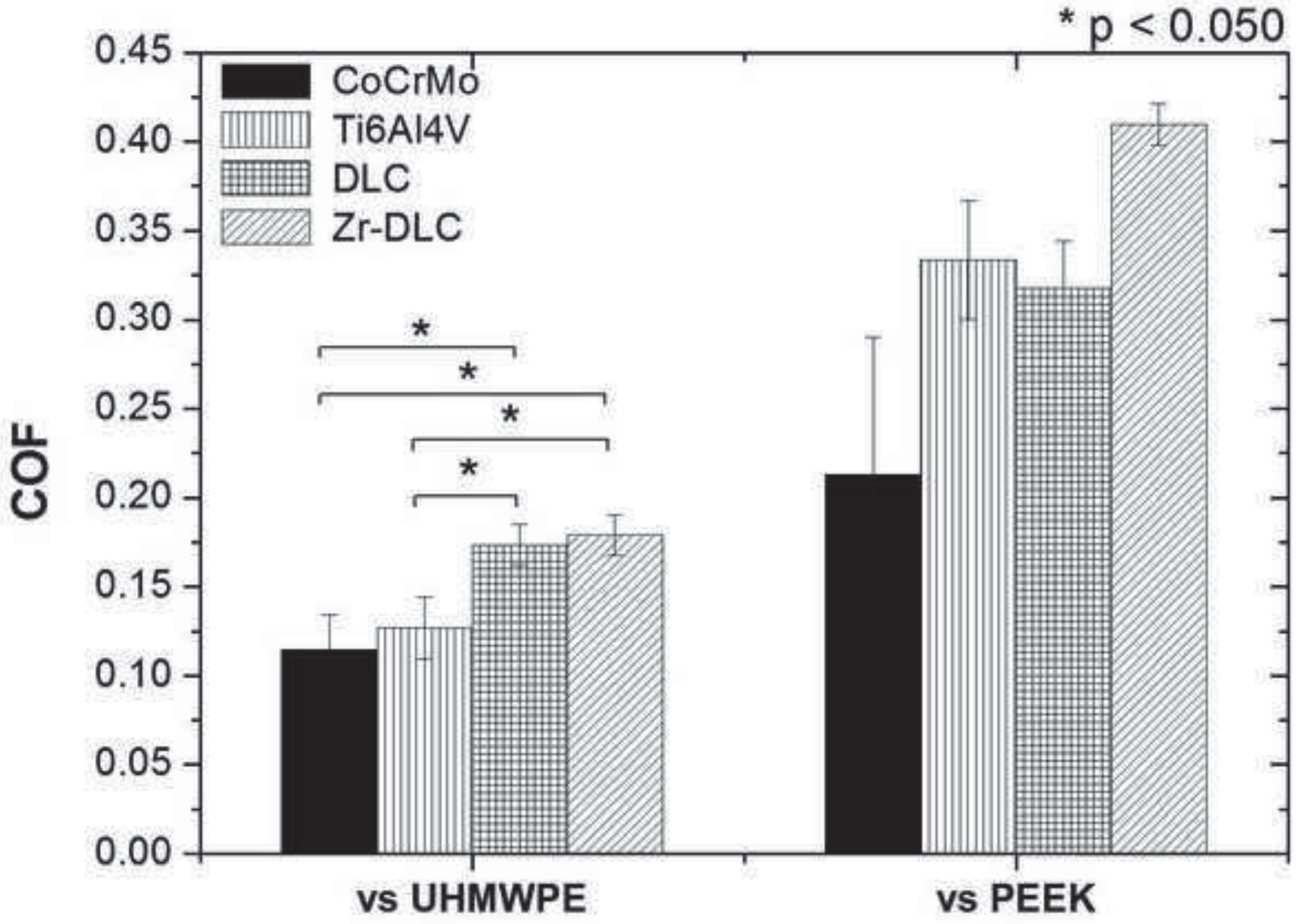
* p < 0.050
COF
0.45
0.40
0.35
0.30
0.25
0.20
0.15
0.10
0.05
0.00
CoCrMo
Ti6Al4V
DLC
Zr-DLC
*
*
*
*
vs UHMWPE
vs PEEK

Figure4a

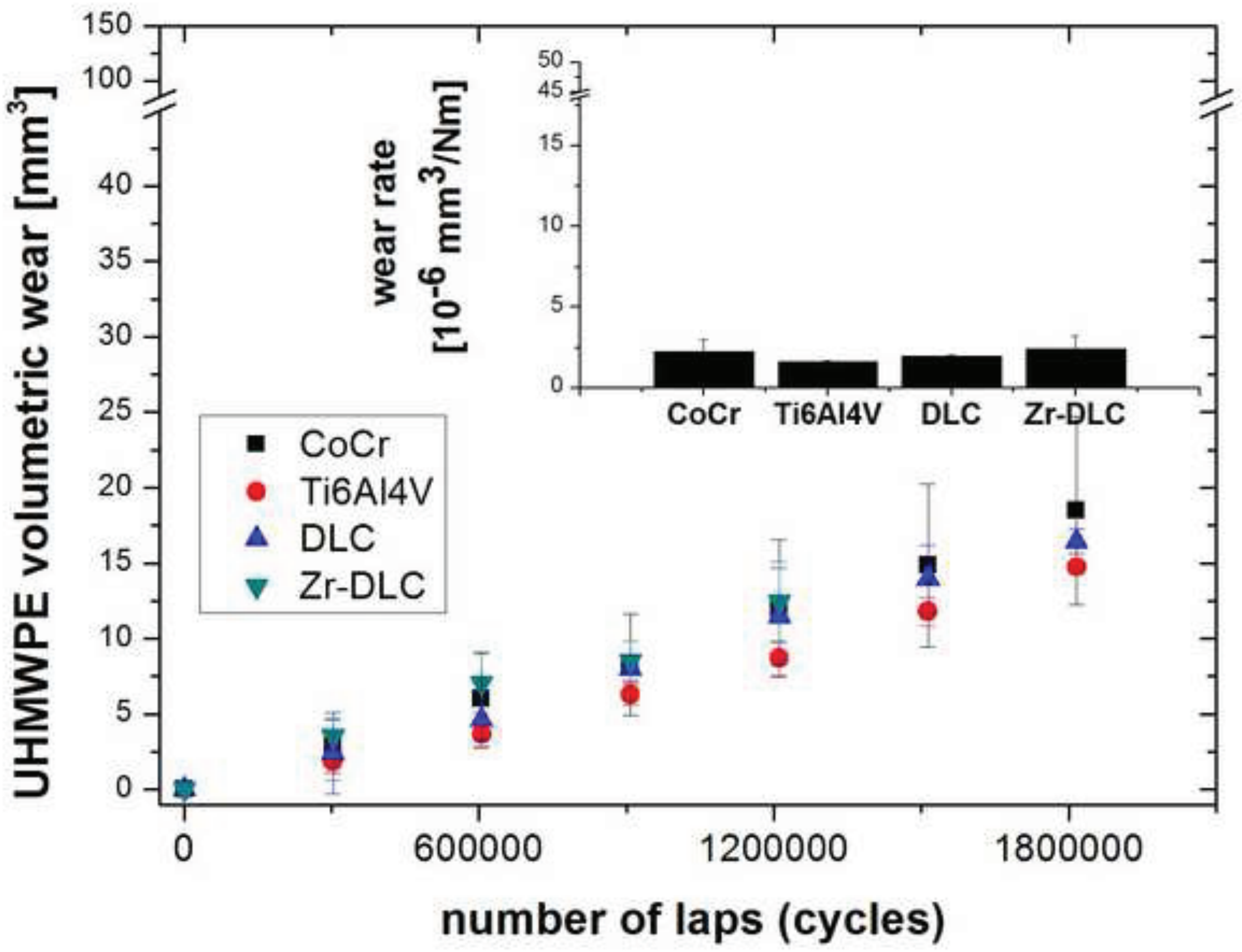
UHMWPE volumetric wear [mm³]
150
100
40
35
30
25
20
15
10
5
0
0
600000
1200000
1800000
number of laps (cycles)
■ CoCr
● Ti6Al4V
▲ DLC
▼ Zr-DLC
wear rate
[10-6 mm3/Nm]
50
45
15
10
5
0
CoCr
Ti6Al4V
DLC
Zr-DLC

Figure4b

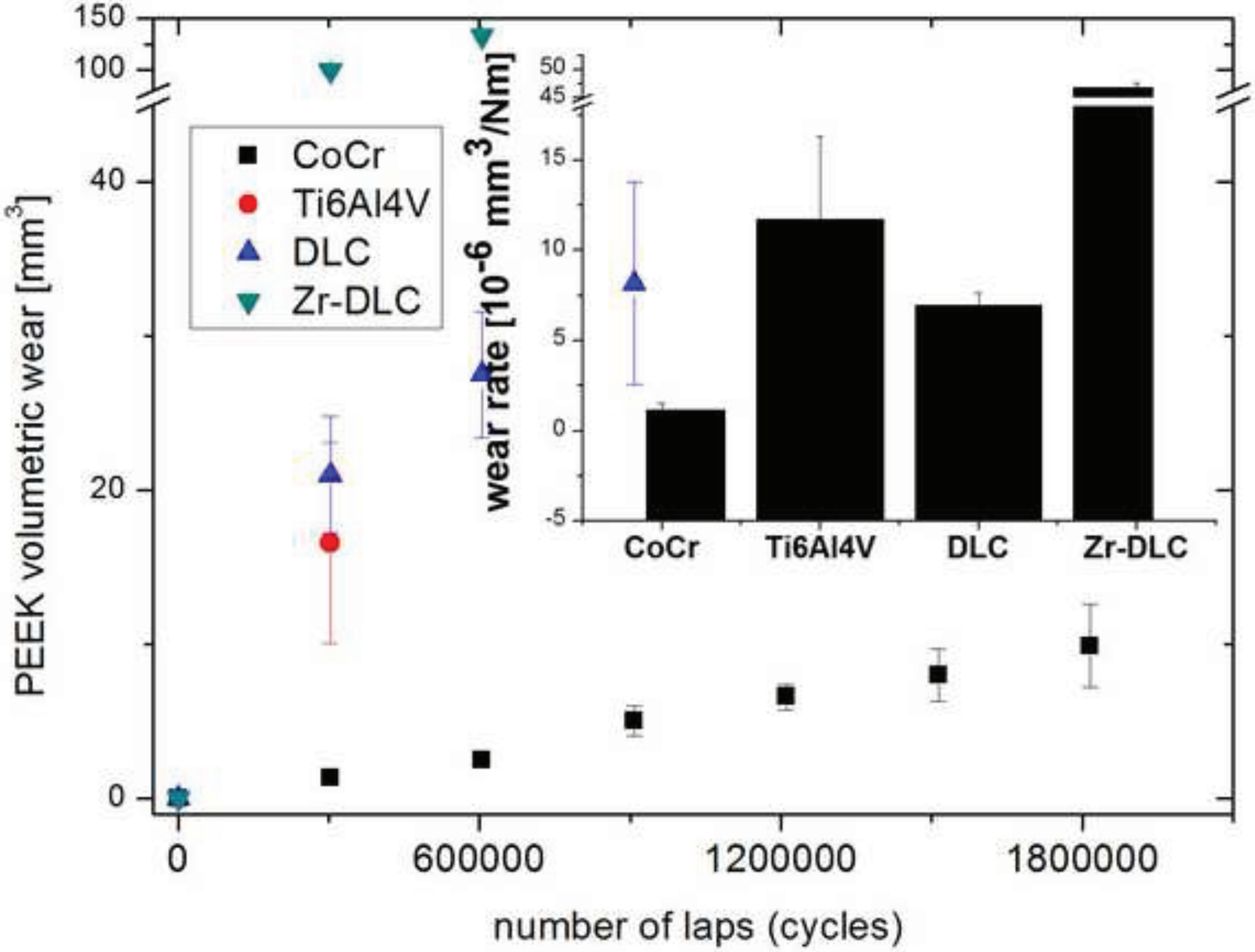
150
100
40
20
0
PEEK volumetric wear [mm^3]
0
600000
1200000
1800000
number of laps (cycles)
CoCr
Ti6Al4V
DLC
Zr-DLC
wear rate [10^{-6} mm^3/Nm]
50
45
15
10
5
0
-5
CoCr
Ti6Al4V
DLC
Zr-DLC

Figure5

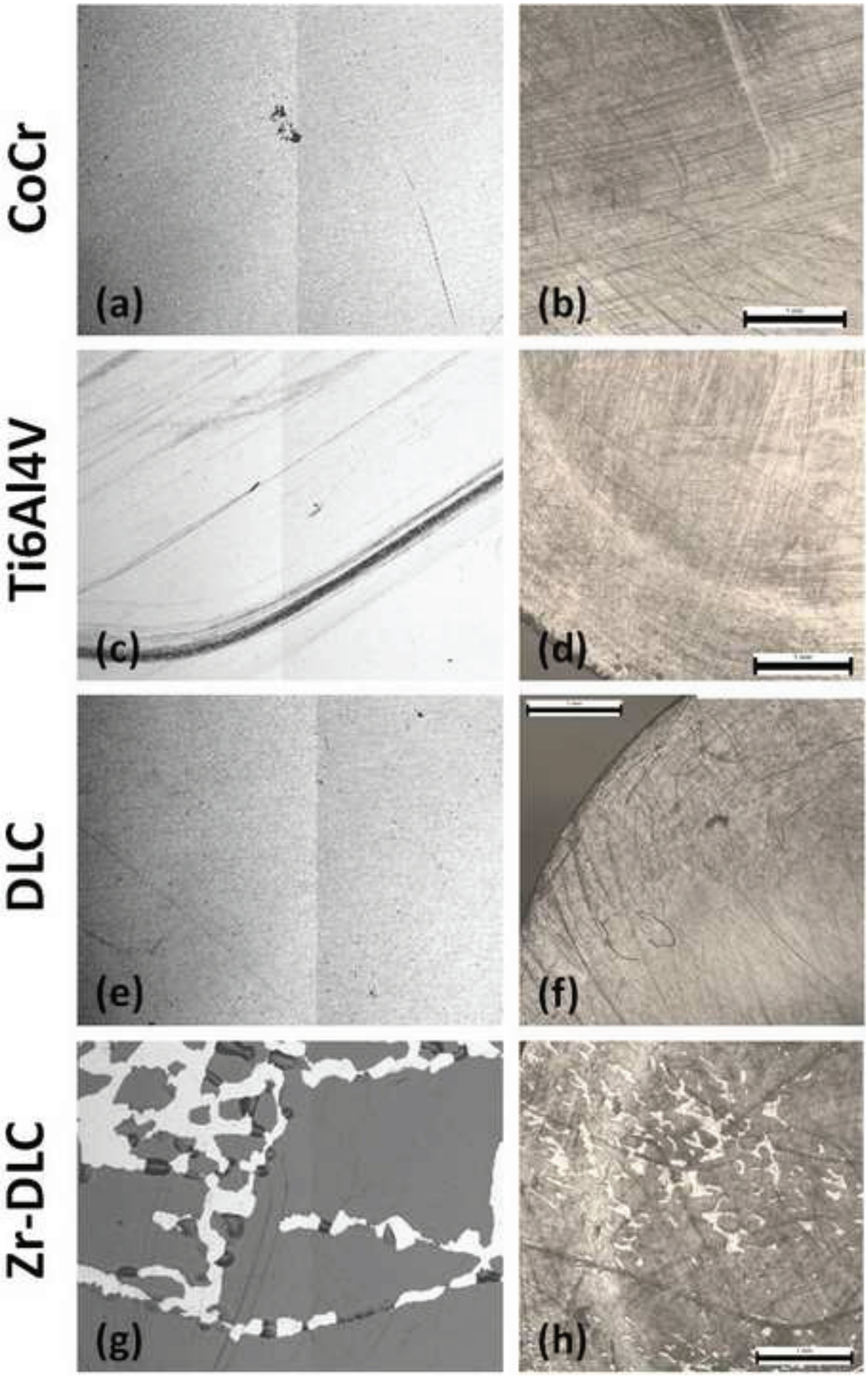

Figure6

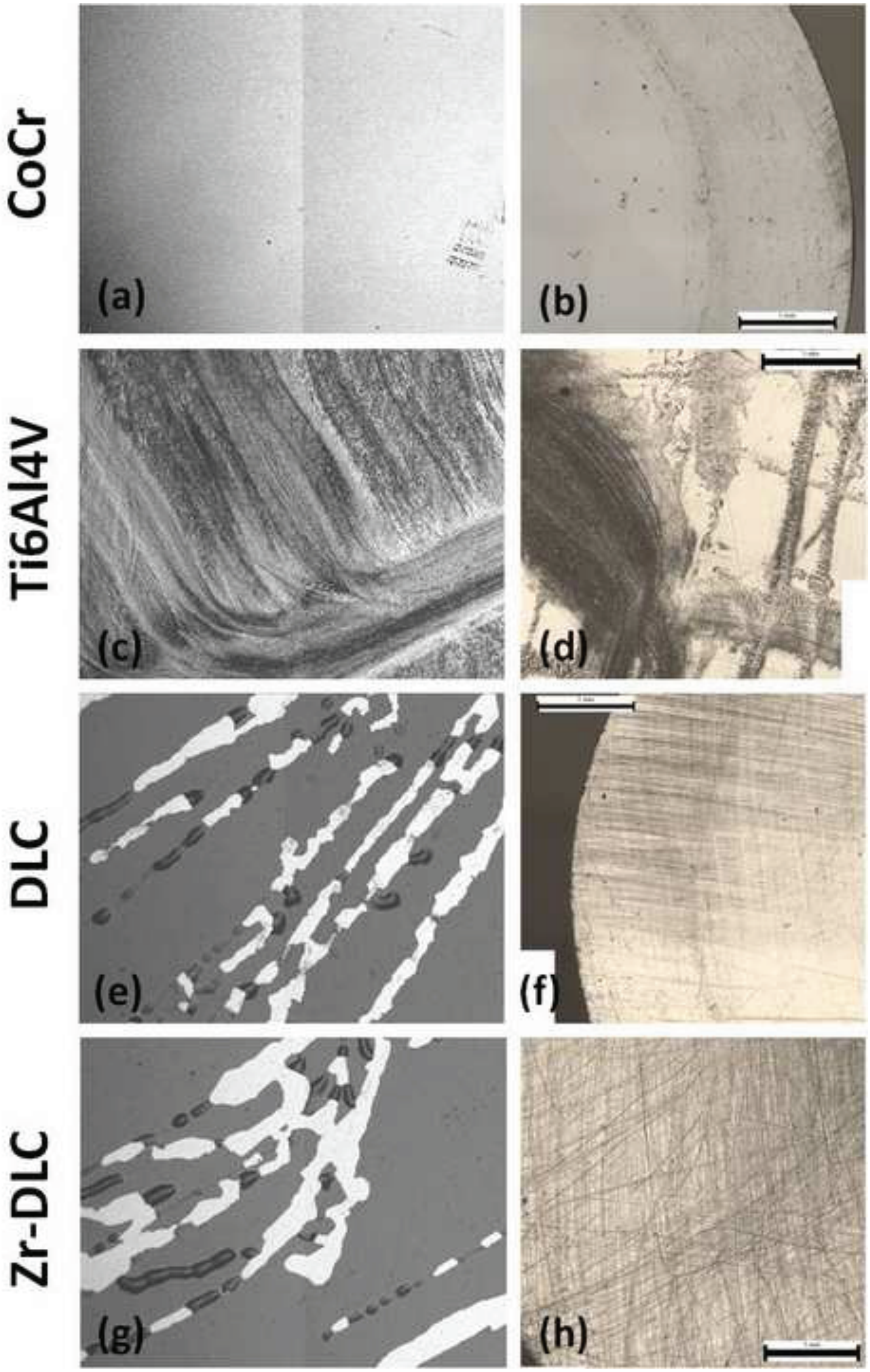

Figure7

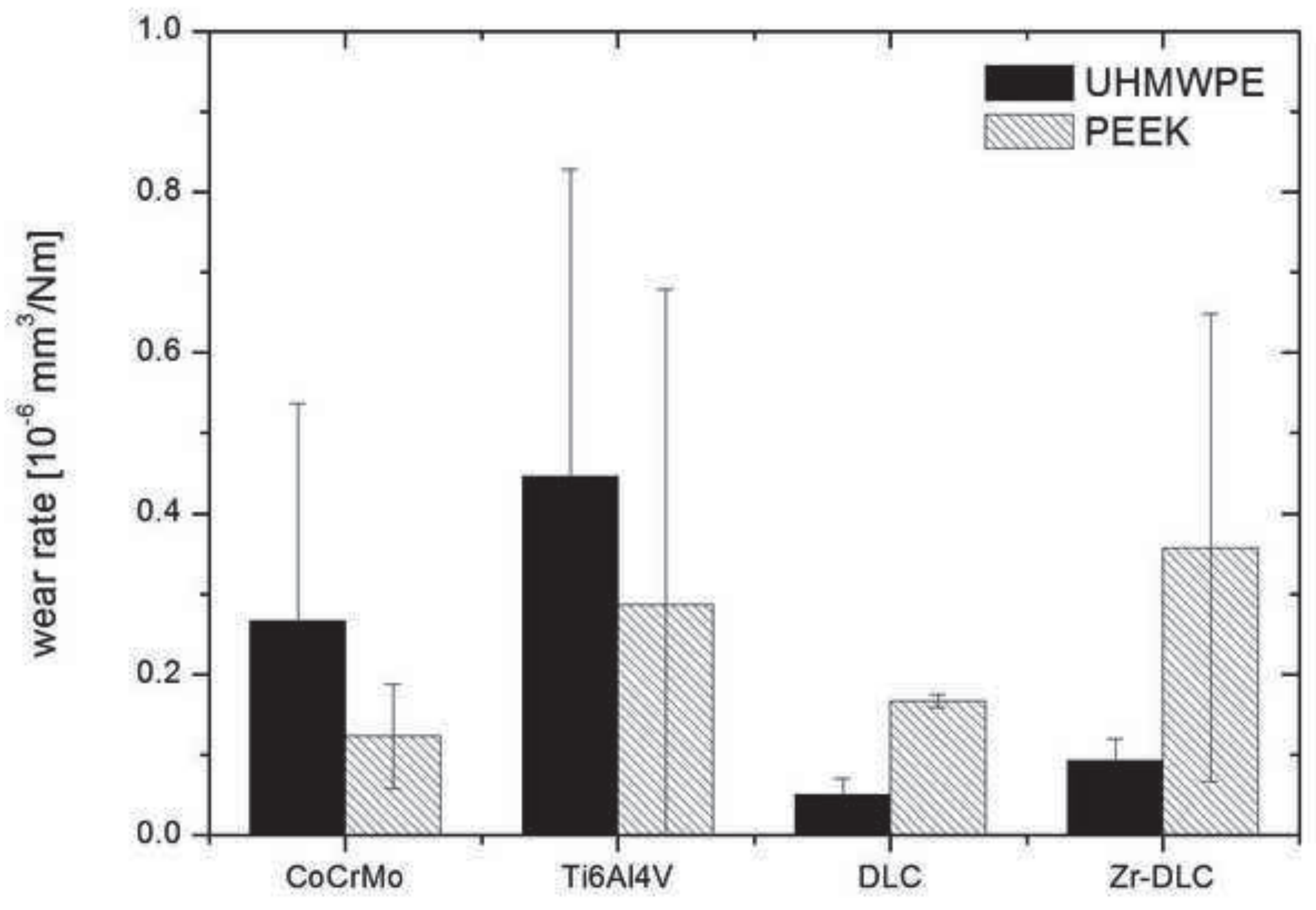
1.0
0.8
0.6
0.4
0.2
0.0
wear rate [10^{-6} mm^3/Nm]
UHMWPE
PEEK
CoCrMo
Ti6Al4V
DLC
Zr-DLC

Figure8

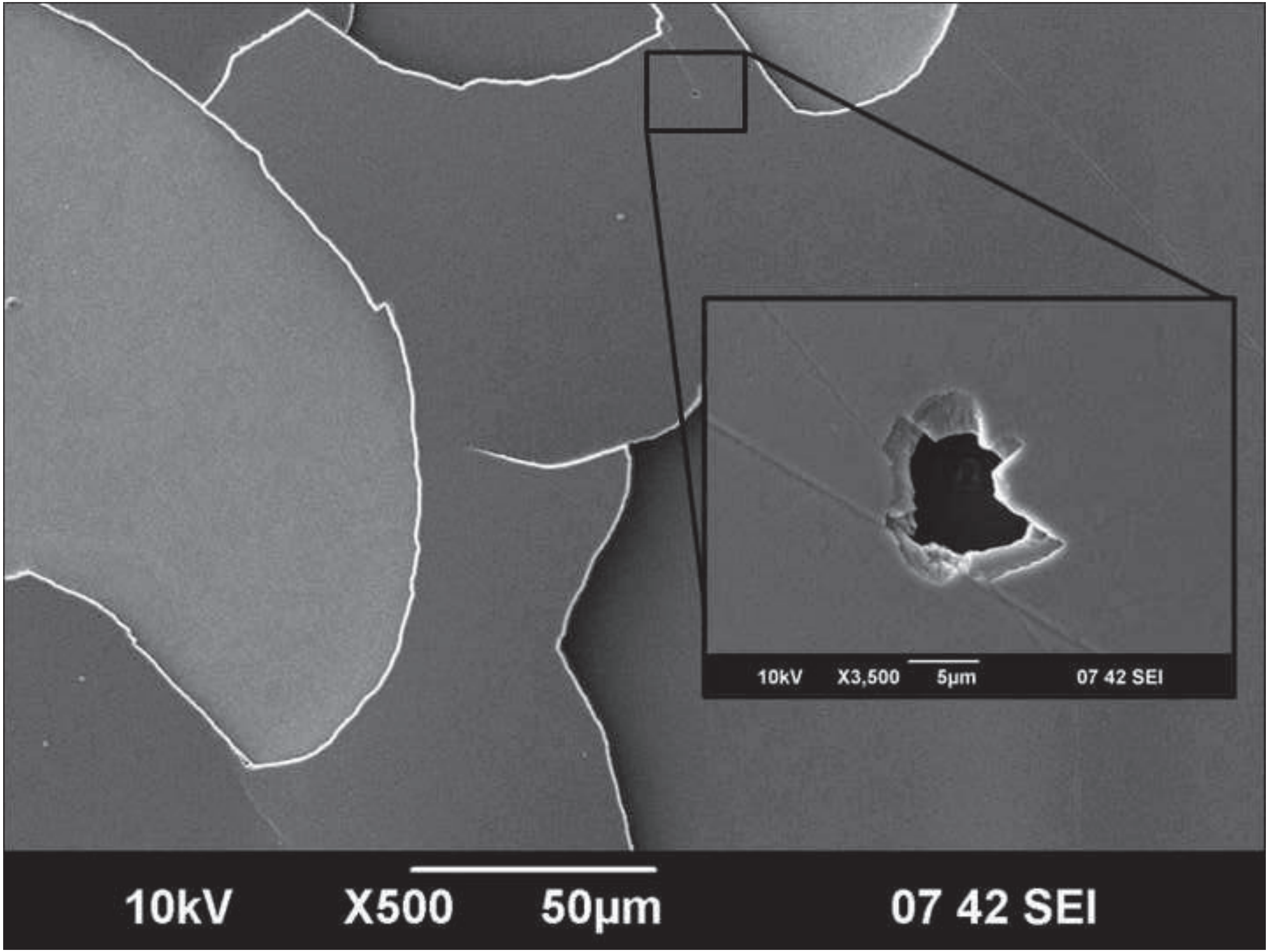

Figure9

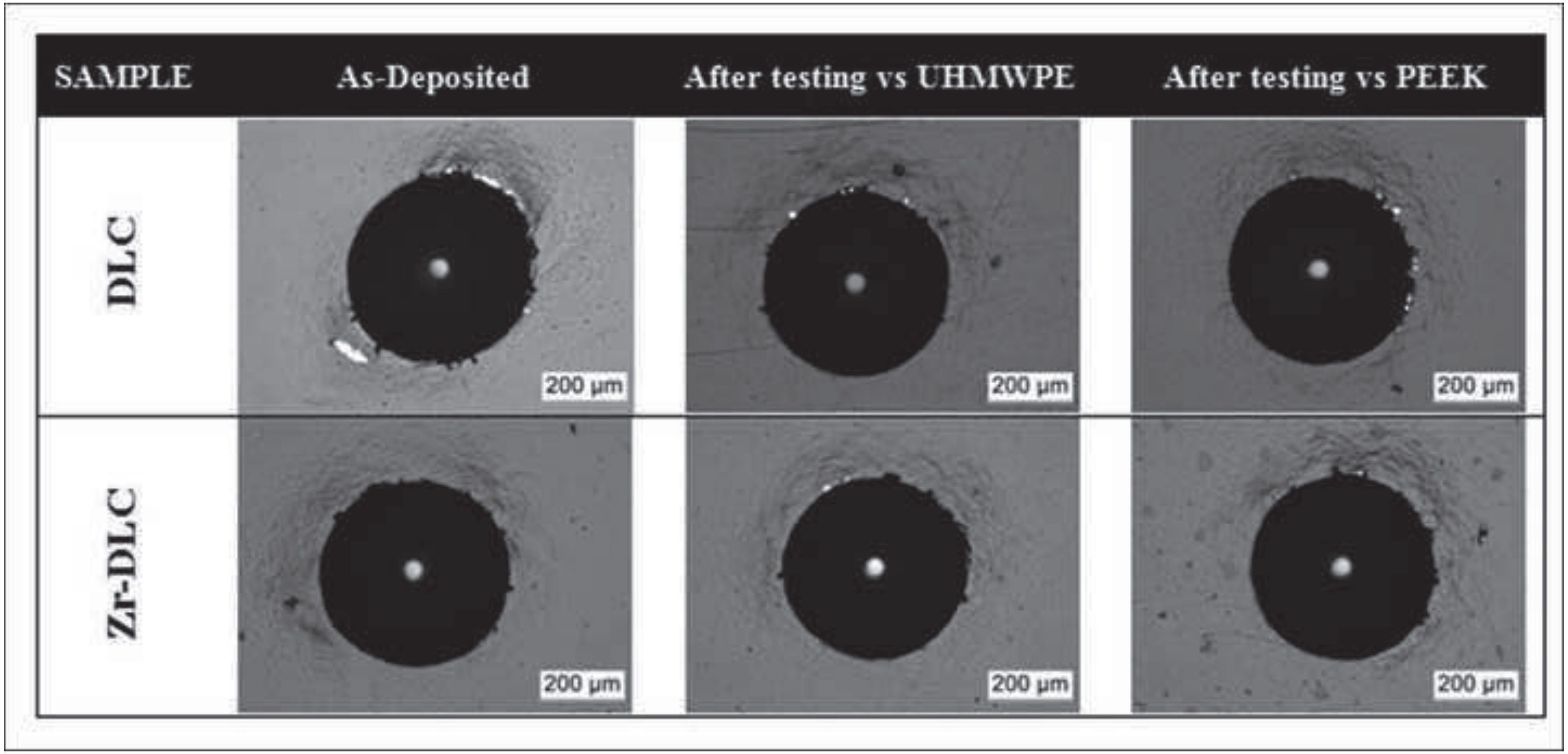
SAMPLE
As-Deposited
After testing vs UHMWPE
After testing vs PEEK
DLC
Zr-DLC
200 µm
200 µm
200 µm
200 µm
200 µm
200 µm

Table1

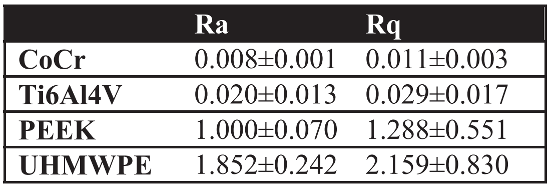

	Ra	Rq
CoCr	0.008±0.001	0.011±0.003
Ti6Al4V	0.020±0.013	0.029±0.017
PEEK	1.000±0.070	1.288±0.551
UHMWPE	1.852±0.242	2.159±0.830

Table2

Samples	Zr/C	I_D/I_G	G peak [μm^{-1}]	H [GPa]	E [GPa]	σ [GPa]	Lc_1 [N]	Lc_2 [N]	Lc_3 [N]	R-C test
DLC	0	1.6	1564	10.7±1	111.1±20	-1.92±0.1	5.4±1	10.7±3	21.5±10	HR3
Zr-DLC	0.04	1.9	1564	10.0±1	143.5±4	-1.46±0.1	6.6±3	13.0±4	34.7±18	HR2

[a] Lc_1, lower critical load is defined as the load where the first cracks occur (cohesive failure) and Lc_2, upper critical load, is defined as the load where the first spallation/flaking on the film is observed (adhesive failure). Lc_3 is then defined as the load where the coating is penetrated by the scratch indenter [22]

[b] HF1-HF4 is typically considered as an acceptable failure, whereas HF5-HF6 is not accepted as a sufficient adhesion [23].

Table3

Sample	Area coverage [%]	Average size [µm]
DLC	7.6±0.7	4.1±0.3
Zr-LC	2.9±0.4	6.8±1.3

PAPER VII

Structural and mechanical properties of nanocrystalline Zr co-sputtered a-C(:H) amorphous films

A. Escudeiro, N.M. Figueiredo, T. Polcar and A. Cavaleiro

Applied Surface Science, under review

Applied Surface Science 325 (2015) 64–72

Contents lists available at ScienceDirect

Applied Surface Science

journal homepage: www.elsevier.com/locate/apsusc

Structural and mechanical properties of nanocrystalline Zr co-sputtered a-C(:H) amorphous films

A. Escudeiro[a,*], N.M. Figueiredo[a], T. Polcar[b,c], A. Cavaleiro[a]

[a] SEG-CEMUC DEM University of Coimbra, Coimbra, Portugal
[b] Engineering Materials, Faculty of Engineering and the Environment, University of Southampton, SO17 1BJ, United Kingdom
[c] Department of Control Engineering, Czech Technical University in Prague, Technicka 2, Prague 6, Czech Republic

ARTICLE INFO

Article history:
Received 28 August 2014
Received in revised form 3 November 2014
Accepted 3 November 2014
Available online 25 November 2014

Keywords:
Nanocrystalline ZrC
Amorphous carbon
XPS
ZrC/a-C(:H)

ABSTRACT

The aim of this study was to investigate the effect of Zr as alloying element to carbon films, particularly in respect to film structure and mechanical properties. The films were deposited by magnetron sputtering in reactive ($Ar+CH_4$) and non-reactive (Ar) atmosphere with different Zr contents (from 0 to 14 at.%) in order to achieve a nanocomposite based films. With an increase of Zr content a broad peak was observed in X-ray diffraction spectra suggesting the presence of nanocrystalline (nc) ZrC phase for the coatings with Zr content higher than 4 at.%. The application of Scherrer formula yielded a grain sizes with a dimension of 1.0–2.2 nm. These results were supported by X-ray photoelectron spectroscopy showing typical charge transfer at Zr—C nanograins and carbon matrix interface. The nc-ZrC phase was also observed by transmission electron microscopy. The hardness of the coatings was approximately independent of Zr content. However, the Young modulus increased linearly. The residual stress of the coatings was strongly improved by the presence of nc-ZrC phase embedded in the a-C matrix. Finally, the incorporation of H into the matrix led to denser and harder films.

1. Introduction

Diamond-like carbon (DLC) coatings are considered an attractive protective surface treatment which combines high hardness and wear resistance with low coefficient of friction, helping to reduce friction losses and to increase load carrying capacity. At the same time, hard DLC coatings are generally characterized by high compressive stress which limits their adhesion to the metallic substrate and makes them brittle under the applied loading. Fortunately, their doping or alloying with non-metallic (N, H, O) and/or metallic (Ti, Cr, W, Ag) elements helps to relax the amorphous carbon (a-C) network by forming a nanocomposite structure [1–4]. Moreover, transition metal-carbides show unique combination of materials of solid-state properties such as very high hardness and excellent electrical and thermal conductivity [5]. If transition metals are introduced into the carbon matrix above a certain concentration, nanocrystalline (nc) particles are formed acting as a reinforcing phase. In fact, Meng et al. [6,7] reported a maximum limit of dissolution of Ti atoms into an a-C:H (hydrogenated) matrix between 0.9 and 2.5 at.% and for a-C matrix between 4 and 8 at.%; for higher Ti concentration, nanocomposite materials could be formed. Mechanical, thermal and electrical properties of the coatings can be then enhanced controlling the size and the volume fraction of the nc-phase [8,9]. Voevodin and co-workers pioneered nanostructured materials [10,11]. For instance, when alloying with Ti, the TiC/DLC systems exhibit a large amount of grain boundaries between the nc-TiC phase and the amorphous DLC matrix, which effectively enhances the hardness and toughness of the coatings, limiting crack initiation and/or terminating further crack growth and film delamination [8–10,12–14]. Moreover, such nanocomposite structure could also lower the friction and wear and significantly improve load carrying capacity [11]. Apparently, encapsulation of finer grains of hard nc-TiC within the amorphous DLC matrix restricts dislocation activity, diverts and arrests macrocracks development, and maintains the high level of hardness [9,13]. The interface between both phases also plays an important role, since interfacial fraction in nanocomposites is very high [15]. It was found that the charge transfer from the Ti 3d to C 2p orbitals may contribute to the mechanical stability of the material by enhancing the inter-phase bonding [15–17]. Therefore, nanocomposite coatings are expected to have high hardness and fracture toughness since the carbide crystals are small and help to block (micro-)crack propagation together with the amorphous carbon phase which provides self-lubrication properties [8,9,13,18,19].

---

[*] Corresponding author. Tel.: +351 239790745.
E-mail address: ana.escudeiro@dem.uc.pt (A. Escudeiro).

http://dx.doi.org/10.1016/j.apsusc.2014.11.015
0169-4332/© 2014 Elsevier B.V. All rights reserved.

Table 1
Coatings deposition parameters (A_{Zr}/A_C is the relative Zr pellets coverage of the erosion area,), chemical composition measured by XPS, deposition rate (Dep rate), thickness (t) and average roughness (Ra).

Sample	A_{Zr}/A_C (%)	[O] (at.%)	[C] (at. %)	[Zr] (at. %)	Dep rate (nm s^{-1})	t (μm)	Ra (nm)
a-C	–	1	99	**–**	7.9	1.7	13.4 ± 1
a-C_Zr(4)	2	2	94	**4**	8.4	1.7	7.3 ± 1
a-C_Zr(7)	3	4	89	**7**	10.5	1.5	5.9 ± 1
a-C_Zr(14)	6	8	78	**14**	11.4	1.5	5.8 ± 1
a-C:H_Zr(10)[a]	6	3	87	**10**	13.2	1.6	4.4 ± 1

[a] Chemical composition not considering H content; H ~ 30 at.% [24].

In this study, Zr, as a strong carbide forming element, was chosen as doping element and incorporated into amorphous carbon matrix in order to form nanocomposite coatings. Coating microstructure is studied in detail and related with mechanical properties.

2. Materials and experimental details

2.1. Coatings deposition

The coatings were deposited using dc magnetron sputtering under reactive (Ar + CH_4,) and non-reactive atmosphere (Ar) in order to deposit hydrogenated and non-hydrogenated coatings, respectively. Two targets were used: Ti, to deposit the gradient interface layer (Ti/TiN/TiCN), and graphite, to deposit the functional coating. Zr-containing films were produced through the incorporation of Zr pellets into the erosion area of the graphite target (see Table 1). Prior to deposition the substrates (Si wafers, mirror polished thin 304 SS and M2 steel discs) were ultrasonic cleaned in acetone, alcohol and distilled water. The substrates were then placed into the vacuum chamber and sputtered etched, via Ar^+ bombardment (−650 V bias voltage), for cleaning any additional oxides and surface contaminants. The Ti-based gradient layer (~650 nm) was then deposited in order to improve adhesion. The deposition parameters were maintained constant for all depositions: 7.5 W cm^{-2} target power density, total pressure 0.4 Pa, sample rotation 18 rpm, bias voltage applied to substrates −50 V. In order to produce hydrogenated coatings, CH_4 was introduced into the deposition chamber while the number of Zr pellets was maintained. The Ar/CH_4 flux was adjusted in order to maintain the total pressure constant. The deposition time was set to deposit coatings approximately 1.6 μm thick. Further deposition details can be found elsewhere [20]. To facilitate reading, the coatings were denominated as a-C_Zr(X) and a-C:H_Zr(X) for non-hydrogenated and hydrogenated coatings, respectively, where X is the approximate Zr content.

2.2. Microstructure, composition and morphology

The phase identification was performed using synchrotron radiation at the Materials Research station of the Rossendorf beam line (ROBL-MRH) located at the bending magnet 20 (BM20) at the European Synchrotron Radiation Facility (ESRF) in Grenoble. The incident X-ray beam was monochromatized to an energy of 11.5 keV (λ = 0.1078 nm). To increase the signal from the coating and in order to identify any crystalline phase, grazing angle incidence X-ray diffraction was performed; hereby the sample surface was tilted 2° in relation to the synchrotron beam. The chemical bonding of the films was evaluated by XPS analysis using a Kratos AXIS Ultra HSA, with VISION software for data acquisition. The analysis was carried out with a monochromatic Al Kα X-ray source (1486.7 eV), operating at 15 kV (90 W), in FAT mode (Fixed Analyser Transmission), with a pass energy of 40 eV for regions ROI and 80 eV for survey. Data acquisition was performed at a pressure lower than 1×10^{-6} Pa and charge neutralization system was used. The samples were sputter-cleaned with Ar^+ ion gun (4 keV) prior to spectra acquisition (30 min) in order to remove any residual contamination, corresponding to a sputter depth of 0.01 nm/min (~0.3 nm). The modeling of the spectra was performed using the CasaXPS program, in which an adjustment of the peaks was performed using peak fitting with Gaussian–Lorentzian peak shape and Shirley type background subtraction. The charging effects were corrected at the surface by assuming C—C bond binding energy (BE) at 285 eV in the C 1s spectrum. For the deconvolution of Zr 3d peaks the spin–orbital splitting was assumed to be constant for all phases (2.4 eV) and the integrated area relatively to that of the Zr $3d_{5/2}$ peak was considered as equal to the spin–orbit multiplicity of 2/3 [21]. The chemical composition was also evaluated by XPS from the relative peak intensity, corrected by experimentally determined sensitivity factors.

The surface morphology and cross-section of the coatings were investigated using a scanning electron microscope (SEM, FEI Quanta 400FEG E SEM–EDAX Genesis X4M) and atomic force microscopy (AFM, AFM–Bruker Innova). The average roughness (Ra) was evaluated by AFM on a 5 μm × 5 μm line scan. The investigation of the nanostructure was carried out by transmission electron microscopy (TEM) with a FEI Tecnai G2 T20 microscope with a LaB_6 filament operated at 200 kV and a FEI Titan 80-300 microscope equipped with field emission gun (FEG) and Gatan image filter (GIF) Tridium and operated at 300 kV. Both bright field (BF) imaging and selected area electron diffraction (SAED) were carried out. SAED was performed with an aperture size of ~100 nm in diameter. TEM specimens were prepared using an FEI Versa3D focus ion beam–scanning electron microscope (FIB-SEM).

2.3. Mechanical properties

The hardness of the coatings was evaluated by depth-sensing indentation (Micromaterials Nanotest) using a Berkovich indenter. The normal stylus load was 5 mN (indentation depth approx. 150 nm); 32 indentations from 2 distinct areas on the sample were carried out to evaluate hardness. Moreover, the reduced Young modulus was derived from the indentation measurements by standard Oliver and Pharr method [22]. The residual stress was calculated using the corrected Stoney equation [23] by measuring the curvature of the SS304 thin disk substrate radii by 2D profilometer (Perthometer S4P) before and after coating deposition.

3. Results and discussion

3.1. Coating deposition and microstructure

Table 1 summarizes the deposition parameters and the corresponding chemical composition of the films (H excluded). The increase of the number of Zr pellets led to higher Zr content in the coatings and, consequently, the deposition rate also increased due to the higher sputtering rate of Zr in relation to C [20,24]. The introduction of CH_4 further increased the deposition rate; however, Zr content was lower due to the presence of a second C source. The

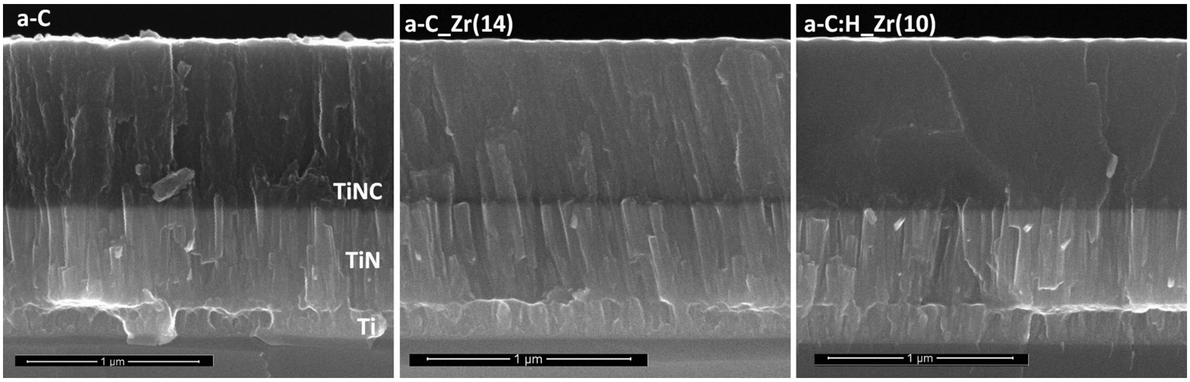

Fig. 1. SEM micrographs showing the fractured cross-section of a-C, a-C_Zr(13) and a-C:H_Zr(10) films.

oxygen contamination originated from the chamber atmosphere was very low (2 at.% data from EDX). The oxygen content measured by XPS was found to be dependent on the Zr content (see Table 1). Prior to XPS signal acquisition, the surfaces were sputter-clean by ion bombardment to clean the surface from contamination. For high Zr contents (14 at.%), the presence of oxygen was detected even after very long ion bombardment (40 min). We assume that the increase of metal/carbon ratio caused by preferential sputtering led to a higher oxygen adsorption and the generation of oxide films on the exposed ZrC nanocrystallines, as will be discuss later [25–27].

The SEM micrographs presented in Fig. 1 show fractured cross-section of selected coatings. The columnar intermediate layer (Ti/TiN/TiCN) is visible between substrate and functional top coating. The same morphology was observed when TiN was deposited by reactive magnetron sputtering at low temperature and low bias voltage [28,29]. a-C films revealed a columnar morphology, which led to a cauliflower-like patterned surface resulting from

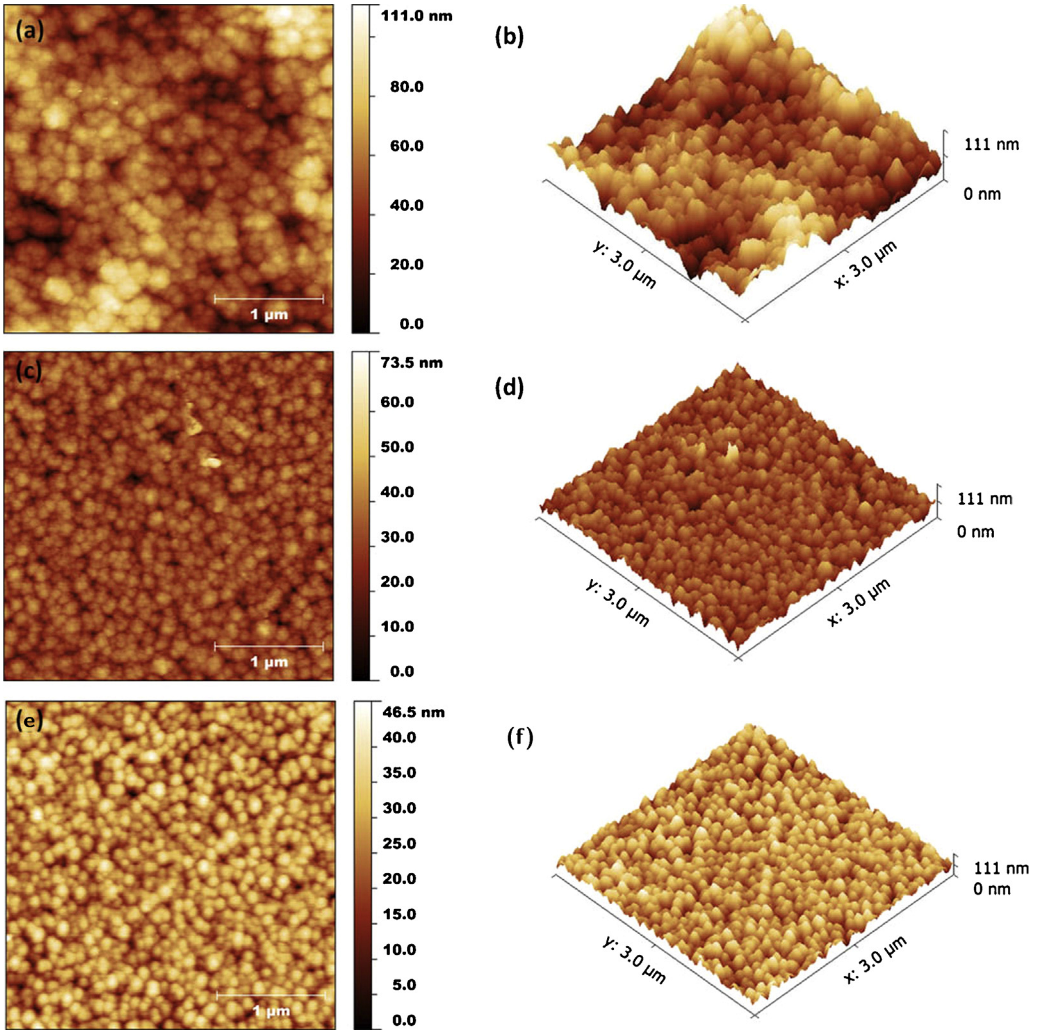

Fig. 2. AFM micrographs showing the topography of (a and b) a-C, (c and d) a-C_Zr(14) and (e and f) a-C:H_Zr(10) films deposited on Si wafers.

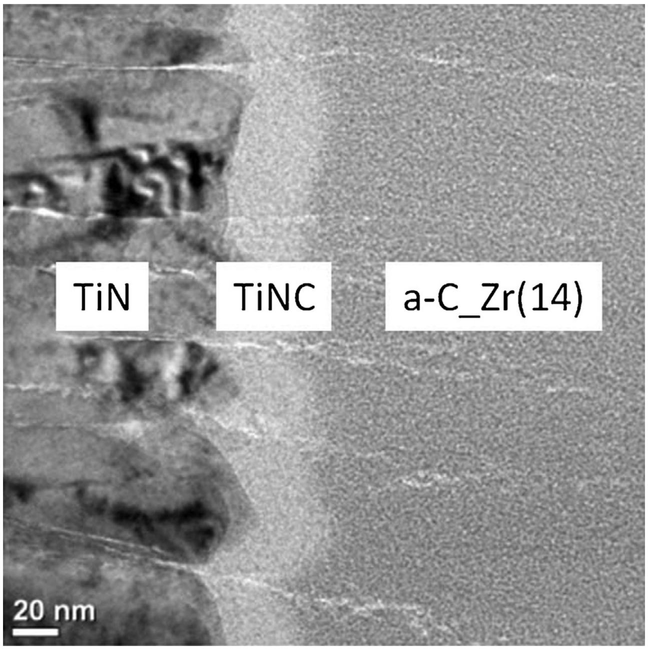

Fig. 3. Cross-sectional TEM BF images of a-C_Zr(14) coating.

the shadow effects and low adatom mobility (see Fig. 2). Columnar growth is commonly associated with growth defects and low toughness coatings which may led to crack initiation/propagation through the columnar boundaries after high load contact [9]. The incorporation of Zr did not produce any significant morphological change; however, the films became denser and smoother. In our previous study, we found that the density was higher with the increase of Zr content. Fig. 3 shows a TEM BF image from the interface between adhesion interlayer and a-C_Zr(14) functional coating. The pronounced columnar structure from the Ti-based interlayer quickly transforms to a rather featureless structure, where only thin and discontinuous columnar boundaries can be seen along the coating growth direction. The presence of heavier atoms, such as Zr, causes preferential growth of ZrC islands while carbon, as lighter atom with expected higher mobility, will be knocked-down to fill the voids reaching the shadowing portions of the coatings and thus promoting the structure rearrangement [13]. The introduction of CH_4 enhances the compact microstructure and eliminated the columnar structure of the films due to two factors: (i) the incorporation of H in the carbon coatings prevent formation of the column boundaries due to high mobility of hydrocarbon species [14] and (ii) a quick fill up of the shadowed areas, since the carbonaceous phases can land from any angle smoothing the growing interface and thus restraining the columnar growth [13].

3.2. Structure and chemical bonding

Fig. 4 shows the X-ray diffractograms of the alloyed non-hydrogenated films. The presence of Si, Ti and TiN peaks originated in a graded Ti/TiN/TiCN interlayer and Si substrate. With the increase of Zr content, a broad peak appeared at ZrC phase position (ICDD card no. 74-1221). The presence of broad peaks is common in nanocomposite and nanostructured films, where the limited size of the diffracting crystals causes broadening of the peak. The peaks were fitted using a pseudo-Voigt function (see Fig. 4 inset) and by fixing the position the interlayer correspondent peaks and allowing the background and the position areas of ZrC peaks to vary. For low Zr content (4 at.%), the deconvolution was found to be very difficult due to the extremely low intensity peak. The particle size estimated by the Scherrer formula [30] slightly increased from 1.0 to 2.2 nm for Zr content 4 and 14 at.%, respectively. The same was observed for the hydrogenated coating (not shown). Raman spectra was used to characterized the amorphous C-matrix. The incorporation of Zr and H led to the formation of aromatic rings and the organization and size of the C-clusters in the C-matrix as seen in our previous study [20].

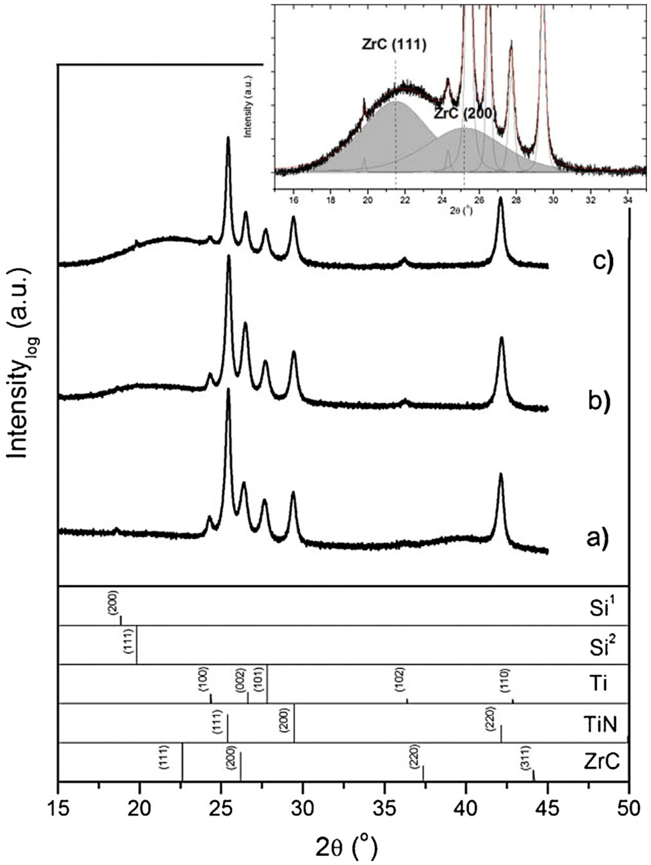

Fig. 4. XRD diffractograms of (a) a-C_Zr(4), (b) a-C_Zr(7) and (c) a-C_Zr(14) films with selected patterns. The inset shows the fitted curve s of the peak phases present in the a-C_Zr(14) diffractogram, highlighting the ZrC phase (gray filling).

TEM investigations were performed on selected samples to verify the XRD results. Fig. 5 shows the TEM micrographs and the schematic representation of the particle distribution of a-C_Zr(14) and a-C_Zr(4). The schematic representation was obtained by using the Mathematica software to model the particle distribution taking into consideration the nanoparticle volume fraction (V_F) and the ZrC nanoparticles size for a unit cell of $20 \times 20 \times 5\,\text{nm}^3$. TEM of a-C_Zr(14) coating clearly shows ~2 nm nanocrystalline ZrC grains randomly distributed in an amorphous carbon matrix (see Fig. 5a). Other smaller nanoparticles are also expected to be present; however, their very small size (<1.5 nm) makes them almost imperceptible to the BF TEM. For a-C_Zr(4) coating (see Fig. 5b) only smaller nanoparticles are expected to be dispersed in the a-C matrix. Again, such small sizes (<1 nm) should be rather difficult to identify in TEM micrographs. Fast Fourier transform (FFT) analysis of the a-C_Zr(14) revealed sharp and discrete rings between the lattice planes corresponding to that of ZrC (not shown). Using the model, the average inter-particle distance was found to be around 9 nm, irrespectively of the Zr content. Thus, in all cases the separation of ZrC nanograins by an amorphous carbon phase is high enough (≫particle size) to isolate the nanoparticles effectively and limits the grain growth via diffusion and coalescence [31].

Information about the chemical state and chemical environment of C and Zr in the coatings was evaluated by XPS. Fig. 6 shows

(a) a-C_Zr(14)

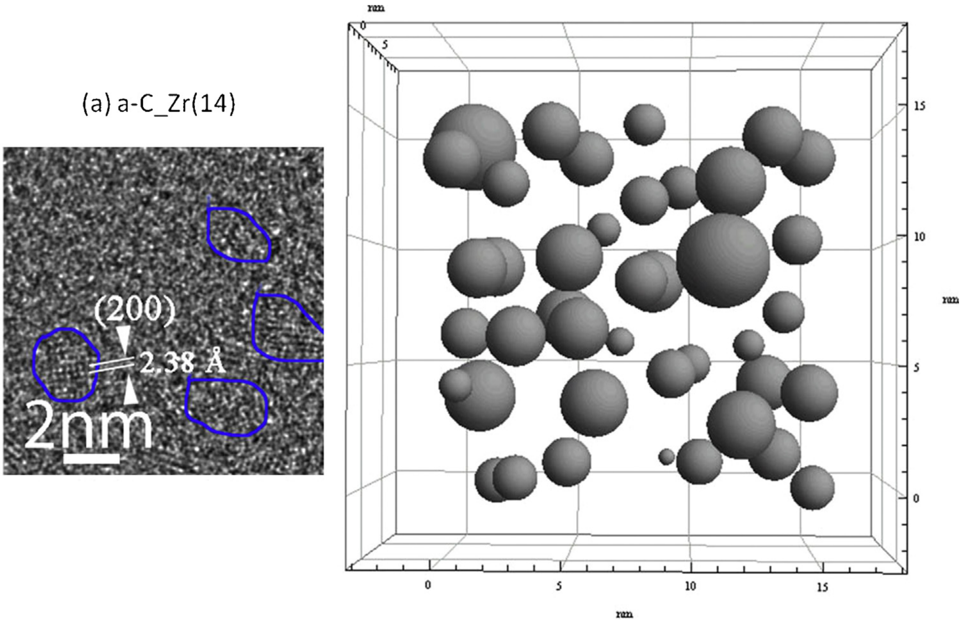

(b) a-C_Zr(4)

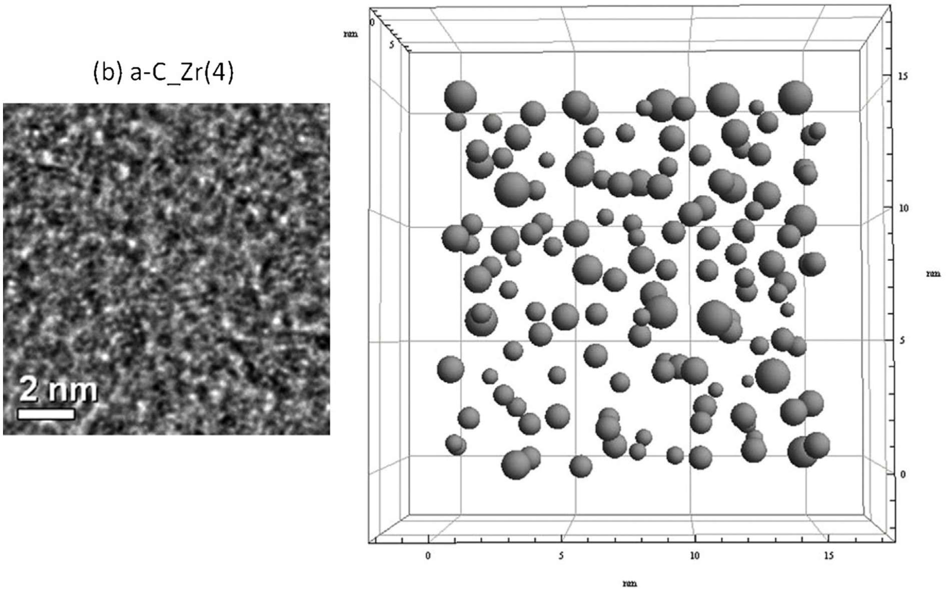

Fig. 5. TEM BF images and particle distribution schematic representation of a-C_Zr(14) and a-C_Zr(4).

the core-level spectra of the analyzed elements: C 1s, Zr 3d and O 1s after Ar^+ sputter cleaning. Tables 2 and 3 show, respectively, the relevant BE found in literature and the experimental BE values obtained after fitting the XPS spectra according to the different types of bonds expected in the coatings.

Fig. 6a shows the carbon C 1s spectral fitting for non-hydrogenated samples. The carbon peak was fitted using the main peak (285 eV) ascribed as alkyl type carbon (C—C, C—H). A second peak was added (286.3 eV) with the same FWHM as the main peak ascribing the alcohol (C—OH) and/or ester (C—O—C) functionality. Two other components were also added corresponding to the C═O and O—C═O at 287.8 eV and 289.3 eV, respectively. When Zr was incorporated in the matrix an extra peak appeared with BE close to 283.5 ± 0.1 eV (see Table 3). The position of this peak (BE value) stayed approximately constant with Zr content in the films. A peak between typical C—Me and C—C bonds has been reported by many authors for nc-MeC/a-C systems (Me = Zr, Ti and Nb) [15–17,31,38,42]; it was suggested to originate from an interfacial state at the carbide and amorphous matrix interface (Me—C*). The presence of nanocrystallites can enhance the charge transfer between the positive metal element and the C-matrix through adsorption of stable building units of a-C(:H) (e.g. extended sp^2-bonded islands with their stabilizing π-system) [42,44]. In fact, Magnuson et al. [17] suggested that, for nc-TiC/a-C films, electron transfer occurs between Ti 3d and C 2p. The electron deficiency, caused by such net charge transfer from Ti to the C-matrix, can be then spread out across the entire carbide grain [17,45]. For larger grains such deficiency is negligible; however, for nanograins the electron deficiency will weaken the Me—C bond within carbide. These interface regions were predicted to be around 1 nm thick [16]. A higher total charge transfer from the Zr nearest neighbors to interfacial C atoms is expected leading to higher chemical shift [42,45]. Thus, for the present case, the ZrC bonds are expected to be characteristic of small ZrC nanoparticles (C—Zr*).

Zr 3d spectra are shown in Fig. 6c. The Zr metallic phase (178.0–179.1 eV) was not observed in any sample. Likewise in the C 1s spectra, Zr 3d peak also shifts approximately 1.0 eV to HBE when compared to typical ZrC peak of a bulk material (179.9 ± 1.8 eV).

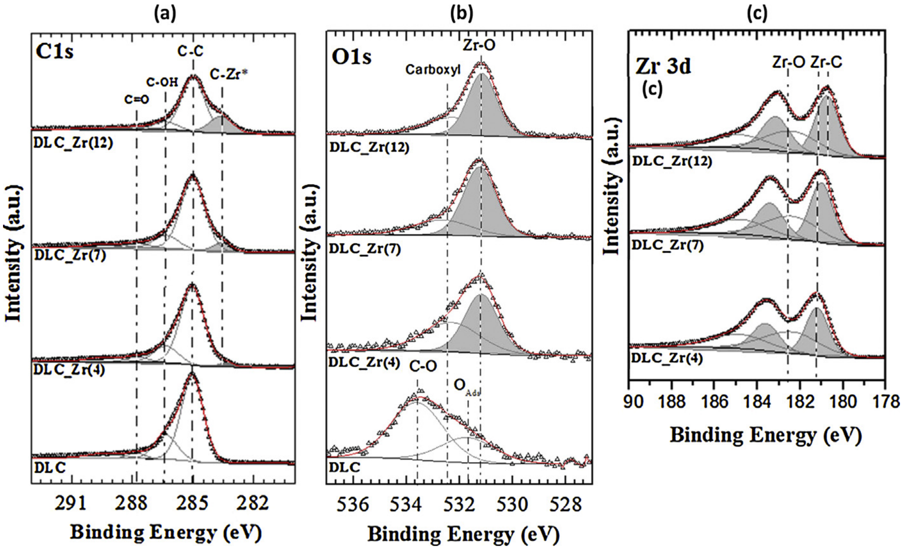

Fig. 6. XPS (a) C1s, (b) O1s and (c) Zr 3d spectra for the non-hydrogenated films with different Zr contents after Ar$^+$ etching of the surface oxides.

Many authors [38,44,46,47] reported similar shifts for small grain sizes. Contrarily to the C 1s, for the Zr 3d case it was observed a reduction of the BE shift with increasing Zr content (Fig. 6c and Table 2). For smaller cluster sizes the electron deficiency in Zr atoms is expected to be higher, leading to HBE shifts [45].

The presence of Zr—O bonds in the Zr 3d spectra (182.4 eV) was also observed, even after ion bombardment. Despite the low oxygen content in the film, the O—Zr contribution in the Zr 3d spectra was around 50% for higher Zr contents. The ion bombardment may induce carbon preferential sputtering causing ZrC nanocrystals exposure to the environment resulting in ZrO_2 formation [27]. Zr is easily oxidized (ZrO_2) showing its high ability to passivate, which might be a beneficial property for corrosion resistance. These bonds were also confirmed in O 1s range of energies revealing a peak at 531.2 eV previously reported as Zr—O bond (Fig. 6b).

3.3. *Mechanical properties*

DLC films are known to have high compressive residual stress due to their peculiar amorphous structure (>3 GPa) [48]. Table 4 shows the compressive residual stress for Zr-free and Zr-containing films. In our case, thermal mismatch is minimized since magnetron sputtering is characterized by a low deposition temperature [49] and no external heating was used. Furthermore, the use of graded layers (Ti/TiN/TiNC) helped to decrease the abrupt composition changes between the film and the substrate and thus decreasing the residual stress and improving the adhesion. The intrinsic stress was strongly dependent on the chemical composition, morphology and microstructure of the films. The incorporation of Zr relaxed the stresses in the films: the higher the Zr content, the lower the stress. Zr acted as a catalyst forming a nanophase of ZrC and reacting with the C-matrix by overlapping Zr d-orbitals with C p-orbitals. The

Table 2
Literature values on BE of the C1s, O1s and Zr 3d core-levels relevant for this study.

Bond type	Spectra	Referenced BE (eV)	FWHM (eV)	Ref.
Zr (metal)	Zr $3d_{5/2}$	178.5	1.8	[32]
		178–179.1	–	[21,33]
Zr—C	Zr $3d_{5/2}$	179.8	~1.2	[34]
		181.1	~ 2	[35]
		178.6–180.2	–	[33,36–39]
Zr—O (Zr^{4+})	Zr $3d_{5/2}$	182.3–182.4	~2.6	[34]
		185.1	~2.5	[35]
		182.9 (Zr^{4+})	1.8	[32]
		181.9–183	–	[21,33,37]
C—C	C 1s	284.2–285	–	[21,37,40,41]
C—O—C, C—OH	C 1s	285–286.5	–	[21,37,40,41]
C=O	C 1s	287.8–288	–	[21,37,40]
O—C=O	C 1s	288.6–289.3	–	[37,40,41]
Zr—C	C 1s	282.5	~2	[34]
		282.9	~1.5	[35]
		281.7–282.3	–	[33,36–38]
Zr-C*	C 1s	282.6–283.3	–	[20,38,42]
OAds	O 1s	531.9	–	[37]
		531.5	2.2	[41]
Zr—O	O 1s	531.2	1.7	[32]
		530.2–530.6	–	[21,33,37]
C—O, C=O, O—C=O (carbonyl)	O 1s	533.2–533.6	–	[41]
		532.4–532.7		[34,43]

Table 3
XPS BE for the deconvolution of the peaks after Ar^+ sputtering.

Sample	Spectra	C—C		C—O, C═O, O—C═O (carbonyl)		Zr—C		Zr—O ($Zr_{5/2}$)		O (adsorbed moisture)	
		BE (eV)	FWHM (eV)	BE (eV)	FWHM (eV)	BE (eV)	FWHM (eV)	BE (eV)	FWHM (eV)	BE (eV)	FWHM (eV)
DLC	C 1s	285.0	1.3	286.3	1.3	–	–				
				287.8	1.0						
				289.3	2.0						
	O 1s			533.6	2.3			–	–	531.8	2.4
DLC_Zr(4)	C 1s	285.0	1.4	286.3	1.4	283.4	1.0				
				287.8	1.4						
				289.3	2.0						
	O 1s			532.3	2.5			531.2	1.4	–	–
	Zr 3d					181.2	1.2	182.4	3.1		
DLC_Zr(7)	C 1s	285.0	1.4	286.3	1.4	283.6	1.1				
				287.8	1.3						
				289.3	2.0						
	O 1s			532.4	2.7			531.2	1.4	–	–
	Zr $3d_{5/2}$					181.0	1.3	182.4	2.9		
DLC_Zr(12)	C 1s	285.0	1.3	286.4	1.3	283.6	1.4				
				287.8	1.4						
				289.3	2.0						
	O 1s			532.3	2.5			531.2	1.3	–	–
	Zr $3d_{5/2}$					180.8	1.3	182.4	2.8		
DLC:H_Zr(8)	C 1s	285.0	1.4	286.3	1.4	283.6	1.3				
				287.8	1.5						
				289.3	2.0						
	O 1s			532.4	2.8			531.2	1.5	–	–
	Zr $3d_{5/2}$					180.7	1.2	182.4	2.6		

break of the C bonds may release the stress through the formation of a more graphite-like film as seen in our previous study [20]. The same tendency was also observed by Zou et al. [50] for DLC coatings doped with low Cr contents. On the other hand, simultaneous incorporation of both H and Zr did not promote such relaxation. The presence of a reactive gas (CH_4) enhanced the bombardment of the film by the hydrocarbon species and their consequent penetration in the structure. Thus, a denser network structure was formed (see Section 3.1) which led to an increase in the residual stress [13,48].

The presence of ZrC nanograins did not significantly change the hardness of the coatings compared to Zr-free ones. The hardness of nanocomposite films is typically influenced by the size, orientation and shape of the embedded nanograins [11]. For hard coatings the key challenge is to avoid grain boundary sliding leaving the grain rotation as the deformation mechanism: small interparticle separation (few atomic layers) and higher volume fraction (V_F) of nano particles (3–5 nm) is required. On the other hand, toughness is achieved by larger interparticle separation and thus, lower V_F, which allows shear delocalization [11,44,51]. Since small nanograins of ZrC (<3 nm) were separated by a thick carbon layer (see Section 3.2) the classical Hall–Petch effect cannot be considered; moreover, two factors contribution to high hardness could be well balanced in our system – higher amount of carbides results in lower compressive stress, so the final hardness could be almost identical for different Zr contents and similar to pure carbon films. On the other hand, the Young modulus increased with the increase of Zr-content (see Table 4), since the embedded ZrC phase presents higher elastic modulus compared to a-C matrix [5].

Other important parameters for hard coatings are H/E and H^3/E^2 which are closely related to the wear resistance and the plastic behavior under Hertzian contact, respectively [52]. Since the hardness was almost independent of Zr content, both parameters slightly decreased with the increase of Zr content. The methane flux during the deposition resulted in an increase of H/E and H^3/E^2 when compared to non-hydrogenated films. As expected, the lack of columnar boundaries (i.e. glassy microstructure, see Fig. 1) together with modified nature of carbon matrix by hydrogen led to slightly higher hardness value. The wear resistance is thus expected to be higher for Zr-containing hydrogenated samples.

Table 4
Mechanical properties of the coating: compressive residual stress ($\sigma_{\text{compressive}}$), hardness ($H$), young modulus ($E$), H/E and H^3/E^2 ratios.

Samples	$\sigma_{\text{compressive}}$ (GPa)	H (GPa)	E (GPa)	H/E	H^3/E^2 (GPa)
a-C	1.9 ± 0.6	11.2 ± 0.6	110.4 ± 6.5	0.10	0.12
a-C_Zr(4)	1.6 ± 0.3	11.7 ± 0.5	118.2 ± 0.9	0.10	0.12
a-C_Zr(7)	1.0 ± 0.6	11.4 ± 0.6	126.6 ± 4.4	0.09	0.09
a-C_Zr(13)	0.3 ± 0.1	11.9 ± 0.5	137.2 ± 1.6	0.09	0.09
a-C:H_Zr(10)	1.7 ± 0.4	12.7 ± 0.6	120.2 ± 1.0	0.11	0.14

4. Conclusion

The formation of nanocomposite structures consisting of ZrC nano-particles in an amorphous carbon matrix has been analyzed in detail by SEM, XRD, XPS and TEM. The incorporation of 4 at.% of Zr resulted in the presence of ZrC nanophase embedded in a carbon matrix. The grain size estimated by XRD peak fitting and directly measured by TEM was between 1.0 and 2.5 nm. The presence of such nanophase ZrC was also confirmed by XPS where additional bonding states were identified due to the small grain size of the carbide phase. The interaction of ZrC with the matrix led to significant charge transfer, which shifted ZrC XPS peak to HBE. Mechanical properties were related to chemical bonding and coating microstructure. With the increase of Zr content the columnar microstructure of the coatings became featureless. The hardness was almost independent of Zr content; however, the change in Young modulus led to different H/E and H^3/E^2, which decreased with the increase of Zr content. Higher amount of Zr decreased residual stress. The introduction of the reactive gas into the chamber further enhanced the properties of the coatings. The high mobility of the hydrocarbon species led to a more compact/glassy microstructure, constraining the typical columnar microstructure and improving the mechanical properties.

Acknowledgments

This research was sponsored by FEDER funds through the program COMPETE–Programa Operacional Factores de Competitividade–and by national funds through FCT–Fundação para a Ciência e a Tecnologia–, under the project PEst-C/EME/UI0285/2011 and QREN-POPH for funding support under the grant SFRH/BD/75071/2010 which was co-funded by FSE and MSTES. The authors would also like to acknowledge support under the project 108/10/1782 from Czech Science Foundation. The research has also received funding from the European Union Seventh Framework Programme under Grant Agreement 312483 – ESTEEM2 (Integrated Infrastructure Initiative–I3). The authors would like as well to thank André J. Cavaleiro from University of Coimbra, Portugal and C. Baehtz from Helmholtz-Zentrum Dresden-Rossendorf, Germany for performing and supporting the synchrotron radiation experiments, respectively. We also thank Lunjie Zeng from Chalmers University of Technology and Liliana Alves from CEMUP for TEM measurements and XPS analysis, respectively, and for all valuable discussions.

References

[1] N.K. Manninen, F. Ribeiro, A. Escudeiro, T. Polcar, S. Carvalho, A. Cavaleiro, Influence of Ag content on mechanical and tribological behavior of DLC coatings, Surf. Coat. Technol. 232 (2013) 440–446.

[2] R.M. Balestra, A.M.G. Castro, M. Evaristo, A. Escudeiro, P. Mutafov, T. Polcar, A. Cavaleiro, Carbon-based coatings doped by copper: tribological and mechanical behavior in olive oil lubrication, Surf. Coat. Technol. 205 (2011) S79–S83.

[3] C.W. Moura e Silva, J.R.T. Branco, A. Cavaleiro, How can H content influence the tribological behaviour of W-containing DLC coatings, Solid State Sci. 11 (2009) 1778–1782.

[4] J.C. Sánchez-López, A. Fernández, Doping and alloying effects on DLC coatings, in: C. Donnet, A. Erdemir (Eds.), Tribology of Diamond-Like Carbon Films, Springer, USA, 2008, pp. 311–338.

[5] W. Lengauer, A. Eder, Carbides transition metal solid-state chemistry, in: Encyclopedia of Inorganic Chemistry, John Wiley & Sons, Ltd., 2006.

[6] W.J. Meng, R.C. Tittsworth, L.E. Rehn, Mechanical properties and microstructure of TiC/amorphous hydrocarbon nanocomposite coatings, Thin Solid Films 377–378 (2000) 222–232.

[7] B. Feng, D.M. Cao, W.J. Meng, J. Xu, R.C. Tittsworth, L.E. Rehn, et al., Characterization of microstructure and mechanical behavior of sputter deposited Ti-containing amorphous carbon coatings, Surf. Coat. Technol. 148 (2011) 153–162.

[8] Y.T. Pei, D. Galvan, J.T.M. De Hosson, C. Strondl, Advanced TiC/a-C:H nanocomposite coatings deposited by magnetron sputtering, J. Eur. Ceram. Soc. 26 (2006) 565–570.

[9] Y.T. Pei, D. Galvan, J.T.M. De Hosson, A. Cavaleiro, Nanostructured TiC/a-C coatings for low friction and wear resistant applications, Surf. Coat. Technol. 198 (2005) 44–50.

[10] A. Voevodin, S. Prasad, J. Zabinski, Nanocrystalline carbide/amorphous carbon composites, J. Appl. Phys. 82 (1997) 855–858.

[11] P.M. Martin, Handbook of Deposition Technologies for Films and Coatings: Science, Applications and Technology, Elsevier Science, 2009.

[12] A. Voevodin, M. Capano, S. Laube, M. Donley, J. Zabinski, Design of a Ti/TiC/DLC functionally gradient coating based on studies of structural transitions in Ti–C thin films, Thin Solid Films 298 (1997) 107–115.

[13] Y.T. Pei, D. Galvan, J.T.M. De Hosson, Nanostructure and properties of TiC/a-C:H composite coatings, Acta Mater. 53 (2005) 4505–4521.

[14] Y.T. Pei, C.Q. Chen, K.P. Shaha, J.T.M. De Hosson, J.W. Bradley, S.A. Voronin, et al., Microstructural control of TiC/a-C nanocomposite coatings with pulsed magnetron sputtering, Acta Mater. 56 (2) (2008) 696–709.

[15] U. Jansson, E. Lewin, Sputter deposition of transition-metal carbide films—a critical review from a chemical perspective, Thin Solid Films 536 (2013) 1–24.

[16] E. Lewin, P.O.Å. Persson, M. Lattemann, M. Stüber, M. Gorgoi, A. Sandell, et al., On the origin of a third spectral component of C1s XPS-spectra for nc-TiC/aC nanocomposite thin films, Surf. Coat. Technol. 202 (2008) 3563–3570.

[17] M. Magnuson, E. Lewin, L. Hultman, U. Jansson, Electronic structure and chemical bonding of nanocrystalline-TiC/amorphous-C nanocomposites, Phys. Rev. B 80 (2009) 235108.

[18] D. Martínez-Martínez, C. López-Cartes, A. Fernández, J.C. Sánchez-López, Influence of the microstructure on the mechanical and tribological behavior of TiC/a-C nanocomposite coatings, Thin Solid Films 517 (2009) 1662–1671.

[19] A.A. Voevodin, J.S. Zabinski, Supertough wear-resistant coatings with ‘chameleon’ surface adaptation, Thin Solid Films 370 (2000) 223–231.

[20] A. Escudeiro, T. Polcar, A. Cavaleiro, a-C(:H) and a-C(:H)_Zr coatings deposited on biomedical Ti-based substrates: tribological properties, Thin Solid Films 538 (2013) 89–96.

[21] C.D. Wagner, W.M. Riggs, L.E. Davis, J.F. Moulder, G.E. Muilenberg, Handbook of X-Ray Photoelectron Spectroscopy, Perkin-Elmer Corporation, Minnesota, 1979.

[22] W.C. Oliver, G.M. Pharr, An improved technique for determining hardness and elastic modulus using load and displacement sensing indentation experiments, J. Mater. Res. 7 (1992) 1564–1583.

[23] G.G. Stoney, The tension of metallic films deposited by electrolysis, Proc. R. Soc. Lond. Ser. A 82 (1909) 172–175.

[24] A. Escudeiro, T. Polcar, A. Cavaleiro, Adsorption of bovine serum albumin on Zr co-sputtered a-C(:H) films: implication on wear behaviour, J. Mech. Behav. Biomed. 39 (2014) 316–327.

[25] P. Frantz, S.V. Didziulis, Detailed spectroscopic studies of oxygen on metal carbide surfaces, Surf. Sci. 412–413 (1998) 384–396.

[26] J.A. Rodriguez, P. Liu, J. Gomes, K. Nakamura, F. Viñes, C. Sousa, et al., Interaction of oxygen with ZrC(0 0 1) and VC(0 0 1): photoemission and first-principles studies, Phys. Rev. B 72 (2005) 075427.

[27] A.A. El Mel, B. Angleraud, E. Gautron, A. Granier, P.Y. Tessier, XPS study of the surface composition modification of nc-TiC/C nanocomposite films under in situ argon ion bombardment, Thin Solid Films 519 (2011) 3982–3985.

[28] F. Fernandes, A. Loureiro, T. Polcar, A. Cavaleiro, The effect of increasing V content on the structure, mechanical properties and oxidation resistance of Ti–Si–V–N films deposited by DC reactive magnetron sputtering, Appl. Surf. Sci. 289 (2014) 114–123.

[29] F. Vaz, P. Machado, L. Rebouta, J.A. Mendes, S. Lanceros-Méndez, L. Cunha, et al., Physical and morphological characterization of reactively magnetron sputtered TiN films, Thin Solid Films 420–421 (2002) 421–428.

[30] M. Birkholz, Line profile analysis, in: Thin Film Analysis by X-Ray Scattering, Wiley-VCH Verlag GmbH & Co. KGaA, 2006, pp. 85–141.

[31] W. Gulbiński, S. Mathur, H. Shen, T. Suszko, A. Gilewicz, B. Warcholiński, Evaluation of phase, composition, microstructure and properties in TiC/a-C:H thin films deposited by magnetron sputtering, Appl. Surf. Sci. 239 (2005) 302–310.

[32] C. Morant, J.M. Sanz, L. Galán, L. Soriano, F. Rueda, An XPS study of the interaction of oxygen with zirconium, Surf. Sci. 218 (1989) 331–345.

[33] Y.F. Zheng, D. Liu, X.L. Liu, L. Li, Enhanced corrosion resistance of Zr coating on biomedical TiNi alloy prepared by plasma immersion ion implantation and deposition, Appl. Surf. Sci. 255 (2008) 512–514.

[34] S.V. Calderon, R.E. Galindo, N. Benito, C. Palacio, A. Cavaleiro, S. Carvalho, Ag^+ release inhibition from ZrCN–Ag coatings by surface agglomeration mechanism: structural characterization, J. Phys. D Appl. Phys. 46 (2013) 325303.

[35] Y.S. Won, Y.S. Kim, V.G. Varanasi, O. Kryliouk, T.J. Anderson, C.T. Sirimanne, et al., Growth of ZrC thin films by aerosol-assisted MOCVD, J. Cryst. Growth 304 (2007) 324–332.

[36] R. Kaufmann, H. Klewe-Nebenius, H. Moers, G. Pfennig, H. Jenett, H.J. Ache, XPS studies of the thermal behaviour of passivated Zircaloy-4 surfaces, Surf. Interface Anal. 11 (1988) 502–509.

[37] M. Balaceanu, M. Braic, V. Braic, A. Vladescu, C.C. Negrila, Surface chemistry of plasma deposited ZrC hard coatings, J. Optoelectron. Adv. Mater. 7 (2005) 2557–2560.

[38] M. Andersson, S. Urbonaite, E. Lewin, U. Jansson, Magnetron sputtering of Zr–Si–C thin films, Thin Solid Films 520 (2012) 6375–6381.

[39] D. Craciun, G. Bourne, G. Socol, N. Stefan, G. Dorcioman, E. Lambers, et al., Characteristics of ZrC/ZrN and ZrC/TiN multilayers grown by pulsed laser deposition, Appl. Surf. Sci. 257 (2011) 5332–5336.

[40] H. Hantsche, in: G. Beamson, D. Briggs (Eds.), High Resolution XPS of Organic Polymers, the Scienta ESCA300 Database, Wiley, Chichester, 1992, p. pp295.

[41] A. Schroeder, G. Francz, A. Bruinink, R. Hauert, J. Mayer, E. Wintermantel, Titanium containing amorphous hydrogenated carbon films (a-C:H/Ti): surface analysis and evaluation of cellular reactions using bone marrow cell cultures in vitro, Biomaterials 21 (2000) 449–456.

[42] Q.N. Meng, M. Wen, F. Mao, N. Nedfors, U. Jansson, W.T. Zheng, Deposition and characterization of reactive magnetron sputtered zirconium carbide films, Surf. Coat. Technol. 232 (2013) 876–883.

[43] S.S. Premathilaka, M.M. Hyland, Z.D. Chen, L.R. Watkins, B. Bansal, Interaction of whey protein with modified stainless steel surfaces, presented at the Proceedings of 7th International Conference on Heat Exchanger Fouling and Cleaning – Challenges and Opportunities, Tomar, Portugal, 2007.

[44] T. Zehnder, J. Patscheider, Nanocomposite TiC/a–C:H hard coatings deposited by reactive PVD, Surf. Coat. Technol. 133–134 (133) (2000) 138–140.

[45] E. Lewin, M. Råsander, M. Klintenberg, A. Bergman, O. Eriksson, U. Jansson, Design of the lattice parameter of embedded nanoparticles, Chem. Phys. Lett. 496 (2010) 95–99.

[46] A. Nakao, M. Iwaki, J. Takahashi, K. Terashima, X-ray photoelectron spectroscopy study of zirconium-implanted iron and carbon-implanted zirconium, Surf. Coat. Technol. 66 (1994) 373–376.

[47] K.H.T. Raman, M.S.R.N. Kiran, U. Ramamurty, G.M. Rao, Structure and mechanical properties of TiC films deposited using combination of pulsed DC and normal DC magnetron co-sputtering, Appl. Surf. Sci. 258 (2012) 8629–8635.

[48] X.L. Peng, T.W. Clyne, Residual stress and debonding of DLC films on metallic substrates, Diam. Relat. Mater. 7 (1998) 944–950.

[49] Y. Pauleau, Residual stresses in DLC films and adhesion to various substrates, in: C. Donnet, A. Erdemir (Eds.), Tribology of Diamond-Like Carbon Films, Springer, USA, 2008, pp. 102–136.

[50] C.W. Zou, H.J. Wang, L. Feng, S.W. Xue, Effects of Cr concentrations on the microstructure, hardness, and temperature-dependent tribological properties of Cr-DLC coatings, Appl. Surf. Sci. 286 (2013) 137–141.

[51] T. Polcar, T. Vitu, L. Cvrcek, R. Novak, J. Vyskocil, A. Cavaleiro, Tribological behaviour of nanostructured Ti–C:H coatings for biomedical applications, Solid State Sci. 11 (2009) 1757–1761.

[52] A. Leyland, A. Matthews, On the significance of the H/E ratio in wear control: a nanocomposite coating approach to optimised tribological behaviour, Wear 246 (2000) 1–11.